FACULTY OF BIOLOGICAL SCIENCES

Biochemistry and Molecular Biology Department

Doctoral Program:

Biochemistry & Biomedicine

CENTRO DE INVESTIGACIÓN PRÍNCIPE FELIPE

Polymer Therapeutics Laboratory

Well-defined polypeptide-based systems as non-viral vectors for cytosolic delivery

AMAYA NIÑO PARIENTE

Doctoral Thesis UV/2017

Thesis Director: María J. Vicent Docón

Dr. María J. Vicent Docón, Ph.D. in Chemistry and Head of the Polymer Therapeutics Laboratory at the Centro de Investigación Príncipe Felipe (Valencia, Spain)

CERTIFIES, that the work

"WELL-DEFINED POLYPEPTIDE-BASED SYSTEMS AS NON-VIRAL VECTORS FOR CYTOSOLIC DELIVERY"

has been developed by Amaya Niño Pariente under her supervision in the Centro de Investigación Príncipe Felipe in Valencia, as a thesis project to obtain a Ph.D. degree in Biochemistry and Biomedicine from the University of Valencia, Faculty of Biological Sciences, Biochemistry and Molecular Biology Department.

A mis padres

INDEX

ACKNOWLEDGEMENTS

Al principio pensé que ésta sería la parte de la tesis que más fácilmente escribiría, pero no ha sido así. Como cada capítulo, lo he leído, releído, cambiado y vuelto a cambiar. Nunca estará completo. Nunca estará bien. Hay demasiado que agradecer. Habéis sido muchos los que habéis hecho posible este viaje, el viaje que emprendí y cambió radicalmente mi vida:

"*En ocasiones tenemos que abandonar la vida que habíamos planeado porque ya no somos la misma persona que hizo aquellos planes*" Javier Iriondo.

Este viaje comenzó con una llamada de teléfono. Gracias María Jesús Vicent, mi directora de tesis, por estar al otro lado del teléfono y darme la oportunidad de emprender esta nueva aventura que tantas cosas me ha enseñado y me sigue enseñando. Gracias por abrirme las puertas a un grupo que sigue creciendo y que se lleva un poquito de mí. Un grupo de gente genial, que he sentido como parte mi familia. A toda esa gente quiero decirles GRACIAS. Mi relación ha sido mayor con unos que con otros y, también, unos más que otros habéis sufrido mi forma de ser. Gracias a cada uno de vosotros por todo este tiempo vivido y perdón por aquellos momentos en los que mi genio salió a pasear. Me voy del laboratorio con muy buenas experiencias vividas, con muy buenos amigos y con muchos lugares donde seguiros. Sin vosotros nada hubiera sido igual.

Dentro de esta aventura no puedo olvidarme de las personas que me acogieron es sus laboratorios: Prof. Dr. Ernst Wagner (Múnich) y Dr. Alison Paul (Cardiff). Fueron grandes experiencias que nunca podré olvidar, ni laboral ni personalmente.

Fuera de lo científico, están todos esos amigos que han permanecido junto a mí en este duro camino. Los que ya estaban y a los que me fui encontrando. Esos momentos de desconexión con vosotros conseguían que volviera a conectarme con más fuerza. Gracias también por esas visitas, seguidas de duras despedidas, que me hacían recordar lo que más echaba de menos y todo lo que me estaba perdiendo.

Por último y más importante: mi familia. Sin ellos nunca hubiera llegado hasta aquí. Su apoyo, confianza y orgullo han hecho que pasito a pasito haya llegado donde estoy. Especialmente mis padres. Realmente no tengo palabras, pero me gustaría que llegarais a entender lo enormemente orgullosa que estoy de vosotros y, aunque ya tenía la certeza, confirmasteis que haríais lo imposible para que lograra lo que me propusiera. Con vuestro gran esfuerzo y paciencia habéis hecho que se cumpla este sueño.

Gracias a mi madre por decirme las palabras que me darían el empujón que necesitaba: “No me preguntes lo que hacer, pregúntame lo que yo haría”. Y lo hice, y comenzó una de las mejores etapas de mi vida. Una etapa llena de esfuerzo, trabajo y dedicación. Llena de millones de experiencias personales. El comienzo de mi nueva vida. Gracias por tu sonrisa al recibirme y tus lágrimas al despedirme. Ojalá no existieran esas despedidas y pudiera estar siempre a tu lado.

Gracias a mi padre, por no cansarte de hablar de mí por todos los rincones, con el orgullo que te caracteriza. Por hacerme sentir importante y por demostrarme lo contento que estás con el trabajo que he desempeñado.

Gracias a mis hermanos que me han seguido allá donde he ido y se han interesado por cada paso que he ido dando. Gracias por todo el esfuerzo que habéis hecho a todos los niveles para que yo pudiera empezar, continuar y terminar mi aventura. Sin vuestro esfuerzo no hubiera podido hacerlo nunca.

Y…Miguel. Lo más duro de marcharme de Valladolid fue el separarme de ti y saber que no iba a vivir tu día a día. Decidir dejar Valladolid fue decidir dejarte y fue realmente difícil. Pero cada reencuentro contigo ha sido mejor que el anterior. El saber que a pesar de estar lejos me tienes presente hace un poquito menos duro el saber que no estoy contigo. Tan pequeño y tan grande a la vez.

Y siguiendo con mi familia estás tú, Alberto. Eres el que ha sufrido todo este camino, haciéndome siempre la vida más fácil con pequeños

detalles y grandes sonrisas. Gracias por estar ahí y gracias por ser tú. Nunca podré compensártelo.

Todos y cada uno de vosotros en conjunto habéis hecho que un camino difícil lo sea mucho menos.

GRACIAS

+/-	Charge-ratio
3D	Three-dimensional
6-FAM	6-Fluorescein amidite
A	Absorbance
AFM	Atomic force microscopy
AGT	Alanine:glyoxylate aminotransferase
Ala	Alanine
ALL	Acute lymphocytic leukaemia
AMD	Age-related macular degeneration
Antp	Antennapedia
ApOH	Amino-2-propanol
Arg	Arginine
ATR-FTIR	Attenuated total reflection Fourier transform infrared spectroscopy
BDMC	Bisdemethoxycurcumin
B_{inc}	Flat background
bp	Base pairs
CAC	Critical aggregation concentration
CaOx	Calcium oxalate
CD	Cyclodextrin
CD	Circular dichroism
CDP	Cyclodextrin polymer
CHO	Chinese hamster ovary
CI	Combination index
CKD	Chronic kidney disease
CMC	Critical micellar concentration
CMV	Cytomegalovirus
CPP	Cell-penetrating peptide
CrEl	Cremophor EL
Cryo-TEM	Cryogenic transmission electron microscopy
Cys	Cysteine
D	Diffusion coefficient
Đ	Polydispersity
d.	Diameter
DACH	1,2-Diaminocyclohexane
DBU	1,8-Diazabicyclo[5.4.0]undec-7-ene
DCM	Dichloromethane
DCX	Docetaxel
DDS	Drug delivery systems
DES	Diethylstilbestrol
df	Dilution factor

DIPEA	*N*,*N*-Diisopropylethylamine
DLinDMA	1,2-Dilinoleyloxy-*N,N*-dimethylaminopropane
DLS	Dynamic light scattering
D_{max}	Maximum dimension
DMEM	Dulbecco's Modified Eagle's Medium
DMF	*N,N*-Dimethylformamide
DMPE	1,2-Dimyristoyl-sn-glycero-3-phosphoethanolamine
DMRIE	*N*-[1-(2,3-Dimyristyloxy)propyl]-*N,N*-dimethyl-N-(2-hydroxyethyl)ammonium bromide
DMSO	Dimethyl sulfoxide
DMTMM·Cl	4-(4,6-Dimethoxy-1,3,5-triazin-2-yl)-4-methylmorpholinium chloride
DOOA	3,6-Dioxa-octanediamine
DOPC	1,2-Dioleoyl-sn-glycero-3-phosphocholine
DOPE	L-Dioleoyl phosphatidylethanolamine
DOSY	Diffusion-ordered spectroscopy
DOTAP	Dioleoyl-trimethylammonium propane
DOX	Doxorubicin
DP	Degree of polymerisation
dPBS	Deuterated PBS
DPC	Dynamic polyconjugate
DP^{theo}	Monomer concentration / initiator concentration
DPyPE	1,2-Diphytanoyl-sn-glycero-3-phosphoethanolamine
DR	Differential refractometry
dsDNA	Double stranded DNA
dsRNA	Double stranded RNA
ds-siRNA	Double stranded siRNA
DTNB	5,5-Dithiobis(2-nitrobenzoate)
DTT	1,4-Dithiothreitol
EDTA	Ethylenediaminetetraacetic acid
EGF	Epithelial growth factor
EPO	Epoetin beta
EPR	Enhanced permeability and retention
eq.	Equivalent
ESEM	Environmental scanning electron microscopy
EtBr	Ethidium bromide
Fab	Fragment antigen-binding
FBS	Fetal bovine serum
FCS	Fluorescence correlation spectroscopy
FDA	Food and Drug Administration
FITC	Fluorescein isothiocyanate

Fmoc	9-Fluorenylmethoxycarbonyl
FRET	Fluorescence resonance energy transfer
FS	Fluorescence spectroscopy
g	Gradient strength
GalNAc	*N*-Acetyl galactosamine
GAP-DMORIE	(±)-*N*-(3-Aminopropyl)-*N,N*-dimethyl-2,3-bis(syn-9-tetradeceneyloxy)-1-propanaminium bromide
GAU	Glutamic acid unit
GFP	Green fluorescent protein
GL67A-DOPE	1,2-Dimyristoyl-sn-glycero-3-phosphoetanolamine
Glu	Glutamic acid
GO	Glycolate oxidase
Hb	Haemoglobin
HEPES	4-(2-Hydroxyethyl)-1-piperazineethane-sulfonic acid
HGH	Human growth hormone
Hist	Histidine
HIV-1	Human immunodeficiency virus type 1
HMW	High molecular weight
HMWC	HMW conjugates
HOBt	1-Hydroxybenzotriazole
HPLC	High performance liquid chromatography
HPMA	N-(2-Hydroxypropyl)methacrylamide
hrGCSF	Human recombinant granulocyte-colony stimulating factor
HSV	Herpes virus protein
I	Observed intensity
I(Q)	Scattering intensity
I_0	Reference intensity
IFM	Immunofluorescence microscopy
IM	Intramuscular
IR	Infrared spectroscopy
ITC	Isothermal titration calorimetry
IV	Intravenous
k	Wave vector of the incident radiation
k'	Wave vector of the scattered radiation
kDa	Kilodalton
LDL	Low-density lipoprotein
LMW	Low molecular weight
LNP	Lipid-based nanoparticle
LPEI	Linear PEI

MDR	Multidrug resistance
MeOD	Deuterated methanol
MeOH	Methanol
Met	Methionine
Mn	Number average MW
mol%	Mol percent
Morph	Morpholine
mRNA	Messenger RNA
MTBE	*Tert*-butyl methyl ether
MTS	3- (4,5-dimethylthiazol-2-yl)-5- (3-carboxymethoxyphenyl)-2- (4- sulfophenyl)-2H-tetrazolium
MW	Molecular weight
MWCO	Molecular weight cut-off
n.s.	Non-significant
N/P ratio	Nitrogen to phosphate ratio
nanoDDS	Nanoscale drug delivery systems
NCE	New chemical entity
Nf	Scale (Dozier model)
NMR	Nuclear magnetic resonance
NOESY NMR	Nuclear overhauser effect spectroscopy NMR
NSCLC	Non-small cell lung cancer
NTA	Nanoparticle tracking analysis
P(Orn)	Poly-L-ornithine
P(Q)	Form factor
P(r)	Pair-distribution function
PAGE	Polyacrylamide gel electrophoresis
PAMAM	Polyamidoamine
PArg	Poly-L-arginine
PBLG	Poly-(ɣ-benzyl-L-glutamate)
PBS	Phosphate buffer saline
PCB	Polycarboxybetaine
PD	Pyridyl dithiol
PDEPT	Polymer-directed enzyme produg therapy
PdI	Polydispersity index
pDNA	Plasmid DNA
PEG	Polyethyleneglycol
PEI	Polyethylenimine
PELT	Polymer enzyme liposome therapy
PGA	Poly-L-glutamic acid
P-gp	P-glycoprotein

PGSE NMR	Pulsed-gradient spin-echo NMR
PH1	Primary hyperoxaluria type I
PLK1	Polo-like kinase 1
PLL	Poly-L-lysine
PLP	pyridoxal 5'-phosphate
PMS	Phenazinemethosulfate
pSar	Polysarcosine
PSB	Polysulfobetaine
PT	Polymer Therapeutics
PT	Potentiometric titration
PTS	Peroxisomal targeting sequence
PTS1	Type 1 PTS
PTX	Paclitaxel
PyBOP	(Benzotriazol-1-yl)oxy-tris-pyrrolidino-phosphonium hexafluorophosphate
Q	Scattering vector
RAFT	Reversible addition-fragmentation chain transfer
RBC	Red blood cell
RES	Reticulo-endothelial system
R_g	Radius of gyration
R_h	Hydrodynamic radius
RISC	RNA-induced silencing complex
RLU	Relative light units
RNAi	RNA interference
ROS	Reactive oxygen species
RRM2	Ribonucleotide reductase M2
RS	Raman spectroscopy
RT	Room temperature
S(Q)	Structure factor
SANS	Small angle neutron scattering
SAR	Structure-activity relationship
SAS	Small angle scattering
SAXS	Small angle X-ray scattering
SC	Subcutaneous
SD	Standard deviation
SDS	Sodium dodecyl sulphate
SEC	Size exclusion chromatography
SEM	Standard error mean
Ser	Serinol
siRNA	Small interfering RNA
SLS	Small angle light scattering

SMANCS	Styrene maleic anhydride neocarzinostatin
SNALP	Stale nucleic acid-lipid particle
SPPS	Solid phase peptide synthesis
SPR	Surface plasmon resonance
ssDNA	Single stranded DNA
SSE	Sum of square errors
STD NMR	Saturation transfer difference NMR
Stp	Succinyl tetraethylene pentamine
Stp_5	Pentameric Stp
Tat	Transactivating transcriptional activator
Tat-AGT	AGT-cell-penetrating Tat-peptide fusion protein
tBoc	*Tert*-butoxycarbonyl
TCEP	tris(2-carboxyethyl)phosphine
TEM	Transmission electron microscopy
TFA	Trifluoroacetic acid
Tfn	Transferrin
TIS	Triisopropylsilane
TNF	Tumor necrosis factor
TTR	Transthyretin
Tyr	Tyrosine
UV-Vis	Ultraviolet-visible spectroscopy
VEGFR	Vascular endothelial growth factor receptor
V_p	Volume of a single particle
wt%	Weight percent
x	Percentage of modification
α/Nf	Relative scale of the fractal term (Dozier model)
γ	Gyromagnetic ratio
δ	Length of the gradient
Δ	Diffusion time
Δρ	Contrast term
ζ-potential	Zeta-potential
λ_{em}	Emission wavelength
λ_{ex}	Excitation wavelength
ξ	Exponential damping length (Dozier model)
$\rho_{polymer}$	Polymer scattering length density
$\rho_{solvent}$	Solvent scattering length density
χ	Flory-Huggins interaction parameters
ϕ	Polymer volume fraction
ν	Flory exponent (Dozier model)

Abstract

A convenient cytosolic drug delivery constitutes a very powerful tool for the treatment and/or prevention of several relevant human diseases. Along with recent advances in therapeutic technologies based on biomacromolecules (*e.g.* oligonucleotides or proteins), we also require the development of technologies which improve the transport of therapeutic molecules to the cell of choice. This has led to the emergence of a variety of promising methods over the last 20 years. Despite significant progress, these methods still suffer from several shortcomings including low/variable delivery efficiency, high cytotoxicity, and perhaps most importantly, ineffective endosomal/lysosomal escape. In this context, Polymer Therapeutics (PT) have emerged as an exciting alternative to overcome such limitations. Specifically, well defined polypeptide-based therapeutics could be considered excellent candidates for drug delivery due to their suitable biodegradability, versatility, multivalence and high drug loading capacity. On the other hand, a comprehensive understanding of therapeutic molecules is also required for the rational selection and design of an appropriate intracellular delivery carrier.

The application of new, robust, and sophisticated characterisation techniques has complemented existing techniques to meet the challenge of working under physiological or near-physiological conditions. The remarkable development in the design of drug delivery systems has forced the establishment of design guidelines to achieve the specific therapeutic effect. The importance of an exhaustive physicochemical characterisation has given rise to more efficient therapeutic strategies via better control of the pharmacokinetics and biodistribution of such nanomedicines.

On this basis, the main aim of this thesis is focused on two main topics: (i) the design, development, and validation of nanosized polypeptide-based carriers capable of facilitating the cytosolic transport of bioactive agents which are not able to cross biological membranes by themselves or exhibit low lysosomal stability, such as plasmid DNA (pDNA), small interfering RNA (siRNA), or proteins, and (ii) the exhaustive physicochemical characterisation of polymeric drug delivery

systems to determine their solution conformation and its correlation with their therapeutic output.

In order to accomplish the above-mentioned goals and based on well-established properties of poly-L-glutamic acid (PGA) as a polymer carrier, firstly, we synthesised and evaluated different conjugates of PGA with succinyl tetraethylene pentamine (Stp) oligoaminoamides as non-viral carriers for pDNA or siRNA delivery. We hypothesised that these zwitterionic bioresponsive and biodegradable carriers may achieve similar transfection efficiencies as those achieved for analogous polycations, but with greater safety in biological scenarios by avoiding polycation-triggered side effects. After physicochemical characterisation of the obtained conjugates, we evaluated cytotoxicity in both N2a and 4T1 cell lines to assess cell viability. We also performed transfection and cell internalisation assays to assess conjugate functionality.

We also continued exploring different alternatives within the field of polypeptides. We synthesised and characterised multifunctional polymeric platforms based on natural or synthetic polyaminoacids, such as PGA, poly-L-arginine (PArg), poly-L-ornithine (P(Orn)), and their derivatives to find an encouraging vehicle for effective siRNA delivery as anticancer treatment. We obtained several oligonucleotide conjugates and complexes and performed preliminary *in vitro* studies in B16F10-luc-G5 cell line. Upon comparing the obtained results of silencing, we established that P(Orn)-based systems offered the most promising results.

Additionally, the feasibility of the delivery of a protein, alanine:glyoxylate aminotransferase (AGT), in order to promote enzyme-replacement therapy in a rare disease Hyperoxaluria Type I by conjugating the enzyme with a polyethyleneglycol (PEG)-PGA block-*co*-polymer based nanocarrier was also evaluated. This conjugation strategy does not significantly alter the functional properties of AGT and endows the protein with the ability to cross the plasma membrane and localise in the cytosol of a cellular model of PH1. Engineering AGT by the insertion of a stronger peroxisomal targeting sequence (PTS) and the

mutation of one of the polymer anchoring points located on the “extended PTS1” partly decreases the conjugation efficiency. However, this allows peroxisomal targeting of the conjugates, resulting in the enhanced ability to detoxify intraperoxisomal glyoxylate with respect to the wild-type protein.

We obtained all mentioned systems from polymers with very low polydispersity (Đ∼1.2) and, therefore, precise and well-defined structures, so allowing reproducibility and the determination of a clear structure-activity relationship (SAR). We also exhaustively investigated physicochemical properties of all obtained polypeptides in terms of size and solution conformation.

Finally, in order to deeply understand the importance of solution conformation in conjugate therapeutic output, highly advanced physicochemical techniques such as small angle neutron scattering (SANS) or small angle X-ray scattering (SAXS) were used always trying to mimic physiological conditions. A rigorous and detailed structural investigation of polymeric nanosystems already classified as successful drug delivery nanocarriers were performed.

Aims of the research

The present thesis dissertation aims to discuss the design and development of nanosized polypeptide-based carriers for cytosolic delivery of biomacromolecules such as plasmid DNA (pDNA), small interfering RNA (siRNA), and proteins. Likewise, this thesis is also focused on the exhaustive physicochemical characterisation in solution of several polymer therapeutics containing similar polymeric base in order to elucidate structure-activity relationships between conjugate solution conformation and their therapeutic output. These principal objectives can be summarised in the following specific tasks:

(i) Design of poly-L-glutamate (PGA)-based complexes for gene-based therapy. Chapter II aims include the design, synthesis, physicochemical characterisation, and *in vitro* biological evaluation of PGA-based systems functionalised with linear synthetic polyamidoamines to be used as oligonucleotide intracellular delivery systems.

(ii) Development of non-viral polypeptide-based carriers for siRNA delivery. Chapter III aims involve the development and biological evaluation of a versatile methodology for the modification of polyaminoacids, both synthetic and natural, in order to obtain appropriate carriers for cytosolic siRNA delivery.

(iii) Development of PGA-based conjugates for intracellular protein delivery. As an example, intraperoxisomal delivery of engineered human alanine:glyoxylate aminotransferase (AGT). Chapter IV aims to the delivery of AGT to liver peroxisomes by conjugating the enzyme with a polyethyleneglycol (PEG)-PGA block-*co*-polymer based nanocarrier.

(iv) Use of Small Angle Neutron Scattering (SANS) and Small Angle X-Ray Scattering (SAXS) to study solution conformation of Polymer Therapeutics. Chapter V aims to elucidate, by means of scattering techniques, the solution conformation of complex nanosystems in order to better correlate size and shape with their biological output. The exhaustive physicochemical characterisation of different nanosystems in solution through advanced techniques such as SANS or SAXS mimicking physiological conditions will be performed.

Chapter I

General Introduction

I.1. POLYMER THERAPEUTICS (PT)

I.1.1. Introduction and Background

Biopharmaceuticals such as proteins, peptides or nucleic acids are eminent candidates in the development of macromolecular drugs for the treatment of several diseases. They generally offer the advantage of biocompatibility and biodegradability since many are naturally produced by the human body and hence are well tolerated and excreted. Nevertheless, one of the most important rate-limiting steps of their efficiency relates to the successful delivery to the desired site of action and subsequent release inside the target cell [1]. Therefore, the development of an appropriate delivery vehicle that combines high specificity for the target cell, high therapeutic payload, relatively low toxicity, and stability during passage through the body still represents an important challenge. A variety of promising methods have emerged in the last 20 years including, for example, the use of cell-penetrating peptides (CPPs), liposomes, or polymers (further explained in Section I.2.2). Despite significant progress, these examples still present with several shortcomings including low/variable delivery efficiency, high cytotoxicity, and perhaps most importantly, ineffective endosomal/lysosomal escape.

In order to further enhance the pharmacological behaviour and stability of these macromolecules, polymers have played an essential role.

I.1.2. Definition and Classification

The descriptor “Polymer Therapeutics”(PT), firstly introduced by Ruth Duncan [2], encompasses a variety of rationally designed polymer-based constructs: polymeric drugs, polymers with inherent activity [3], polymer conjugates of proteins, drugs and aptamers [4-7], polymeric micelles containing covalently bound drug [8-10], and multicomponent polyplexes that are being developed as non-viral vectors [2, 11, 12] (Figure I.1). All of these examples are amongst the most successful first-generation nanomedicines, with 16 products already in routine clinical use [13]. Furthermore, two polymer therapeutics are within the US Top

10 selling drugs: the polymeric drug Glatiramer acetate for the treatment of multiple sclerosis (Copaxone®, Teva Pharm) and the polymer conjugate polyethyleneglycol (PEG)-filgrastim for the treatment of neutropenia (Neulasta®, Amgen) [14]. These subclasses use specific water-soluble polymers, either as the bioactive agent itself or as an inert functional part of a multifaceted construct for improved drug, protein, or gene delivery [15].

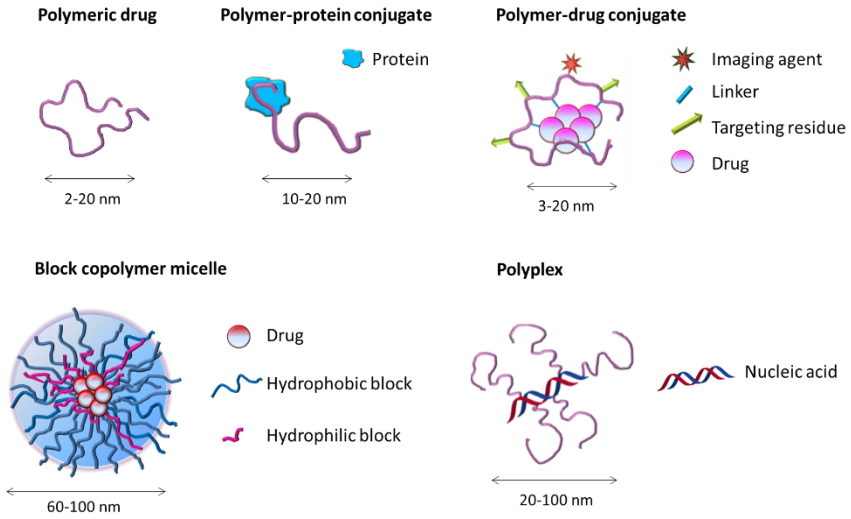

Figure I.1. Schematic representation of Polymer Therapeutics. Redrawn from Duncan [11].

After more than two decades, development of PT has resulted in several products entering the market (Table I.1) and a growing number of as new chemical entities (NCEs) in clinical development (Table I.2). Through the knowledge and understanding acquired regarding biodistribution, clearance, mechanism of action, and stability of first generation PT, a second generation is now being designed with improved and promising features.

Table I.1. First generation marketed polymer therapeutics. Adapted and update from refs [16-18]. IV=intravenous, IM=intramuscular, SC=subcutaneous.

Product name	Technology	Indication	Route	Information source
Polymer-protein conjugates				
Zinostatin stimaler®	Styrene maleic anhydride neocarzinostatin (SMANCS)	Cancer-hepatocellular carcinoma	Local via hepatic artery infusion	Yamanouchi Japan
Oncaspar®	PEG-asparaginase	Cancer-acute lymphocytic leukaemia (ALL)	IV/IM	Enzon
Peg-intron®	PEG-interferon alpha 2b	Hepatitis C	SC	Schering-Plough
Pegasys®	PEG-interferon alpha 2a	Hepatitis C	SC	Roche
Neulasta™	PEG-hrGCSF (human recombinant granulocyte-colony stimulating factor)	Chemotherapy-induced neutropenia	SC	Amgen
Andagen®	PEG-adenosine deaminase	Severe combined immune deficiency syndrome	IM	Enzon
Somavert®	PEG-HGH (human growth hormone) antagonist	Acromegalia	SC	Pfizer

Mircera®	PEG-EPO (epoetin beta)	Treatment of anaemia associated with chronic kidney disease	IV/SC	Roche
Cimzia® (certolizumab pegol)	PEG-anti-TNF Fab (tumor necrosis factor fragment antigen-binding)	Rheumatoid arthritis, Crohn´s disease	SC	UCB
Krystexxa™ pegloticase	PEG-uricase	Chronic gout	IV	Savient Pharmaceuticals
ADYNOVATE	Antihemophilic Factor(recombinant), PEGYlated	Hemophilia A	IV	Nektar and Baxalta
Polymer-aptamer conjugate				
Macugen®	PEG-aptamer (apatinib)	Age-related macular degeneration (AMD)	Local intravitreal	OSI-Eyetech
Polymer-drug conjugate				
MovantikTM/Moventig® (NKTR-118)	PEG-naxolol	Opioid-induced constipation	Oral	AstraZeneca/Daiichi Sankyo Co, Ltd.
Polymeric drugs				
Copaxone®	Glutamic acid (Glu), Alanine (Ala), Tyrosine (Tyr) copolymer	Multiple sclerosis	SC	Teva
Renagel®	Phosphate binding polymer	End stage renal failure	Oral	Genzyme (Daiichi Co, LTD. Licensed)

Welchol®	Cholesterol binding polymer	Type 2 diabetes	Oral	Genzyme

Table I.2. Examples of polymer therapeutics in clinical development. Adapted and updated form refs [16-18]. IV=intravenous.

Product name	Technology	Indication	Route	Stage	Information source
Polymer-protein conjugates					
ADI-PEG 20	PEG-arginine deaminase	Cancer-hepatocellular carcinoma, melanoma	IV	Phase III	Polaris Group
Hemospan® MP40X	PEG-Haemoglobin	Delivery of O_2 in post-surgery and trauma patients	IV	Phase III	Sangart
CDP 791	PEG anti vascular endothelial growth factor receptor (VEGFR)-2-Fab	Cancer-non-small cell lung cancer (NSCLC)	IV	Phase II	UCB Pharma
Polymer-aptamer conjugate					
ARC1779	PEG-anti-platelet-binding function of von Eillebrand Factor	Thrombotic microangiopathies	IV	Phase II	Archemix
E10030	PEG-anti-platelet derived growth factor	AMD	Local intravitreal	Phase III	Ophthotech

	(PDGF) aptamer combination with Lucentis®				
Polymeric drugs					
AMG 223	Phosphate binding polymer	Hyperphosphatemia in chronic kidney disease (CKD) patients on haemodialysis	Oral	Phase II	Amgem
VivaGel®	Lysime-based dendrimer	Microbiocide	Topical	Phase III	Starpharma
Polymer-drug conjugates					
CT2103; Xyotax; Opaxio™	PGA-paclitaxel	Ovarian, Stomach	IV	Phase III	Cell Therapeutics Inc
Prolindac®	N-(2-Hydroxypropyl)methacrylamide (HPMA)-copolymer-1,2-diaminocyclohexane (DACH) platinate	Cancer-melanoma, ovarian	IV	Phase III	Acces Pharmaceuticals
FCE 28068 (PK1)	HPMA-copolymer-doxorubicin (DOX)	Breast, lung and colon cancer	IV	Phase II	Pfizer

FCE 28069 (PK2)	HPMA-copolymer-DOX	Hepatocellular carcinoma	IV	Phase I/II	Pfizer
PEG-SN38	Multiarm PEG-camptothecin	Cancer-various	IV	Phase II/III	Enzon Inc
CRLX101	Cyclodextrin (CD)-PEG-Camptothecin	Cancer-various only in combinations	IV	Phase II	Cerulean Pharma
CRLX301	CD-PEG-Docetaxel	Solid tumours	IV	Phase I	Cerulean Pharma
DEP^{TM} Docetaxel	Docetaxel	Solid tumours	IV	Phase I	Starpharma/AstraZeneca
CriPEC^{TM} Docetaxel	Docetaxel	Solid tumours	IV	Phase I	Cristal Therapeutics
NKTR-181	PEG-naloxone	Chronic pain	Oral	Phase III	Nektar
NKTR-171	PEG-Na^+ channel blocker	Neuropathic pain	Oral	Phase I	Nektar
NKTR-102	PEG-Irinotecan	Advanced breast cancer and brain metastases	IV	Phase III	Nektar
XMT-1001 (Fleximer® based)	Polyacetal-camptothecin	Cancer-various	IV	Phase II	Mersana
XMT-1107	Polyacetal-fumagillin	Solid tumours	IV	Phase I	Mersana/Teva

Polymeric Micelles					
SP1049C Biotransport™	Pluronic® based formulation of DOX	Cancer-Upper GI, NSCLC colorectal	IV	Phase III	Supratek Pharma Inc
NK 105 (Nanocarrier ® technology)	Paclitaxel block copolymer micelle	Breast cancer, Stomach cancer	IV	Phase III	Nippon Kayaku Co
NC-6004, Nanoplatin™	Cisplatin block copolymer micelle	Cancer-various	IV	Phase III	NanoCarrier Co./Orient Neuropharma
NC-4016 (Nanocarrier® technology)	Oxaliplatin block copolymer micelle	Solid tumours	IV	Phase I	NanoCarrier Co
NC-6300 (K-912)	Epirubicin block copolymer micelle	Solid tutors	IV	Phase I	NanoCarrier Co/Kowa
Nanoxel™	Paclitaxel	Advanced Breast cancer	IV	Phase I	Samyang Biopharmaceuticals

As mentioned previously, the main objectives of any drug delivery system (DDS), and therefore of polymer therapeutics, are the release of the active agent at the correct location of action (*targeting*) and the maintenance of the bioactive drug concentration within a therapeutic window for an adequate duration (*controlled drug release*) [19]. The examples given in the previous tables demonstrate that the preferred administration route for intracellular delivery is via intravenous injection. This allows rapid bioavailability in the bloodstream when compared to other parenteral routes explored. Therefore, this enhances the benefits of intrinsic targeting mechanisms, such as the EPR (Enhanced Permeability and Retention) effect [20-24], and bypasses specific biological barriers.

I.1.3. Passive Targeting: Enhanced Permeability and Retention (EPR) Effect

Since the mid-80s, the design of nanosized therapeutic agents, such as polymer therapeutics, has been inspired by the EPR effect, a passive tumour targeting phenomenon which considerably increases therapeutic effect. This evolving theory, firstly described by Matsumura & Maeda [23], is based on the unique pathophysiological features of most solid tumours, such as extensive angiogenesis (hyper-vasculature), defective vascular architecture, and impaired lymphatic drainage. Once a given macromolecule is in the bloodstream, it will extravasate more selectively at tumour tissues due to the enhanced permeability of the angiogenic tumour vasculature. Furthermore, the macromolecule will be retained and accumulate at the tumour site assisted by the lack of an effective lymphatic drainage (Figure I.2). The EPR effect is also an important factor in inflammatory tissues, thereby justifying the development and use of these nanodrugs in infectious and inflammatory conditions [25].

The EPR effect is ultimately driven by the circulating plasma concentration of the polymer therapeutic [26, 27], but it is also highly dependent on tumour vascularisation, which may change between different tumour regions as well as from patient to patient [28]. Typically, the peripheral area of damaged tissues is well-vascularised,

the core is semi-necrotic, and the central region is vascularly necrotic. Poor-vascularised damaged tissues are less susceptible to therapies based on nanosystems. Therefore, simply utilising the hyperpermeability of this vasculature alone may not provide equal treatment throughout the entire tumour [29]. Reports suggest that the ideal molecular size needed to take full advantage of the EPR effect is larger than 40 kDa [30, 31].

There are other characteristics and limitations that have to be taking into account when discussing the EPR effect [21]. These include (i) the fact that the macromolecule may not be able to interact with blood components or blood vessels; (ii) the total surface charges have to be weakly negative to near neutral; (ii) and EPR requires systemic circulation times of several hours. These reasons highlight the need to also employ active targeting strategies to improve disease-to-normal tissue ratios.

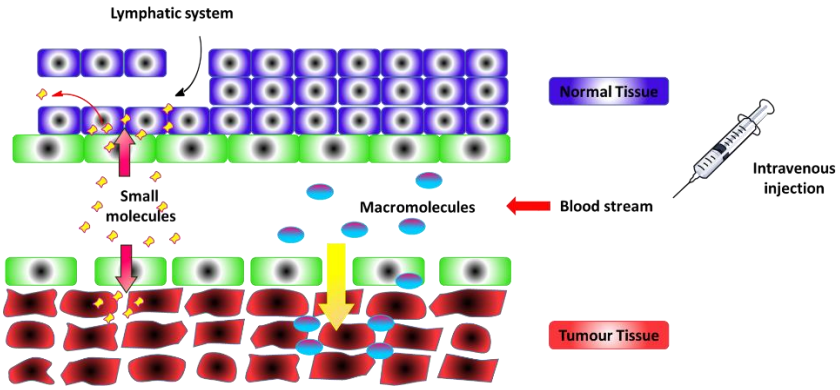

Figure I.2. Schematic representation of the enhanced permeability and retention (EPR) effect.

The EPR effect had been thought of as a universal approach to direct nanoparticles to tumours, and so drug have been designed in a manner that exploits this effect. However, this topic has come under discussion in more recent times. Tumours *in vivo* manifest great diversity and some demonstrate a poor EPR effect. The effect varies depending on a patient's pathological and physiological characteristics and clinical condition. Due to the fact that cancer is highly diverse and heterogeneous, there will be also heterogeneity associated with the

EPR effect [32-34]. This heterogeneity has provoked a debate regarding the real value of this effect, and has led to differing opinions. Some studies support EPR-mediated accumulation of nanomedicines within tumours, while others show that the EPR effect is highly dependent on the tumour model and suggest that the EPR alone may not provide the entire solution. Dr. Maeda himself recognizes such heterogeneity and has developed methods to enhance the EPR effect in order to overcome the heterogeneity and improve drug delivery to tumours [34].

I.2. CYTOSOLIC DELIVERY

Some drugs are large hydrophilic and/or charged molecules and this represents a major obstacle to their intracellular delivery through the lipidic environment of biological membranes. Additionally, after endocytosis (if it has taken place), lysosomal enzymatic degradation must be avoided. Therefore, a comprehensive understanding of the therapeutic in question is required to rationally design an appropriate intracellular drug delivery carrier. As a result, several strategies to promote the cytosolic delivery of macromolecular therapeutics have been developed over recent years. These strategies include the use of CPPs, pH sensitive and cationic liposomes, and cationic lipids and polymers, among others. Different strategies can be classified into those that exploit the biochemical aspects of the endosomal cavity to promote endosome-to-cytosol transfer (*e.g.* pH-responsive carriers or endosome disrupting agents) and those approaches that bypass the endocytic pathway by facilitating direct transport of macromolecules across the plasma membrane (*e.g.* some CPPs) [35]. Additionally, for more efficient/specific delivery, various targeting moieties can be attached to the surface of the delivery system, *e.g.* folate and transferrin (Tfn) for tumour cells [36], and polysaccharides for hepatoma cells [37].

I.2.1. Pathways for Intracellular Drug Delivery

All eukaryotic cells exhibit one or more forms of endocytosis. Endocytosis encompasses multiple mechanisms by which the internalisation of the plasma membrane takes place with the simultaneous dipping of extracellular molecules or fluid into small

membrane-bounded vesicles effectively reducing the extracellular volume that the cell must process. Traditionally, endocytosis is subdivided into two main types: phagocytosis (uptake of large particles or "cell eating") and pinocytosis (uptake of fluid and solutes or "cell drinking"). The former is typically carried out by phagocytes, *i.e.* macrophages, neutrophils and dendritic cells, responsible for clearing large pathogens such as bacteria or yeast as well as large debris such as the remnants of dead cells, arterial deposits of fat, *etc.* [38, 39]. Pinocytosis is utilised by essentially all nucleated cell types and occurs by multiple pathways including clathrin-mediated endocytosis, caveolae-mediated endocytosis, clathrin and caveolae-independent endocytosis, and macropinocytosis. The last three pathways are collectively referred to as non-clathrin dependent endocytosis (Figure I.3) [40].

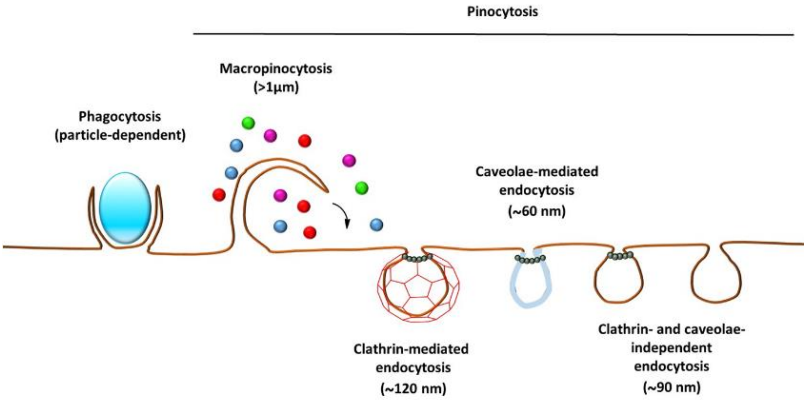

Figure I.3. Multiple portals of entry into the cell. Adapted from [40].

Conventional small molecule drugs, such as amino acids, sugars, and ions, generally enter cells via transmembrane diffusive transport or non-specific adsorptive pinocytosis. Cellular uptake of macromolecules, due to their polarity and large hydrodynamic diameter, is mostly restricted to receptor-mediated endocytosis. When transported by diffusion, the drug will reach the cytoplasm of the cell, whereas all pinocytic processes are lysosomotropic.

Clathrin-mediated endocytosis, an energy-dependent process, is the best characterised mode of cellular internalisation [41]. Clathrin-

coated pits have been proposed as molecular “filters” and are 100-150 nm in size. Clathrin-mediated endocytosis is used for the uptake of specific ligands such as transferrin (Tfn) and low-density lipoproteins (LDLs) [40, 42, 43]. Initial uptake of ligands into coated vesicles, encapsulated by a polygonal clathrin coat, is followed by fusion with early tubule-vesicular endosomes near the plasma membrane.

There are also clathrin-independent mechanisms for endocytosis for which caveolae-mediated endocytosis has been widely investigated. Caveolae are small caveolin-coated invaginations of the plasma membrane that are rich in cholesterol and glycosphingolipids. Caveolae are present in many cell types and are primarily involved in transcytosis in blood vessels wall endothelial cells. Caveolae are smaller in size (50-80 nm) and differ in receptor disposition from clathrin-coated vesicles in that they do not separate from the plasma membrane while unloading their cargo. This pathway is advantageous for drug delivery because it avoids acidic compartments (endosomal/lysosomal pathways) [44]. However, some of these uncoated vesicles deliver their contents to endosomes and lysosomes. The process has been termed potocytosis, being exemplified by folate, which is the best characterised cargo molecule undergoing potocytosis [45].

Macropinocytosis is another type of actin-dependent endocytotic pathway in which irregular sized and shaped vesicles are formed. The macropinocytosis process can be stimulated by growth factors, such as epithelial growth factor (EGF). Large endocytic vesicles (macropinosomes, generally 0.5-2.5 μm in diameter) formed after stimulation have no coat and do not concentrate receptors [46] and represent a non-selective phenomenon for the uptake of large volumes of fluid. In macropinocytosis, the macropinosomes do not fuse with endosomes or lysosomes despite fusing with each other, although macromolecules internalised in macropinosomes can be delivered to lysosomes.

I.2.2. Intracellular Targeted Drug Carriers

Many nanosized drug delivery carriers are intended to deliver the drug to a specific intracellular compartment, such as the cytosol. The

time taken to internalise the therapeutic agent and deliver it to the cytosol, as well as the steady-state level of the nanoparticle and its cargo, influenced by degradation and dose, will ultimately determine the overall efficacy of the drug delivery system. Nanopharmaceuticals are able to enter cells via multiple endocytic pathways or even using non-endocytic pathways. Although targeting to lysosomal pathways is generally undesirable and actively avoided in drug delivery due to the possible enzymatic degradation, some DDS take advantage of this pathway in order to improve their efficiency. In this section, various examples of drug delivery carriers currently under investigation will be discussed together with their different internalisation mechanisms.

I.2.2.1. Polymer Conjugates

Increased understanding on the mechanisms of action of polymer conjugates is aiding the design of the next generation of conjugates and the optimisation of clinical protocols for their evaluation. Rapid blood clearance after intravenous administration needs to be avoided to maintain the high plasma concentration essential for EPR-mediated targeting. Once accumulated in the tumour or target tissue, the conjugates are generally internalised into cells by endocytic mechanisms driven by interactions with proteins and receptors on the cell surface. Drug conjugation to a water-soluble polymer restricts cellular uptake to the endocytic pathway and, therefore, bypasses mechanisms of resistance such as MDR (multidrug resistance) induced by P-gp (P-glycoprotein) overexpression in the plasma membrane [47]. As previously mentioned, macromolecules are captured by invaginations of the cell plasma membrane forming vesicles named endosomes. Such vesicles undergo a complex sequence of fusion events directing the substances to the correct compartment. In this process, the endosomal compartment pH drops from the early to late endosome to values around 5.5. At the end of the fusion process, the formed lysosomes contain a battery of enzyme machinery utilised to degrade complex molecules such as lipids or proteins. Most polymer conjugates rely on the lysosomotropic drug delivery pathway, where either proteolytic enzymes or acidic pH triggers drug release. However, the hostile environment of lysosomes must be avoided if the presence of

hydrolytic enzymes and acidic pH drives the inactivation/degradation of the bioactive agent. This issue is particularly important in peptide/protein and nucleic acid delivery. To circumvent this problem, pH-responsive endosomolytic carriers are being developed to promote endosomal escape upon pH stimuli [48].

I.2.2.2. Lipoplexes/Polyplexes

Complexes between cationic lipids (such as Lipofectin®) and oligonucleotides (lipoplexes) [49] and complexes between cationic polymers (such as polyethylenimine, PEI) [50] and oligonucleotides (polyplexes) are mediated by strong electrostatic interactions between the positively charged carrier and negatively charged nucleic acid. The slight net positive charge of the resulting lipoplexes and polyplexes facilitates their interaction with negatively charged cells, so improving transfection efficiency.

Endocytosis (including receptor-mediated endocytosis) has been repeatedly confirmed as the main mechanism of lipoplex/polyplex internalisation by cells [51]. Despite endocytosis-mediated uptake, oligonucleotides do not accumulate in lysosomes, but instead are released into the cytoplasm due to the destabilisation of the endosomal membrane provoked by the lipid or polymeric component of the complexes. In particular, lipoplexes fuse with the endosomal membrane when they contain a fusogenic lipid such as L-dioleoyl phosphatidylethanolamine (DOPE) [52], which easily undergoes the transition from bilayer to hexagonal phase, facilitating the fusion.

In the case of polyplexes, which cannot directly destabilise the endosomal membrane, the mechanism of oligonucleotide escape from endosomes is still not completely understood. However, the “proton sponge hypothesis”, first proposed by Boussif *et al.* [53], may explain oligonucleotide escape. In this hypothesis, the substantial buffering capacity of polycations (dependent on their pKa) raises intra-vesicle pH, induces chloride influx, causes vesicle swelling, and leads to membrane destabilisation.

However, the proton sponge mechanism is still debated due to several different aspects [54]. For example, there is a requirement for transporters (and channels) for ions and aquaporins for water during normal cellular homeostasis as neither water nor ions move readily over membranes of their own volition. Moreover, the osmotic pressure required for the rupture of endosomes has been calculated to be greater than that generated by internalised PEI, the gold standard [55]. Given that different cell types exhibit different trafficking pathways, and may well also exhibit different pHs, the proton-sponge effect may contribute differently according to the vector tested and cellular model. Other mechanisms to explain polycation-induced membrane permeabilisation include direct membrane interaction, induction of pore formation, and colloidal osmotic effects.

I.2.2.3. Cell Penetrating Peptides (CPPs)

CPPs are short peptides with the ability to transport molecules or colloidal drug carriers systems across the cell membrane to the cell interior [56]. The most extensively studied CPPs are derived from the human immunodeficiency virus type 1 (HIV-1) encoded Tat (transactivating transcriptional activator)-peptide [57, 58], HSV (herpes virus protein)-VP22 [59], and Antennapedia (Antp, transcription factor of *Drosophila*) [60]. These peptides are water-soluble, partly hydrophobic, and structurally similar in that they all contain a short sequence of less than 30-35 amino acids with positively charged arginine and/or lysine residues giving them a net positive charge at physiological pH. These peptides have been used for intracellular delivery of various cargoes with molecular weights several times greater than their own. The main feature of these CPPs is their ability to penetrate cell membranes at low micromolar concentrations *in vitro* and *in vivo* without using chiral receptors and without causing significant membrane damage. Moreover, they are efficient over a range of cell types and hold great potential for therapeutic application.

The mechanism of internalisation of CPPs is not completely understood. Recent studies point to more than one mechanism, depending on the experimental conditions, but endocytosis and direct

penetration have been suggested as the two major uptake forms [61]. CPP-mediated intracellular delivery of large molecules and nanoparticles proceed via energy-dependent macropinocytosis, with subsequent enhanced escape from endosome into the cell cytoplasm. Individual CPPs or CPP-conjugated small molecules penetrate cells via electrostatic interactions and hydrogen bonding and do not seem to depend on energy. Direct contact between the translocating moiety and cell membrane or cell-membrane-interacting proteoglycans is required for successful intracellular delivery.

I.2.2.4. Liposomes

Liposomes are artificial vesicular nanosystems (50-1000 nm) consisting of a hydrophilic core surrounded by a lipid bilayer. Liposomes have been extensively investigated as potential carriers for the cytosolic delivery of substances such as drugs, proteins, and oligonucleotides. They are biologically inert and completely biocompatible, they cause practically no toxicity or antigenic reactions, and drugs packaged into liposomes are protected from the destructive action of the external environment. Packaged elements can be water-soluble drugs (loaded into their inner aqueous compartment) and sometimes even water-insoluble drugs (loaded into the hydrophobic compartment of the phospholipid bilayer). Alteration of the lipid composition (sometimes using cationic or anionic lipids) and/or the cholesterol:lipid ratio has been used to modulate liposomal properties. For example, cationic liposomes have been used to complex DNA and oligonucleotides on their surface [62].

Association of drugs with liposomes has pronounced effects on the pharmacokinetic profile of the drug, resulting in delayed drug absorption, restricted drug biodistribution, decreased volume of drug biodistribution, delayed drug clearance, and retarded drug metabolism. Non-stealth liposomes are rapidly eliminated from the blood and captured by the cells of the reticulo-endothelial system (RES), primarily in the liver and spleen, as the result of rapid opsonisation of the liposomes. Although liposomes can be internalised by endocytosis, studies suggest that delivery of entrapped anti-tumour agents is largely

due to diffusion of the drug from the liposomes into tumour cells. The use of targeted liposomes may increase the efficacy of the liposomal drug and decrease the loss of liposomes and their contents in the RES.

Different formulation strategies have been developed to increase the ability of liposomes to mediate cytosolic delivery of therapeutics. These include the development of “fusogenic” and “pH-sensitive” liposomes. Fusogenic lipids, such as unsaturated DOPE, contain weak acids as head groups. These lipids, when incorporated into liposomes, facilitate an interaction and fusion or destabilisation of liposomes with the endosomal membranes, resulting in the release of the encapsulated therapeutic agent in the cytoplasm. pH-sensitive liposomes are stable at physiological pH but undergo destabilisation and acquire fusogenic properties under acidic conditions. Different hypothetical mechanisms have been proposed for the endosomal escape of pH-sensitive liposomes: (i) Destabilisation of pH-sensitive liposomes destabilises the endosomal membrane possibly through pore formation, (ii) destabilisation of pH-sensitive liposomes allows cargo to diffuse through the endosomal membrane, and (iii) liposomal membrane fusion with the endosomal membrane.

I.3. PHYSICOCHEMICAL CHARACTERISATION

Molecular weight, polydispersity, purity, identity, drug content, free drug content, and quantification of targeting units are some of the intrinsic quality characteristics of a given therapeutic agent that need to be controlled during the manufacturing process in order to enter clinical development. Many drug delivery systems fail in this purpose due to impractical scale-up production and manufacturing processes that do not meet the required criteria. Other systems have not progressed because of problems related to toxicity, other undesirable side effects, low correlation of performance from *in vitro* to *in vivo* in animal models to humans, or an imbalance in the safety-efficacy relationship [63-66].

The design of drug delivery systems is hampered both by their intrinsic complexity and the multiple complex interactions with the multiple biological environments encountered following delivery to a biological system [67].

The selection of a nanosized carrier for a given pathology must take into account considerations such as the route of administration, site of action, and therapeutic window of the bioactive species. This will describe the pathway taken by the therapeutic as it passes through the different biological barriers and physiological environments to reach the site of action and, therefore, will define the restrictions and rules in the design of the therapeutic. Therefore, there is a general agreement for the need of characterisation methodologies that, beyond quality control parameters, would allow for the identification and study of representative physicochemical descriptors [11]. These findings will be useful for structure-activity relationships which themselves will enable the rational design of nanomedicines towards improved biological performance. Altogether, such a strategy requires a deeper and more comprehensive approach to the study of conformation, dimensions, dynamics, and interactions with the biological environment to provide robust tools towards rational design of DDS to overcome biological barriers.

I.3.1. Rational Design of Drug Delivery Systems (DDS)

The therapeutic efficacy of conventional drugs is usually limited by their low bioavailability, low stability in physiological media, fast clearance, and unspecific or ineffective pharmacokinetic profile. In order to overcome these issues, the nanoscale manipulation of drugs can facilitate the modulation of their physicochemical properties and so enhance their biological output. In this regard, a multitude of strategies have been described, encompassing the use of various colloidal, polymeric, and supramolecular systems (*e.g.* liposomes, polymeric micelles, polymer conjugates, and polyplexes). These have provided a myriad of nano drug delivery systems (nanoDDS) with differential structural, compositional, responsive, and conformational properties. Additionally, cargos may be incorporated into these nanoDDS through physical entrapment (encapsulation), non-covalent interactions (*e.g.* siRNA polyplexes), or relying on responsive covalent linkages, allowing for the stimuli controlled release of the therapeutic agent (*e.g.* polymer conjugates). The degree of complexity can be increased if an active targeting strategy is required using selected targeting moieties (*e.g.*

antibody, peptide, or glyco-compounds) towards specific receptors. This toolbox of nanosized carriers provides scientists with multiple solutions towards the design of nanomedicines to treat a given pathology. Therefore, any accurate design must include the consideration of several parameters, including the pathology to treat, the biological target, the therapeutic strategy (chemotherapy, gene therapy, photodynamic therapies or their combinations, *etc.*), the associated pharmacokinetic requirements for effective therapeutic output, and the route of administration.

I.3.2. Physicochemical Descriptors

Any attempt to carry out an exhaustive physicochemical characterisation of a given therapeutic agent must be driven towards the establishment of structure-activity relationships. This fact allows the prior prediction of biological outputs enabling an improved rational design [68-70]. Given the heterogeneity and complexity in the chemical structural and conformational nature of nanomedicines, general descriptions of physicochemical parameters covering all the involved features would not be accurate and each nanocarrier family should be studied individually. The same line of reasoning applies to the biomedical application pursued in terms of pathology, biological target, site of action, route of administration, and pharmacokinetic requirements for an effective therapeutic outcome of the active species with minimal or no associated toxicity. The experimental design strategies for the precise characterisation of both physicochemical descriptors and the biological activities must be built from a step-wise and holistic perspective [71].

The choice of an appropriate drug carrier, based on the pathway transited through the body to reach the site of action, will significantly reduce the number of feedback design cycles required. This choice should also account for the variable environmental conditions that the nanosized medicine will encounter, as these conditions will affect the physicochemical properties of the soft nanomaterial. Indeed, interactions at the bio-nano interface comprise reciprocal multiple, complex and dynamic interactions, producing responses at the

biological and nanomedicinal interface, involving multiple colloidal forces [72]. Recorded changes to the physicochemical parameters in response to the environmental changes experienced along the route through the body and the study of interactions with biological macromolecules in relevant physiological conditions will allow for a better understanding and enhanced candidate selection towards the successful progression into biological *in vitro* and *in vivo* experimentation.

I.3.3. Techniques to Study DDS in Biological Relevant Media

As nanomedicine characterisation in terms of identity, molecular weight, composition, purity, solubility, and stability have been successfully achieved, DDS performance in relevant physicochemical environments must now be addressed. A progressive increase in media complexity would allow a more complete understanding of DDS performance based on the physicochemical descriptors extracted in solvated states. Characterisation in hydrated states and relevant physiological media is accessible through a battery of complementary techniques entailing a multitude of different principles. Table I.3 summarises several of the most important techniques used in physicochemical characterisation of the different nanosystems, some of which will be explained in detail in the following chapters.

Table I.3. Summary of the most relevant techniques used to elucidate physicochemical descriptors in physiological media. Adapted from ref [73].

Technique	Strengths	Descriptor Measured	Drawbacks
UV-Vis **(Ultraviolet Visible Spectroscopy)**	Quantitative, non-destructive, fast measurements, time-course studies, physiological conditions (aqueous, pH, ionic strength)	Composition, conformation, non-covalent interactions	Necessity of chromophores, signal overlapping
DR (Differential Refractometry)	Quantitative, non-destructive, fast measurements, time-course studies, physiological conditions (aqueous, pH ionic strength), universal	Concentration	Reference cell, not specific
FS (Fluorescence Spectroscopy)	Quantitative, selective, time-course studies, non-destructive, physiological conditions (aqueous, pH, ionic strength)	Concentration, composition, Critical micellar concentration (CMC), stability	Necessity of fluorophores, fluorescence quenching
FRET (Fluorescence Resonance Energy Transfer)	Quantitative, selective, low sample concentration, physiological conditions (aqueous, pH, ionic strength)	Structure, binding affinities, stability, conformational change	Insufficient spectral separation (false negatives), donor reabsorbs emission, high background noise
FCS	Sensitive to single-entities, very small sample volumes, fast measurement, in vivo measurement	Size (R_h), size distribution	Dimerization not observable, high preparation time, requires fluorophores

(Fluorescence Correlation Spectroscopy)			
IR (Infrared Spectroscopy)	Fast measurement, small sample volumes, time-course studies	Composition, conformation, non-covalent interactions	Water mask part of the spectra, signal overlap
ATR-FTIR (Attenuated Total Reflection Fourier Transform Infrared Spectroscopy)	Fat measurement, small sample volumes, null sample preparation, aqueous samples, time-course studies	Composition, conformation, interactions	Needs ATR correction software, signal overlap
RS (Raman Spectroscopy)	Quantitative, minimal sample preparation, relative fast measurements, physiological conditions (pH, ionic strength, biological fluids), mapping of biological tissues	Composition, conformation, interaction with biological environment	Auto-fluorescence, signal overlap
CD (Circular Dichroism)	Quantitative, non-destructive, fast measurement, minimal sample preparation, time-course studies, physiological conditions (aqueous, pH ionic strength)	Conformation, non-covalent interactions, binding affinities	Signal overlap
1D-NMR **^{1}H NMR** **^{19}F NMR** (Nuclear Magnetic Resonance)	Non-destructive, minimal sample preparation, semi-quantitative, time-course studies, physiological conditions (aqueous, pH, ionic strength), highly selective, water	Composition, binding affinities, interactions, quantification in tissues	Relatively long measurements, expertise required, relatively large concentration required, signal overlapping, biological sample preparation

	signals can be eliminated, biological samples, tissues		
NOESY NMR (Nuclear Overhauser Effect Spectroscopy NMR)	Non-destructive, minimal sample preparation, semi-quantitative, physiological conditions (aqueous, pH, ionic strength), highly selective, water signals can be eliminated	Conformation at the molecular level, non-covalent interactions, epitope mapping, dynamics	Very long measurements times, expertise required, relatively large concentration required, signal overlap
PGSE NMR (Pulsed-gradient Spin-echo NMR)	Non-destructive, minimal sample preparation, semi-quantitative, complex mixtures, physiological conditions (aqueous, pH, ionic strength), highly selective, water signals can be eliminated, biological fluids	Size (R_h), conformation, non-covalent interactions, co-assembling systems, fast screening of interacting components within complex mixtures, dynamics	Relatively long measurement times, expertise required, relatively large concentration required, signal overlap
STD NMR (Saturation Transfer Difference NMR)	Non-destructive, minimal sample preparation, semi-quantitative, physiological conditions (aqueous, pH, ionic strength), highly selective, water signals can be eliminated	Binding affinities, epitope mapping, screening of interacting components within complex mixtures, dynamics	Long measurement times, expertise required, relatively large concentration required, signal overlap
NMR Relaxometry	Non-destructive, minimal sample preparation, semi-quantitative, physiological conditions (aqueous, pH, ionic strength), highly selective, water signals can be eliminated	Conformation, mobility, flexibility (or rigidity), structure topology, dynamics	Long measurement times, expertise required, relatively large concentration required, signal overlap

SANS (Small Angle Neutron Scattering)	Non-destructive, minimal sample preparation, semi-quantitative, physiological conditions (aqueous, pH, ionic strength), possibility of contrast variation scattering studies	Size, conformation, flexibility (or rigidity), 3D shape	Long measurements, expertise required, relatively large concentration required
SAXS (Small Angle X-ray Scattering)	Non-destructive, minimal sample preparation, physiological conditions (aqueous, pH ionic strength)	Size, conformation, flexibility (or rigidity), 3D shape	Expertise required, relatively large concentration required, heavier elements mask the scattering from lighter elements
SLS (Static Light Scattering)	Non-destructive, small sample volumes, physiological conditions (aqueous, pH, ionic strength)	Size (R_h, R_g), size distribution, form factor (ρ), molecular weight	Requires sample preparation, interference (dust, aggregation)
DLS (Dynamic Light Scattering)	Non-destructive, small sample volumes, physiological conditions (aqueous, pH, ionic strength), biological fluids	Size (R_h), size distribution	Requires sample preparation, interference (dust, aggregation), can´t differentiate similar sized populations
ITC (Isothermal Titration Calorimetry)	Quantitative, aqueous samples	Non-covalent interactions, binding affinities and associated thermodynamic data	High preparation time, high precision in sample preparation

ESEM (Environmental Scanning Electron Microscopy)	Non-destructive, 3D mapping, physiological conditions	Size, size distribution, surface morphology, shape	Expertise required
Cryo-TEM (Cryogenic Transmission Electron Microscopy)	Physiological conditions, 3D mapping	Size, size distribution, surface morphology, shape	Expertise required
AFM (Atomic Force Microscopy)	Non-destructive, 3D mapping, minimal sample preparation	Size, size distribution, surface, morphology, shape	Overestimation of measurements
PT (Potentiometric Titration)	Non-destructive, aqueous sample	Salt ration, ionisation state, pK_a	Salts and pH might interfere the measurements
ζ-potential (Zeta Potential)	Non-destructive, physiological conditions (aqueous, pH, ionic strength)	Surface charge, stability, binding affinities	Salts and pH might interfere the measurements
NTA (Nanoparticle Tracking Analysis)	Small sample volumes, minimal sample preparation, physiological conditions (aqueous, pH, ionic strength), selective measurement through fluorescent labelling	Size (R_h), size distribution, particle size, concentration, selective filtering through fluorescence	Interferences (dust, aggregation), limited particle concentration range
SPR (Surface Plasmon Resonance)	Quantitative, small sample volumes, physiological conditions	Interactions, binding rates	Artefacts

REFERENCES

1. Au, J.L.S., et al., *Delivery of cancer therapeutics to extracellular and intracellular targets: Determinants, barriers, challenges and opportunities.* Advanced Drug Delivery Reviews, 2016. **97**: p. 280-301.
2. Duncan, R., *The dawning era of polymer therapeutics.* Nat Rev Drug Discov, 2003. **2**(5): p. 347-360.
3. Seymour, L., *Review : Synthetic Polymers with Intrinsic Anticancer Activity.* Journal of Bioactive and Compatible Polymers, 1991. **6**(2): p. 178-216.
4. Greco, F. and M.J. Vicent, *Polymer-drug conjugates: current status and future trends.* Front Biosci, 2008. **13**: p. 2744-56.
5. Vicent, M.J., et al., *Polymer conjugates as therapeutics: future trends, challenges and opportunities.* Expert Opinion on Drug Delivery, 2008. **5**(5): p. 593-614.
6. Duncan, R., *Polymer conjugates as anticancer nanomedicines.* Nat Rev Cancer, 2006. **6**(9): p. 688-701.
7. Roncador, A., et al., *Use of polymer conjugates for the intraperoxisomal delivery of engineered human alanine:glyoxylate aminotransferase as a protein therapy for primary hyperoxaluria type I.* Nanomedicine, 2016. **18**(16): p. 30228-3.
8. Masayuki, Y., et al., *Polymer micelles as novel drug carrier: Adriamycin-conjugated poly(ethylene glycol)-poly(aspartic acid) block copolymer.* Journal of Controlled Release, 1990. **11**(1): p. 269-278.
9. Matsumura, Y. and K. Kataoka, *Preclinical and clinical studies of anticancer agent-incorporating polymer micelles.* Cancer Sci, 2009. **100**(4): p. 572-9.
10. Asyikin binti Abdul Aziz, Z., et al., *Recent Advances in Drug Delivery of Polymeric Nano-Micelles.* Current Drug Metabolism, 2017. **18**(1): p. 16-29.
11. Duncan, R. and M.J. Vicent, *Polymer therapeutics-prospects for 21st century: The end of the beginning.* Advanced Drug Delivery Reviews, 2013. **65**(1): p. 60-70.
12. Cheng, Y., et al., *Development of switchable polymers to address the dilemma of stability and cargo release in polycationic nucleic acid carriers.* Biomaterials, 2017. **127**: p. 89-96.

13. Duncan, R. and R. Gaspar, *Nanomedicine(s) under the Microscope.* Molecular Pharmaceutics, 2011. **8**(6): p. 2101-2141.
14. Duncan, R., *Polymer therapeutics: Top 10 selling pharmaceuticals — What next?* Journal of Controlled Release, 2014. **190**: p. 371-380.
15. Duncan, R., *Polymer therapeutics as nanomedicines: new perspectives.* Current Opinion in Biotechnology, 2011. **22**(4): p. 492-501.
16. Gaspar, R. and R. Duncan, *Polymeric carriers: Preclinical safety and the regulatory implications for design and development of polymer therapeutics.* Advanced Drug Delivery Reviews, 2009. **61**(13): p. 1220-1231.
17. England, R.M., I. Conejos-sanchez, and M.J. Vicent*, *Chapter 8.2 Drug Delivery Strategies: Polymer Therapeutics*, in *Nanostructured Biomaterials for Overcoming Biological Barriers*. 2012, The Royal Society of Chemistry. p. 456-482.
18. Hare, J.I., et al., *Challenges and strategies in anti-cancer nanomedicine development: An industry perspective.* Advanced Drug Delivery Reviews.
19. Liechty, W.B., et al., *Polymers for Drug Delivery Systems.* Annual review of chemical and biomolecular engineering, 2010. **1**: p. 149-173.
20. Maeda, H., *The link between infection and cancer: Tumor vasculature, free radicals, and drug delivery to tumors via the EPR effect.* Cancer Science, 2013. **104**(7): p. 779-789.
21. Maeda, H., H. Nakamura, and J. Fang, *The EPR effect for macromolecular drug delivery to solid tumors: Improvement of tumor uptake, lowering of systemic toxicity, and distinct tumor imaging in vivo.* Advanced Drug Delivery Reviews, 2013. **65**(1): p. 71-79.
22. Maeda, H., et al., *Vascular permeability enhancement in solid tumor: various factors, mechanisms involved and its implications.* International Immunopharmacology, 2003. **3**(3): p. 319-328.
23. Matsumura, Y. and H. Maeda, *A New Concept for Macromolecular Therapeutics in Cancer Chemotherapy: Mechanism of Tumoritropic Accumulation of Proteins and the Antitumor Agent Smancs.* Cancer Research, 1986. **46**(12 Part 1): p. 6387-6392.

24. Prabhakar, U., et al., *Challenges and Key Considerations of the Enhanced Permeability and Retention Effect for Nanomedicine Drug Delivery in Oncology.* Cancer Research, 2013. **73**(8): p. 2412-2417.
25. Greish, K., et al., *Macromolecular therapeutics: advantages and prospects with special emphasis on solid tumour targeting.* Clin Pharmacokinet, 2003. **42**(13): p. 1089-105.
26. Seymour, L.W., et al., *Influence of molecular weight on passive tumour accumulation of a soluble macromolecular drug carrier.* European Journal of Cancer, 1995. **31**(5): p. 766-770.
27. Vicent, M.J., H. Ringsdorf, and R. Duncan, *Polymer therapeutics: Clinical applications and challenges for development.* Advanced Drug Delivery Reviews, 2009. **61**(13): p. 1117-1120.
28. Lammers, T., et al., *Drug targeting to tumors: Principles, pitfalls and (pre-) clinical progress.* Journal of Controlled Release, 2012. **161**(2): p. 175-187.
29. Danquah, M.K., X.A. Zhang, and R.I. Mahato, *Extravasation of polymeric nanomedicines across tumor vasculature.* Advanced Drug Delivery Reviews, 2011. **63**(8): p. 623-639.
30. Maeda, H., *The enhanced permeability and retention (EPR) effect in tumor vasculature: the key role of tumor-selective macromolecular drug targeting.* Advances in Enzyme Regulation, 2001. **41**(1): p. 189-207.
31. Maeda, H., *Tumor-Selective Delivery of Macromolecular Drugs via the EPR Effect: Background and Future Prospects.* Bioconjugate Chemistry, 2010. **21**(5): p. 797-802.
32. Allen, C., *Why I'm Holding onto Hope for Nano in Oncology.* Molecular Pharmaceutics, 2016. **13**(8): p. 2603-2604.
33. Maeda, H., K. Tsukigawa, and J. Fang, *A Retrospective 30 Years After Discovery of the Enhanced Permeability and Retention Effect of Solid Tumors: Next-Generation Chemotherapeutics and Photodynamic Therapy—Problems, Solutions, and Prospects.* Microcirculation, 2016. **23**(3): p. 173-182.
34. Maeda, H., *Toward a full understanding of the EPR effect in primary and metastatic tumors as well as issues related to its heterogeneity.* Advanced Drug Delivery Reviews, 2015. **91**: p. 3-6.
35. Asokan, A., R. Cheung, and M.J. Cho, *Strategies for the Cytosolic Delivery of Macromolecules: An Overview*, in *Pharmaceutical Sciences Encyclopedia*. 2010, John Wiley & Sons, Inc.

36. Sriraman, S.K., et al., *Anti-cancer activity of doxorubicin-loaded liposomes co-modified with transferrin and folic acid.* European Journal of Pharmaceutics and Biopharmaceutics, 2016. **105**: p. 40-49.
37. Li, D., et al., *Self-Targeted Polysaccharide Prodrug Suppresses Orthotopic Hepatoma.* Molecular Pharmaceutics, 2016. **13**(12): p. 4231-4235.
38. Aderem, A. and D.M. Underhill, *MECHANISMS OF PHAGOCYTOSIS IN MACROPHAGES.* Annual Review of Immunology, 1999. **17**(1): p. 593-623.
39. Lee, W.L., R.E. Harrison, and S. Grinstein, *Phagocytosis by neutrophils.* Microbes and Infection, 2003. **5**(14): p. 1299-1306.
40. Conner, S.D. and S.L. Schmid, *Regulated portals of entry into the cell.* Nature, 2003. **422**(6927): p. 37-44.
41. Brown, M.S. and J.L. Goldstein, *A Receptor-Mediated Pathway for Cholesterol Homeostasis (Nobel Lecture).* Angewandte Chemie International Edition in English, 1986. **25**(7): p. 583-602.
42. Schmid, S.L., *CLATHRIN-COATED VESICLE FORMATION AND PROTEIN SORTING:An Integrated Process.* Annual Review of Biochemistry, 1997. **66**(1): p. 511-548.
43. Brodsky, F.M., et al., *Biological Basket Weaving: Formation and Function of Clathrin-Coated Vesicles.* Annual Review of Cell and Developmental Biology, 2001. **17**(1): p. 517-568.
44. Cohen, A.W., et al., *Role of Caveolae and Caveolins in Health and Disease.* Physiological Reviews, 2004. **84**(4): p. 1341-1379.
45. Ritter, T.E., et al., *Folate receptors targeted to clathrin-coated pits cannot regulate vitamin uptake.* Proceedings of the National Academy of Sciences of the United States of America, 1995. **92**(9): p. 3824-3828.
46. Swanson, J.A. and C. Watts, *Macropinocytosis.* Trends in Cell Biology, 1995. **5**(11): p. 424-428.
47. Dong, X. and R.J. Mumper, *Nanomedicinal strategies to treat multidrug-resistant tumors: current progress.* Nanomedicine (London, England), 2010. **5**(4): p. 597-615.
48. Bazban-Shotorbani, S., et al., *Revisiting structure-property relationship of pH-responsive polymers for drug delivery applications.* Journal of Controlled Release.
49. Felgner, P.L., et al., *Nomenclature for Synthetic Gene Delivery Systems.* Human Gene Therapy, 1997. **8**(5): p. 511-512.
50. Kunath, K., et al., *Low-molecular-weight polyethylenimine as a non-viral vector for DNA delivery: comparison of*

physicochemical properties, transfection efficiency and in vivo distribution with high-molecular-weight polyethylenimine. Journal of Controlled Release, 2003. **89**(1): p. 113-125.

51. Ogris, M., et al., *DNA/polyethylenimine transfection particles: Influence of ligands, polymer size, and PEGylation on internalization and gene expression.* AAPS PharmSci, 2001. **3**(3): p. 43-53.
52. Farhood, H., N. Serbina, and L. Huang, *The role of dioleoyl phosphatidylethanolamine in cationic liposome mediated gene transfer.* Biochimica et Biophysica Acta (BBA) - Biomembranes, 1995. **1235**(2): p. 289-295.
53. Boussif, O., et al., *A versatile vector for gene and oligonucleotide transfer into cells in culture and in vivo: polyethylenimine.* Proceedings of the National Academy of Sciences of the United States of America, 1995. **92**(16): p. 7297-7301.
54. Duncan, R. and S.C.W. Richardson, *Endocytosis and Intracellular Trafficking as Gateways for Nanomedicine Delivery: Opportunities and Challenges.* Molecular Pharmaceutics, 2012. **9**(9): p. 2380-2402.
55. Won, Y.-Y., R. Sharma, and S.F. Konieczny, *Missing pieces in understanding the intracellular trafficking of polycation/DNA complexes.* Journal of Controlled Release, 2009. **139**(2): p. 88-93.
56. Guidotti, G., L. Brambilla, and D. Rossi, *Cell-Penetrating Peptides: From Basic Research to Clinics.* Trends in Pharmacological Sciences.
57. Green, M. and P.M. Loewenstein, *Autonomous functional domains of chemically synthesized human immunodeficiency virus tat trans-activator protein.* Cell. **55**(6): p. 1179-1188.
58. Vivès, E., P. Brodin, and B. Lebleu, *A Truncated HIV-1 Tat Protein Basic Domain Rapidly Translocates through the Plasma Membrane and Accumulates in the Cell Nucleus.* Journal of Biological Chemistry, 1997. **272**(25): p. 16010-16017.
59. Elliott, G. and P. O'Hare, *Intercellular Trafficking and Protein Delivery by a Herpesvirus Structural Protein.* Cell. **88**(2): p. 223-233.
60. Joliot, A., et al., *Antennapedia homeobox peptide regulates neural morphogenesis.* Proceedings of the National Academy of Sciences, 1991. **88**(5): p. 1864-1868.

61. Madani, F., et al., *Mechanisms of Cellular Uptake of Cell-Penetrating Peptides.* Journal of Biophysics, 2011. **2011**.
62. Ewert, K.K., et al., *Synthesis of linear and cyclic peptide–PEG–lipids for stabilization and targeting of cationic liposome–DNA complexes.* Bioorganic & Medicinal Chemistry Letters, 2016. **26**(6): p. 1618-1623.
63. Greco, F. and M.J. Vicent, *Combination therapy: Opportunities and challenges for polymer–drug conjugates as anticancer nanomedicines.* Advanced Drug Delivery Reviews, 2009. **61**(13): p. 1203-1213.
64. Eaton, M.A.W., *Improving the translation in Europe of nanomedicines (a.k.a. drug delivery) from academia to industry.* Journal of Controlled Release, 2012. **164**(3): p. 370-371.
65. Crist, R.M., et al., *Common Pitfalls in Nanotechnology: Lessons Learned from NCI's Nanotechnology Characterization Laboratory.* Integrative biology : quantitative biosciences from nano to macro, 2013. **5**(1): p. 10.1039/c2ib20117h.
66. Zamboni, W.C., et al., *Best Practices in Cancer Nanotechnology: Perspective from NCI Nanotechnology Alliance.* Clinical Cancer Research, 2012. **18**(12): p. 3229-3241.
67. Maeda, H., et al., *Tumor vascular permeability and the EPR effect in macromolecular therapeutics: a review.* Journal of Controlled Release, 2000. **65**(1–2): p. 271-284.
68. Bygd, H.C., K.D. Forsmark, and K.M. Bratlie, *Altering in vivo macrophage responses with modified polymer properties.* Biomaterials, 2015. **56**: p. 187-197.
69. Rege, K., et al., *Investigation of DNA-Binding Properties of an Aminoglycoside-Polyamine Library Using Quantitative Structure−Activity Relationship (QSAR) Models.* Journal of Chemical Information and Modeling, 2005. **45**(6): p. 1854-1863.
70. Hofmeister, I., K. Landfester, and A. Taden, *Controlled Formation of Polymer Nanocapsules with High Diffusion-Barrier Properties and Prediction of Encapsulation Efficiency.* Angewandte Chemie International Edition, 2015. **54**(1): p. 327-330.
71. Cheng, C.J., et al., *A holistic approach to targeting disease with polymeric nanoparticles.* Nat Rev Drug Discov, 2015. **14**(4): p. 239-247.
72. Nel, A.E., et al., *Understanding biophysicochemical interactions at the nano-bio interface.* Nat Mater, 2009. **8**(7): p. 543-557.

73. Niño-Pariente, A., V.J. Nebot, and M.J. Vicent, *Relevant Physicochemical Descriptors of "Soft Nanomedicines" to Bypass Biological Barriers.* Current Pharmaceutical Design, 2016. **22**: p. 1-1.

Chapter II

Design of Poly-L-Glutamate-Based Complexes for Gene Therapy

The work presented in this thesis chapter was made possible by a collaboration between the Polymer Therapeutics lab at the Centro de Investigación Príncipe Felipe, in Valencia and The Pharmaceutical Biotechnology Department from Ludwig-Maximilians-Universität (LMU), in Munich in Prof Wagner's group. A publication entitled "Design of Poly-L-glutamate based Complexes for pDNA delivery" in the journal Macromolecular Bioscience has been the result of this collaborative work.

II.1. INTRODUCTION AND BACKGROUND

Gene therapy is an experimental technique that offers a wide spectrum of applications including regulation, repair, and replacement of the genes which affect genetic disease. The ability to influence change at the genetic level is a promising and encouraging strategy for several diseases. Such diseases include cancer which can be promoted by complex genetic alterations and still represents an often incurable disease and one of the main causes of mortality in humans.

Gene therapy is designed to introduce genetic material (nucleic acids) into cells to compensate for an abnormal gene or to promote the production of a protein required by the cell for proper function. For example, if a mutated gene causes a necessary protein to be faulty or missing, gene therapy may be able to introduce a normal copy of the gene to restore the function of the protein. While this concept appears simple, the reality is much more problematic given the difficulty of correctly and efficiently introducing a genetic sequence into a cell of choice. This strategy usually employs genetically engineered carriers, so-called "*vectors*", to deliver the genetic material. Such vectors can be categorized as viral or non-viral, although, despite their high efficiency, viral vectors exhibit significant disadvantages. These include immunogenicity, limited cargo loading, high production costs, and the risk of promoting cancer by insertional mutagenesis.

Over recent decades, the field of gene therapy has evolved tremendously with regard to both employed nucleic acid and vector diversity [1]. However, numerous technical barriers have limited the success of gene therapy in clinical trials [2].

Lipid-based vectors are amongst the most widely used non-viral gene carriers. Various liposomal formulations continue to be developed clinically, even though Allovectin-7, a locally administered formulation comprising a cationic lipid (N-[1-(2,3-dimyristyloxy)propyl]-N,N-dimethyl-N-(2-hydroxyethyl)ammonium bromide, DMRIE), a neutral phospholipid (dioleoyl phosphatidylethanolamine, DOPE), and a plasmid DNA (pDNA), recently failed to meet its efficacy endpoints in a Phase III clinical trial for the treatment of advanced metastatic melanoma [3]. Other examples include DOTAP (dioleoyl-trimethylammonium propane)-cholesterol, GAP-DMORIE [(±)-N-(3-aminopropyl)-N,N-dimethyl-2,3-bis(syn-9-tetradeceneyloxy)-1-propanaminium bromide]-DPyPE (1,2-diphytanoyl-sn-glycero-3-phosphoethanolamine), and GL67A-DOPE (1,2-dimyristoyl-sn-glycero-3-phosphoetanolamine)-DMPE (1,2-dimyristoyl-sn-glycero-3-phosphoethanolamine)-PEG (polyethylene glycol) (Table II.1).

Small interfering RNA (siRNA) species have been combined with a lipid-based nanoparticle (LNP) family known as stable nucleic acid-lipid particles (SNALP) for clinical applications [4] (Table II.2). Such combinations have been used in the treatment of hypercholesterolemia. PRO-040201 (TKM-ApoB, Tekmira Pharmaceuticals Corporation) and ALNPCS02 (Alnylam Pharmaceuticals) [4, 5] have been reported to substantially reduce expression of their target genes (ApoB and ALN) and subsequently of low-density lipoprotein (LDL) cholesterol in Phase I trials. Also, two separate clinical trials are currently assessing the effects of SNALP-based siRNA delivery in patients with hepatocellular carcinoma; TKM080301 (Tekmira Pharmaceuticals Corporation) suppresses polo-like kinase 1 (PLK1) and ALN-VSP02 (Alnylam Pharmaceuticals) simultaneously targets KIF11 and VEGF. A second generation SNALP:siRNA formulation called ALNTTR02 (also known as Patisiran, Alnylam Pharmaceuticals) aims to suppress mutant transthyretin (TTR) in TTR-mediated amyloidosis. This formulation features a 1,2-dilinoleyloxy-N,N-dimethylaminopropane (DLinDMA) analogue that has allowed a tenfold increase in efficacy in preclinical studies [6].

There are also two clinical trials that feature LNP formulations other than SNALP. AtuPLEX (Silence Therapeutics) becomes internalised by mouse vascular endothelium after intravenous injection [7, 8]. The AtuPLEX-based formulation Atu027 is also under evaluation for the treatment of patients with advanced solid cancer (Table II.2) [9].

Finally, the MD Anderson Cancer Center has also initiated a clinical trial for their siRNA-EphA2-DOPC (1,2-dioleoyl-sn-glycero-3-phosphocholine) formulation in patients with advanced cancers. In this case, the siRNA is incorporated into neutral liposomes composed of DOPC (Table II.2) [10].

Cationic carriers [11, 12], capable of condensing large nucleic acids into smaller structures and masking negative DNA or RNA charges, are also an attractive alternative class of non-viral vectors due to their immense chemical diversity and their potential for functionalisation. The clinical potential of the PEGylated poly-L-lysine (PLL) vector has been investigated in the treatment of cystic fibrosis; a Phase I clinical trial supports the safety and tolerability of these DNA nanoparticles and provides some evidence for vector gene transfer [13]. Polyethylenimine (PEI) and its variants are also amongst the most studied polymeric materials for gene delivery and have been applied widely in local gene therapy of various cancers (Table II.1). However, cationic carriers can be targets of the innate immune system [14, 15]. These and numerous other challenges may be met by new design processes that also must take into account the requirement for dynamic responsiveness during the delivery process [16]. Thus, instead of taking a static stable form, polymers need to change their properties with time and position in order to protect the nucleic acid outside the cell, facilitate the transfer across the endosomal barrier triggered by acidification, and support intracellular release and bioavailability of the nucleic acid in the required cellular compartment. The sum of all these factors points to the implementation of an intricate design strategy [17].

Naturally occurring biodegradable cationic polymers such as chitosan derivatives [18, 19], cationic cyclodextrin polymers (CDPs) [20, 21], or cationised collagens [22] have been also assessed as pDNA

carriers to solve biocompatibility issues. A CDP-siRNA formulation has been evaluated in several therapeutically relevant animal models of cancer [23, 24] and in Phase I clinical trials. A CDP-based RNA interference (RNAi) delivery system has also been successfully applied in a Phase I clinical trial (Table II.2). In this case, targeting ribonucleotide reductase M2 (RRM2) messenger RNA (mRNA) in patients with solid cancers. This trial noted a reduction in target mRNA levels and the presence of the specific mRNA cleavage product, supporting a RNA interference (RNAi) mechanism of action [25]. However, while these carriers do present certain advantages, it is important to be aware of their limitations. These include an inherent heterogeneity (polydispersity >1.6) which masks precise structure-activity relationships (SARs) [26, 27]. It is extremely important to use controlled polymerisation techniques to diminish the variability of these dynamic vehicles looking towards an efficient clinical translation.

Numerous other polymers are currently being preclinically evaluated for DNA delivery to address issues of efficacy and toxicity associated with commonly used cationic polymers. This includes the evaluation of a non-ionic poloxamer (CRL1005) and cationic surfactant benzalkonium chloride formulation in a Phase II/III study as a genetic vaccine to prevent cytomegalovirus (CMV) infection in patients undergoing allogeneic haematopoietic stem cell transplantation (Table II.1).

Several promising delivery systems have been developed through covalent attachment of delivery ligands to a siRNA cargo. This strategy yields precisely defined single-component systems that require minimal delivery material. The most clinically advanced conjugate platforms are dynamic polyconjugates (DPCs) and carbohydrate N-acetyl galactosamine (GalNAc) conjugates. siRNA-GalNAc conjugates under development by Alnylam Pharmaceuticals contain a highly modified siRNA stably conjugated to a multivalent targeting ligand.

Table II.1. Non-viral DNA vectors under clinical evaluation. Adapted from reference [28] and updated from [29].

Delivery System	Gene Therapy Drug	Sponsor	Indications	Phase	Status
DOTAP-cholesterol	DOTAP-Chol-fus 1	MD Anderson Cancer Center	Non-small-cell lung cancer	I	Completed
				I/II	Recruiting
GAP-DMORIE-DPyPE	Tetravalent dengue vaccine	US Army Medical Research and Materiel Command	Dengue disease vaccine	I	Completed
GL97A-DOPE-DMPE-PEG	pGM169/GL67A	Imperial College London	Cystic fibrosis	II	Completed
PEI	BC-819/PEI	BioCancell Ltd.	Bladder cancer	II	Unknown
	BC-819	BioCancell Ltd.	Ovarian cancer	I/II	Completed
	DTA-H19	BioCancell Ltd.	Pancreatic cancer	I/II	Completed
	SNS01-T	Senesco Technologies, Inc.	Multiple myeloma and B cell lymphoma	I/II	Unknown
	CYL-02	University Hospital Toulouse	Pancreatic ductal adenocarcinoma	I	Completed

PEG-PEI cholesterol	EGEN-001	Gynecologic Oncology Group	Ovarian, tubal and peritoneal cancers	I	Unknown
				II	Active, not recruiting
	EGEN-001-301	EGEN Inc.	Colorectal peritoneal cancer	I/II	Terminated
PEI-mannose-dextrose	DermaVir/LC002	Genetic Immunity	HIV vaccine	II	Unknown
Poloxamer CR L005-benzakonium chloride	ASP0113	Astellas Pharma Inc.	CMV vaccine	III	Active, not recruiting
				II	Completed
	VCL-CB01	Astellas Pharma Inc.	CMV vaccine	II	Completed

Table II.2. Non-viral siRNA vectors under clinical evaluation. Adapted from reference [28] and updated from [29].

Delivery System	Drug	Sponsor	Target gene	Disease	Phase	Status
Naked siRNA	ALN-RSV01	Alnylam Pharmaceuticals	Nucleocaspid gene of RSV	RSV Infections	II	Completed

	TD101	Pachyonychia Congenita Project	KRT6A (N171 mutation)	Pachyonychia congenital	I	Completed
	AGN211745	Allergan	FLT1	Age-related macular degeneration and choroidal neovascularisation	II	Completed
	QPI-1007	Quark Pharmaceuticals	CASP2	Optic atrophy and non-arteritic anterior ischemic optic neuropathy	I	Completed
				Acute primary angle-closure glaucoma	II	Completed
	ISNP	Quark Pharmaceuticals	TP53	Kidney injury and acute renal failure	I	Completed
				Delayed graft function and complications of kidney transplant	I/II	Completed
	PF-655 (PF-04523655)	Quark Pharmaceuticals	DDIT4	Choroidal neovascularisation, diabetic retinopathy	II	Completed

				and diabetic macular oedema		
				Age-related macular degeneration	II	Completed
	Bevasiranib	OPKO Health, Inc.	VEGFA	Diabetic macular oedema	II	Completed
				Macular degeneration	II	Completed
	SYL1001	Sylentis S.A.	TRPV1	Ocular pain and dry eye syndrome	I/II	Completed
	SYL040012	Sylentis S.A.	ADRB2	Ocular hypertension and open angle glaucoma	II	Completed
	RXI-109	RXi Pharmaceuticals	CTGF	Cicatrix and scar prevention	I	Completed
				Hypertrophic scar	II	Completed
				Keloid	II	Completed
Lipid-based nanoparticles	ALN-VSP02	Alnylam Pharmaceuticals	KIF11 and VEGF	Solid tumours	I	Completed

sRNA-EphA2-DOPC	MD Anderson Cancer Center	EPHA2	Advanced cancers	I	Recruiting
Atu027	Silence Therapeutics	PKN3	Advanced solid cancers	I/II	Completed
TKM-080301	Tekmira Pharmaceuticals Corporation	PLK1	Cancer	I/II	Completed
TKM-100201	Tekmira Pharmaceuticals Corporation	VP24, VP35 and Zaire Ebola L-polymerase gene	Ebola virus Infection	I	Terminated
PRO-040201	Tekmira Pharmaceuticals Corporation	APOB	Hypercholesterolemia	I	Terminated
ALN-PCS02	Alnylam Pharmaceuticals	PCSK9	Hypercholesterolemia	I	Completed
ALN-TTR02	Alnylam Pharmaceuticals	TTR	TTR-mediated amyloidosis	III	Active, not recruiting

	ND-L02-s0201	Nitto Denko Corporation	SERPINH1	Fibrosis	I	Completed
CDP-based nanoparticle	CALAA-01	Calando Pharmaceuticals	RRM2	Solid tumours	I	Terminated
Dynamic Poly-Conjugate	ARC-520	Arrowhead Research Corporation	Two conserved regions of HBV transcripts	Hepatitis B	I II	Completed Recruiting
siRNA-GalNAc conjugate	ALN-TTRsc	Alnylam Pharmaceuticals	TTR	TTR-mediated amyloidosis	I II	Completed Completed
LODER polymer	siG12D LODER	Silenseed Ltd.	KRAS	Pancreatic cancer	II	Not yet recruiting

Synthetic peptide-based polymers represent a simpler, cost-effective, and potentially less immunogenic classes of gene delivery agents as compared to viruses [30]. As stated before, PLL has been frequently explored due to its cationic character [31], although only a few studies with well-controlled systems have been published. Using reversible addition-fragmentation chain transfer polymerisation (RAFT-polymerisation) Zentel and co-workers [32, 33] generated cationic PLL-poly[2-(hydroxypropyl methacrylamide)] (p[HPMA]) block copolymers which display transfection activity at minimal cytotoxicity in cell models. Barz and colleagues synthesised a series of well-defined polypeptide-polypeptoid block copolymers (PLL-block-polysarcosine (pSar)) by ring opening polymerisation for pDNA polyplex formation (renamed as PeptoPlexes) [34]. Polyplexes consisting of a cationic block for pDNA complexation and a non-ionic hydrophilic block for shielding of the cargo were also studied by Kataoka and co-workers [35, 36] and Martin *et al.* [37]. The hydrophilic polymer corona of these systems can reduce/suppress unspecific interactions with serum proteins caused by hydrophobic or electrostatic interactions. Thereby, circulation times are elongated and inadvertent effects such as coagulation or complement activation are reduced.

Several studies have attempted to eliminate *in vivo* cytotoxicity of polyplexes by masking their high cationic surface charge with PEG [38] or proteins such as albumin or transferrin in DNA complexes [39-41]. However, conjugating hydrophilic PEG segments into delivery systems markedly reduced gene transfection efficiency as the inserted PEG segments reduced polyplex association with cells. As an alternative, shielding of positive charges of cationic polymers with polyanions has been extensively studied [42]. These polyanions are able to stabilise the complexes, minimise nonspecific interactions, and prolong *in vivo* circulation times. However, there has been little development in polyplex design with regard to the use of polymer conjugates containing both cationic and anionic domains. One of the few examples following a zwitterionic strategy are polycarboxybetaine (PCB) or polysulfobetaine (PSB), which have shown promising properties for gene delivery (such as appreciable transfection efficiency and relatively

low cytotoxicity) [43]. These encouraging characteristics are due to their ability to resist non-specific adsorption of proteins caused by electrostatically induced hydration.

Poly-L-glutamic acid (PGA) is a negatively charged, multifunctional, biodegradable polymer already tested in Phase III trials [44, 45]. PGA can markedly improve the cytocompatibility and reduce the cytotoxicity of carriers in gene delivery [46] and several examples in the literature have explored the use of PGA as a vector for effective and safe gene delivery. Some of these examples studied neutral or cationic PGA derivatives such as poly-(ɣ-benzyl-L-glutamate) (PBLG) functionalised with different amines with the ability to be protonated under physiological conditions [46-48]. After aminolysis, PBLG can be converted into polyglutamine and can be used as a potential gene delivery vector. However, suitable aminolysis agents are vitals factor in preparing an efficient gene vector [49]. Further research lines have focused on the use of the anionic PGA chain to shield non-viral vectors for effective and safe gene delivery [50-52].

The current study addresses the fundamental question of whether negatively charged well-defined PGA polymers functionalised with positively charged oligomer domains can be used as oligonucleotide delivery systems. Succinyl tetraethylene pentamine (Stp)-based oligomers were selected for PGA derivatisation [53]. The artificial oligo-amino acid Stp has been prepared in a properly protected form as a building block for standard solid-phase peptide synthesis (SPPS) [54-56].

SPPS can be defined as a process in which a peptide attached by its C-terminus to an insoluble polymer is assembled by the successive addition of protected amino acids constituting its sequence (Figure II.1).

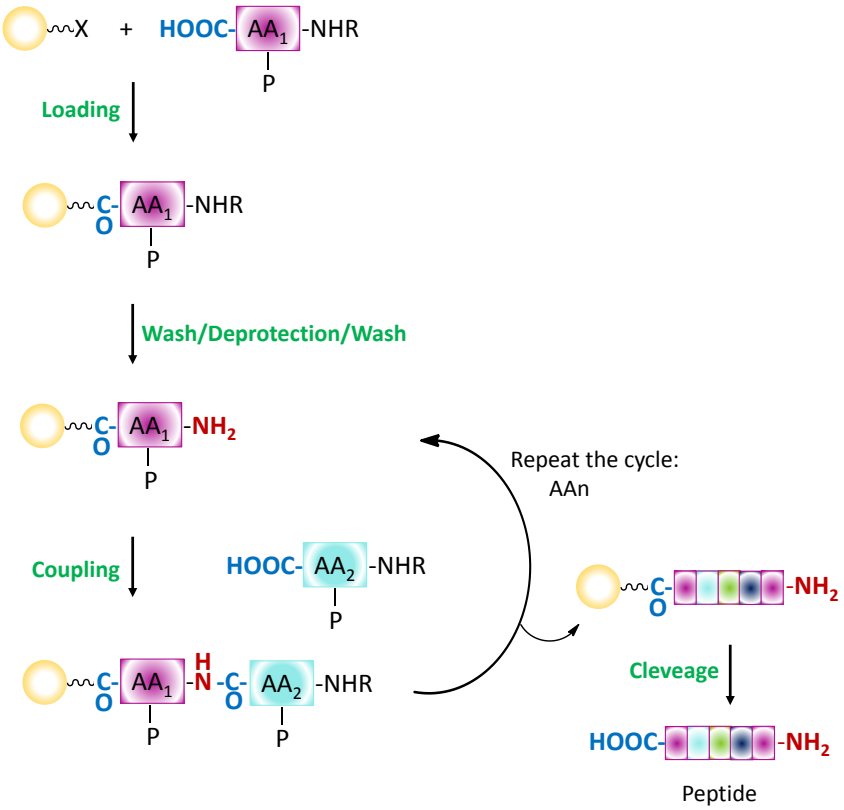

Figure II.1. General scheme of SPPS.

SPPS, first introduced for peptide synthesis [57] and peptidic nucleic acid carriers [54-56], is a widely studied method that provides defined monodisperse products by the control of position and structure of every unit in a polymer. Hartmann *et al.* [58-61] adopted standard *Fmoc*- (9-fluorenylmethoxycarbonyl) protective group-based SPPS to build up a small library of monodisperse, sequence-defined polyamidoamine polymers. An extension of this strategy permitted the generation of artificial oligo-amino acids such as Stp (Figure II.2) [53] in *tBoc*- (*tert*-butoxycarbonyl)/*Fmoc*-protected form, containing the diaminoethane motif (three protonatable secondary amino nitrogen atoms per unit), also present in the gold standard PEI [62-67].

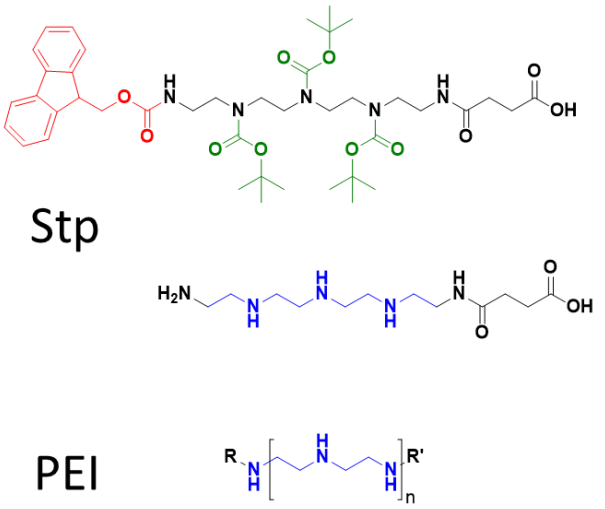

Figure II.2. Schematic representation for the synthetic amino acid Stp (succinimidyl tetraethylene pentamine: protected (up) and deprotected (down) forms) and for the polycationic transfection agent linear polyethyleneimine (LPEI).

Schaffert *et al.* [68] demonstrated that this protonatable Stp repeat unit is responsible for favourable transfection properties by mediating electrostatic binding with oligonucleotides. Furthermore, Stp provides the additional protonation capacity upon cell entry to endolysosomal compartments giving rise to the hypothesized *proton sponge effect* [63, 69, 70]. This effect allows residual unprotonated nitrogens with lower basicity to become cationised within the endolysosomal pH range (from pH 7.4 to pH < 5.0) and thus may trigger vesicular escape. Other than osmotic pressure triggered by chloride and water influx, alternative mechanisms such as direct membrane destabilisation by the protonated polycation may also account for endosomal escape [36, 71, 72].

A recently published study [73] synthesised linear sequences of the Stp building block in order to investigate the effect of increasing molecular weight (MW) of linear oligo(ethanamino) amides in nanosized pDNA particle formation. These Stp-based oligomers differ from standard linear PEI (LPEI) by an amide-bonded succinic acid linker every fifth ethanamino unit, which contributes favourably to

biocompatibility. The study revealed that only above a certain length threshold (more than 10 Stp units), DNA polyplex formation and gene transfer occurred [73]. Moreover, at an optimum length of 30 Stp units (8.4 kDa, 90 protonatable nitrogens), the study observed a six-fold higher transfection efficiency compared with LPEI (22 kDa, 500 ± 200 protonatable nitrogens). Importantly, oligomers with 30 Stp units displayed a ten-fold lower level of toxicity when compared with LPEI. Further studies also demonstrated that a simple linear sequence of 5 Stp units did not trigger gene transfer due to the small number of protonatable nitrogens present (16) compared to standard LPEI [68, 73, 74]. The small, precise oligomer could not form stable complexes with nucleic acids. Importantly, as outlined in previous studies [73], the development of effective transfection carriers required the addition of additional moieties such as cysteines (stabilisation of polyplexes by disulphide formation between oligomers) [74, 75], tyrosine trimmers [76], or fatty acids (hydrophobic stabilisation of formed particles) [68, 74, 77].

On this basis, different conjugates of PGA with Stp oligoaminoamides (PGA-Stp) were synthesised and evaluated as non-viral carriers for pDNA delivery. (i) System 1: PGA-based polymers modified through amide bond formation with oligoaminoamide **S**, which is a Stp-based oligomer containing 5 Stp units with a C-terminal tryptophan (Figure II.3). (ii) System 2: PGA-based polymers modified through amide bond formation with oligoaminoamide **SH** (bearing additional histidines), or **SC** (additional cysteine), or **SHC** (additional histidines and cysteine). (iii) System 3: PGA-based polymers modified with oligomer **SHC** via disulphide bond formation. (iv) System 4: In addition, pDNA polyplexes were formed with oligomer **SHC** and subsequently coated with different PGA-based structures (PGA_{50}, PGA_{100} and PEG_{5000}-PGA_{88} (DB_{88})).

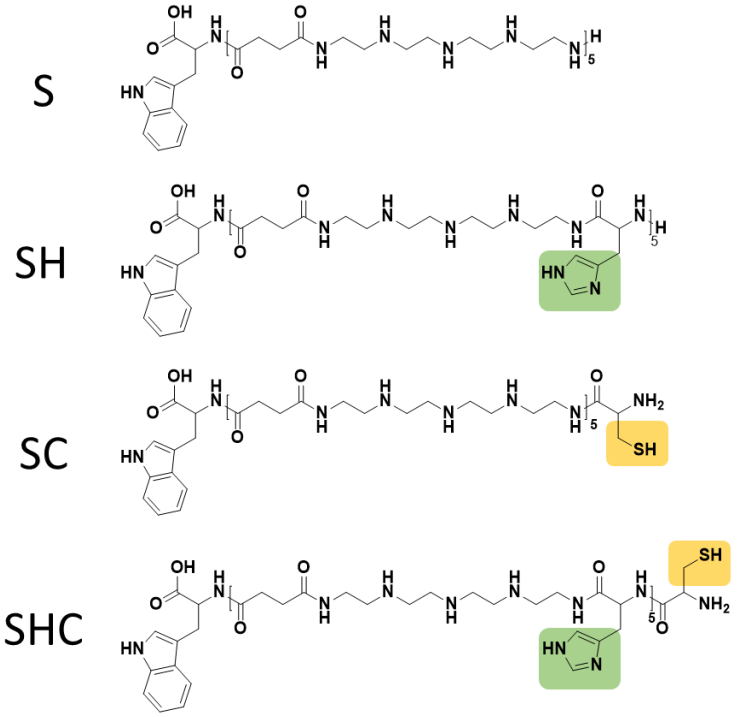

Figure II.3. Schematic representation of the used defined oligomers: S, SH (containing histidines), SC (containing cysteine), and SHC (containing histidines and cysteine).

The first three systems are based on PGA polymers (homopolymers or block-copolymers) modified with a monodisperse Stp-based polyamidoamine (Figure II.4).

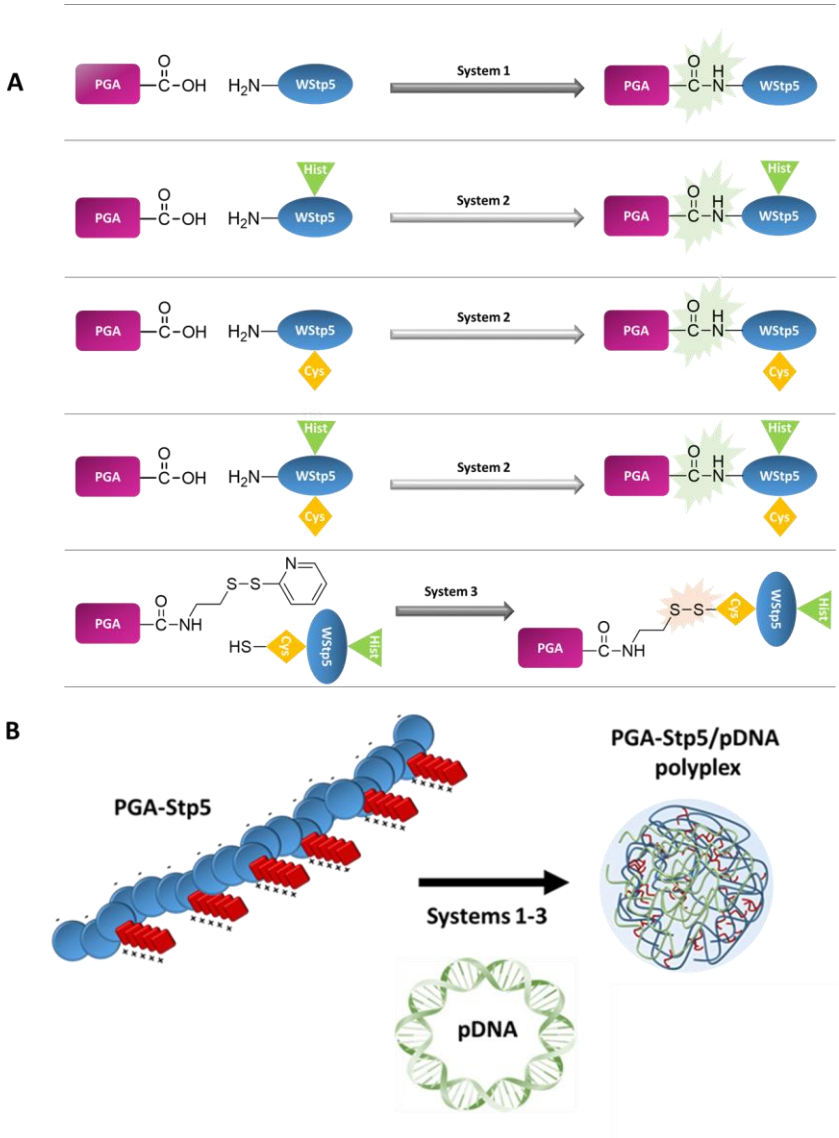

Figure II.4. Schematic representation of the synthetic process for Systems 1-3: (A) PGA-Stp$_5$ synthesis; (B) PGA-Stp$_5$/pDNA polyplex formation.

System 4 differs from the previous three systems in several ways. Firstly, we generated a polyplex between pDNA and SHC polyamidoamine, and subsequently coated the positively charged pDNA complex with a negatively charged PGA-polymer in an attempt to improve the pharmacokinetics and biodistribution of SHC (Figure II.5).

We employed two different lengths of PGA and diblock PEG-PGA as coating agents.

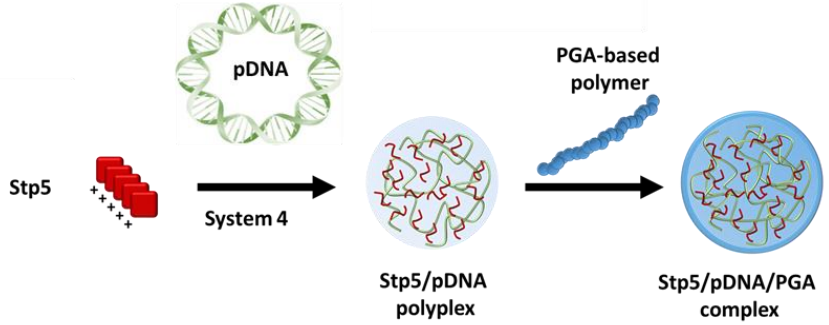

Figure II.5. Schematic representation for System 4.

We hypothesised that the zwitterionic bioresponsive and biodegradable carriers designed in the current study may achieve similar transfection efficiencies as those achieved for analogous polycations, but with greater safety in biological scenarios by avoiding polycation-triggered side effects.

II.2. RESULTS AND DISCUSSION

II.2.1. Synthesis of Sequence-Defined Oligomers

SPPS of cationic oligomers using artificial oligo-amino acids has been previously used to establish polymer libraries which included effective carriers for gene delivery [68, 74, 75]. In the current work, we applied *Fmoc*-based SPPS to generate a small library of linear oligo(ethanamino)amides containing 5 Stp units (25 nitrogens), optionally bearing histidines as protonatable buffering units [78] and cysteines as disulphide-forming polyplex stabilising units or disulphide-forming PGA-based-conjugates (Table II.3, Figure II.3) [68, 77]. A C-terminal tryptophan was also included for better analytical characterisation.

Table II.3. Sequences of oligomer structures written from the C- terminus to the N- and the corresponding calculated molecular weights.

Compound Id	Sequence	Molecular formula	$[M-H]^{-a}$ (Da)	$[M-H]^{-b}$ (Da)
S	W-Stp_5	$C_{71}H_{137}N_{27}O_{12}$	1559.1	1558.2
SH	W-$(StpH)_5$	$C_{74}H_{142}N_{28}O_{13}S$	2244.4	2243.4
SC	W-Stp_5-C	$C_{101}H_{172}N_{42}O_{17}$	1662.1	1661.3
SHC	W-$(StpH)_5$-C	$C_{104}H_{177}N_{43}O_{18}S$	2347.4	2346.9

[a] Calculated; [b] Determined by MALDI-TOF mass analysis.

II.2.2. System 1: PGA Chain Modified with S via Amide Bond Formation

Three different designs were considered within System 1: i) PGA homopolymers of different MW, as starting carriers; ii) PEG-*co*-PGA block-*co*-polymers, to explore both altered cell trafficking; and iii) histidine methyl ester (Hist) as an extra moiety conjugated to PEG-*co*-PGA side-chains, aiming for an enhancement in endosomolytic capacity [79] and thus ensure the release of the nucleic acid into the cytosol.

We obtained a family of defined PGA-based conjugates of different net charges (Table II.4) by means of DMTMM·Cl (4-(4,6-Dimethoxy-1,3,5-triazin-2-yl)-4-methylmorpholinium chloride) coupling chemistry [80], keeping oligoaminoamide **S** content between 13 to 26 mol% as determined by ^{1}H NMR (Figure II.6A) in the hope of facilitating a comparison between the different conjugates. At the same time, adequate reaction conditions (concentration, timings, *etc.*) were implemented in order to minimise possible side reactions due to the presence of carboxylates in the oligoaminoamides.

Table II.4. System 1 conjugates tested as possible non-viral vectors.

Conjugate Polymer	Id	GAU	S loading [a] (mol%)	MW [b] (g/mol)	Positive [b] Charges	D [c] (m^2/s)	R_h [c] (nm)
W-Stp_5	S	-	-	-	16	1.40e-11	14.35
PGA_{50}-S17%	PS2	50	17	25073	86	ND	ND
PGA_{50}-S20%	PS3	50	20	28165	110	7.20e-12	27.86
PGA_{50}-S21%	PS4	50	21	29196	110	ND	ND
PGA_{100}-S14%	PS5	100	14	43961	124	ND	ND
PEG_{5000}-PGA_{40}-S20%	PPS1	40	20	27532	88	ND	ND
PEG_{5000}-PGA_{40}-Hist12%-S26%	PPHS1	40	26	33099	131	ND	ND
PEG_{2000}-PGA_{80}-Hist35%-S13%	PPHS2	80	13	40434	114	ND	ND
PEG_{2000}-PGA_{80}-Hist35%-S19%	PPHS3	80	19	51953	191	ND	ND

[a] Determined by ^{1}H NMR; [b] Estimated after ^{1}H NMR analysis; [c] Diffusion coefficient (D) and hydrodynamic radius (R_h) determined by fitting the intensities of the arrayed DOSY NMR spectra into Stejskal-Tanner equation. GAU= glutamic acid units. ND= not determined.

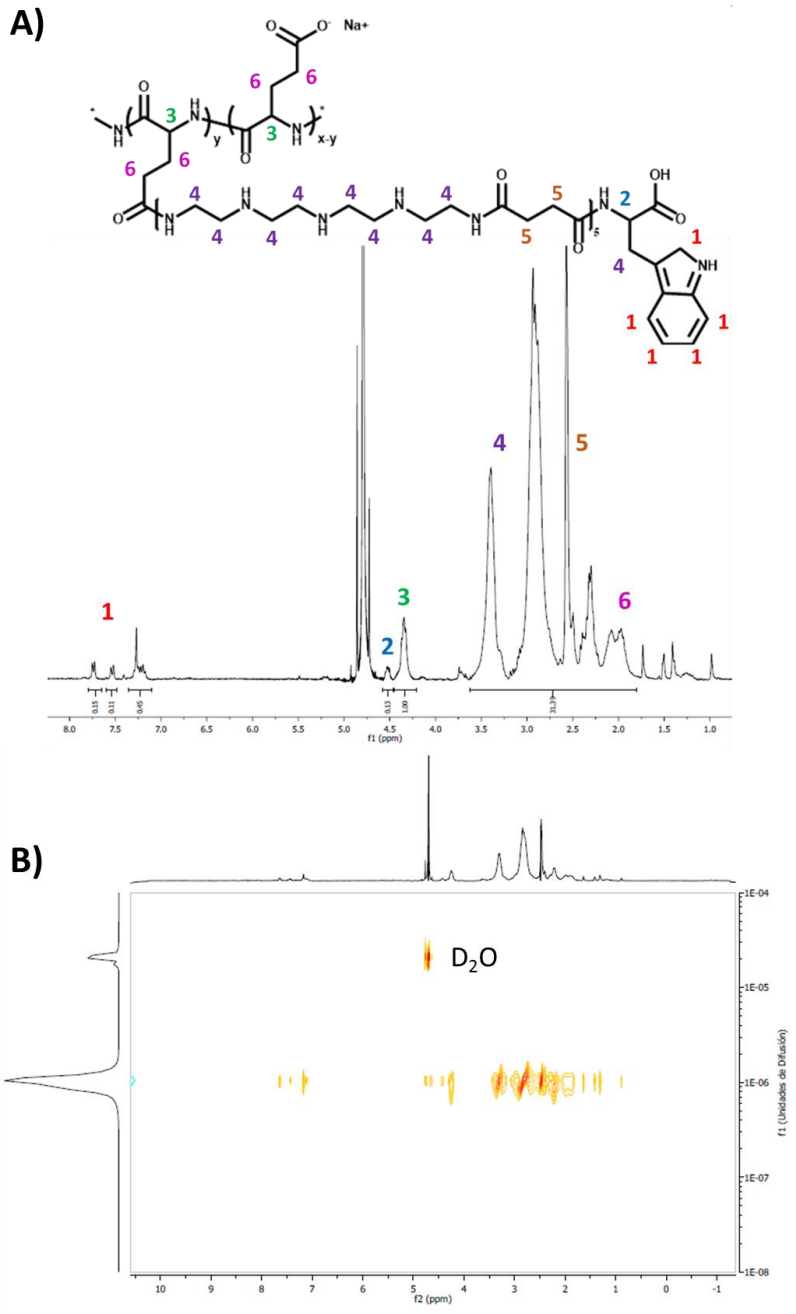

Figure II.6. Example of (A) ^{1}H NMR spectrum and (B) DOSY NMR for PS conjugates in D_2O.

DMTMM·Cl is a common coupling reagent that facilitates an efficient one-step condensation of both small molecules and polymers and provides high reaction yields [81]. DMTMM·Cl is relative inexpensive and can be easily synthesised (Figure II.7) [82]. An easily isolatable white solid appears within several minutes.

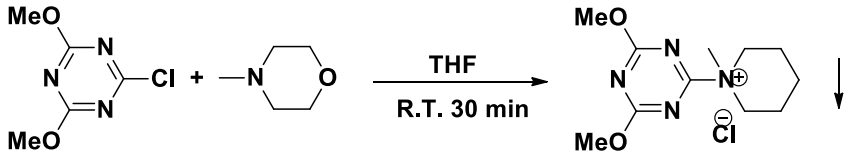

Figure II.7. DMTMM·Cl synthesis according to Kunishima *et al.* [82].

Concerning the synthesis of PGA-WStp_5 conjugates, the mechanism of action of DMTMM·Cl consists of the formation of the corresponding activated ester with the release of 4-methylmorpholine in a first step (Figure II.8). This activated ester then reacts with the terminal amino group in W-Stp_5 at pH 8 to favour its nucleophilic character.

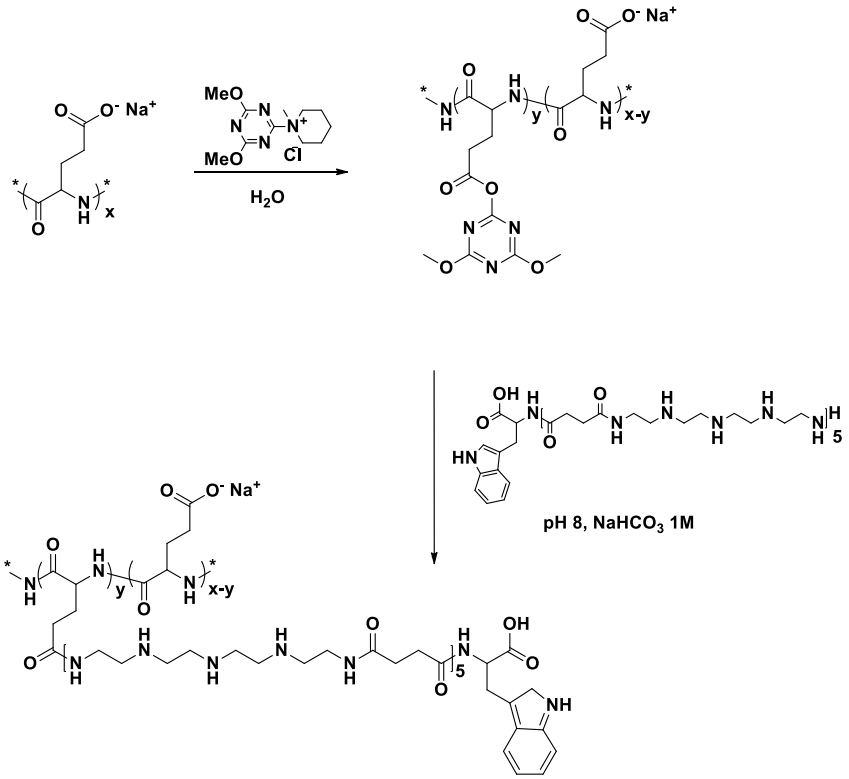

Figure II.8. General scheme of PS synthesis via DMTMM·Cl activation.

II.2.2.1. pDNA and siRNA Binding Assay by Electrophoresis

The ability of synthetic carriers to condense pDNA or siRNA represents a crucial requirement for successful gene delivery. For this reason, after the synthesis process, we carried out agarose gel electrophoresis for every polyplex obtained to evaluate the strength of the electrostatic interaction between the polymers and negatively charged pDNA (Figure II.9) as well as siRNA (Figure II.10). Free nucleic acid migrates in the gel due to its negative charge, whereas polyplexes are retained and can even remain in the loading pockets of the agarose gel.

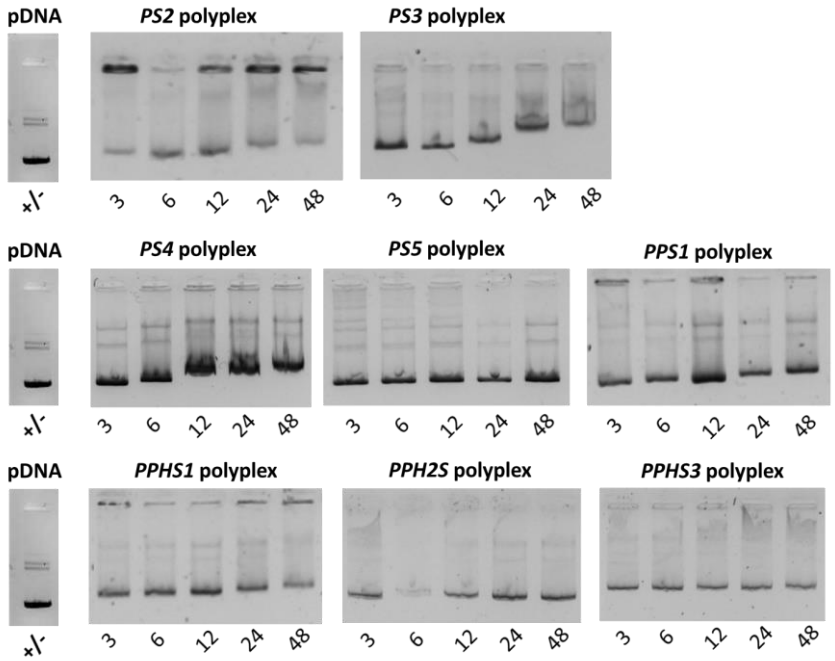

Figure II.9. pDNA binding ability of System 1 family determined by agarose gel shift assay at different charge-ratios (+/-).

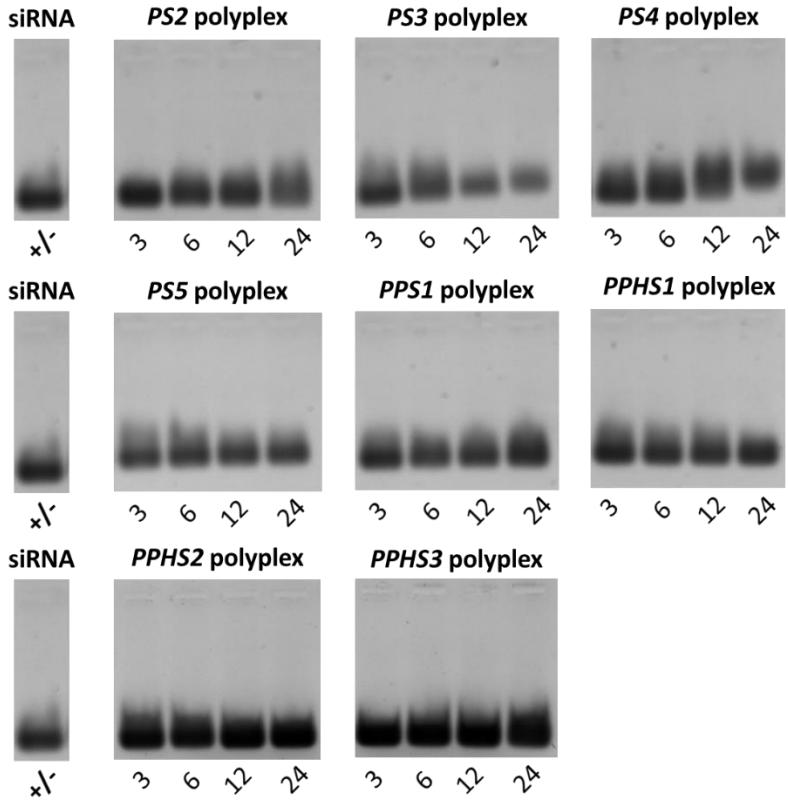

Figure II.10. siRNA binding ability of System 1 family determined by agarose gel shift assay at different +/- ratios.

These gels provide an idea of how binding strength correlates to the amount of polymer needed for complete oligonucleotide retardation. Evaluation of pDNA binding capability demonstrated that only homopolymers with shorter PGA chain (**PS2-PS4**) at high charge-ratios (Figure II.9) possessed adequate pDNA binding properties. We verified this binding ability via an ethidium bromide (EtBr) exclusion assay (Section II.2.2.2, Figure II.11) finding that neither the PEG-PGA block-*co*-polymers (**PPS1-PPHS3**) nor the longer polyglutamate (**PS5**) demonstrated any pDNA condensation ability. Concerning siRNA (Figure II.10), no compound inhibited siRNA migration at the tested concentrations. Moreover, the presence of histidine moieties did not affect the complex formation for any of the nucleotides.

II.2.2.2. Ethidium Bromide (EtBr) Exclusion Assay

In order to investigate the influence of the +/- ratio on the binding capability in more detail, we evaluated all the PGA-based systems presented in Table II.4 via EtBr exclusion assay using both pDNA and siRNA. LPEI was used as a positive control, displaying the fastest and the greatest decrease in the intercalated fluorescence and the highest compaction ability already at low +/- ratios. We measured the effect of stepwise addition of oligomer solution to pDNA or siRNA in HEPES (4-(2-hydroxyethyl)-1-piperazineethane-sulfonic acid) containing EtBr at increasing +/- ratios. We set the maximal fluorescence intensity at 100% for the EtBr solution containing free nucleic acid, and the measured fluorescence decrease after each addition of oligomer aliquot.

In the case of pDNA (Figure II.11A), the structures composed of homopolymers demonstrated improved pDNA condensation ability compared to the diblock structures with the exception of **P5** polyplex, which presented similar behaviour to the PEG-PGA block-*co*-polymers. These results are in agreement with the gel shift assay data reported above. Surprisingly, when siRNA was used as oligonucleotide (Figure II.11B), the **P5** polyplex offered better results followed by the **PPH3** polyplex.

At this stage, the results indicated that the PGA-homopolymers formed more stable complexes with pDNA as compared to siRNA. However, the results obtained with the block-*co*-polymers were not conclusive and require further analysis.

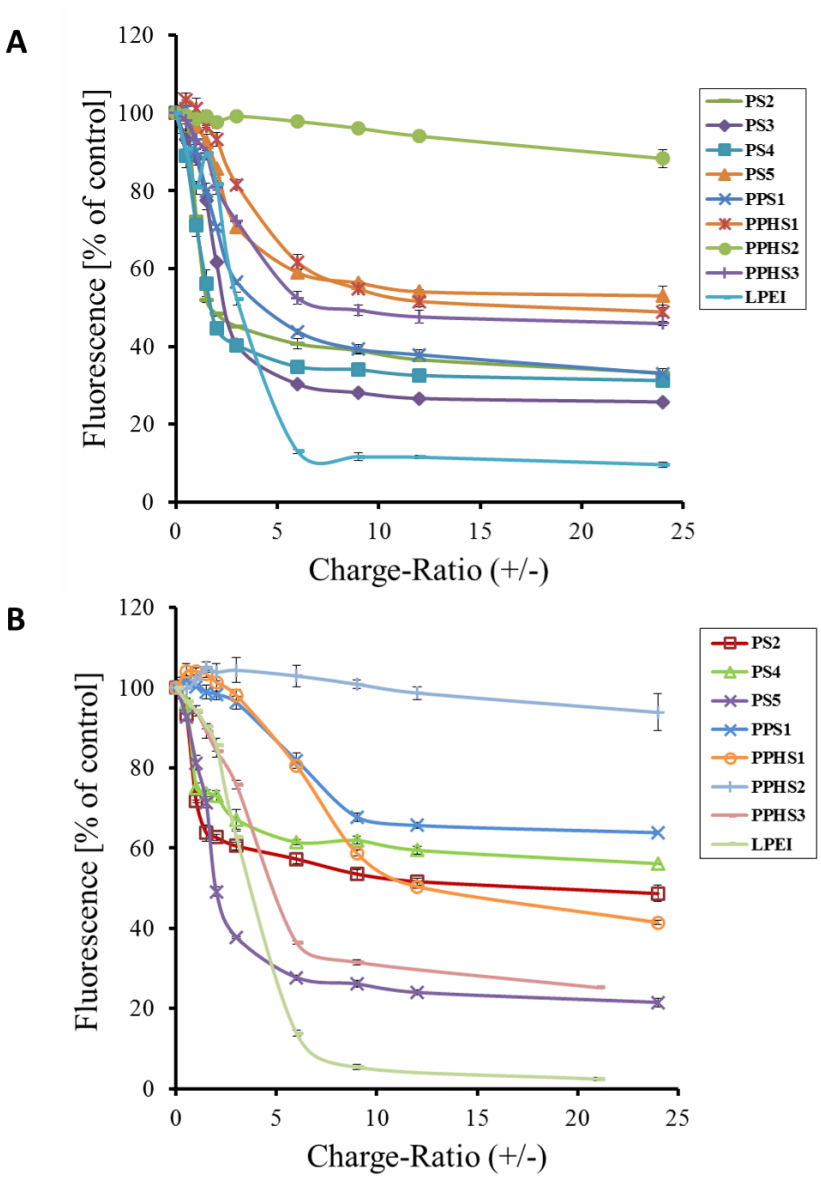

Figure II.11. Nucleic acid binding ability of System 1 polymers determined by EtBr assay at different +/- ratios. (A) pDNA; (B) siRNA.

II.2.2.3. Dynamic Light Scattering (DLS) Measurements - Particle Size and Zeta (ζ)-Potential

The determination of polyplex sizes and Zeta (ζ)-potential by dynamic light scattering (DLS) of selected homopolymers (**PS2- PS4**) indicated a particle size between 150 and 190 nm diameter. Moreover, small differences in the content of oligomer **S** resulted in significant differences in terms of ζ-potential, presumably caused by conformational changes (see **PS3** *vs.* **PS4**, Table II.5).

Table II.5. Physicochemical characterisation of System1/pDNA polyplexes.

Conjugate Polymer	pDNA polyplex Id	Size[a] (d. nm)	ζ-potential[a] (mV)	PdI[a]
PGA_{50}-S17%	PS2 polyplex	166.9 ± 7.2	**1.1 ± 0.3**	0.233 ± 0.011
PGA_{50}-S20%	PS3 polyplex	151.9 ± 9.3	**17.8 ± 0.8**	0.287 ± 0.033
PGA_{50}-S21%	PS4 polyplex	188.9 ± 81.7	**8.3 ± 0.4**	0.224 ± 0.015

[a] As determined by DLS at +/- 12 in 20 mM HEPES buffer at 25˚C. Polyplexes were diluted 1:20 before measurement. Size values are expressed in terms of number. d.= diameter. PdI= polydispersity index. Variations refer to the median of three measurements of the sample.

Regarding siRNA complexation, we analysed the same conjugates by DLS and obtained very different results, as presented in Table II.6. We did not identify any stable species with siRNA for **PS3** and only less compact polyplexes with **PS2** and **PS4**. This fact indicates weaker interactions than that observed for pDNA or more heterogeneous aggregates.

Table II.6. Physicochemical characterisation of System1/siRNA polyplexes.

Conjugate Polymer	siRNA polyplex Id	Size[a] (d., nm)	ζ-potential[a] (mV)	PdI[a]
PGA_{50}-S17%	PS2 polyplex	357.1 ± 50.6	**3.6 ± 0.2**	0.529 ± 0.085
PGA_{50}-S21%	PS4 polyplex	259.3 ± 5.6	**10.1 ± 0.5**	0.304 ± 0.025

[a] As determined by DLS at +/- 12 in 20 mM HEPES buffer at 25˚C. Polyplexes were diluted 1:20 before measurement. Size values are expressed in terms of number. Variations refer to the median of three measurements of the sample.

II.2.2.4. Biological Evaluation: Gene Transfer, Gene Silencing and Cell Viability *In Vitro*

We then examined transfection efficiency by luciferase pDNA gene transfer to N2a neuroblastoma cells. The presence of oligomer **S** in PGA homopolymers (Figure II.12A) had a positive impact (better efficiency than PEI at nitrogen to phosphate ratio (N/P) 6), except for the **PS5** polyplex which was used as negative control due to absence of pDNA binding ability. This clearly demonstrated that a greater S mol% modification correlated with improved efficiency (**PS3-PS4**). PGA-S17% (**PS2**) also demonstrated robust transfection results, but did not exceed the efficacy of PEI. However, polyplexes formed by PEG-PGA block-*co*-polymers did not transfect pDNA, supporting the results obtained by previous assays (Figure II.12B).

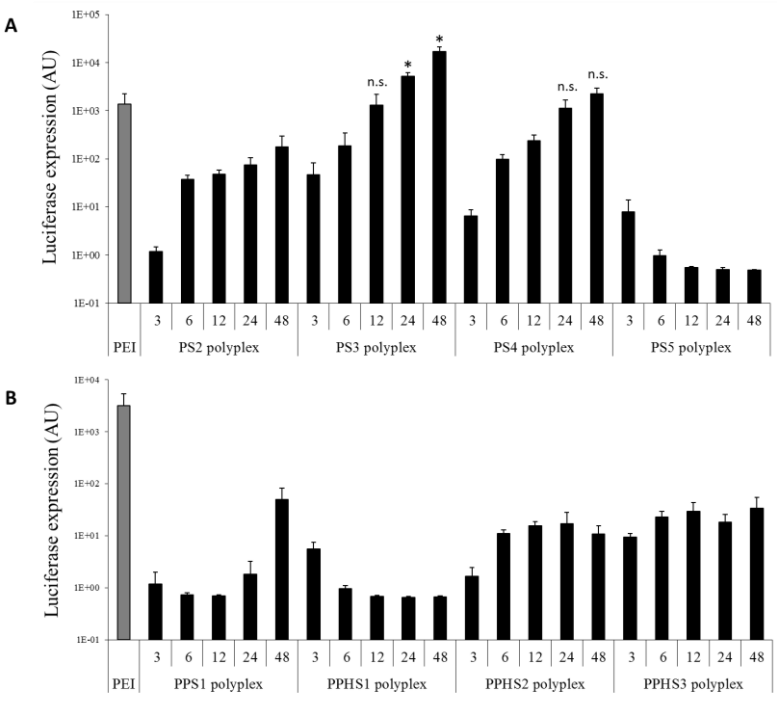

Figure II.12. Gene transfer in System 1 homopolymers (A) and diblocks (B) in N2a neuroblastoma cell line. Luciferase activity was normalised to HEPES (control) luciferase activity. Data expressed as mean ± SD, n≥3. Statistical significance between polyplexes and PEI (n.s. = $p > 0.05$; *$p < 0.01$), determined using one-sided ANOVA.

We also tested the synthesised polymers for siRNA-mediated gene silencing, with results confirming the data obtained by gel electrophoresis and EtBr assays. Neither homopolymers (Figure II.13) nor block-c*o*-polymers (Figure II.14) formed stable complexes with siRNA.

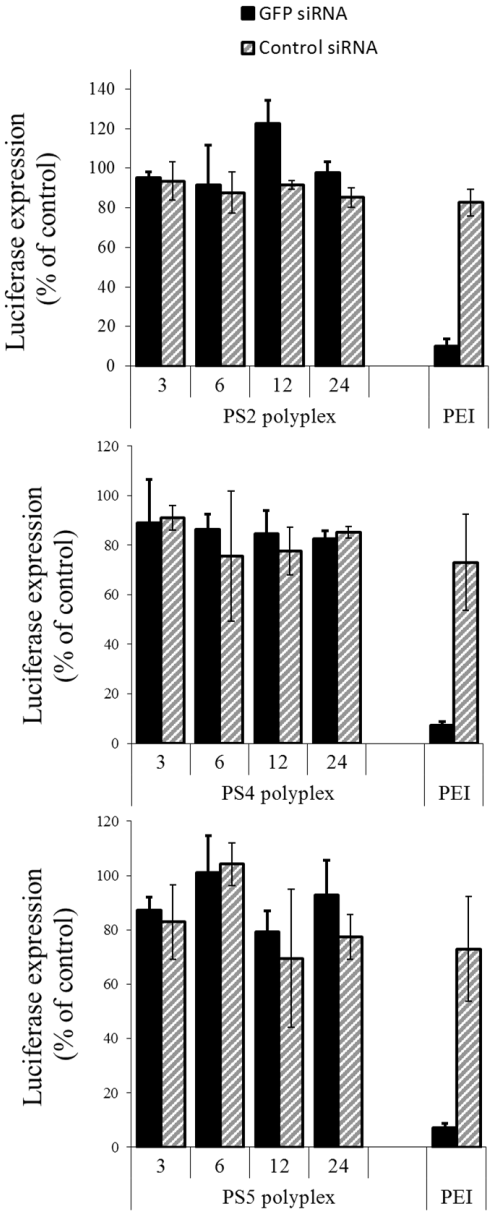

Figure II.13. Gene silencing data from PS2, PS4 and PS5 in N2a EGFPLuc cells.

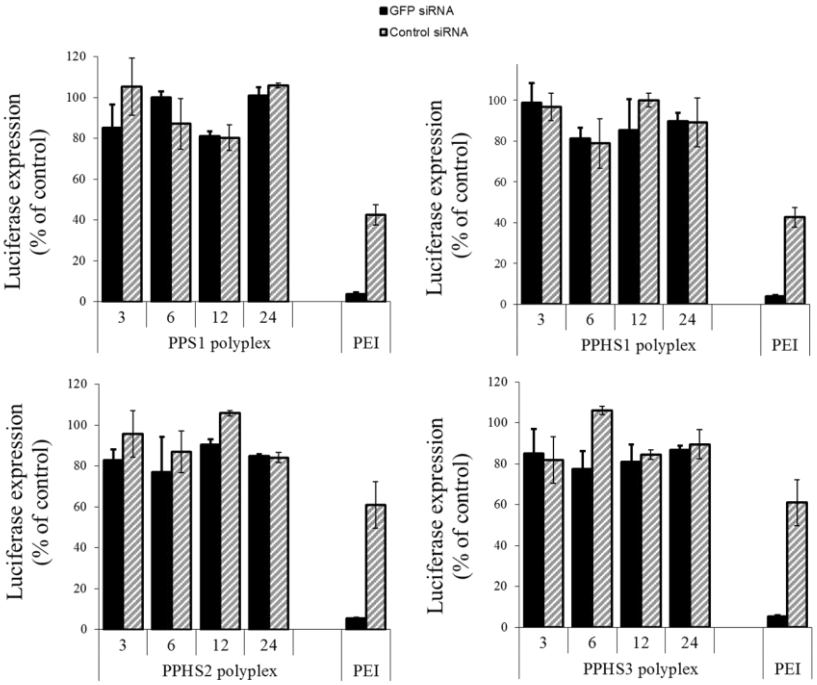

Figure II.14. Gene silencing data from PPS1 and PPHS1-3 in N2a EGFPLuc cells.

A possible reason for the absence of activity could be poor endosomolytic character of the tested polymers. In an attempt to surpass this limitation, we covalently conjugated INF-7, a lytic peptide known to promote endosomal escape [83, 84], to siRNA and complexed the resulting INF-7-siRNA to *PS5* polymer.

Unlike previous cases, we used the defined polycationic carrier **386** (Figure II.15) [85] as a positive control to avoid the toxic effects arising from PEI use.

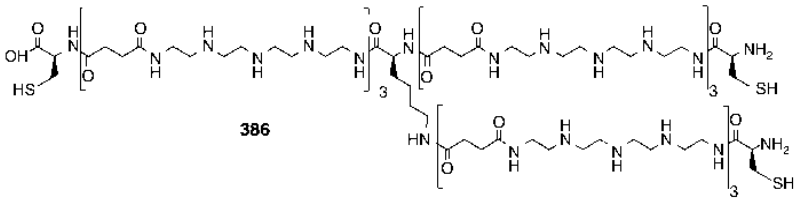

Figure II.15. Defined polycationic carrier 386 [85] used as positive control.

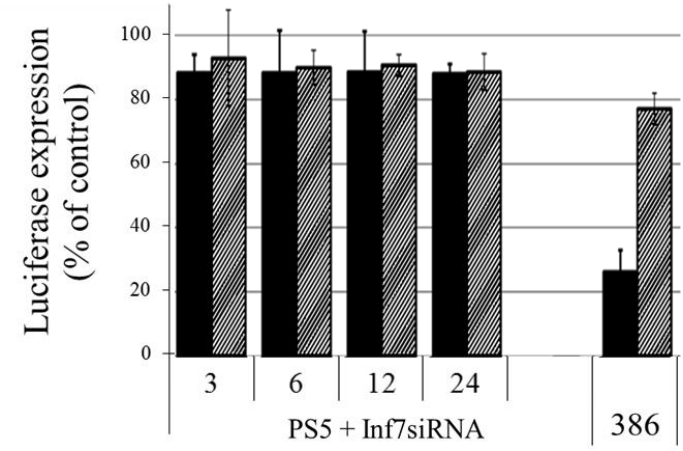

Figure II.16. Gene silencing using PS5/INF-7-siRNA in N2a EGFPLuc cells.

Unfortunately, the inclusion of the INF-7 residue did not provide any improvements to gene silencing (Figure II.16), perhaps due to the poor availability of the INF-7 moiety and, therefore, diminished lytic effect.

It is important to note the absence of cytotoxicity in N2a cells for all of the studied polyplexes at any optimum +/- ratio and concentrations tested, as determined by the MTS assay (Figure II.17).

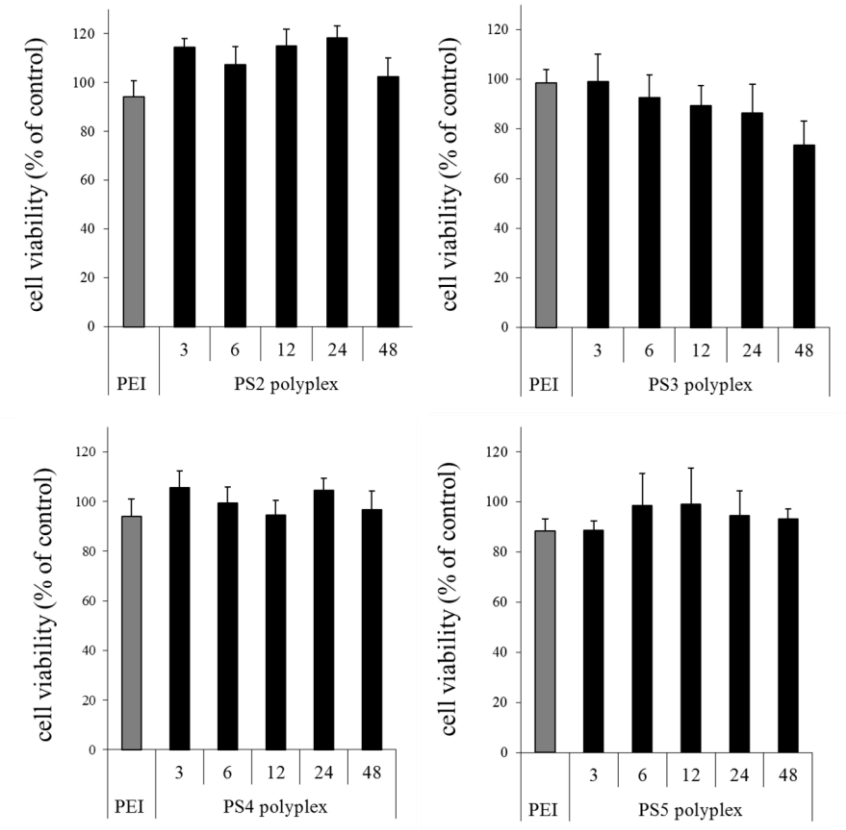

Figure II.17. Cell viability of PEI (N/P 6) and pDNA polyplexes at different +/- ratios developed in N2a cells, determined MTS assay 24 h post-incubation. Data expressed as mean ± SD, n≥4.

II.2.3. System 2: PGA Chain Modified with Oligomers SH, SHC or SC, Bearing Histidine and/or Cysteine via Amide Bond Formation

In an attempt to improve the transfection efficiency of System 1, we introduced N-terminal cysteine and histidines in the **S** polyamidoamine structure with the aim of increasing polyplex stabilisation by internal disulphide linkages [68, 77] and also improving endosomal protonation and escape [78].

By using **SH**, **SC**, and **SHC** polyamidoamines (Figure II.3), we obtained three different PGA-based (50 glutamic acid units, GAU) conjugates following the synthetic approach reported above (Table II.7).

Table II.7. System 2 conjugates tested as possible non-viral vectors.

Conjugate Polymer	Id	GAU	S loading[a] (mol%)	MW[b] (g/mol)	Positive Charges[b]	D^c (m^2/s)	$R_h{}^c$ (nm)
PGA_{50}-SH40%	PSH	50	40	62458	270	5.65e-12	35.52
PGA_{50}-SC30%	PSC	50	30	39980	190	1.56e-11	12.84
PGA_{50}-SHC40%	PSHC	50	40	64510	270	1.25e-11	16.05

[a] Determined by ^1H NMR; [b] Estimated after ^1H NMR analysis; [c] Diffusion coefficient (D) and hydrodynamic radius (R_h) determined by fitting the intensities of the arrayed DOSY NMR spectra into Stejskal-Tanner equation.

II.2.3.1. pDNA Binding Assay by Electrophoresis

As in the case of System 1, we evaluated the ability of synthetic gene carriers to condense oligonucleotides by agarose gel electrophoresis (Figure II.18).

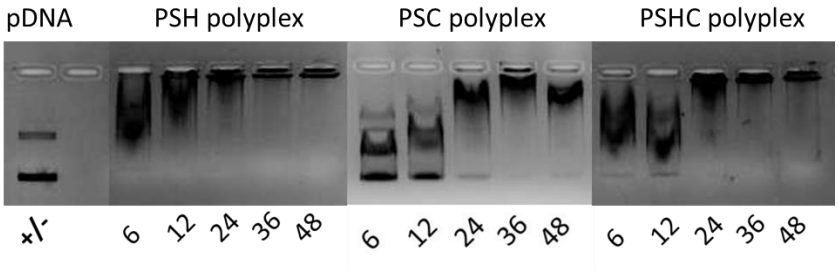

Figure II.18. pDNA binding ability of System 2 family determined by agarose gel shift assay at different +/- ratios.

As shown in Figure II.18, all compounds formed complexes at high +/- ratios, but insertion of a histidine motif (**PSH** and **PSHC**) led to better complexation capabilities.

II.2.3.2. Biological Evaluation: Gene Transfer and Cell Viability *In Vitro*

In agreement with gel shift assay findings, at high +/- ratios, results in the N2a cell line demonstrated a positive impact of histidine motif on transfection efficiency (Figure II.19).

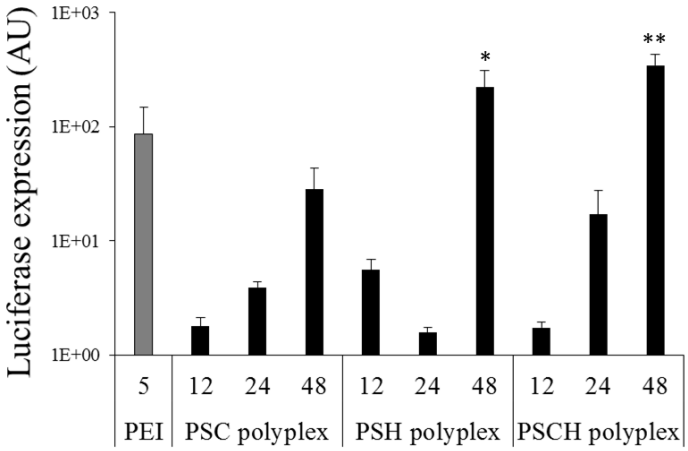

Figure II.19. Normalised transfection efficiency of carriers with (PSCH and PSH polyplexes) and without histidine (PSC polyplex) in the N2a cell line. PEI data is representative of two different experiments. Luciferase activity was normalised to HEPES (control) luciferase activity. Data expressed as mean ± SD, n≥3. Statistical significance between polyplexes and PEI (*p < 0.01, **p < 0.001), determined using one-sided ANOVA.

Although the addition of a greater number of histidine residues led to a slight reduction in cell viability, no compound displayed significant cytotoxicity even at high +/- ratios (Figure II.20).

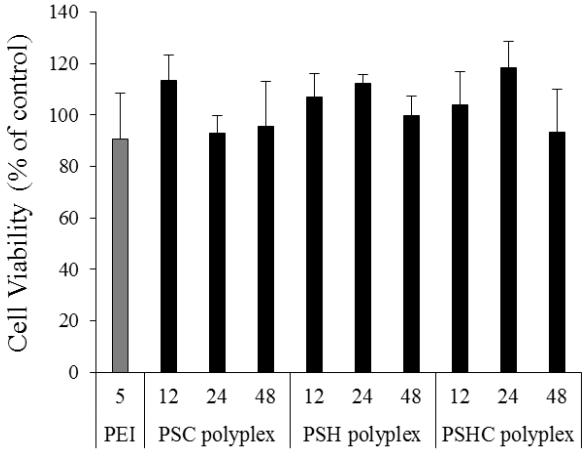

Figure II.20. Cell viability of the polyplexes developed in the N2a cell line by MTS assay at 24 h post-incubation and different +/- ratios. Data expressed as mean ± SD, n≥4.

We confirmed results in the 4T1 cell line with the selected highest +/- ratio for each compound showing similar trends as those observed in N2a cells regarding transfection efficiency (Figure II.21) as well as cell viability (Figure II.22).

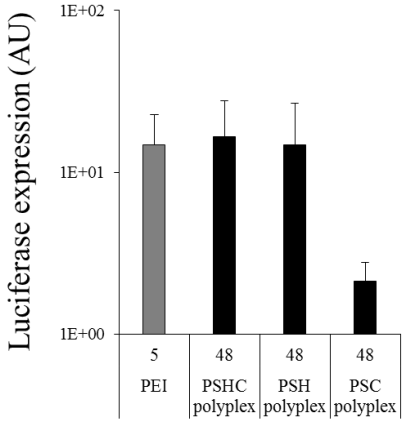

Figure II.21. Transfection efficiency of carriers with (PSCH and PSH polyplexes) and without histidine (PSC polyplex) in the 4T1 cell line. Luciferase activity was normalised to HEPES (control) luciferase activity. Data expressed as mean ± SD, n≥3.

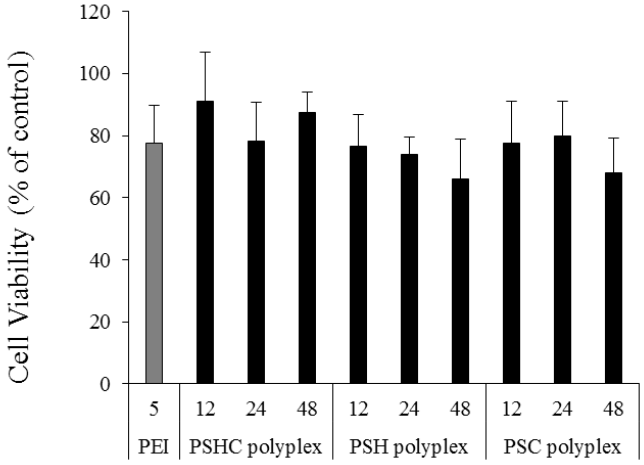

Figure II.22. Cell viability of the polyplexes in the 4T1 cell line by MTS assay at different +/- ratios and 24 h post-incubation. Data expressed as mean ± SD, n≥4.

Whereas the overall data supports the beneficial effect of additional histidine residues on the polyglutamates, the effect of cysteine residues was not fully conclusive (Figure II.23).

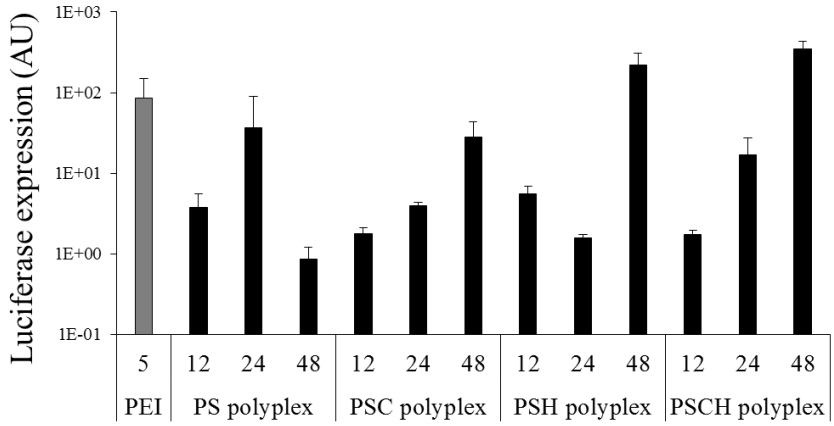

Figure II.23. Comparison between System 1 and System 2 in N2a cells. Luciferase activity was normalised to HEPES (control) luciferase activity. Data expressed as mean ± SD, n≥3.

II.2.3.3. DLS Measurements- ζ-Potential

DLS measurements determined the ζ-potential of System 2 polyplexes (Table II.8). As expected for a non-viral vector, we identified a correlation between ζ-potential and transfection efficiency, with the positively charged polyplexes presenting the highest activity.

Table II.8. Physicochemical characterisation of System 2/pDNA polyplexes.

Conjugate Polymer	Id	+/-	ζ –potential[a] (mV)	PdI[a]
PGA_{50}-SH40%	PSH polyplex	6	**-5.2 ± 0.7**	0.392 ± 0.007
		12	**-1.4 ± 0.6**	0.459 ± 0.031
		24	**3.7 ± 0.5**	0.544 ± 0.127
		36	**6.0 ± 0.2**	0.700 ± 0.130
		48	**7.7 ±0.3**	0.741 ± 0.060
PGA_{50}-SC30%	PSC polyplex	6	**-1.1 ± 0.4**	0.429 ± 0.057
		12	**-0.6 ± 1.9**	0.518 ± 0.090
		24	**-1.6 ± 2.6**	0.488 ± 0.052
		36	**4.6 ± 0.3**	0.966 ± 0.032
		48	**6.1 ± 0.2**	0.675 ± 0.063
PGA_{50}-SHC40%	PSHC polyplex	6	**-1.1 ± 0.2**	0.399 ± 0.023
		12	**-1.5 ± 0.3**	0.416 ± 0.047
		24	**1.6 ± 0.3**	0.499 ± 0.040
		36	**3.1 ± 0.2**	0.645 ± 0.040
		48	**5.7 ± 0.2**	0.891 ± 0.102

[a] As determined by DLS in 20 mM HEPES buffer at 25˚C. Polyplexes were diluted 1:20 before measurement. PdI= polydispersity index. Variations refer to the median of three measurements of the sample.

II.2.3.4. Transmission Electron Microscopy (TEM)

As we observed heterogeneity in size distribution, indicating the formation of large aggregates, we performed transmission electron microscopy (TEM) measurements to gain a better idea of size distribution. We recorded TEM images at different pDNA concentrations: from 10 µg/mL pDNA (equivalent to those in DLS measurements, *i.e.* polyplex formation concentration, Figure II.24A) to 2 µg/mL pDNA (Figure II.24C) and observed a main polyplex population of around 30-40 nm. However, at higher concentrations large aggregates (> 500 nm) could also be found, demonstrating an important dependence of size on concentration (Figure II.24).

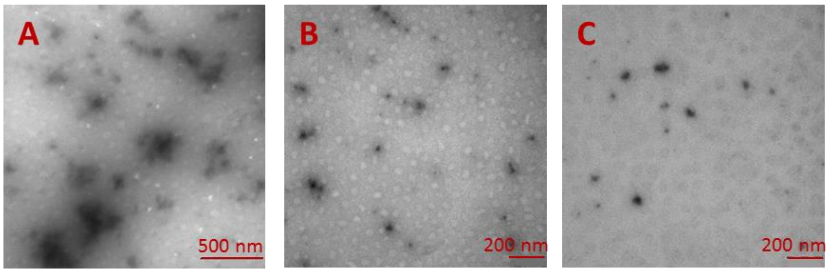

Figure II.24. TEM images of PSHC polyplex at +/- 48 measured at different pDNA concentrations: (A) 10 µg/mL pDNA; (B) 4 µg/mL pDNA; (C) 2 µg/mL pDNA.

II.2.4. System 3: PGA-Based Conjugates Obtained via Disulphide Bond Formation

System 3 was developed to attach the oligomer **SHC** by bioreducible disulphide linkage and to avoid possible side-chain crosslinking reactions hoping for a more controlled polymer structure. For this purpose, we employed a pyridyl disulphide modified PGA (PGA-PD) as the starting material, obtained as previously reported (Figure II.25) [80].

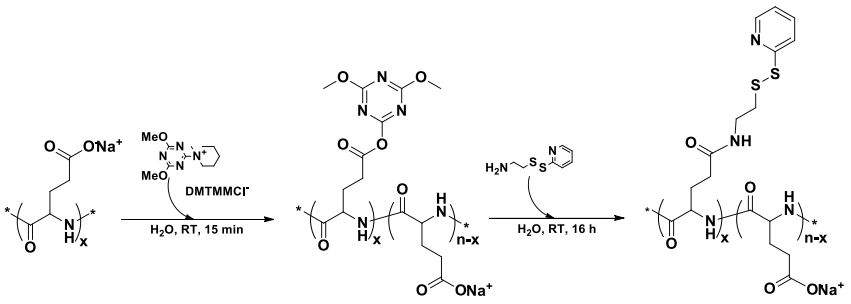

Figure II.25. Modification of PGA chain with pyridyl dithiol ethylamine via DMTMM·Cl activation.

We determined the modification degree by ^{1}H NMR and UV-Vis (ultraviolet-visible spectroscopy), using the average of both results (Figure II.26, Table II.9).

Table II.9. Characteristics of obtained PGA-PD.

Conjugate Polymer	PD loading (%mol)[a]	PD loading (%mol)[b]	MW (g/mol)[c]
PGA_{50}-PD	22	24	9170

[a] Determined by ^{1}H NMR; [b] Determined by UV-Vis; [c] Estimated after ^{1}H NMR and UV-Vis assays.

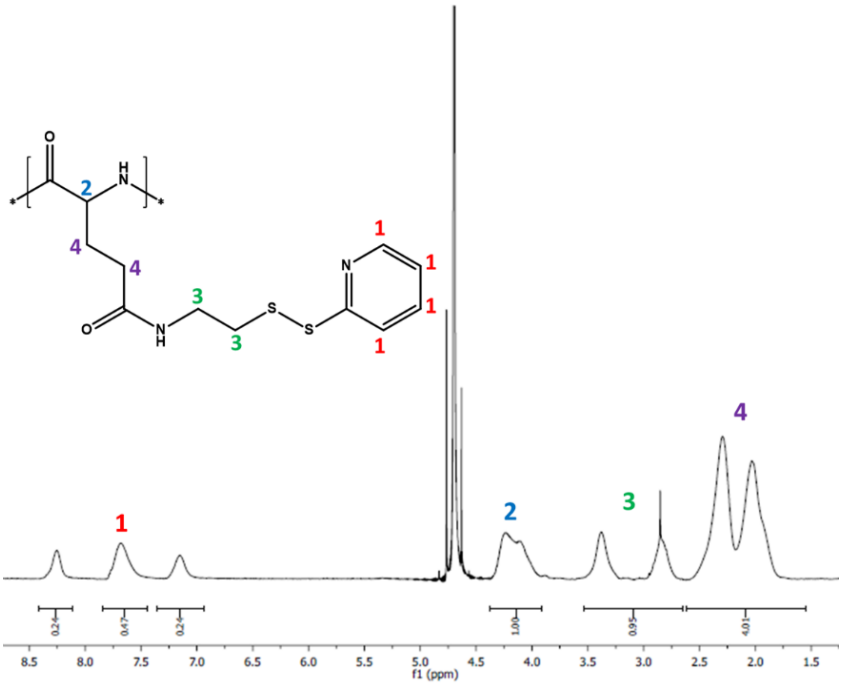

Figure II.26. ^{1}H NMR spectrum in D_2O of PGA-PD.

We conjugated **SHC** (Figure II.3) to PGA-PD through disulphide bonds yielding a new family of polyglutamates (Table II.10). ^{1}H NMR and DOSY NMR in D_2O verified SHC content and purity of the obtained conjugated polymers (Figure II.27).

Table II.10. System 3 conjugates tested as possible non-viral vectors.

Conjugate Polymer	Id	GAU	S loading [a] (mol%)	MW [b] (g/mol)	Positive Charges[b]	D^c (m^2/s)	R_h^c (nm)
PGA_{50}-PCSH21%	PCSH1	50	21	32849	129	ND	ND
PGA_{50} PCSH10%	PCSH2	50	10	19565	35	ND	ND
PGA_{50}-PCSH22%	PCSH3	50	22	33983	137	1.27e-11	15.70

[a] Determined by ^{1}H NMR; [b] Estimated after ^{1}H NMR analysis; [c] Diffusion coefficient (D) and hydrodynamic radius (R_h) determined by fitting the intensities of the arrayed DOSY NMR spectra into Stejskal-Tanner equation. ND= not determined.

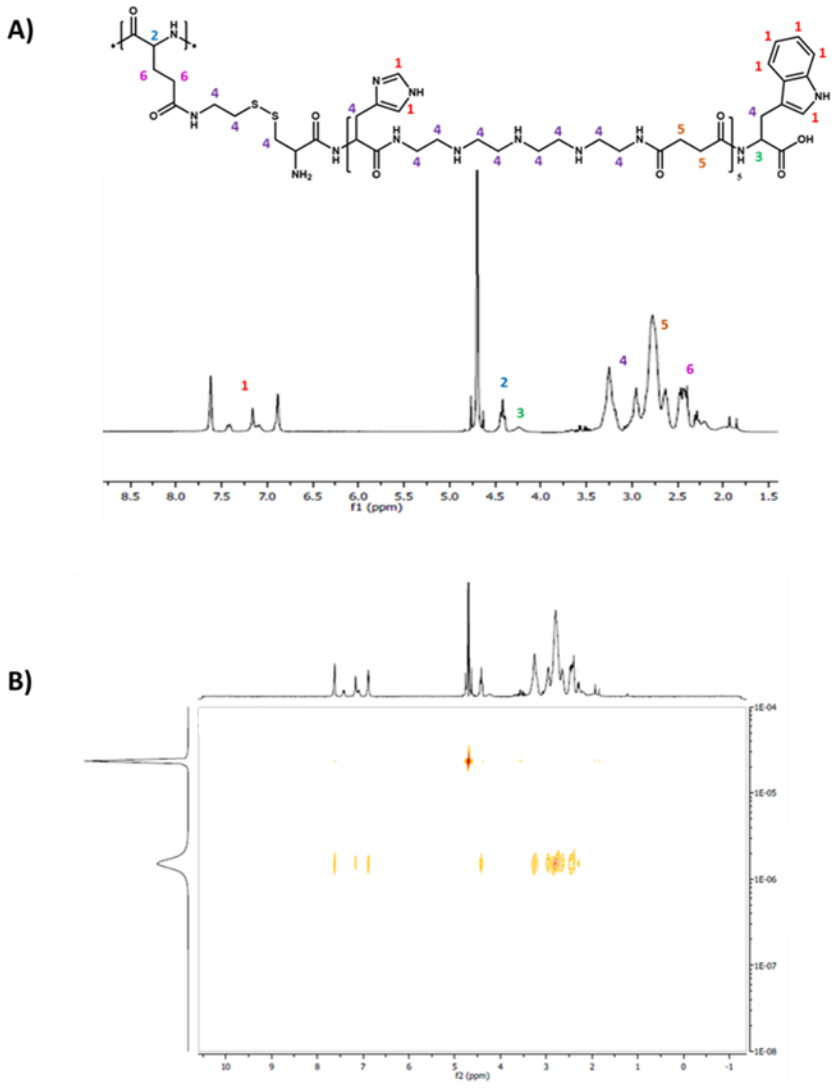

Figure II.27. NMR spectra of PCSH3 in D_2O: (A) ^1H NMR; (B) DOSY NMR.

II.2.4.1. DLS Measurements- ζ-Potential

To select the best candidate and the best +/- ratio, we performed DLS measurements, finding negative ζ-potential values for **PCSH1** and for **PCSH2** polyplexes (Table II.11) even at a high +/- ratio. However, **PCSH3** polyplexes demonstrated a positive net charge and, therefore, were selected to move forward.

Table II.11. Physicochemical characteristics of System 3 polyplexes.

pDNA polyplex Id	+/-	ζ-potential [a] (mV)	PdI [a]
PCSH1 polyplex	3	**-24.3 ± 3.4**	0.377 ± 0.074
	6	**-21.3 ± 1.8**	0.434 ± 0.128
	12	**-25.4 ± 2.1**	0.455 ± 0.032
	24	**-18.6 ± 7.0**	0.808 ± 0.161
	36	**-8.8 ± 0.6**	0.195 ± 0.012
	48	**-14.5 ± 0.6**	0.245 ± 0.022
	60	**-10.4 ± 0.5**	1.000
PCSH2 polyplex	3	**-16.8 ± 0.3**	0.319 ± 0.038
	6	**-17.9 ± 0.2**	0.498 ± 0.064
	12	**-12.4 ± 0.8**	0.341 ± 0.040
	24	**-14.6 ± 0.6**	0.361 ± 0.057
	36	**-11.4 ± 0.4**	0.698 ± 0.059
PCSH3 polyplex	3	**2.0 ± 0.242**	0.347 ± 0.008
	6	**1.1 ± 0.0**	0.550 ± 0.109
	12	**-2.6 ± 0.104**	0.440 ± 0.054
	24	**6.3 ± 0.413**	0.489 ± 0.036
	36	**5.2 ± 0.265**	0.796 ± 0.050
	48	**5.0 ± 0.297**	0.993 ± 0.012

[a] As determined by DLS in 20 mM HEPES buffer at 25˚C. Polyplexes were diluted 1:20 before measurement. PdI= polydispersity index. NA= not appropriate. Variations refer to the median of three measurements of the sample.

II.2.4.2. Biological Evaluation: Gene Transfer and Cell Viability *In Vitro*

We examined the influence of the **SHC** oligomer used on transfection efficiency by luciferase pDNA gene transfer to N2a cells, finding that the **PCSH** efficiently transferred pDNA (Figure II.28).

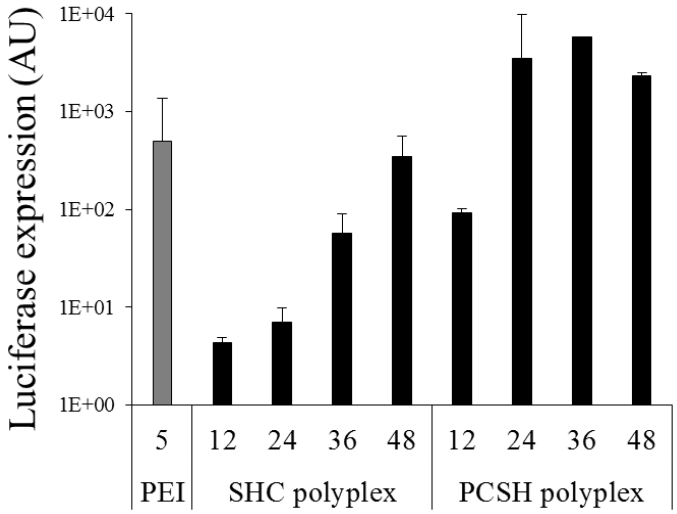

Figure II.28. Normalised transfection efficiency of SHC and PCSH polyplexes at low +/- and N/P ratios in the N2a cell line. PEI data is representative of two different experiments. Luciferase activity was normalised to HEPES (control) luciferase activity. Data expressed as mean ± SD, n≥3. No statistical significance found between polyplexes and PEI (n.s.= $p > 0.05$) as determined using one-sided ANOVA.

A recently published study by Scholz *et al.* [73] demonstrated that linear sequences of 5 Stp building block units could not form stable complexes with nucleic acids. The development of effective transfection carriers required the addition of extra moieties such as cysteines (stabilisation of polyplexes by disulphide formation between oligomers) [74, 75], tyrosine trimmers [76], or fatty acids (hydrophobic stabilisation of formed particles) [68, 74, 77]. In the case of **SHC** polyplexes, the addition of histidine and cysteine moieties improved gene transfer when compared with **S** polyplexes, although not to the level obtained for **PCSH**. Hence, such moieties can positively influence pDNA transfer at high N/P ratios without affecting cell viability.

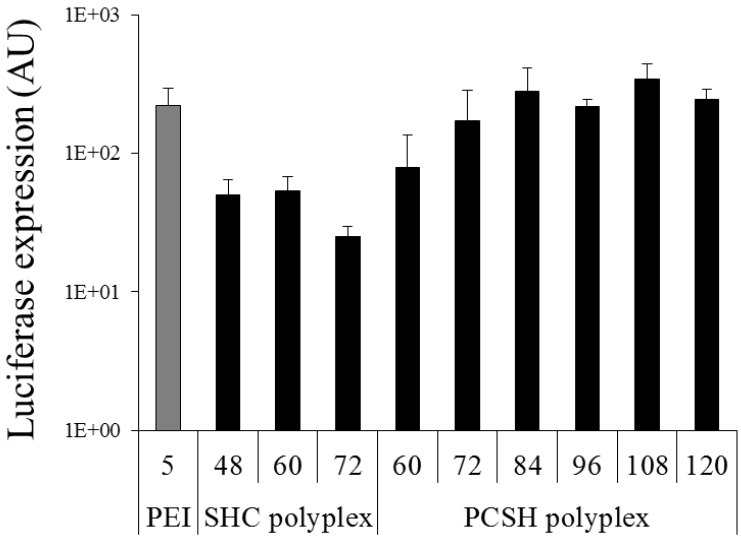

Figure II.29. Normalised transfection efficiency of SHC and PCSH polyplexes at high +/- and N/P ratios in the N2a cell line. PEI data is representative of two different experiments. Luciferase activity was normalised to HEPES (control) luciferase activity. Data expressed as mean ± SD, n≥3. No statistical significance found between polyplexes and PEI (n.s.= $p > 0.05$) as determined using one-sided ANOVA.

Given the low cytotoxicity of both compounds (**PCSH** and **SCH** polyplexes), we tested higher +/- and N/P values to select the best ratio. As shown in Figure II.29, whereas transfection efficiency did not improve with increased **SHC** polyplex N/P ratio, in the case of **PCSH**, the limit was +/- 84, surpassing the efficiency of **SHC** at N/P 48 with no significant reduction in cell viability against N2a cells (Figure II.30 and II.31).

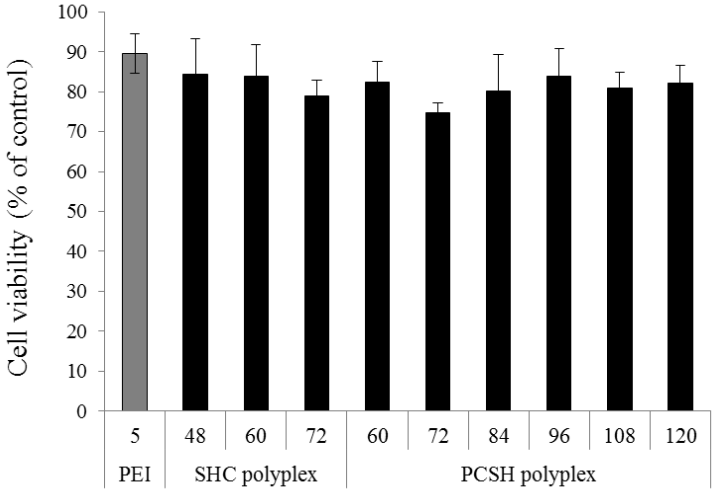

Figure II.30. Determination of cell viability for SHC and PCSH polyplexes in the N2a cell line. Data expressed as mean ± SD, n≥4.

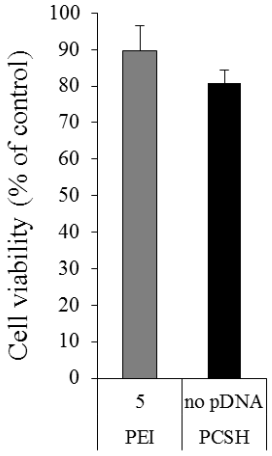

Figure II.31. Determination of cell viability for PCSH polymer. Data expressed as mean ± SD, n≥4.

To further elucidate gene delivery efficacy, confocal fluorescence microscopy (24 h incubation) was used to study the successful transcription in the nucleus of PSCH polyplex at its optimal conditions (+/- 84) in N2a cells. pDNA encoding for green fluorescent protein (GFP) was selected in order to form the complexes. After transfection, we

mainly observed the GFP signal dispersed in the cytosol of N2a cells (Figure II.32) in a comparable manner to the results obtained with PEI.

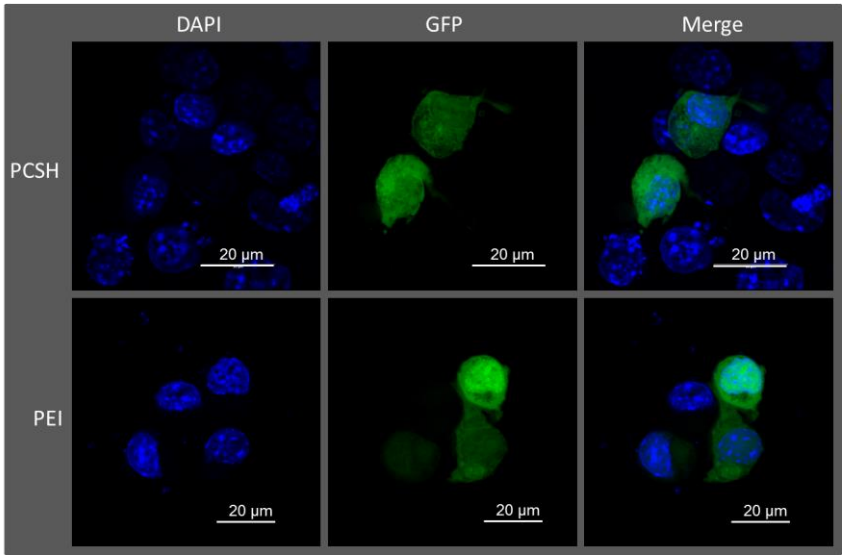

Figure II.32. Confocal microscopy images of PSCH conjugate (+/- 84) and PEI (positive control, N/P 5) after 24 h of transfection in N2a cell line. Green fluorescence corresponds to GFP and blue fluorescence to the nuclei marker DAPI.

II.2.4.3. Red Blood Cell (RBC) Lysis Assay

We performed a red blood cell (RBC) lysis assay to evaluate the lytic activity of both **SHC** and **PCSH** and its possible contribution to endosomal escape. For this purpose, we measured haemoglobin release at different pH values (pH 7.4, 6.5, 5.5) using a range of concentrations (0.1, 0.05 and 0.01 mg/mL). No significant lytic activity was observed for the tested compounds, consistent with their low cytotoxicity (Figure II.33).

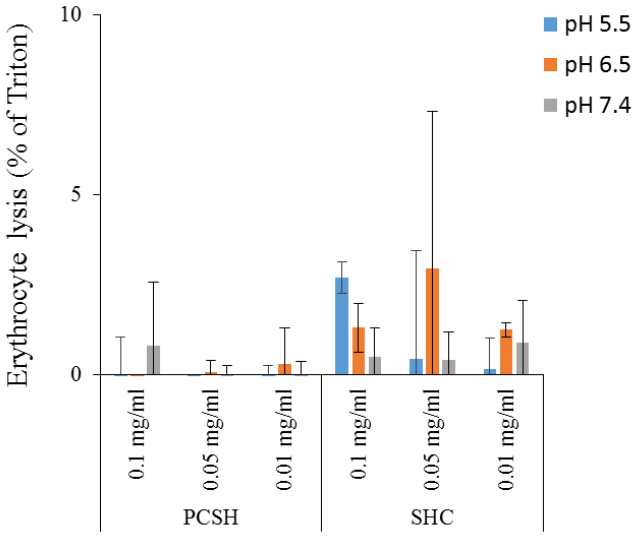

Figure II.33. Erythrocyte leakage assay at different pH values: compounds were incubated with erythrocytes at different concentrations at 37°C at indicated pH values. Haemoglobin release was measured after 1 h. Data expressed as mean ± SD, n≥4.

II.2.5. System 4: PGA-Coated SHC Polyplexes

Due to the similar behaviour of **SHC** and **PCSH** polyplexes, we designed an alternative system aimed at improving the activity of SHC by promoting complex stability. For this purpose, we coated SHC polyplex with several different PGA-based compounds (PGA_{50}, PGA_{100} and PEG_{5000}-PGA_{88} (DB_{88})). Initially, we created **SHC** polyplexes in the same manner as previously described, although with shorter pDNA incubation time (15 min *vs.* 30 min). Following this step, we added the PGA-based coating solutions and incubated for an additional 15 min yielding three different families of coated systems (Table II.12).

Table II.12. Families of studied coated systems.

Coated System	Id
SHC polyplex coated with PGA_{50}	P_{50}SHC polyplex
SHC polyplex coated with PGA_{100}	P_{100}SHC polyplex
SHC polyplex coated with DB_{88}	DB_{88}SHC polyplex

II.2.5.1. pDNA Binding Assay by Electrophoresis

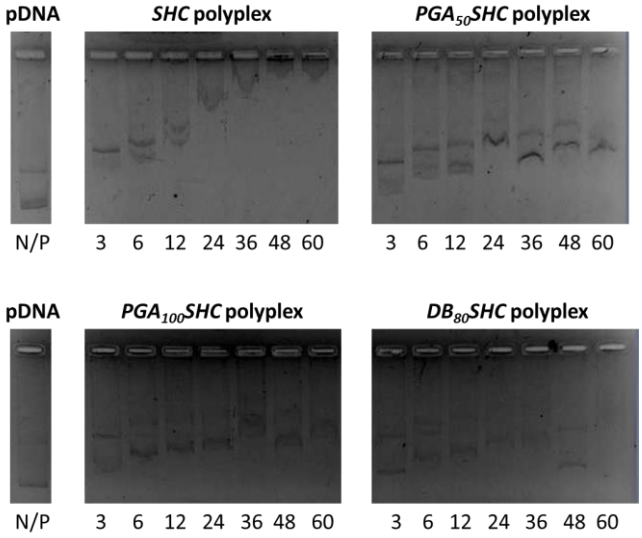

Figure II.34. pDNA binding ability determined by agarose gel shift assay at different N/P ratios and different coatings.

Figure II.34 demonstrates the different pDNA binding ability of **SHC** polyplexes compared with the coated systems. After coating with PGA_{50}, the resulting system presented a negative ζ-potential (Table II.13), a possible reason for the more rapid migration compared with **SHC** polyplexes, even given the remaining difference between the pDNA control and the sample. In the case of the PGA_{100} and DB_{88} coatings, the retention was also different, although the DB_{88}SHC polyplex system presented a positive ζ-potential at high N/P ratios. Moreover, for the DB_{88} system, the PdI value improved with a greater N/P ratio.

II.2.5.2. DLS Measurements- Particle Size and ζ-Potential

We performed DLS measurements at pH 7.4 (pH of complex formation) (Table II.13).

Table II.13. Physicochemical characteristics of System 4 polyplexes.

Polyplex	Id	+/-	Size[a] (d., nm)	ζ –potential[a] (mV)	PdI[a]
SHC polyplex	SHC polyplex	3	137.9 ± 4.0	**11.3 ± 0.3**	0.244 ± 0.015
		6	93.7 ± 1.4	**12.7 ± 0.5**	0.271 ± 0.024
		12	123.2 ± 4.0	**13.8 ± 0.3**	0.158 ± 0.008
		24	121.0 ± 8.9	**20.9 ± 0.9**	0.384 ± 0.019
SHC polyplex coated with PGA_{50}	P_{50}SHC polyplex	3	105.3 ± 78.9	**-32.4 ± 1.6**	0.473 ± 0.039
		6	100.9 ± 13.2	**-33.2 ± 1.0**	0.263 ± 0.019
		12	89.45 ± 42.45	**-33.0 ± 0.5**	0.327 ± 0.031
		24	66.38 ± 21.17	**-31.5 ± 0.5**	0.267 ± 0.002
SHC polyplex coated with PGA_{100}	P_{100}SHC polyplex	3	122.1 ± 1.3	**-34.7 ± 0.8**	0.217 ± 0.009
		6	195.4 ± 5.8	**-38.5 ±0.8**	0.294 ±0.014
		12	126.1 ± 20.3	**-36.3 ± 1.1**	0.400 ± 0.043
		24	106.7 ± 10.4	**-33.6 ± 0.3**	0.223 ± 0.013
SHC polyplex coated with DB_{88}	DB_{88}SHC polyplex	3	131.2 ± 7.9	**-32.7 ± 0.8**	0.659 ± 0.017
		6	131.9 ± 18.7	**-32.4 ±0.6**	0.383 ±0.004
		12	66.70 ± 17.74	**-20.5 ± 0.2**	0.357 ± 0.021
		24	86.04 ± 3.15	**-10.6 ± 0.4**	0.227 ± 0.010
		36	77.58 ± 2.58	**3.23 ± 0.374**	0.155 ± 0.009

[a] As determined by DLS in 20 mM HEPES buffer at 25˚C. Polyplexes were diluted 1:20 before measurement. Size values are expressed in terms of number. Variations refer to the median of three measurements of the sample.

II.2.5.3. Biological Evaluation: Gene Transfer and Cell Viability *In Vitro*

We evaluated transfection efficiency in the N2a cell line using three coatings (PGA_{50}, PGA_{100}, and DB_{88}) and the same amount as for **SHC** (c). Preliminary results (Figure II.35) demonstrated lower transfection activity with coated polyplexes compared to pure **SHC** polyplexes, but improved cell viability (Figure II.36).

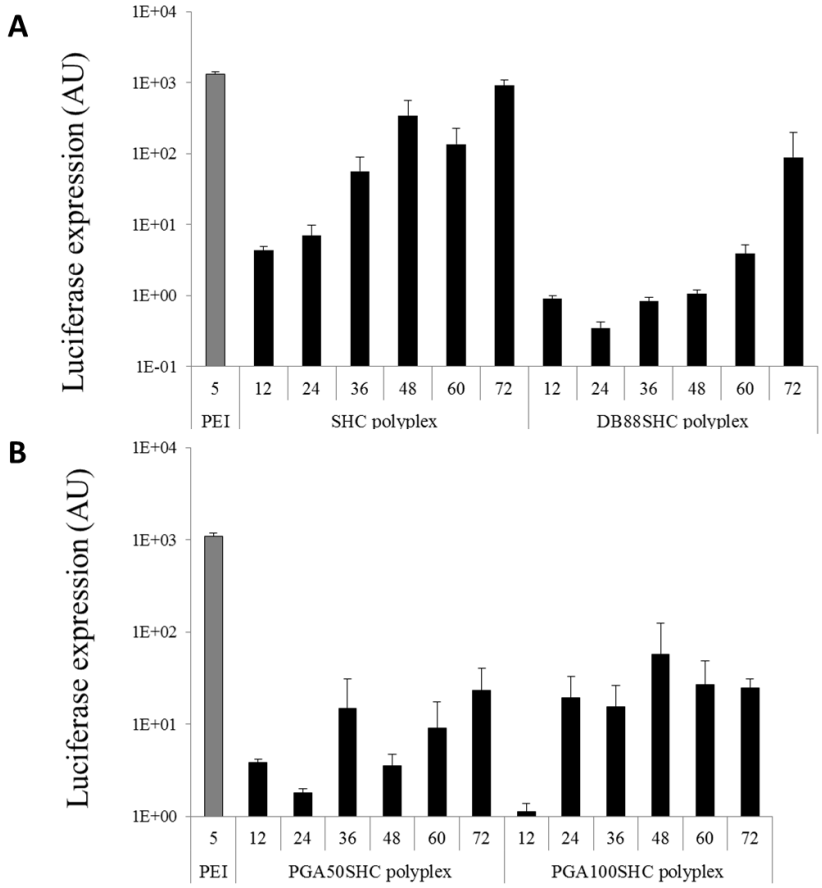

Figure II.35. Normalised gene transfer in N2a cells at different N/P ratios for (A) SHC, and DB_{88}SHC polyplexes, and (B) PGA_{50}SHC and PGA_{100}SHC polyplexes.

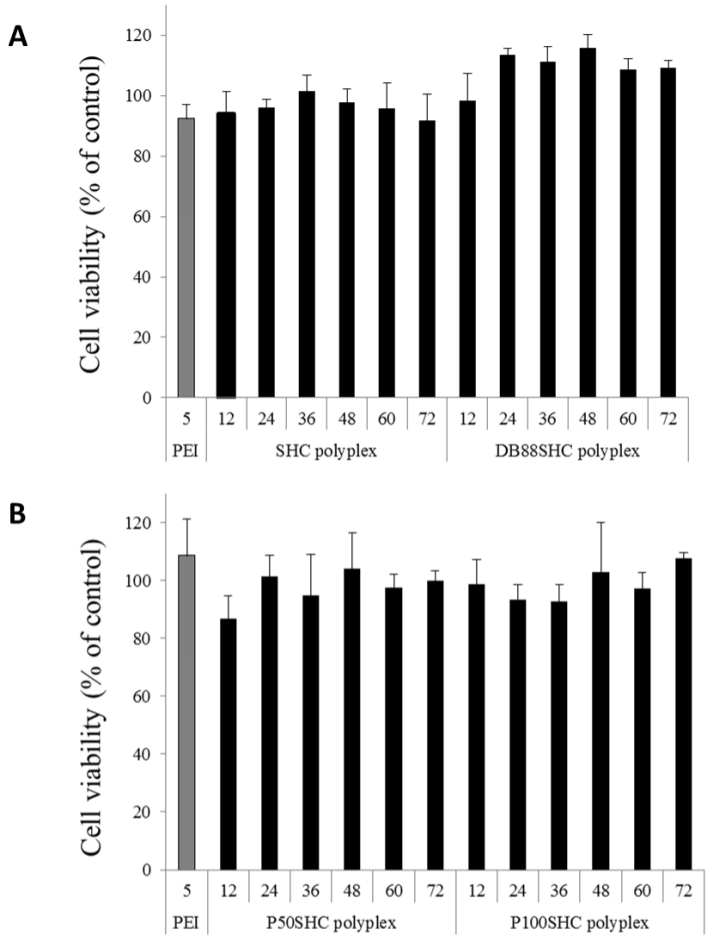

Figure II.36. Cell viability of (A) SHC and DB_{88}SHC polyplexes, (B) PGA_{50}SHC and PGA_{100}SHC polyplexes at different N/P ratios. Data expressed as mean ± SD, n≥4.

In view of these results, we selected the DB_{88} coating as the best candidate at increasing concentrations (c, 2c and c/2) showing that the c/2 system presented similar behaviour to the **SHC** polyplexes with better cell viability profile. However, higher ratios did not improve the activity as much as anticipated (Figure II.37).

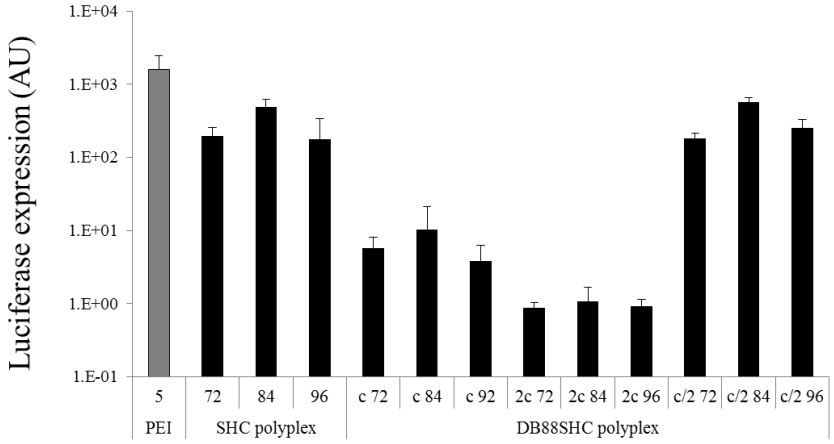

Figure II.37. Normalised gene transfer for DB_{88}SHC polyplexes at different N/P ratios and different amount of coating agent. Luciferase activity was normalised to HEPES (control) luciferase activity. Data expressed as mean ± SD, n≥3.

II.3. CONCLUSIONS

Due to the polyanionic nature of DNA or RNA, typically cationic or neutral delivery vehicles have been used for gene delivery. As a new approach, this thesis chapter focused on the design, development and validation of non-viral polypeptide-based carriers for oligonucleotide delivery based on a negatively-charged PGA backbone partly derivatised with oligoaminoamide residues. To this end, PGA-derivatives modified with different pentameric succinyl tetraethylene pentamines (Stp_5) were designed. Optionally, histidines for modulation of endosomal buffer capacity and cysteines for pDNA or siRNA complex stabilisation were included, followed by characterisation of biophysical properties and gene transfer efficiency in N2a neuroblastoma or 4T1 breast cancer cell culture.

The first three developed systems were based on PGA polymers (homopolymers or block-*co*-polymers) modified with a monodisperse Stp-based oligoaminoamide. In System 1, we orthogonally modified PGA side-chains with oligomer **S** by means of amide bond formation using the **S** terminal amine (Figure II.3). In System 2, we modified PGA side-chains analogously with **SH** (additionally containing histidines to improve the endosomolytic effect) [78], **SC** (containing cysteine to

stabilise the pDNA complex via disulphide formation) [68, 77], or **SHC** (containing both histidines and cysteine). To generate System 3, we performed the conjugation via bioreducible disulphide bonds using the terminal cysteine of **SHC**. System 4 differed from the previous systems in several ways. Firstly, we generated a polyplex between pDNA and oligoaminoamide **SHC**, and subsequently coated the positively charged pDNA complex with a negatively charged PGA-polymer in an attempt to improve the biocompatibility of **SHC**. We employed two different lengths of PGA and diblock PEG-PGA as coating agents.

Unfortunately, our studies suggest that the systems assessed are not suitable for siRNA delivery. We propose the poor stability of complexes as the major factor contributing to a lack of transfection ability. Nanoparticle formulation with siRNA presents some important differences to plasmid formulation. Although both self-assemble by electrostatic forces, plasmids are several hundred-fold larger than siRNA, suggesting that different kinds of polycations may be optimal. This again demonstrates that pDNA and siRNA differ considerably in their properties and suitable delivery vectors must be tailored individually [86].

Concerning pDNA, the conjugation of Stp derivatives to the PGA chain through amide bond formation (System 1 and System 2) resulted in stable non-toxic nanosystems with the ability to efficiently transfer pDNA. This improved the efficiency of both PGA and Stp-based compounds as transfection agents, with a more pronounced effect for Stp derivatives bearing histidine moieties. Moreover, the complexation capacity depended on the content of the oligoaminoamide. Complexation of pDNA with System 1 or 2 polymers exceeded the effectiveness of PEI in gene delivery. Thus, the presence of PGA promoted the enhanced transfection capacity of the Stp_5 family.

In the case of System 3, **SHC** conjugated to PGA by disulphide bonds improved cell viability, even given the relatively high amount of PGA-based polymer required. Upon coating (System 4), no significant improvements were observed regarding gene transfer efficiency, mainly as **SHC** itself already demonstrated a high gene transfer

capability. However, coating did allow for a slight enhancement in cell viability. We also expected that a coating strategy will provide advantages when compared with **SHC** in an *in vivo* settings due to the enhanced permeability and retention (EPR) effect and possible alterations to pharmacokinetics. Further experiments are ongoing to demonstrate this point.

II.4. MATERIALS AND METHODS

II.4.1. Materials

All chemicals were reagent grade and used without further purification. Protected *Fmoc*-α-amino acids, 2-chlorotrityl chloride resin, N,N-dimethylformamide (DMF), N,N-diisopropylethylamine (DIPEA) and trifluoroacetic acid (TFA) were purchased from Iris Biotech. Triisopropylsilane (TIS), 1-hydroxybenzotriazole (HOBt), and phenazinemethosulfate (PMS) were purchased from Sigma-Aldrich. (Benzotriazol-1-yloxy)tripyrrolidinophosphonium hexafluorophosphate (PyBOP®) and microreactors were obtained from MultiSynTech. HEPES was purchased from Biomol GmbH, agarose NEEO Ultra-Qualität from Carl Roth GmbH and GelRed™ from VWR. The pCMVLuc and pCMV-GFP pDNAs were obtained from Plasmid Factory. PGA sodium salt and PEG-*co*-PGA block-*co*-polymers were provided from Polypeptide Therapeutic Solutions SL (PTS, Spain). The DMTMM·Cl coupling reagent was synthesised according to previous descriptions [82]. Pyridyl dithiol ethylamine HCl salt was synthesised essentially as described in van der Vlies *et al.* [87]. Jet-PEI was obtained from Polyplus-Transfection. Dulbecco's Modified Eagle's Medium (DMEM), RPMI, phosphate buffer saline (PBS), fetal bovine serum (FBS) and trypsin, were provided from Gibco. 3-(4,5-dimethylthiazol-2-yl)-5-(3-carboxymethoxyphenyl)-2-(4-sulfophenyl)-2H-tetrazolium (MTS) was supplied by Promega. Paraformaldehyde electron microscopy grade was purchased from Electron Microscopy Sciences. All solvents were of analytical grade and used as received. Deuterated solvents $CDCl_3$ and D_2O were purchased from Deutero GmbH. Dialysis was performed by using a Float-A-Lyzer®. Sephadex G-10 material for size exclusion chromatography was

obtained from GE Healthcare. MilliQ water is defined as deionised water with a conductance below 0.06 µS.

II.4.2. Cell Culture

Mouse neuroblastoma cells (N2a) were grown in DMEM supplemented with 10% FBS, 4 mM stable glutamine, 100 U/mL penicillin, and 100 µg/mL streptomycin, at 37 °C in a humidified atmosphere containing 5% CO_2 and 95% air.

Murine neuroblastoma cells, stably transfected with an enhanced green fluorescent protein GL3 firefly luciferase fusion protein (N2a/eGFPLuc) [77, 85, 88], were cultured at 37 °C in DMEM with 1 g/L glucose, supplemented with 10% FBS, 4 mM glutamine, 100 U/mL penicillin, and 100 µg/mL streptomycin. For maintenance, the cells were detached with a trypsin-ethylenediaminetetraacetic acid (EDTA) solution (0.25%) and seeded at the desired concentration.

Metastatic murine breast cancer murine (4T1) were grown in RPMI medium supplemented with 10% FBS at 37 °C in a humidified atmosphere containing 5% CO_2 and 95% air.

II.4.3. Characterisation Techniques

II.4.3.1. Nuclear Magnetic Resonance (NMR) Spectroscopy

^1H and DOSY NMR spectra were recorded on a Bruker AC 300 or on a Bruker AV500 at room temperature (RT) and at a frequency of 300 MHz and 500 MHz respectively. Pulsed field gradient NMR spectroscopy was used to measure translational diffusion by fitting the integrals or intensities of the NMR signals to the Stejskal-Tanner [89, 90] equation: $I= I_0 \exp[-D\gamma^2g^2\delta^2(\Delta-\delta / 3)]$ where I is the observed intensity, I_0 the reference intensity (unattenuated signal intensity), D the diffusion coefficient, γ the gyromagnetic ratio of the observed nucleus, g the gradient strength, δ the length of the gradient, and Δ the diffusion time. Two-dimensional diffusion-ordered NMR spectroscopy (DOSY) was performed with a stimulated echo sequence using bipolar gradient pulses. The lengths of delays were held constant at Δ= 100 ms, and 32 spectra of 64 scans each were acquired with the strength of the

diffusion gradient varying between 5% and 95%. The lengths of the diffusion gradient and the stimulated echo were optimised for each sample. Typical values were δ = 3 ms for the analysis of both oligomers and PGA-based conjugates. All data were processed and analysed using the MestreNova 6.2 software.

II.4.3.2. Matrix-Assisted Laser Desorption/Ionization (MALDI) Mass Spectrometry

A 0.8 µL matrix droplet consisting of a saturated solution of Super-DHB (sum of 2,5-dihydroxybenzoic acid and 2-hydroxy-5-methoxybenzoic acid) in acetonitrile / water (1 : 1) containing 0.1 % (v/v) TFA was spotted on a MTP AnchorChip (Bruker Daltonics, Bremen, Germany). After the Super-DHB matrix crystallized, 0.8 µL of the sample solution (10 mg/mL in water) was added to the matrix spot. Samples were analysed using an Autoflex II mass spectrometer (Bruker Daltonics, Bremen, Germany).

II.4.3.3. Dynamic Light Scattering (DLS)

The polyplex solution was measured in a cell DTS 1070 with laser light scattering using a Zetasizer Nano ZS with backscatter detection (Malvern Instruments, Worcestershire, UK). For size measurements, the equilibration time was 0 min, the temperature was 25˚C, and an automatic attenuator was used. The refractive index of the solvent (MilliQ water) was 1.330 and hence, the viscosity was 0.8872. For analysis of the polyplexes, the refractive index of polystyrene latex (1.590) was used. Each sample was measured 3 times with 10 sub-runs. The ζ-potential was calculated using the Smoluchowski model. Therefore, 10-30 sub-runs of 10 s at 25°C (n=3) were measured.

II.4.3.4. Transmission Electron Microscopy (TEM)

Pictures were obtained from a FEI Tecnai G2 Spirit (FEI Europe, Eindhoven, Netherlands) transmission electron microscope using the Morada digital camera (Olympus Soft Image Solutions GmbH, Münster, Germany). Samples were prepared as detailed: a Mesh grid was placed over one sample solution drop for 3 min and then the grid was transferred to a drop of uranyl acetate (2% in milliQ water for 1 min).

Excess of uranyl acetate was dried and the grid was placed in the grid holder and observed under the microscope.

II.4.4. Protocols

II.4.4.1. Loading of a 2-Chlorotrityl Chloride Resin with an *Fmoc*-protected Amino Acid

After swelling of 750 mg of a 2-chlorotrityl chloride resin (1.2 mmol chloride) in water-free DCM for 10 min, the first *Fmoc*- protected amino acid *Fmoc*-L-Trp(*Boc*)-OH (0.75 equivalents, eq.) and DIPEA (1.5 eq.) were added to the resin for 1 h. The reaction solvent was drained and a mixture of DCM/MeOH/DIPEA (80/15/5) was added twice for 10 min. After the removal of the reaction mixture, the resin was washed 5 times with DCM.

About 30 mg of the resin was removed and dried to determine the loading of the resin. Therefore, an exact amount of resin was treated with 1 mL deprotection solution (20% piperidine in DMF) for 1 h. Following these steps, the solution was diluted and absorption was measured at 301 nm. The loading was then calculated according to the equation: resin load [mmol/g] = (A*1000)/(m [mg]*7800*df) with df as dilution factor.

The resin was treated twice with 20% piperidine in DMF and twice with 20% piperidine DMF with 2% DBU (1,8-Diazabicyclo[5.4.0]undec-7-eneto) remove the *Fmoc*- protection group. Reaction progress was monitored by Kaiser test [91]. Afterwards, the resin was washed with DMF, DCM and n-hexane and dried in a vacuum.

II.4.4.2. Synthesis of Stp Oligomers S, SH, SC, and SHC

Stp oligomers (**S**, **SH**, **SC**, and **SHC)** were synthesised using a 2-chlorotrityl resin preloaded with the first C-terminal amino acid (*Fmoc*-L-Trp(*Boc*)-OH) as solid support (resin-loading protocol can be found in Section II.4.4.1). Artificial *Fmoc*-oligoamino acid *Fmoc*-Stp(Boc_3)-OH was synthesised as previously described [68, 75]. Oligomers of this artificial oligoamino acid, optionally together with the natural amino acids histidine (*Fmoc*-L-His(Trt)-OH) and/or cysteine (*Boc*-L-Cys(Trt)-OH),

were synthesised manually under standard *Fmoc* solid phase peptide synthesis conditions using syringe microreactors. Coupling steps were carried out using 4 eq. *Fmoc*-amino acid, 4 eq. HOBt, 4 eq. PyBOP and 8 eq. DIPEA in DCM-DMF 1 : 1 (10 mL g^{-1} resin) for 90 min. *Fmoc* deprotection was accomplished by 4 × 10 min with 20% piperidine in DMF (10 mL g^{-1} resin). After each coupling and deprotection step, a washing procedure comprising 3 × 1 min DMF, 3 × 1 min DCM incubation (10 mL g^{-1} resin), and a Kaiser test were performed. In the case of a positive Kaiser test result after coupling, the last coupling step was repeated. In case of a negative result after deprotection, the last deprotection step was repeated. Finally, all oligomers were cleaved from the resin by incubation with TFA-TIS-H_2O 95 : 2.5 : 2.5 (10 mL g^{-1} resin) for 90 min. The cleavage solution was concentrated by flushing nitrogen and the oligomers were precipitated in 40 mL of pre-cooled methyl tert-butyl ether (MTBE)-n-hexane 1 : 1. All oligomers were purified by size exclusion chromatography using an Äkta purifier system (GE Healthcare Bio-Sciences AB, Uppsala, Sweden), a Sephadex G-10 column, and 10 mM hydrochloric acid solution-acetonitrile 7 : 3 as a solvent. All oligomers were lyophilised. Oligomer sequences were validated by mass spectrometry and ^{1}H NMR.

Oligomer **S**, W-Stp_5: ^{1}H NMR (500 MHz, D_2O, δ): 2.3-2.6 (m, 20 H), 2.95-3.55 (m, 82 H), 4.40-4.55 (t, 1 H), 7.05-7.65 (m, 5 H).

Oligomer **SC**, W-Stp_5-C: ^{1}H NMR (500 MHz, D_2O, δ): 2.3-2.6 (m, 20 H), 2.95-3.55 (m, 84 H), 3.95-4.55 (m, 2 H), 7.05-7.65 (m, 5 H).

Oligomer **SH**, W-$(StpH)_5$: ^{1}H NMR (500 MHz, D_2O, δ): 2.3-2.6 (m, 20 H), 2.95-3.55 (m, 92 H), 3.90-4.55 (m, 6 H), 7.05-7.65 (m, 10 H), 8.40-8.75 (m, 5 H).

Oligomer **SHC**, W-$(StpH)_5$-C: ^{1}H NMR (500 MHz, D_2O, δ): 2.3-2.6 (m, 20 H), 2.95-3.55 (m, 94 H), 4.10-4.55 (m, 7 H), 7.05-7.65 (m, 10 H), 8.40-8.75 (m, 5 H).

II.4.4.3. General Synthesis of PGA-Stp-Based Conjugates via Amide Bond Formation

One eq. of PGA sodium salt (MW 151 per unit, 50 GAU) was dissolved in a minimum amount of milliQ water. Then one eq. of DMTMM·Cl (MW 276.1) was added, also dissolved in milliQ water. Ten min later, 0.5 eq. of Stp-based polyamidoamine was added and the pH adjusted to 8 with 1M $NaHCO_3$. The reaction was allowed to proceed for 16 h stirring at RT. Dialysis using Float-A-Lyzer® at the corresponding molecular weight cut-off (MWCO) was performed in order to purify the polymer. A white powder was obtained after freeze-drying.

^{1}H NMR (300 MHz, D_2O, δ): 7.75-7.19 (m, 5xH), 4.51 (m, 1xH), 4.35 (m, 1H), 3.39-1.98 (m, 80xH + 4H). x: percentage of modification.

II.4.4.4. Synthesis of PGA-Based Conjugates via Disulphide Bond Formation

Synthesis of pyridyl disulphide modified PGA (PGA-PD). PGA-PD was synthesised using DMTMM·Cl with a modification of a previously published method [80]. One eq. of PGA sodium salt (MW 151 per unit, 50 GAU) was dissolved in milliQ water. Then 0.6 eq. of DMTMM·Cl, also dissolved in milliQ water was added. 10 min later, 0.3 eq. of pyridyl disulphide was added and the pH adjusted to 8 with 1M $NaHCO_3$. The reaction was allowed to proceed overnight stirring at RT. Dialysis using Float-A-Lyzer® was performed in order to purify the polymer. A white powder was obtained after freeze drying.

^{1}H NMR δ (300 MHz, D_2O, δ): 8.43 (1xH, m), 7.88 (2xH, m), 7.33 (1xH, m), 4.33 (1H, m), 3.48 (2xH, m), 2.95 (2xH, m), 2.39-1.90 (4H, m). x: percentage of modification.

Synthesis of PCSH. One eq. of PGA-PD and 0.5 eq. of oligomer SHC were separately dissolved in PBS at pH 7.4. Both solutions were mixed and the reaction allowed to proceed for 5 h stirring at RT. Dialysis using Float-A-Lyzer® at 3000 MWCO was performed for 16 h. A yellowish powder was obtained after freeze-drying.

^{1}H NMR (300 MHz, D_2O, δ): 7.75-7.19 (m, 15xH), 4.51 (m, 1H), 4.35 (m, 1xH), 3.39-1.98 (m, 118xH + 4H). x: percentage of modification.

II.4.4.5. Polyplex Formation

Polyplex formulations for transfection and gel shift experiments were prepared as follows: 200 ng of pDNA or 500 ng of siRNA and the calculated amount of polymer at indicated +/- or N/P ratios were diluted in separate tubes in 10 µL of 20 mM HEPES at pH 7.4 each. Only protonatable nitrogens, not amide nitrogens, were considered in the +/- ratio and N/P ratio calculations. The nucleic acid and the polymer solution were mixed by rapidly pipetting up and down (at least 5 times) and incubated for 30-40 min at RT.

II.4.4.6. pDNA and siRNA Binding Assay by Electrophoresis

For pDNA, a 1% agarose gel was prepared by dissolving agarose in TAE buffer (Tris base, acetic acid and EDTA) and boiling at 100°C. After cooling to 50°C and after the addition of EtBr, the agarose gel was set in an electrophoresis unit. Polyplexes containing 200 ng of pDNA in 20 µL 20 mM HEPES and loading buffer were placed into the sample lanes. Electrophoresis was performed at 80 V for 80 min. For siRNA, a 2.5% agarose gel containing EtBr was prepared. Polyplexes containing 500 ng of siRNA in 20 µL HEPES and loading buffer were placed into the sample lanes. Electrophoresis was performed at 80 V for 40 min.

II.4.4.7. Ethidium Bromide (EtBr) Exclusion Assay

Oligomer solution was added at increasing +/- ratios to 10 µg pDNA or siRNA in 1 mL HEPES containing 0.4 µg EtBr. After each addition, the EtBr fluorescence was measured at the excitation wavelength λ_{ex}= 510 nm and emission wavelength λ_{em}= 590 nm using a Cary Eclipse spectrophotometer (Varian, Germany). 0.4 µg EtBr in 1mL HEPES presented the blank value. Maximal fluorescence intensity was set 100% for the EtBr solution containing free nucleic acid (10 µg) and decreases in fluorescence were measured after stepwise addition of the oligomer solution.

II.4.4.8. Luciferase Gene Transfer *In Vitro* and Luciferase Assay

N2a cells or 4T1 cells were seeded in 96-well plates in 100 μL medium (10000 or 5000 cells per well respectively). After 24 h, the medium was exchanged for 80 μL fresh medium. The formed polyplexes containing 200 ng of pCMVLuc encoding plasmid per well were added in a volume of 20 μL to each well and incubated at 37˚C. LPEI at non-toxic optimum N/P 6 was used for comparison. All experiments were performed in quintuplicate. 24 h after transfection, cells were treated with 20 μL of Bright-Glo™ reagent. Luciferase activity was read spectrophotometrically using Victor^2 Wallac^{eTM} plate reader.

II.4.4.9. Luciferase Gene Silencing *In Vitro* and Luciferase Assay

Gene silencing experiments were performed in N2a/EGFPLuc cells stably expressing the CMV-EGFPLuc cassette (Clontech) encoding a fusion of enhanced green fluorescent protein and GL3 firefly luciferase under the control of the CMV promoter. Cells were grown in RNase-free cell culture flasks as described above. siRNA delivery (0.5 μg/well of either GFP-siRNA or control-siRNA) was performed in RNase-free 96-well plates (5000 cells per well, triplicates). Cells were seeded 24 h prior to transfection and then the medium replaced with 80 μL fresh growth medium containing 10% FCS. 20 μL of transfection complexes solution for siRNA delivery at different +/- ratios were added to each well and incubated at 37°C. 48 h after transfection, luciferase activity was determined as described above. Relative light units (RLU) were presented as percentage of the luciferase gene expression obtained with buffer treated control cells.

II.4.4.10. MTS Assay for Cell Viability Evaluation

N2a cells or 4T1 cells were seeded into 96-well plates at a density of 10,000 or 5000 cells/well respectively. After 24 h, culture medium was replaced with 80 μL fresh growth medium containing 10% FCS and 20 μL of transfection complexes solution at different +/- ratios were added. All studies were performed in quintuplicate. 24 h post transfection, 20 μL of manufacturer solution containing MTS/PMS (20:1) was added to each well, and the cells were incubated for a further

2 h. Optical density of each well was measured spectrophotometrically at 490 nm using Victor^2 Wallac^{eTM} plate reader. The absorbance values were represented as the percentage of cell viability taken as 100% cell viability of untreated control cells.

II.4.4.11. Red Blood Cell (RBC) Lysis Assay

Erythrocytes (RBC, red blood cells) were isolated from fresh whole mouse blood obtained by cardiac puncture after death and placed in a heparinised tube. Blood was diluted with PBS pH 7.4 up to 10 mL and then it was centrifuged (3000 rpm, 10 min, 4°C) three times, removing the supernatant after each centrifugation and re-suspending the cells in sterile PBS. The final RBC pellet was weighed and re-suspended at 2% (v/v) in PBS. To study the haemolytic activity of the systems, they were dissolved in PBS stock solutions adjusted to pH 6.5 or 7.4 and citrate solution adjusted to pH 5.5. Then samples were added to wells (n=3, 100 µL) covering the concentration range 0.1-0.01 mg/mL of systems. Buffer at the corresponding pH was used as a control together with Triton X–100 1% (w/v) to determine a 100% RBC lysis. The plates were then incubated at 37°C for 1 h. To assess haemoglobin (Hb) release the plates were then centrifuged (3000 rpm, 10 min, 20°C) and the supernatant of each well was transferred into a new plate. The Hb released was assessed by measuring the absorbance at 570 nm using Victor^2 Wallac^{eTM} plate reader. The percentage of haemolysis of each sample was calculated relative to 100% haemolysis obtained from incubation with Triton-X 100.

II.4.4.12. Confocal Fluorescence Microscopy

100 µL of 0.01% PLL were added on Chamber Slide^{TM} (0.8 cm^2/well) to coat the culture surface. After 5 min, the solution was removed by aspiration and PBS was used to wash the surface. Then, PLL was allowed to dry for 2 h before introducing cells and medium. N2a cells were seeded at a density of 25,000 on Chamber Slide™ (31,250 cells/cm^2) in 200 µL of medium and allowed to seed for 24 h at 37˚C. Culture medium was replaced with 160 µL fresh medium and 40 µL of pCMV-GFP polyplex solution was added. The cells were incubated for 24 h, at 37˚C and, then, the medium was removed and cells were washed twice with

PBS. In order to fix the cells, 200 µL of 2% paraformaldehyde at pH 7.4 was added and left to react for 20 min at RT in the dark. The medium was removed again and cells were washed twice with PBS. Then, samples were mounted using VectaShield® mounting medium with DAPI. Images were captured with a confocal microscope Leica TSC SP8 AOBS (Leica Microsystems Heidelberg and MBH, Germany) equipped with a 63 oil immersion objective. GFP was excited at 488 nm by a 496 nm laser and DAPI by a 405 nm. Images were taken on an 8-bit gray scale and processed with LEICA LAS AF Lite Software (Leica Microsystems Heidelberg and MBH, Germany).

II.4.4.13. Statistical Analysis

The results presented are an average of experiments performed in at least triplicate with standard deviation (SD). In all cases, we considered differences to be significant when $p < 0.001$ or $p < 0.01$; n.s. = non-significant > 0.05.

REFERENCES

1. Wang, K., F.M. Kievit, and M. Zhang, *Nanoparticles for cancer gene therapy: Recent advances, challenges, and strategies.* Pharmacological Research, 2016. **114**: p. 56-66.
2. Hill, A.B., et al., *Overcoming Gene-Delivery Hurdles: Physiological Considerations for Nonviral Vectors.* Trends in Biotechnology, 2016. **34**(2): p. 91-105.
3. Hersey, P. and S. Gallagher, *Intralesional immunotherapy for melanoma.* Journal of Surgical Oncology, 2014. **109**(4): p. 320-326.
4. Burnett, J.C., J.J. Rossi, and K. Tiemann, *Current progress of siRNA/shRNA therapeutics in clinical trials.* Biotechnology Journal, 2011. **6**(9): p. 1130-1146.
5. Fitzgerald, K., et al., *Effect of an RNA interference drug on the synthesis of proprotein convertase subtilisin/kexin type 9 (PCSK9) and the concentration of serum LDL cholesterol in healthy volunteers: a randomised, single-blind, placebo-controlled, phase 1 trial.* The Lancet. **383**(9911): p. 60-68.
6. Jayaraman, M., et al., *Maximizing the Potency of siRNA Lipid Nanoparticles for Hepatic Gene Silencing In Vivo.* Angewandte Chemie International Edition, 2012. **51**(34): p. 8529-8533.

7. Santel, A., et al., *A novel siRNA-lipoplex technology for RNA interference in the mouse vascular endothelium.* Gene Ther, 2006. **13**(16): p. 1222-1234.
8. Santel, A., et al., *RNA interference in the mouse vascular endothelium by systemic administration of siRNA-lipoplexes for cancer therapy.* Gene Ther, 2006. **13**(18): p. 1360-1370.
9. Aleku, M., et al., *Atu027, a Liposomal Small Interfering RNA Formulation Targeting Protein Kinase N3, Inhibits Cancer Progression.* Cancer Research, 2008. **68**(23): p. 9788-9798.
10. Landen, C.N., et al., *Therapeutic EphA2Gene Targeting In vivo Using Neutral Liposomal Small Interfering RNA Delivery.* Cancer Research, 2005. **65**(15): p. 6910-6918.
11. Kirtane, A.R. and J. Panyam, *Polymer nanoparticles: Weighing up gene delivery.* Nat Nano, 2013. **8**(11): p. 805-806.
12. Lachelt, U. and E. Wagner, *Nucleic Acid Therapeutics Using Polyplexes: A Journey of 50 Years (and Beyond).* Chem Rev, 2015. **115**(19): p. 11043-78.
13. Konstan, M.W., et al., *Compacted DNA nanoparticles administered to the nasal mucosa of cystic fibrosis subjects are safe and demonstrate partial to complete cystic fibrosis transmembrane regulator reconstitution.* Hum Gene Ther, 2004. **15**(12): p. 1255-69.
14. Merkel, O.M., et al., *In vitro and in vivo complement activation and related anaphylactic effects associated with polyethylenimine and polyethylenimine-graft-poly(ethylene glycol) block copolymers.* Biomaterials, 2011. **32**(21): p. 4936-42.
15. Plank, C., et al., *Activation of the complement system by synthetic DNA complexes: a potential barrier for intravenous gene delivery.* Hum Gene Ther, 1996. **7**(12): p. 1437-46.
16. Wagner, E., *Programmed drug delivery: nanosystems for tumor targeting.* Expert Opinion on Biological Therapy, 2007. **7**(5): p. 587-593.
17. Niño-Pariente, A., V. J. Nebot, and M.J. Vicent, *Relevant Physicochemical Descriptors of "Soft Nanomedicines" to Bypass Biological Barriers.* Current Pharmaceutical Design, 2016. **22**(9): p. 1274-1291.
18. Ragelle, H., et al., *Chitosan Nanoparticles for SiRNA Delivery In Vitro*, in *SiRNA Delivery Methods: Methods and Protocols*, K. Shum and J. Rossi, Editors. 2016, Springer New York: New York, NY. p. 143-150.

19. Rudzinski, W.E., et al., *Targeted delivery of small interfering RNA to colon cancer cells using chitosan and PEGylated chitosan nanoparticles.* Carbohydrate Polymers, 2016. **147**: p. 323-332.
20. Ohyama, A., et al., *In Vitro and In Vivo Tumor-Targeting siRNA Delivery Using Folate-PEG-appended Dendrimer (G4)/α-Cyclodextrin Conjugates.* Bioconjugate Chemistry, 2016. **27**(3): p. 521-532.
21. Eslaminejad, T., S.N. Nematollahi-Mahani, and M. Ansari, *Cationic β-Cyclodextrin–Chitosan Conjugates as Potential Carrier for pmCherry-C1 Gene Delivery.* Molecular Biotechnology, 2016. **58**(4): p. 287-298.
22. An, B., Y.-S. Lin, and B. Brodsky, *Collagen interactions: Drug design and delivery.* Advanced Drug Delivery Reviews, 2016. **97**: p. 69-84.
23. Hu-Lieskovan, S., et al., *Sequence-Specific Knockdown of EWS-FLI1 by Targeted, Nonviral Delivery of Small Interfering RNA Inhibits Tumor Growth in a Murine Model of Metastatic Ewing's Sarcoma.* Cancer Research, 2005. **65**(19): p. 8984-8992.
24. Bartlett, D.W. and M.E. Davis, *Impact of tumor-specific targeting and dosing schedule on tumor growth inhibition after intravenous administration of siRNA-containing nanoparticles.* Biotechnology and Bioengineering, 2008. **99**(4): p. 975-985.
25. Davis, M.E., et al., *Evidence of RNAi in humans from systemically administered siRNA via targeted nanoparticles.* Nature, 2010. **464**(7291): p. 1067-1070.
26. Kadlecova, Z., et al., *Poly(ethyleneimine)-Mediated Large-Scale Transient Gene Expression: Influence of Molecular Weight, Polydispersity and N-Propionyl Groups.* Macromolecular Bioscience, 2012. **12**(5): p. 628-636.
27. Kunath, K., et al., *Low-molecular-weight polyethylenimine as a non-viral vector for DNA delivery: comparison of physicochemical properties, transfection efficiency and in vivo distribution with high-molecular-weight polyethylenimine.* Journal of Controlled Release, 2003. **89**(1): p. 113-125.
28. Yin, H., et al., *Non-viral vectors for gene-based therapy.* Nat Rev Genet, 2014. **15**(8): p. 541-555.
29. *https://clinicaltrials.gov.*
30. Duro-Castano, A., I. Conejos-Sánchez, and M. Vicent, *Peptide-Based Polymer Therapeutics.* Polymers, 2014. **6**(2): p. 515.

31. Zauner, W., M. Ogris, and E. Wagner, *Polylysine-based transfection systems utilizing receptor-mediated delivery.* Advanced Drug Delivery Reviews, 1998. **30**(1–3): p. 97-113.
32. Tappertzhofen, K., et al., *Bioreducible Poly-l-Lysine–Poly[HPMA] Block Copolymers Obtained by RAFT-Polymerization as Efficient Polyplex-Transfection Reagents.* Macromolecular Bioscience, 2016. **16**(1): p. 106-120.
33. Tappertzhofen, K., et al., *Poly-l-Lysine–Poly[HPMA] Block Copolymers Obtained by RAFT Polymerization as Polyplex-Transfection Reagents with Minimal Toxicity.* Macromolecular Bioscience, 2015. **15**(8): p. 1159-1173.
34. Heller, P., et al., *Introducing PeptoPlexes: Polylysine-block-Polysarcosine Based Polyplexes for Transfection of HEK 293T Cells.* Macromolecular Bioscience, 2014. **14**(10): p. 1380-1395.
35. Christie, R.J., N. Nishiyama, and K. Kataoka, *Delivering the code: polyplex carriers for deoxyribonucleic acid and ribonucleic acid interference therapies.* Endocrinology, 2010. **151**(2): p. 466-73.
36. Miyata, K., N. Nishiyama, and K. Kataoka, *Rational design of smart supramolecular assemblies for gene delivery: chemical challenges in the creation of artificial viruses.* Chemical Society Reviews, 2012. **41**(7): p. 2562-2574.
37. Martin, I., et al., *Solid-phase-assisted synthesis of targeting peptide-PEG-oligo(ethane amino)amides for receptor-mediated gene delivery.* Organic & Biomolecular Chemistry, 2012. **10**(16): p. 3258-3268.
38. Grosse, S.M., et al., *Tumor-specific gene transfer with receptor-mediated nanocomplexes modified by polyethylene glycol shielding and endosomally cleavable lipid and peptide linkers.* The FASEB Journal, 2010. **24**(7): p. 2301-2313.
39. Ogris, M., et al., *PEGylated DNA/transferrin-PEI complexes: reduced interaction with blood components, extended circulation in blood and potential for systemic gene delivery.* Gene Ther, 1999. **6**(4): p. 595-605.
40. Kircheis, R., et al., *Polyethylenimine/DNA complexes shielded by transferrin target gene expression to tumors after systemic application.* Gene Ther, 2001. **8**(1): p. 28-40.
41. Simões, S., et al., *Human serum albumin enhances DNA transfection by lipoplexes and confers resistance to inhibition by serum.* Biochimica et Biophysica Acta (BBA) - Biomembranes, 2000. **1463**(2): p. 459-469.

42. Tian, H., et al., *RGD targeting hyaluronic acid coating system for PEI-PBLG polycation gene carriers.* Journal of Controlled Release, 2011. **155**(1): p. 47-53.
43. Li, Y., et al., *Zwitterionic Poly(carboxybetaine)-based Cationic Liposomes for Effective Delivery of Small Interfering RNA Therapeutics without Accelerated Blood Clearance Phenomenon.* Theranostics, 2015. **5**(6): p. 583-596.
44. Singer, J.W., et al., *Paclitaxel poliglumex (XYOTAX; CT-2103): an intracellularly targeted taxane.* Anti-Cancer Drugs, 2005. **16**(3): p. 243-254.
45. Duncan, R. and M.J. Vicent, *Polymer therapeutics-prospects for 21st century: The end of the beginning.* Advanced Drug Delivery Reviews, 2013. **65**(1): p. 60-70.
46. Dubruel, P., et al., *Poly-l-glutamic Acid Derivatives as Multifunctional Vectors for Gene Delivery. Part B. Biological Evaluation.* Biomacromolecules, 2003. **4**(5): p. 1177-1183.
47. Dekie, L., et al., *Poly-l-glutamic acid derivatives as vectors for gene therapy.* Journal of Controlled Release, 2000. **65**(1–2): p. 187-202.
48. Tian, H., et al., *Gene transfection of hyperbranched PEI grafted by hydrophobic amino acid segment PBLG.* Biomaterials, 2007. **28**(18): p. 2899-2907.
49. Chen, L., et al., *Multi-armed poly(L-glutamic acid)-graft-oligoethylenimine copolymers as efficient nonviral gene delivery vectors.* The Journal of Gene Medicine, 2010. **12**(1): p. 64-76.
50. Kurosaki, T., et al., *γ-Polyglutamic acid-coated vectors for effective and safe gene therapy.* Journal of Controlled Release, 2010. **142**(3): p. 404-410.
51. Kurosaki, T., et al., *Ternary complexes of pDNA, polyethylenimine, and γ-polyglutamic acid for gene delivery systems.* Biomaterials, 2009. **30**(14): p. 2846-2853.
52. Guo, S., et al., *Ternary complexes of amphiphilic polycaprolactone-graft-poly (N,N-dimethylaminoethyl methacrylate), DNA and polyglutamic acid-graft-poly(ethylene glycol) for gene delivery.* Biomaterials, 2011. **32**(18): p. 4283-4292.
53. Schaffert, D., N. Badgujar, and E. Wagner, *Novel Fmoc-Polyamino Acids for Solid-Phase Synthesis of Defined Polyamidoamines.* Organic Letters, 2011. **13**(7): p. 1586-1589.

54. Leng, Q., et al., *Highly branched HK peptides are effective carriers of siRNA.* The Journal of Gene Medicine, 2005. **7**(7): p. 977-986.
55. Chen, C.-P., et al., *Gene Transfer with Poly-Melittin Peptides.* Bioconjugate Chemistry, 2006. **17**(4): p. 1057-1062.
56. EL Andaloussi, S., et al., *Design of a peptide-based vector, PepFect6, for efficient delivery of siRNA in cell culture and systemically in vivo.* Nucleic Acids Research, 2011. **39**(9): p. 3972-3987.
57. Merrifield, R.B., *Solid Phase Peptide Synthesis. I. The Synthesis of a Tetrapeptide.* Journal of the American Chemical Society, 1963. **85**(14): p. 2149-2154.
58. Hartmann, L., et al., *Solid-Phase Supported Polymer Synthesis of Sequence-Defined, Multifunctional Poly(amidoamines).* Biomacromolecules, 2006. **7**(4): p. 1239-1244.
59. Hartmann, L., et al., *Tailor-Made Poly(amidoamine)s for Controlled Complexation and Condensation of DNA.* Chemistry – A European Journal, 2008. **14**(7): p. 2025-2033.
60. Hartmann, L. and H.G. Börner, *Precision Polymers: Monodisperse, Monomer-Sequence-Defined Segments to Target Future Demands of Polymers in Medicine.* Advanced Materials, 2009. **21**(32-33): p. 3425-3431.
61. Hartmann, L., *Polymers for Control Freaks: Sequence-Defined Poly(amidoamine)s and Their Biomedical Applications.* Macromolecular Chemistry and Physics, 2011. **212**(1): p. 8-13.
62. Boussif, O., et al., *A versatile vector for gene and oligonucleotide transfer into cells in culture and in vivo: polyethylenimine.* Proceedings of the National Academy of Sciences of the United States of America, 1995. **92**(16): p. 7297-7301.
63. Behr, J.-P., *The Proton Sponge: a Trick to Enter Cells the Viruses Did Not Exploit.* CHIMIA International Journal for Chemistry, 1997. **51**(1-2): p. 34-36.
64. Uchida, H., et al., *Odd–Even Effect of Repeating Aminoethylene Units in the Side Chain of N-Substituted Polyaspartamides on Gene Transfection Profiles.* Journal of the American Chemical Society, 2011. **133**(39): p. 15524-15532.
65. Suma, T., et al., *Enhanced stability and gene silencing ability of siRNA-loaded polyion complexes formulated from polyaspartamide derivatives with a repetitive array of amino groups in the side chain.* Biomaterials, 2012. **33**(9): p. 2770-2779.

66. Russ, V., et al., *Improved in vivo gene transfer into tumor tissue by stabilization of pseudodendritic oligoethylenimine-based polyplexes.* The Journal of Gene Medicine, 2010. **12**(2): p. 180-193.
67. Lee, C.-C., Y. Liu, and T.M. Reineke, *General Structure–Activity Relationship for Poly(glycoamidoamine)s: The Effect of Amine Density on Cytotoxicity and DNA Delivery Efficiency.* Bioconjugate Chemistry, 2008. **19**(2): p. 428-440.
68. Schaffert, D., et al., *Solid-Phase Synthesis of Sequence-Defined T-, i-, and U-Shape Polymers for pDNA and siRNA Delivery.* Angewandte Chemie International Edition, 2011. **50**(38): p. 8986-8989.
69. Sonawane, N.D., F.C. Szoka, and A.S. Verkman, *Chloride Accumulation and Swelling in Endosomes Enhances DNA Transfer by Polyamine-DNA Polyplexes.* Journal of Biological Chemistry, 2003. **278**(45): p. 44826-44831.
70. Akinc, A., et al., *Exploring polyethylenimine-mediated DNA transfection and the proton sponge hypothesis.* The Journal of Gene Medicine, 2005. **7**(5): p. 657-663.
71. Benjaminsen, R.V., et al., *The Possible "Proton Sponge " Effect of Polyethylenimine (PEI) Does Not Include Change in Lysosomal pH.* Molecular Therapy, 2013. **21**(1): p. 149-157.
72. Wagner, E., *Polymers for siRNA Delivery: Inspired by Viruses to be Targeted, Dynamic, and Precise.* Accounts of Chemical Research, 2012. **45**(7): p. 1005-1013.
73. Scholz, C., et al., *Correlation of Length of Linear Oligo(ethanamino) Amides with Gene Transfer and Cytotoxicity.* ChemMedChem, 2014. **9**(9): p. 2104-2110.
74. Schaffert, D., C. Troiber, and E. Wagner, *New Sequence-Defined Polyaminoamides with Tailored Endosomolytic Properties for Plasmid DNA Delivery.* Bioconjugate Chemistry, 2012. **23**(6): p. 1157-1165.
75. Salcher, E.E., et al., *Sequence-defined four-arm oligo(ethanamino)amides for pDNA and siRNA delivery: Impact of building blocks on efficacy.* Journal of Controlled Release, 2012. **164**(3): p. 380-386.
76. Troiber, C., et al., *Stabilizing effect of tyrosine trimers on pDNA and siRNA polyplexes.* Biomaterials, 2013. **34**(5): p. 1624-1633.
77. Fröhlich, T., et al., *Structure–activity relationships of siRNA carriers based on sequence-defined oligo (ethane amino) amides.* Journal of Controlled Release, 2012. **160**(3): p. 532-541.

78. Pichon, C., C. Gonçalves, and P. Midoux, *Histidine-rich peptides and polymers for nucleic acids delivery.* Advanced Drug Delivery Reviews, 2001. **53**(1): p. 75-94.
79. Bertrand, E., et al., *Histidinylated linear PEI: a new efficient non-toxic polymer for gene transfer.* Chemical Communications, 2011. **47**(46): p. 12547-12549.
80. Barz, M., A. Duro-Castano, and M.J. Vicent, *A versatile post-polymerization modification method for polyglutamic acid: synthesis of orthogonal reactive polyglutamates and their use in "click chemistry".* Polymer Chemistry, 2013. **4**(10): p. 2989-2994.
81. Pelet, J.M. and D. Putnam, *An In-Depth Analysis of Polymer-Analogous Conjugation using DMTMM.* Bioconjugate Chemistry, 2011. **22**(3): p. 329-337.
82. Kunishima, M., et al., *Synthesis and Characterization of 4-(4,6-Dimethoxy-1,3,5-triazin-2-yl)-4-methylmorpholinium Chloride.* Tetrahedron Letters, 1999. **40**(29): p. 5327-5330.
83. Plank, C., et al., *The influence of endosome-disruptive peptides on gene transfer using synthetic virus-like gene transfer systems.* J Biol Chem, 1994. **269**(17): p. 12918-24.
84. Lächelt, U., et al., *Fine-tuning of proton sponges by precise diaminoethanes and histidines in pDNA polyplexes.* Nanomedicine: Nanotechnology, Biology and Medicine. **10**(1): p. 35-44.
85. Dohmen, C., et al., *Defined Folate-PEG-siRNA Conjugates for Receptor-specific Gene Silencing.* Molecular therapy. Nucleic acids, 2012. **1**(1): p. e7.
86. Scholz, C. and E. Wagner, *Therapeutic plasmid DNA versus siRNA delivery: Common and different tasks for synthetic carriers.* Journal of Controlled Release, 2012. **161**(2): p. 554-565.
87. van der Vlies, A.J., et al., *Synthesis of Pyridyl Disulfide-Functionalized Nanoparticles for Conjugating Thiol-Containing Small Molecules, Peptides, and Proteins.* Bioconjugate Chemistry, 2010. **21**(4): p. 653-662.
88. Dohmen, C., et al., *Nanosized Multifunctional Polyplexes for Receptor-Mediated SiRNA Delivery.* ACS Nano, 2012. **6**(6): p. 5198-5208.
89. Tsou, C.C. and S.S. Sun, *New fluorescent amide-functionalized phenylethynylthiophene low molecular weight gelator.* Organic Letters, 2006. **8**(3): p. 387-390.

90. Tu, T., et al., *Visual Chiral Recognition through Enantioselective Metallogel Collapsing: Synthesis, Characterization, and Application of Platinum–Steroid Low-Molecular-Mass Gelators.* Angewandte Chemie International Edition, 2011. **50**(29): p. 6601-6605.
91. Kaiser, E., et al., *Color test for detection of free terminal amino groups in the solid-phase synthesis of peptides.* Analytical Biochemistry, 1970. **34**(2): p. 595-598.

Chapter III

Development of Non-Viral Polypeptide-Based Carriers for siRNA Delivery

The work presented within this thesis chapter was carried out in close collaboration with Dr. Elena Gallon and Dr. Inmaculada Conejos Sánchez.

III.1. INTRODUCTION AND BACKGROUND

As stated in Chapter II, gene therapy is an experimental technique offering a wide spectrum of applications including regulation, repair, and replacement of mutated genes to treat genetic diseases. Gene therapy currently represents a promising option for inherited genetic disorders, certain viral infections, and also some types of cancer. Cancer is often associated with complex genetic alterations and constitutes an incurable illness. Classical gene therapy, in terms of the substitution of deficient genes by transfer of genetic material, represents the first therapeutic application of nucleic acids [1, 2]. The first gene therapy achieved market approval by the European Commission in 2012 (alipogene tiparvovec, Glybera® [3]) and by April 2017 [4] 2400 clinical gene therapy trials encompassing three decades of work were completed, ongoing, or approved worldwide. Safety data accumulated during this time has permitted the development and improvement of safer and more efficient gene therapy approaches.

Among the diverse subtypes of oligonucleotides evaluated for gene therapy, perhaps the best-known and most studied is the application of small interfering RNA (siRNA) for RNA interference (RNAi). RNAi gene specific silencing in nematodes was discovered in 1998 by Fire and Mello [5]. However, this technique was not effective in mammalian cells, where the long (over 30 base pairs (bp)) double stranded RNA (dsRNA) induced immune reactions and cell death. The use of a shorter 21 bp RNA avoided unwanted immune responses and allowed effective gene silencing in mammalian cells [6]. The ability to selectively downregulate single genes at the post transcriptional level led to a revolution in basic cell biology, opening a completely new and potent platform for drug development. The siRNA mechanism (Figure III.1) starts with the introduction of dsRNA or synthetic siRNA into cells. When dsRNA enters the cell, it is recognised by the Dicer enzyme which

cleaves the dsRNA into fragments of 21-23 bp (siRNA) [7]. Alternatively, synthetically produced siRNA can be introduced directly [6].

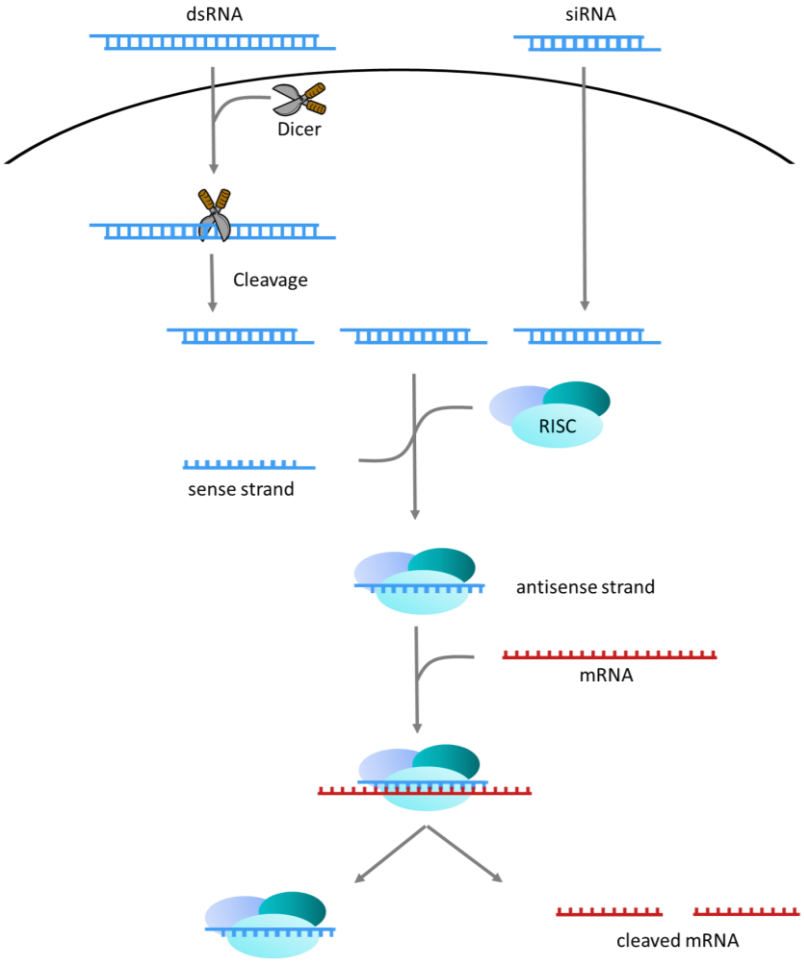

Figure III.1. Mechanism of siRNA silencing by introduction of dsRNA or synthetic siRNA.

Once in the cytosol, siRNA fragments are recognised by the multi-protein RNA-induced silencing complex (RISC), and unwound by Argonaute2 (AGO2). While the sense strand is released and degraded, the antisense strand remains incorporated in the RISC complex [8]. If complementary messenger RNA (mRNA) is present, the siRNA guided RISC complex will bind the mRNA, leading to degradation or translational inhibition [9, 10]. The RISC-antisense strand complex

remains stable during this process and, therefore, can attach to another corresponding mRNA, thereby propagating gene silencing. Overall, this process constitutes an important and precise epigenetic tool for the regulation of gene expression. After unravelling this mechanism, many opportunities for therapeutic purposes emerged and its translation to clinical trials has evolved rapidly [11].

Although siRNA has been extensively studied for application as a pharmaceutical drug [12, 13], "naked" siRNA suffers the same limitations as many other macromolecules (proteins, peptides, antibodies, DNA, *etc.)* during the delivery process. These restrictions include enzymatic degradation over renal clearance, interaction with blood components, activation of the immune system, and inefficient uptake by target cells. Therefore, siRNA requires an appropriate carrier system to fulfil its potential. As natural nucleic acid vehicles, viruses (such as adenovirus, retrovirus, and adeno-associated virus) are the most investigated vectors for gene therapy [4, 14]. Despite their high efficiency, these viral vectors exhibit serious disadvantages which restrict its progress. Immunogenicity, limited cargo loading, high production costs, and the risk of promoting cancer by insertional mutagenesis are their main drawbacks [14-16], which led to the development of more advantageous synthetic structures [17].

New and improved nucleic acid carriers must be multifunctional, bioresponsive to a dynamic environment, and specific. Their design has to consider the delivery route and the individual hurdles which are likely to be encountered [18]. Recently, polypeptides have been evaluated as siRNA carriers [19] as they allow stable nucleic acid complexation/conjugation and encourage cellular uptake, subsequent endosomal escape and intracellular cargo release at the target site. Additionally, polypeptides exhibit reduced cytotoxicity, immunogenicity as well as biodegradability [20]. However, viruses are advantageous over polypeptides in that they have evolved to use natural mechanisms to enter cells [21].

In brief, polypeptides represent a simpler, cost-effective, and potentially less immunogenic class of gene delivery agents than viruses

[22]. However, polypeptides still face some major challenges, including a lack of cell and tissue specificity and inefficient endosomal escape. A manufactured drug substance should be homogenous and composed of a single, defined species. By the contrast, it is important to note that, most of the reported polypeptides used for gene therapy by far have been synthesised through random polymerisation techniques, ending up in high polydispersity products and poor architecture control. Total control of crucial parameters such as chain length, molecular weight (MW), polydispersity, microstructure, final conformation as well as localisation of charge or hydrophobic-hydrophilic balance are key to adequately tailor nanomedicine body distribution, fate, biological activity and toxicity [23-25]. Therefore, the development and exhaustive physicochemical characterisation of defined polypeptides with a fully defined structure and content would provide precise data and enable the design of more efficient delivery systems [26-28].

Improvement of polymerisation techniques (mainly N-carboxyanhydride ring-opening polymerisation (NCA-ROP)) [29] and synthetic chemistry have permitted the production of polypeptides with narrow polydispersity, minimal side product formation, high reproducibility, and precise functionalisation of the polypeptide backbone [30].

This thesis chapter is focused on the design, development, and validation of non-viral polypeptide-based carriers for oligonucleotide delivery. Three different polymeric platforms based on natural or synthetic polyaminoacids were evaluated, aiming to improve gene silencing by conferring them the capability of modulating the endosomal buffer capacity, improving pharmacokinetics and achieving efficient gene transfer by using among others: (i) polypeptides with different ζ-potential in order to explore safety *vs.* transfection efficiency and (ii) covalent conjugation approaches *vs*. complexation to explore the need of trigger release *vs.* nanoconstruct stability. These platforms were based on poly-L-glutamic acid (PGA), poly-L-arginine (PArg) and poly-L-ornithine (P(Orn)) obtained through controlled NCA-ROP techniques [26, 27] and adequately derivatised by post-polymerisation

modification [31] to achieve the adequate ζ-potential and orthogonal conjugation sites (Figure III.2 summarises the different systems studied).

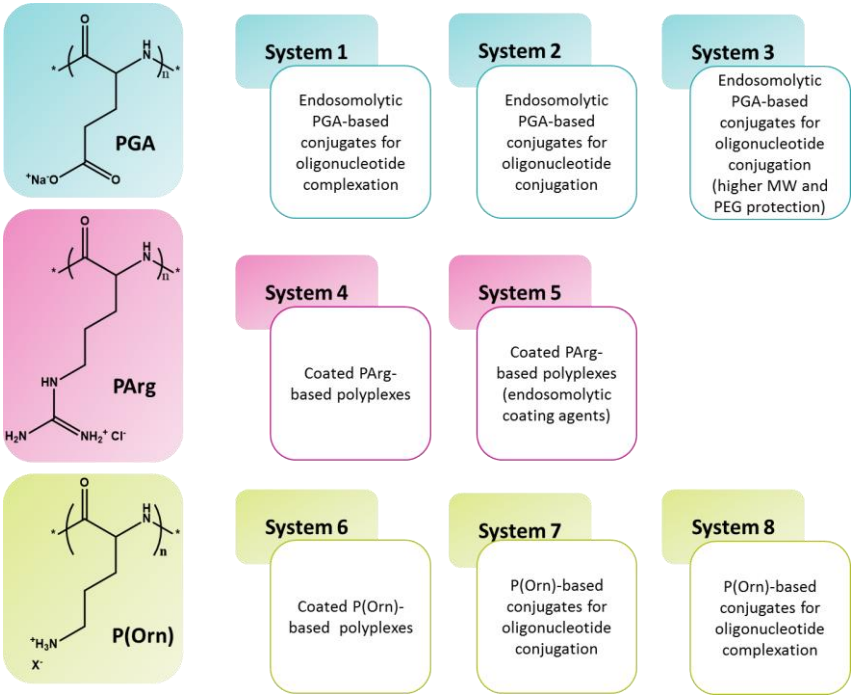

Figure III.2. Summary of the developed systems.

III.2. RESULTS AND DISCUSSION

III.2.1. Poly-L-Glutamic Acid (PGA)-Based Systems (Systems 1-3)

Positively charged cationic polymers have been extensively proposed as vectors for negatively charged oligonucleotides as they readily form complexes due to their intrinsic attraction [32, 33]. However, the major problem of cationic polymers is their unwanted interaction with erythrocytes and the subsequent haemolysis and haemagglutination. Furthermore, many cationic polymers are not biodegradable and repeated administration may, therefore, lead to lysosomal storage disease. To overcome this problem, a well-defined PGA was selected as biocompatible, and biodegradable carrier [34-36], functionalising its main chain with secondary and ternary amines. The

resultant polypeptide-based carriers were evaluated as possible gene delivery vehicles. These modifications aim to diminish the negative charge inherent to PGA providing in addition multiple advantageous qualities, such as an enhancement in endosomolytic capacity [37] enhancing the possible release of the nucleic acid into the cytosol.

III.2.1.1. Systems 1 and 2 - PGA-Based Systems: Functionalisation with Endosomolytic Molecules. Complexation and Conjugation of Oligonucleotides

III.2.1.1.1. Synthetic Approaches

In order to achieve PGA complexation/conjugation with oligonucleotides, a rational design was followed reducing the negative charges in parallel with conferring vector specific functions through the addition of endosomolytic moieties: histidine (Hist) or morpholine (Morph). Both were introduced via DMTMM·Cl (4-(4,6-Dimethoxy-1,3,5-triazin-2-yl)-4-methylmorpholinium chloride) activation of the polypeptide chain carboxyl groups (Figure III.3) [31]. The mechanism of action of DMTMM·Cl was already described in Chapter II, Section II.2.2.

L-histidine methyl ester and 3-morpholinopropylamine contain an imidazole ring (pKa_3 6.5) and a morpholine ring (pKa 6.2), respectively, which increase the buffering capacity of endosomes. This aids the endosomal escape of modified oligonucleotides after cell endocytosis, a crucial and rate-limiting step to trigger transfection. The imidazole and morpholine rings have been previously used for this purpose in several non-viral gene carriers, such as dendrimers [38], cationic polymers [39-41], and lipids [42, 43]. Moreover, various studies have shown that the modification of highly positively charged polymers, peptides, and liposomes with imidazole-containing groups (such as histidine) resulted in reduced cytotoxicity in comparison with the parent systems, without reducing their endosomolytic capacity [44].

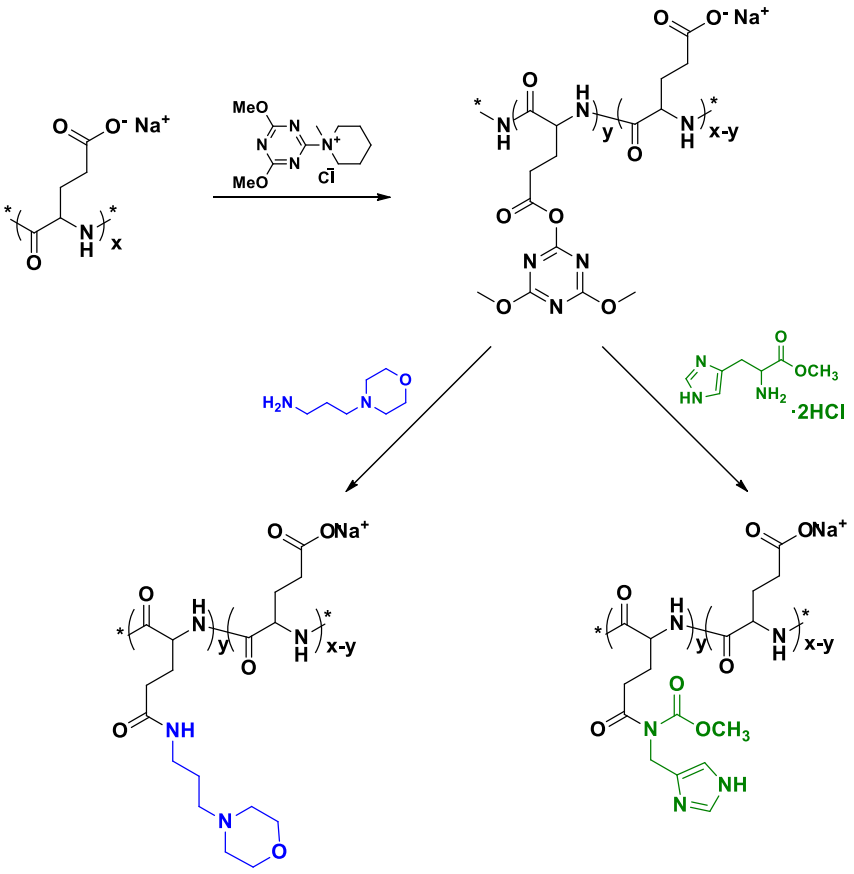

Figure III.3. Schematic representation of PGA-Hist and PGA-Morph synthesis via DMTMM·Cl activation.

System 1 compounds are detailed in Table III.1. Since the length of the PGA backbone may induce significant conformational fluctuations and influence the complexing capacity, different lengths of PGA (20 and 50 GAU (glutamic acid units)) were evaluated to select the best candidate. Reactions proceeded quantitatively as determined by ^{1}H NMR (Figure III.4 and Figure III.5).

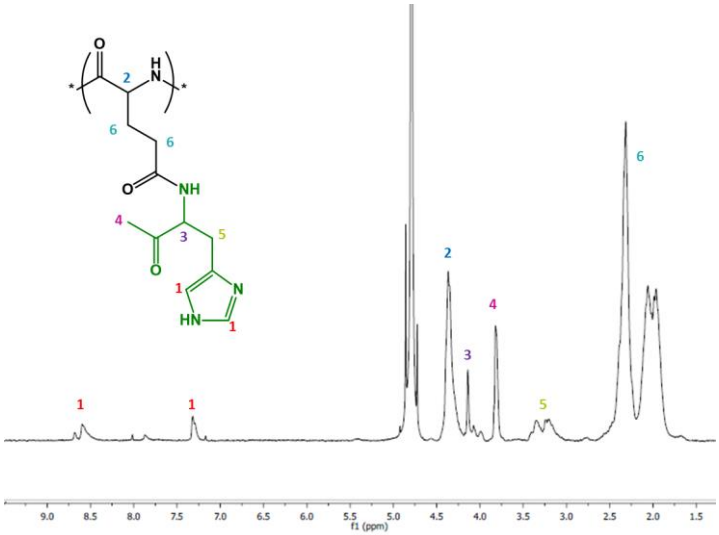

Figure III.4. ^{1}H NMR spectrum with assignments for PGA-Hist.

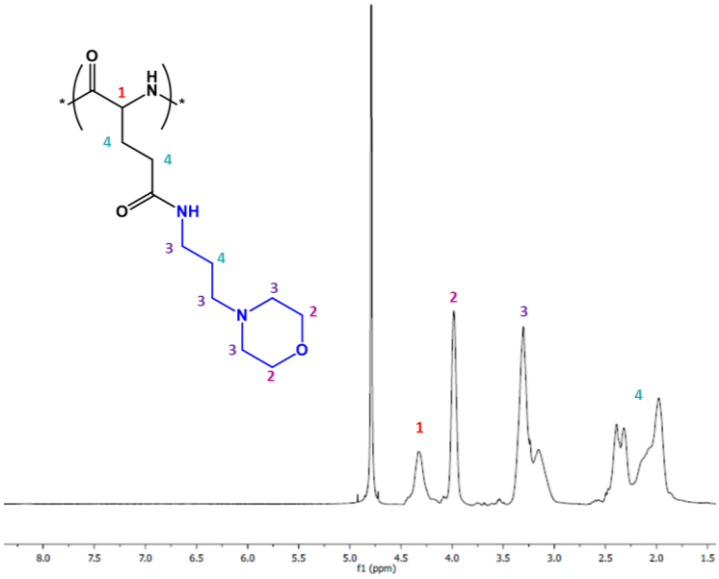

Figure III.5. ^{1}H NMR spectrum with assignments for PGA-Morph.

To further diminish the remaining negative charge of the PGA chain, amino-2-propanol (ApOH) or L-arginine methyl ester (Arg, provides an additional positive charge) were conjugated using the same coupling strategy (Figure III.6).

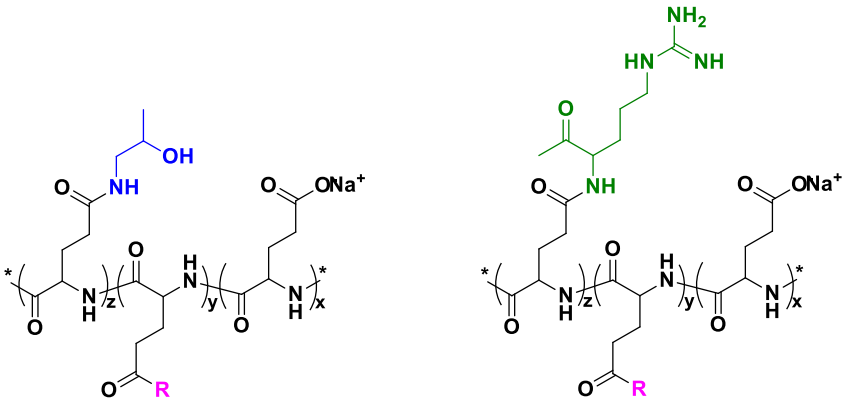

Figure III.6. Schematic representation of PGA-Hist or PGA-Morph functionalised with amino-2-propanol (left) and L-arginine methyl ester (right). R= previously introduced Hist or Morph moieties.

Taking into account the total charge values shown in Table III.1, **PHArg2** (PGA_{50}-Hist15%-Arg75%, 33(+)) and **PMArg2** (PGA_{50}-Morph60%-Arg31%, 11(+)) were expected to induce the least electrostatic repulsion with the oligonucleotide. Binding ability of both conjugates was tested by gel shift assay using a small doubled stranded DNA, dsDNA (22 bp) as a model of oligonucleotide. However, System 1 PGA derivatives did not form stable complexes even at high charge-ratio (+/-). To solve this problem, conjugation of the nucleic acid to the PGA chain (**System 2**) was explored through a biodegradable and reversible linkage (disulphide bond), modifying some of the already synthesised System 1 derivatives. Disulphide bonds guarantee site-specific conjugation and oligonucleotide release in the reducing environment encountered in the cell cytoplasm [45, 46]. Pyridyl disulphide (PD) molecules were incorporated into the already synthesised PGA-vectors (Figure III.7) using the same protocol as described in Chapter II (Section II.2.4). Under the same rational design previously explained, three different lengths of PGA were studied (20, 50 and 100 GAU). All the resulting products are disclosed in Table III.2.

Table III.1. System 1 conjugates synthesis and characterisation.

Conjugate Polymer	Id	GAU	Loading[a] (mol%)					Total charge at pH 7[b]	MW[b] (g/mol)
			Morph	Hist	Arg	ApOH	free COOH		
PGA-Hist-Arg	**PHArg1**	20	-	15	50	-	35	**3 (+)**	4685
	PHArg2	50	-	15	75	-	10	**33 (+)**	13373
PGA-Hist-ApOH	**PHApOH**	50	-	15	-	50	35	**18 (-)**	9288
PGA-Morph-Arg	**PMArg1**	20	52	-	21	-	27	**2 (-)**	4656
	PMArg2	50	60	-	31	-	9	**11 (+)**	12716
PGA-Morph-ApOH	**PMApOH**	50	60	-	-	25	15	**8 (-)**	11108

[a] Determined by ^{1}H NMR; [b] Estimated after ^{1}H NMR analysis. MW= molecular weight.

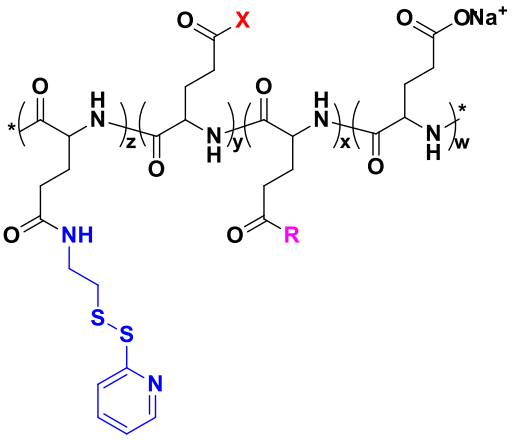

Figure III.7. Schematic representation of pyridyl disulphide conjugates. R= Hist or Morph; X= ApOH or Arg.

The conjugation of dsDNA to the PGA backbone via disulphide bond formation occurs by the simple addition of the oligonucleotide with an additional terminal thiol group, (-SH) into a solution containing the PGA derivative (Figure III.8).

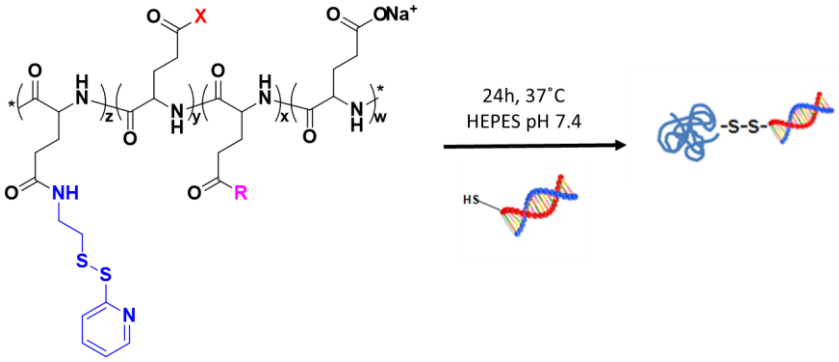

Figure III.8. Schematic representation for the synthesis of PGA-dsDNA conjugates.

Table III.2. System 2 polypeptide family.

Conjugate Polymer	Id	GAU	Loading[a] (mol%)						Total charge at pH 7[b]	MW[b] (g/mol)
			Morph	Hist	Arg	ApOH	PD	free COOH		
PGA-Hist-Arg-PD	**PHArgPD1**	20	-	15	50	-	10	25	**5 (+)**	4977
	PHArgPD2	50	-	24	33	-	7	36	**1 (-)**	12048
	PHArgPD3	100	-	16	23	-	8	53	**30 (-)**	21728
PGA-Morph-Arg-PD	**PMArgPD1**	20	52	-	21	-	5	22	**1 (-)**	4802
	PMArgPD2	50	60	-	31	-	4	5	**13 (+)**	13008
	PMArgPD3	50	50	-	24	-	1	25	**1 (-)**	11807
	PMArgPD4	50	63	-	24	-	6	7	**9 (+)**	12848
	PMArgPD5	50	41	-	20	-	7	32	**6 (-)**	11513
	PMArgPD6	50	50	-	25	-	4	21	**2 (+)**	12092
	PMArgPD7	100	47	-	14	-	6	33	**19 (-)**	22940
PGA-Morph-ApOH-PD	**PMApOHPD**	50	60	-	-	25	7	8	**4 (+)**	11618

[a] Determined by 1H NMR; [b] Estimated after ^{1}H NMR analysis.

Taking into account the total charge values shown in Table III.2, **PMArgPD2** (PGA_{50}-Morph60%-Arg31%-PD4%, 13(+)), **PMApOHPD** (PGA_{50}-Morph60%-ApOH25%-PD7%, 4(+)), and **PHArgPD1** (PGA_{20}-Hist15%-Arg50%-PD10%, 5(+)) were expected to induce the least electrostatic repulsion with the oligonucleotide. These polymers allowed the study of the role of Arg and ApOH on the PGA main chain trying to enhance its cytosolic potential.

III.2.1.1.2. DNA Binding Assay Electrophoresis

Oligonucleotide conjugation with the three selected polymers (**PMArgPD2**, **PMApOHPD** and **PHArgPD1**) was qualitatively evaluated through agarose gel electrophoresis technique. The optimisation of the experimental conditions for dsDNA conjugation to the selected carriers was performed. To certify such conjugation efficiency, 1,4-dithiothreitol (DTT, a reducing agent) was added (Figure III.9) [47].

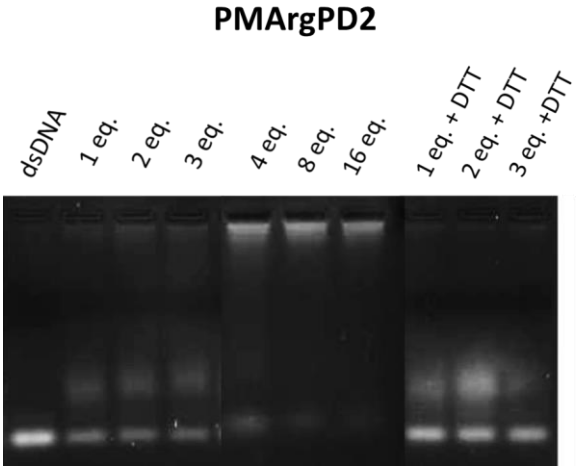

Figure III.9. dsDNA conjugation efficiency to **PMArgPD2** determined by an agarose gel shift assay using different equivalents of the PGA-based polymer (1 to 16 eq **PMArgPD2)** per 0.04 equivalents of dsDNA (500 ng), with and without DTT.

Figure III.9 shows DNA presence (signified by white bands) in the loading wells of the samples without DTT and with lower amounts of free DNA (bottom band) as compared with the control dsDNA. Additionally, the bands in the loading wells disappear upon addition of DTT and the free DNA signal increases. Therefore, it could be said that a successful dsDNA conjugation to the PGA backbone via disulphide

bond formation may has occurred. The best ratio was 16 equivalents of polymer per 0.04 equivalents of dsDNA with almost free DNA absence.

On the other hand, **PMApOHPD** conjugate required polymer/dsDNA ratios of 1-40 equivalents per 0.07 equivalents of dsDNA (500 ng), according to the ratio of PD groups in the PGA derivative (Figure III.10). DNA-conjugate retention was worse as compared to **PMArgPD2**, probably due to the different resulting ζ-potential. Nonetheless, the observed signal for the polymer was different from control (dsDNA) concluding that dsDNA was at least partly conjugated.

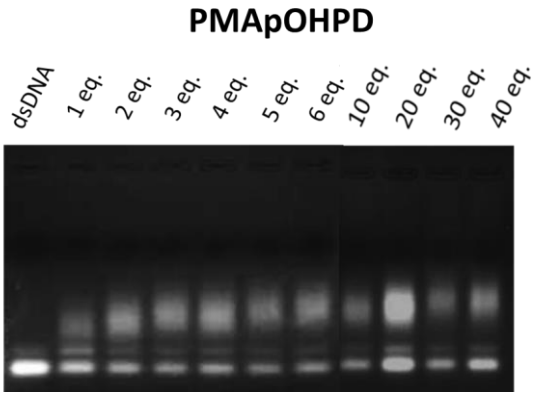

Figure III.10. dsDNA conjugation efficiency to **PMApOHPD** determined by an agarose gel shift assay by using different equivalents of the PGA-based polymer. 1-40 eq. PMApOHPD per 0.07 equivalents dsDNA (500 ng).

Polymer **PHArgPD1** (PGA_{20}-Hist15%-Arg50%-PD10%) did not show dsDNA retention suggesting that DNA conjugation had not occurred. After these results, it is clear that the nature of the molecule used for side-chain modification (morpholine better than histidine) is more important than the degree of PD derivatisation. Therefore, **PMArgPD2** was selected as the best candidate to move forward.

III.2.1.1.3. Red Blood Cell (RBC) Lysis Assay

As the synthesised conjugates are proposed for intravenous (IV) administration, their ability to induce red blood cell (RBC) lysis *in vitro* was carried out as a preliminary measure of haematocompatibility [48]. For this purpose, PMArgPD2, PMApOHPD, and PHArgPD1 polymers

were incubated with RBCs (Figure III.11). None of the conjugates showed haemolytic properties either at physiological pH (7.4) or at endosomal pH (5.5) indicating their suitability for IV administration. Triton X-100 and PBS (pH 7.4) or citrate buffer (pH 5.5) at the corresponding pH were used as positive and negative control, respectively.

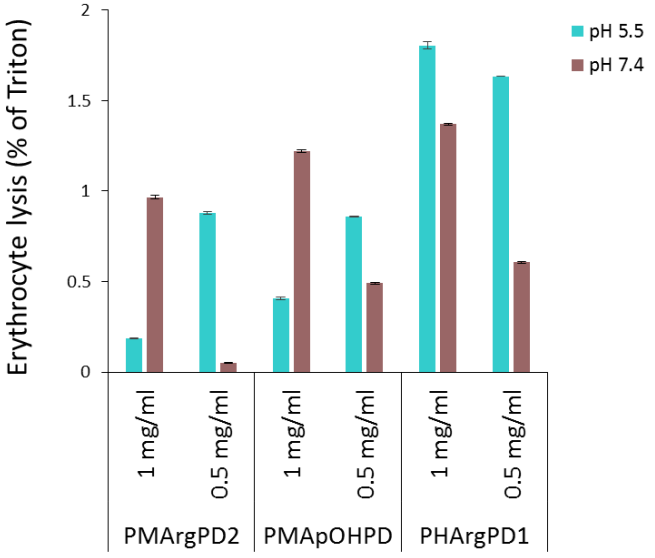

Figure III.11. Erythrocyte leakage assay at different pH values: compounds were incubated with erythrocytes at different concentrations at 37°C at indicated pH values. Haemoglobin release was measured after 1 h. Data expressed as mean ± SD, n=3

III.2.1.1.4. Buffer Capacity- Potentiometric Titration

The buffer capacity of the polymer **PMArg2** (PGA_{50}-Morph60%-Arg31%), a precursor of **PMArgPD2**, was tested by alkalimetric titration at a pH range of 5.0 and 7.4. This range represents the physiologically relevant acidification from pH 7.4 in the blood or cell cytosol to pH 5.0 in the endosome/lysosome. Figure III.12 shows the titration curves with the highlighted endosomal range. The titration curve of **PMArg2** demonstrated a significant difference between both pHs compared with NaCl used as reference titration, mainly indicating an endosomal buffer capacity due to the deprotonation of morpholine rings (35% buffer capacity calculated through Equation III.1, Section III.4.4.16). The

gradient of the curve had its minimum around pH 6. However, above pH 8 the titration curve showed a similar course as NaCl since the amount of morpholine rings available for deprotonation decreases exponentially with increasing pH.

The polymer **PMArg2** exhibited a continuous buffering capability over a broad range, including the endosomal area and above, which suggests that the polymer presents sufficient buffering capacity for endosomal escape.

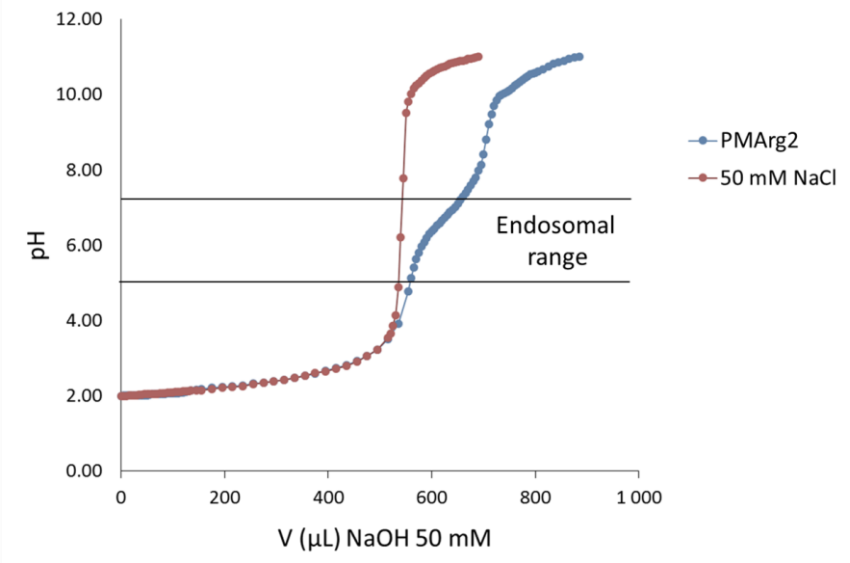

Figure III.12. Potentiometric titration of **PMArg2** (PGA_{50}-Morph60%-Arg31%). Amounts corresponding to 15 µmol protonatable amines.

III.2.1.1.5. Cell Culture Media and Plasma Stability

Stability of the conjugates in cell culture media was carried out using DTT to certify that dsDNA was still conjugated. As observed in Figure III.13 (left), dsDNA release occurs in a time dependent manner in presence of cell media. However, the results with DTT at 5 h suggest that a small amount of stable dsDNA-conjugate still exists.

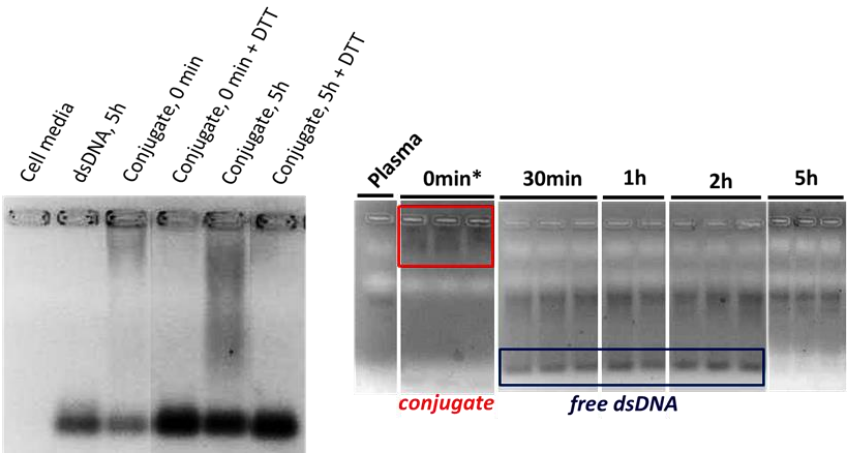

Figure III.13. Stability of PGA-Morph-Arg-PD conjugate to dsDNA in cell culture media without FBS (left) and in plasma (right). *Without plasma.

Additionally, plasma stability by an agarose gel shift assay was also performed trying to mimic physiological conditions. Figure III.13 (right) demonstrates again the low stability of System 2 conjugates even at short incubation times.

III.2.1.1.6. Biological Evaluation of System 2 Conjugates: Cell Viability and Gene Transfer *In Vitro*

Cytotoxicity of the novel DNA conjugates was explored in B16F10 cell line in order to select the highest concentration for later activity studies. As it can be observed in Figure III.14, all the tested concentrations were non-toxic and 37 μM dsDNA concentration was selected for further *in vitro* experiments.

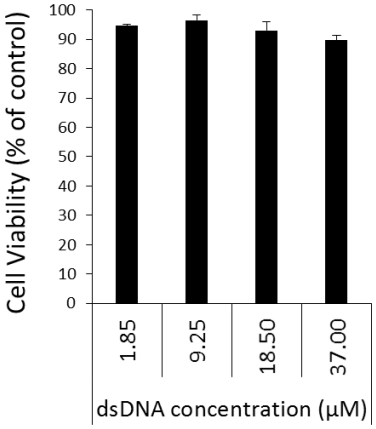

Figure III.14. Cell viability assay of DNA conjugates using different concentrations of dsDNA, developed in B16F10 cells and determined by MTS assay 24 h post-incubation. HEPES was used as control. Data expressed as mean ± SD, n≥4.

Activity studies by means of a silencing luciferase assay were carried out. Evaluation of gene silencing at 24 h and 48 h, using a 21bp thiolated luciferase double stranded siRNA (ds-siRNA), demonstrated that any of System 2 conjugates were not capable to achieve gene silencing, even at high siRNA concentrations (Figure III.15).

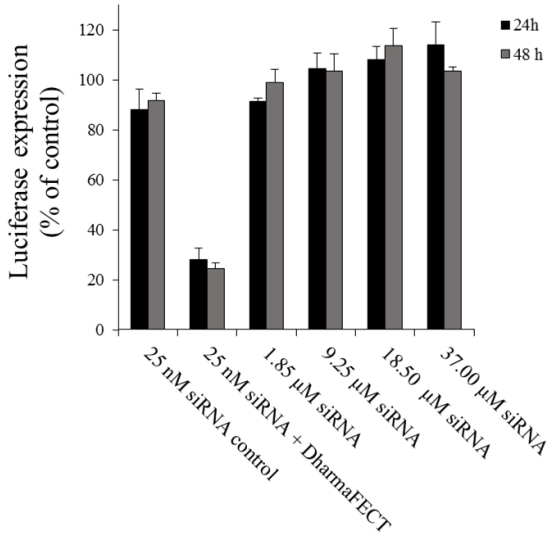

Figure III.15. Gene silencing from System 2 conjugates in B16F10 cell line using different concentrations of ds-siRNA. HEPES was used as control. Data expressed as mean ± SD, n≥4.

These results further corroborated those shown in Section III.2.1.1.5, concerning plasma and cell culture media stability. System 2 conjugates demonstrated low stability even at short incubation times. Otherwise, the endosomal escape would not be efficient enough for the oligonucleotide release. Immunofluorescence assays are being carrying out to resolve such issues.

Taking into account the results obtained for System 2, System 3 was designed using PGA derivatives with higher MW.

III.2.1.2. System 3 - PGA-Based Systems: Functionalisation of Higher Molecular Weight PGA with Endosomolytic Molecules and PEG Protection. Conjugation of Oligonucleotides

III.2.1.2.1. Synthetic Approaches

Greater MW PGA derivatives were explored in order to enhance oligonucleotide stability in plasma, main limitation in previous reported systems. At the same time, such MW enhancement could benefit passive targeting by the Enhanced Permeability and Retention (EPR) effect [49]. Therefore, two novel strategies were evaluated as alternatives to Systems 1 and 2. First, PEG5000-*co*-*b*-PGA_{88} (DB) derivative as a delivery agent was evaluated. PEG is a non-biodegradable hydrophilic polymer which provides stealth properties to the conjugate avoiding conjugate recognition by the immune system and increasing molecule size. Secondly, a higher MW PGA (PGA_{300}) was also used.

PGA post-polymerisation modifications explained above were also used to functionalise PGA_{300} and DB with Morph, Arg, and PD, obtaining the polypeptides presented in Table III.7.

Table III.7. System 3 conjugates tested as possible non-viral vectors.

Conjugate Polymer	Id	GAU	Loading[a] (mol%)				Total Charge at pH 7[b]	MW[b] (g/mol)
			Morph	Arg	PD	free COOH		
DB-Morph-Arg-PD	**DB_{88}MArgPD**	88	52	8	4	36	**8 (-)**	25664
PGA-Morph-Arg-PD	**P_{300}MArgPD**	300	53	14	7	26	**36 (-)**	70446

[a] Determined by 1H NMR; [b] Estimated after ^{1}H NMR analysis.

To verify the identity and purity of each polymer and to compare their sizes and diffusion coefficients, bidimensional DOSY experiments (Figure III.16, Table III.8) were carried out.

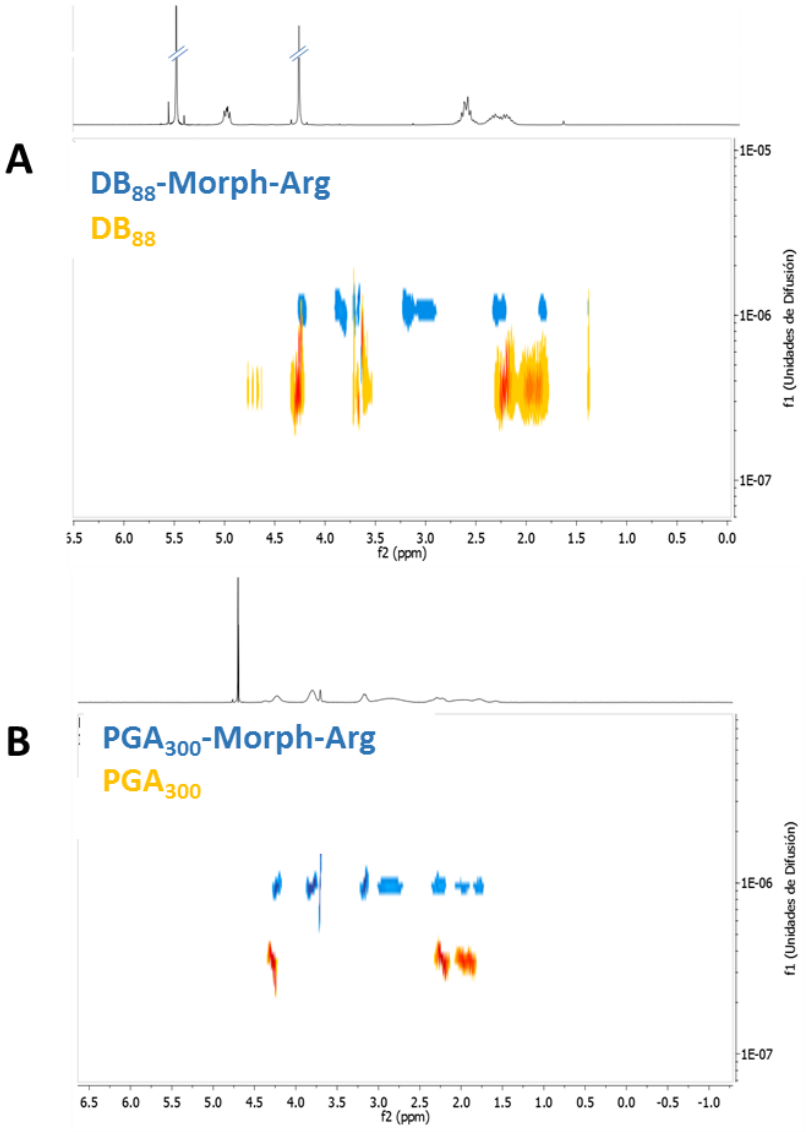

Figure III.16. DOSY NMR spectrum for (A) PGA_{300} and PGA_{300}-Morph-Arg-PD (**P_{300}MArgPD**); and (B) DB_{88} and DB_{88}-Morph-Arg-PD (**DB_{88}MArgPD**).

Table III.8. Diffusion coefficients and hydrodynamic radius (R_h) of System 3 PGA-derivatives.

Conjugate Polymer	D[a] (m^2/s)	R_h[a] (nm)
DB_{88}	8.22e-12	24.4
DB_{88}-Morph-Arg-PD	3.39e-12	64.3
PGA_{300}	8.27e-12	21.8
PGA_{300}-Morph-Arg-PD	3.14e-12	63.9

[a] Diffusion coefficient (D) and hydrodynamic radius (R_h) determined by fitting the intensities of the arrayed DOSY NMR spectra into Stejskal-Tanner equation.

NMR results indicate that, after derivatisation, both polymers (**P_{300}MArgPD** and **DB_{88}MArgPD**) display an increase in size, which further diminishes their diffusion coefficient. This indicates that the size of PGA-derivatives is influenced by the moieties added, which can treble the initial hydrodynamic radius (R_h).

III.2.1.2.2. DNA Binding Assay Electrophoresis

To evaluate System 3 polyplex formation (Table III.7), agarose gel electrophoresis test was performed (Figure III.17).

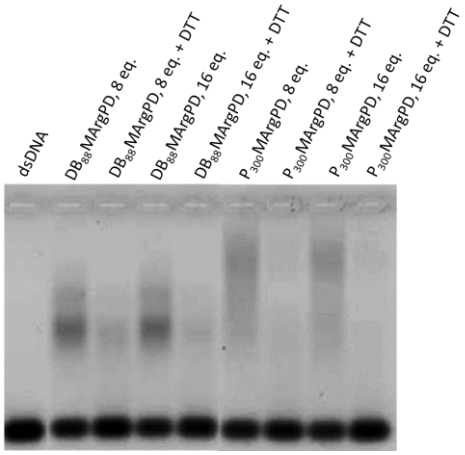

Figure III.17. dsDNA binding ability of **P_{300}MArgPD** and **DB_{88}MArgPD** determined by agarose gel shift assay using different amounts of PGA-based polymer keeping constant the amount of dsDNA, with and without DTT.

As it can be observed in the figure above, a lower DNA binding capacity for P_{300}MArgPD and DB_{88}MArgPD was obtained in comparison to the PGA_{50}-derivatives of Systems 1 and 2. Although the MW of P_{300}MArgPD is higher than the MW of DB_{88}MArgPD (70446 g/mol *vs*. 25664 g/mol), the theoretical total charge at pH7 is lower in the case of P_{300}MArgPD (36(-) for P_{300}MArgPD *vs*. 8(-) for DB_{88}MArgPD). Despite this, polymer P_{300}MArgPD displayed better DNA binding ability as compared to DB_{88}MArgPD. For this reason, we selected P_{300}MArgPD to repeat the agarose gel electrophoresis using increased amounts of polymer while keeping the amount of oligonucleotide constant. However, increasing the amount of polymer only led to a very small improvement of DNA binding.

Given the low effectiveness in the conjugation of the different PGA derivatives to the oligonucleotide (regardless of their MW), another strategy based on poly-L-arginine was developed.

III.2.2. Poly-L-Arginine (PArg)-Based Systems (Systems 4-5)

Cationic polymers, such poly-L-lysine (pLL) and polyethylenimine (PEI), have been extensively studied as vectors for gene therapy as they readily form polyelectrolyte complexes with the corresponding oligonucleotide. This fact results in a greater compaction and an enhanced stability toward nucleases [50, 51]. For this reason, herein, we explored new designs based on the basic amino acid arginine due to its known efficiency as a delivery agent for plasmid DNA (pDNA) and siRNA both *in vitro* and *in vivo* [52]. Additionally, arginine-rich peptides are able to enter cells via endocytosis [53] and, interestingly, there exists a dependence of chain length on cellular localisation, membrane permeability, and toxicity [54]. However, the major disadvantages of using such cationic moieties for *in vivo* proposes are their cytotoxicity and low biodegradability, issues that have been also taken into account in the synthetic processes selected.

III.2.2.1. System 4 - PGA-Coated PArg-Based Polyplexes

III.2.2.1.1. Synthetic Approaches

Under the same rational as PGA, different backbone lengths of PArg (50, 92 and 150 units) were explored to study the potential for complexation. **System 4** would give rise to electrostatic interactions with DNA instead of controlled covalent attachment. After complexation, the systems were coated with PGA or DB in order to secure haemo- and bio-compatible systems and to provide "stealth" properties to polyplexes for future *in vivo* application (Figure III.18).

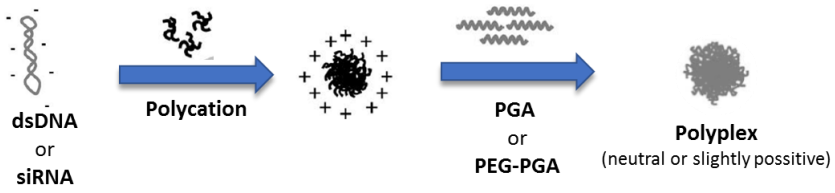

Figure III.18. Schematic representation for System 4 complexes.

III.2.2.1.2. DNA Binding Assay Electrophoresis

After optimising the nitrogen to phosphate (N/P) ratio for each system (Figure III.19), the high capacity of PArg to form stable complexes even at low N/P ratios was observed.

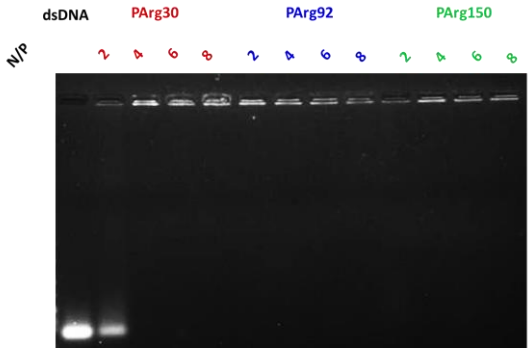

Figure III.19. Optimisation of N/P ratio by checking the dsDNA binding ability of PArg through agarose gel electrophoresis.

Coating optimisation was also performed by gel shift assay (Figure III.20), finding out that PGA destabilised the system and $PArg_{30}$ provided

less stable complexes compared with $PArg_{92}$ and $PArg_{150}$. Thus, **$PArg_{92}$/dsDNA + DB_{88}** and **$PArg_{150}$/dsDNA + DB_{88}** at N/P 6 were selected for subsequent experiments due to their high stability and reproducibility.

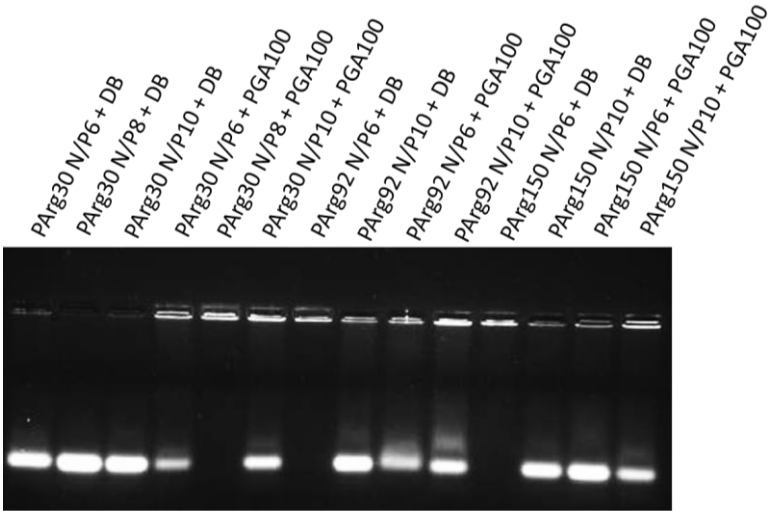

Figure III.20. Optimisation of coating agent by checking the PArg-dsDNA binding ability through agarose gel electrophoresis.

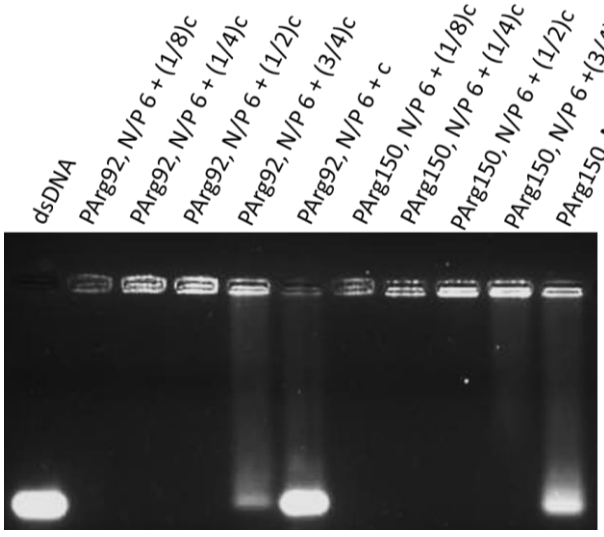

Figure III.21. Binding ability for PArg complexes by using different amounts of coating agent (c= 80 µg/mL PArg per 500 ng of oligonucleotide).

The amount of coating agent (DB_{88}) related to PArg amount (c= 80 µg/mL per 500 ng of oligonucleotide) was also optimised by testing different quantities of DB for each length of PArg (Figure III.25). N/P 6 and (½)c (40 µg/mL per 500 ng of oligonucleotide), half the amount of DB per amount of PArg, were selected as the composition to move forward.

III.2.2.1.3. DLS Measurements- Particle Size and ζ-Potential

Using the selected amount of DB_{88} (DB:PArg ratio 1:2) a reduction in ζ-potential after the coating was observed, as expected. ζ-potential still remained positive in both cases after complexation (Table III.9).

Table III.9. Physicochemical characterisation of System 4/dsDNA polyplexes.

Polyplex	Size[a] (d., nm)	ζ-potential[a] (mV)	PdI[a]
$PArg_{92}$/dsDNA	69.3 ± 5.3	**41.4 ± 1.5**	0.242 ± 0.015
$PArg_{92}$/dsDNA + DB_{88} coating	69.3 ± 5.6	**19.1 ± 0.5**	0.350 ± 0.047
$PArg_{150}$/dsDNA	38.9 ± 25.6	**40.5 ± 1.5**	0.243 ± 0.006
$PArg_{150}$/dsDNA + DB_{88} coating	68.8 ± 11.7	**17.9 ± 0.6**	0.378 ± 0.019

[a] As determined by DLS at N/P 6 and half amount of DB per amount of PArg, in 20 mM HEPES buffer at 25˚C. Polyplexes were diluted 1:20 before measurement. Size values are expressed in terms of number. d.= diameter. PdI= polydispersity index. Variations refer to the median of three measurements of the sample.

III.2.2.1.4. Heparin Displacement Assay

Stability of System 4 compounds was evaluated by measuring dsDNA release in the presence of a competing polyanion: heparin. The lowest concentration of heparin required for dsDNA displacement provides an estimation of the complex stability against polyanions [55]. Following incubation of the studied polyplexes with increasing levels of heparin, all complexes were stable even at 0.25 IU per 20 µL (Figure III.22). This equals to 1250 IU/100 mL, while the average heparin levels in human plasma are 15 IU/100 mL [56].

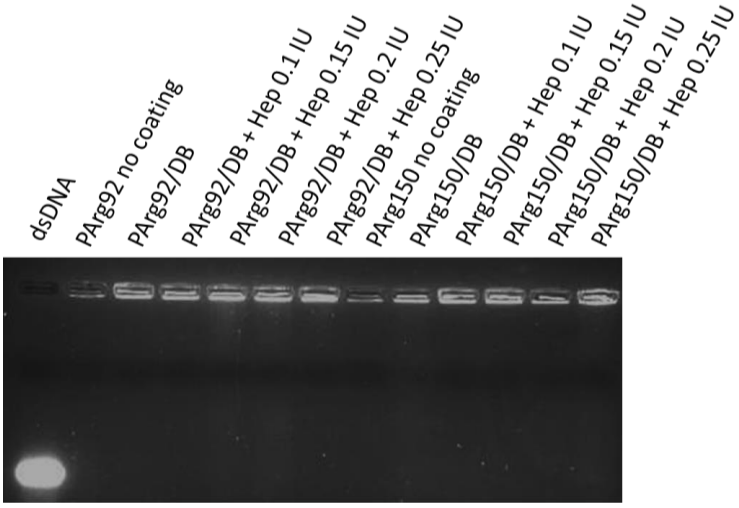

Figure III.22. Heparin displacement assay for System 4 polyplexes by agarose gel electrophoresis.

III.2.2.1.5. Biological Evaluation of System 4 Complexes: Cell Viability and Gene Silencing *In Vitro*

Again, MTS assays were performed to test cell viability in the B16F19 cell line. Different siRNA concentrations were studied keeping constant the PArg/siRNA ratio (Figure III.23). 13.87 µM siRNA (4 mg/mL PArg) was considered the limit to perform the subsequent *in vitro* experiments.

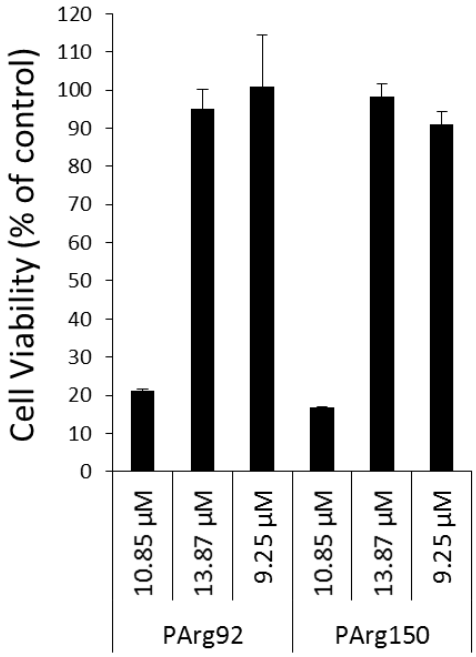

Figure III.23. Cell viability assay of siRNA complexes using different concentrations of siRNA developed in B16F10 cells and determined by MTS assay 24 h post-incubation. HEPES was used as control. Data expressed as mean ± SD, n≥4.

In the subsequent activity study (silencing luciferase expression, protocol described in Section III.4.4.19), significant transfection was not observed, even using high siRNA concentrations. An inefficient endosomal escape could be a possible reason for the absence of silencing. The addition of and endosomolytic agent into the coating agent backbone could solvent this issue. System 5 was then proposed.

III.2.2.2. System 5 - Coated PArg-Based Polyplexes. Endosomolytic PGA-Derivatives as Coating Agents

III.2.2.2.1. DNA Binding Assay Electrophoresis

In order to improve the endosomolytic properties of System 4, PGA-Morph and PGA-Hist (PGA_{50} and PGA_{100}) were employed as coating agents, generating **System 5**. The previously optimised ratio N/P 6 for polyplex formation using $PArg_{92}$ and $PArg_{150}$ was selected.

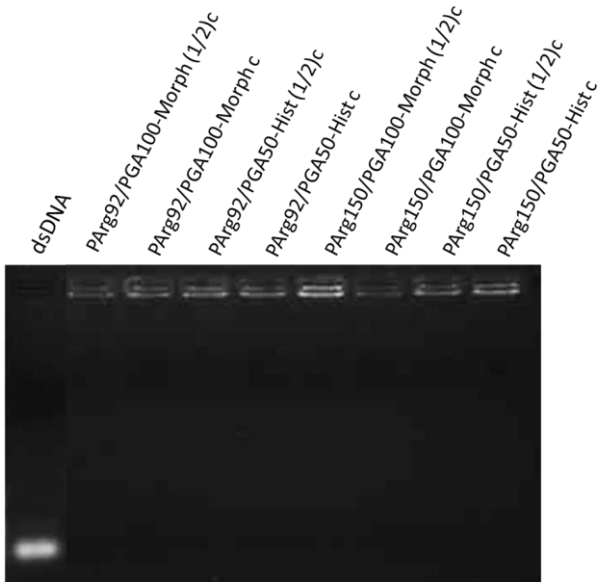

Figure III.24. DNA binding assay electrophoresis for PArg polyplexes at N/P 6 with PGA-Hist and PGA-Morph coatings. The amount of coating agent related to PArg amount (c= 80 μg/mL per 500 ng of oligonucleotide).

Figure III.24 demonstrates that all the systems formed stable coatings even using different amounts of coating agent. In addition, change in ζ-potentials towards positive values were observed (Table III.10, Section III.2.2.2.2).

III.2.2.2.2. DLS Measurements- ζ-Potential

Table III.10. Physicochemical characterisation of System 5 complexes.

PArg	PArg Concentration (µg/mL per 500 ng oligonucleotide)	Coating Agent	Coating Agent Concentration (µg/mL)	ζ-potential[a] (mV)
$PArg_{92}$	80	-	-	**41.4 ± 1.5**
	80	PGA_{100}-Morph	80	**23.8 ± 0.2**
	80	PGA_{50}-Hist	80	**33.2 ± 1.2**
	80	PGA_{50}-Hist	160	**26.0 ± 0.2**
$PArg_{150}$	80	-	-	**40.5 ± 1.5**
	80	PGA_{100}-Morph	80	**21.4 ± 0.9**
	80	PGA_{50}-Hist	80	**32.7 ± 0.9**

[a] As determined by DLS at N/P 6 in 20 mM HEPES buffer at 25˚C. Polyplexes were diluted 1:20 before measurement. Variations refer to the median of three measurements of the sample.

III.2.2.2.3. Biological Evaluation of System 5 Complexes: Cell Viability and Gene Silencing *In Vitro*

MTS assays were performed to test cell viability in the B16F19 cell line. Different siRNA concentrations were studied keeping constant the polymer/siRNA ratio at N/P 6 as well as the amount of coating agent (equal to PArg, in mg/mL) (Figure III.25). 1.85 µM siRNA was considered the limit to perform the subsequent *in vitro* experiments.

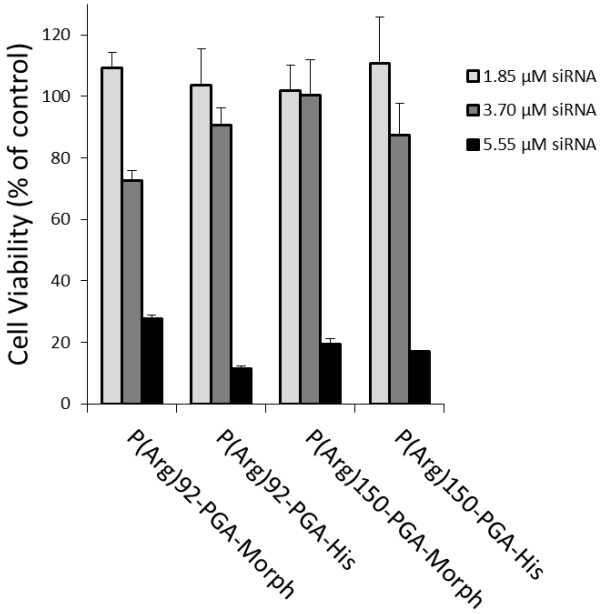

Figure III.25. Cell viability assay of System 5 complexes using different concentrations of siRNA, developed in B16F10 cells and determined by MTS assay 24 h post-incubation. HEPES was used as control. Data expressed as mean ± SD, n≥4.

In the subsequent activity study (silencing luciferase expression, Figure III.26), significant transfection was not observed, even using high siRNA concentrations. The amount of endosomolytic agent in the coating polymer at non-toxic concentrations could be not enough for an efficient endosomal escape. Furthermore, the electrostatic bonding between the oligonucleotide and PArg might be too stable resulting in a lack of dissociation within the endosome.

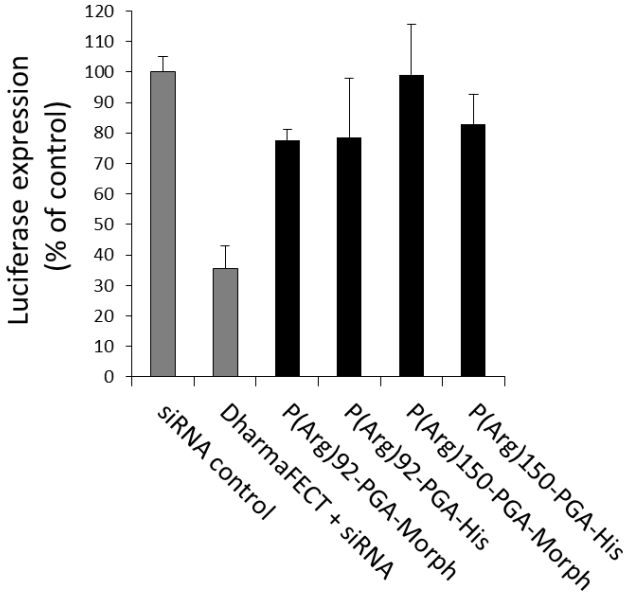

Figure III.26. Gene silencing from System 5 complexes at N/P 6 line using 1.85 µM siRNA and the same amount of coating agent than PArg, in B16F10 cells. HEPES was used as control. Data expressed as mean ± SD, n≥4.

In view of the results, another strategy was proposed based on the synthetic polyaminoacid P(Orn), precursor of PArg.

III.2.3 Poly-L-Ornithine (P(Orn))-Based Systems (Systems 6-8)

Continuing with the exploration of the different alternatives within the field of polypeptides, it was proposed to developed a new strategy based on the positively charged synthetic polyaminoacid P(Orn). As in the case of PArg, ornithine is expected to enhance gene delivery due to the cationic charge of its pendant amino groups at physiological pH. However, P(Orn) binding slightly weaker than PArg (pKa 10.7 ornithine *vs.* pKa 12.5 arginine) will give rise to systems capable of being dissociated within the endosome. The cationic charge contributed to the binding and condensation of the oligonucleotide and, in parallel with lysine, is used in cell penetrating peptides [20, 57, 58]. P(Orn) has been shown to be up to 10-fold more efficient than other cationic polymers such as PLL (the most commonly utilised model cationic

polymer in laboratory gene delivery investigations) in the transfection of a variety of cell lines (*e.g.* B16 murine melanoma cells) [59, 60].

Three different P(Orn)-based designs were developed in order to find the best combination for an effective gene delivery. Complexation (Systems 6 and 8) and conjugation (System 7) strategies were considered for this purpose (Figure III.27)

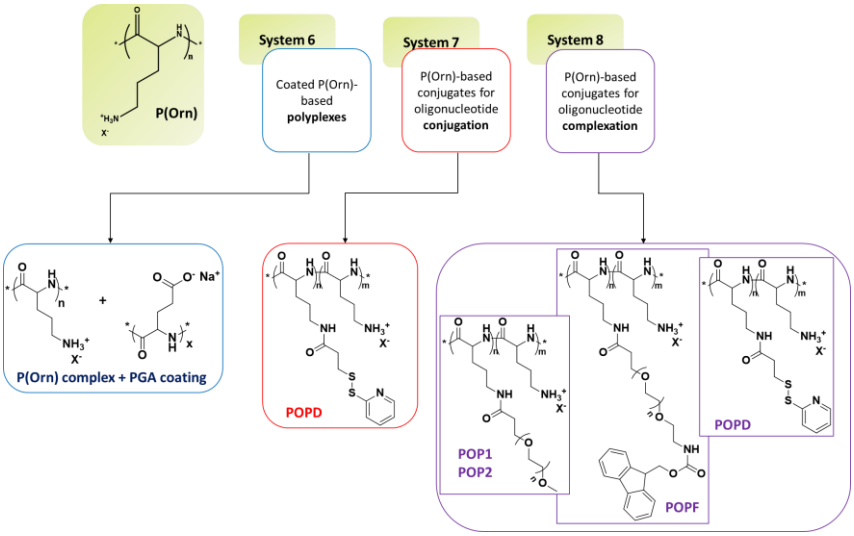

Figure III.27. Schematic representation for the tested P(Orn) systems.

III.2.3.1. System 6 - Coated P(Orn)-Based Polyplexes

III.2.3.1.1. DNA Binding Assay Electrophoresis

In **System 6**, we used P(Orn) (50 ornithine units) as a sequestering agent and PGA-based derivatives as coating agents. N/P ratio and the amount of coating agent (PGA_{100} and DB_{88}) were optimised by gel shift assay proving the P(Orn) ability to form complexes even using small N/P ratios (Figure III.28).

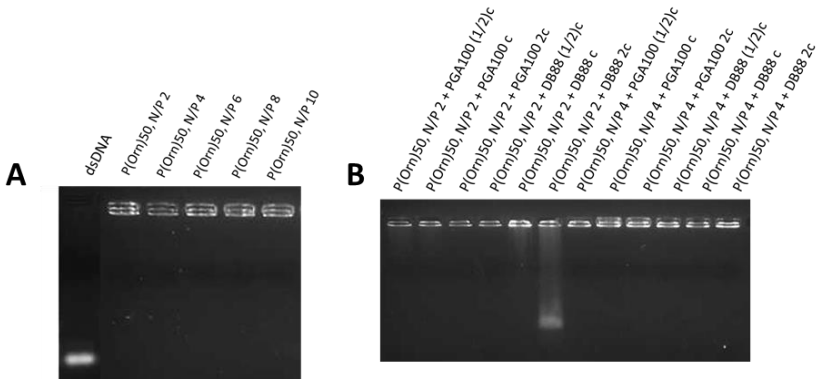

Figure III.28. (A) dsDNA binding ability of P(Orn) at different N/P ratios. (B) Coating agent optimisation by agarose electrophoresis. c= 26.5 µg/mL P(Orn) per 500 ng dsDNA for N/P 2 and 58.5 µg/mL P(Orn) per 500 ng dsDNA for N/P 4.

III.2.3.1.2. DLS Measurements- ζ-Potential

Table III.12 shows how ζ-potential changes according to the coating agent as well as the amount of coating agent used. Systems with positive ζ-potential values were selected as the most appropriate candidates in order to check their stability in the presence of heparin (Section III.2.3.1.3).

Table III.12. ζ-potential for the selected P(Orn) complexes.

P(Orn)	P(Orn) concentration (µg/mL per 500 ng oligonucleotide)	N/P	Coating Agent	Coating Agent Concentration (µg/mL)	ζ-potential[a] (mV)
$P(Orn)_{50}$	26.5	2	-	-	**20.5 ± 0.4**
	26.5	2	PGA_{100}	13.25	**27.2 ± 0.8**
	26.5	2	PGA_{100}	26.5	**-7.2 ± 0.2**
	26.5	2	DB_{88}	26.5	**12.5 ± 0.8**
	26.5	2	DB_{88}	53.0	**-7.0 ± 0.5**
$P(Orn)_{50}$	58.5	4	-	-	**39.2 ± 3.3**
	58.5	4	PGA_{100}	58.5	**24.0 ± 1.15**
	58.5	4	DB_{88}	58.5	**10.9 ± 0.4**

[a] As determined by DLS in 20 mM HEPES buffer at 25˚C. Polyplexes were diluted 1:20 before measurement. Variations refer to the median of three measurements of the sample.

III.2.3.1.3. Heparin Displacement Assay

The relative stability of System 6 compounds was evaluated by measuring dsDNA release in the presence of the heparin as described previously. Following incubation of the studied systems with 10 IU of heparin, we found a poor stability for all the complexes tested at an amount of heparin lower than the average heparin levels in human plasma (15 IU/100 mL) (Figure III.29).

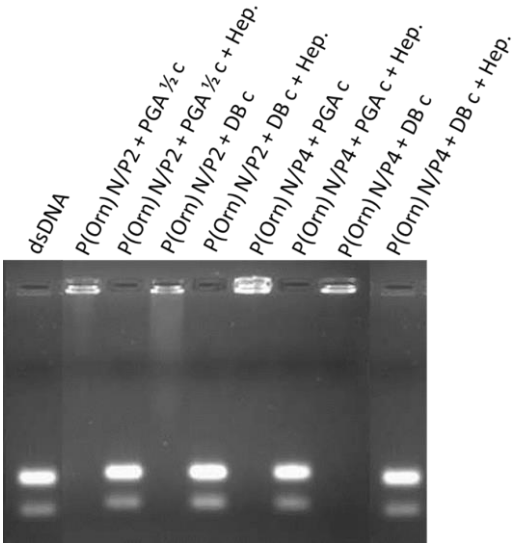

Figure III.29. Heparin displacement assay for System 6 complexes by agarose gel electrophoresis. c= 26.5 µg/mL P(Orn) per 500 ng dsDNA for N/P 2 and 58.5 µg/mL P(Orn) per 500 ng dsDNA for N/P 4.

Seeking greater stability, we designed System 7 aiming to entrap covalently the oligonucleotide, thus resisting the path to the desired target without suffering any damage.

III.2.3.2. System 7 - P(Orn)-Based Conjugates for Oligonucleotide Conjugation

III.2.3.2.1. Synthetic Approaches

In order to compare the coated P(Orn) complexes with P(Orn) conjugates, **System 7** was developed by functionalising the P(Orn) (50 units ornithine) backbone with PD (Figure III.30). The P(Orn)-derivative obtained, POPD (8 mol% PD), is presented in Table III.13.

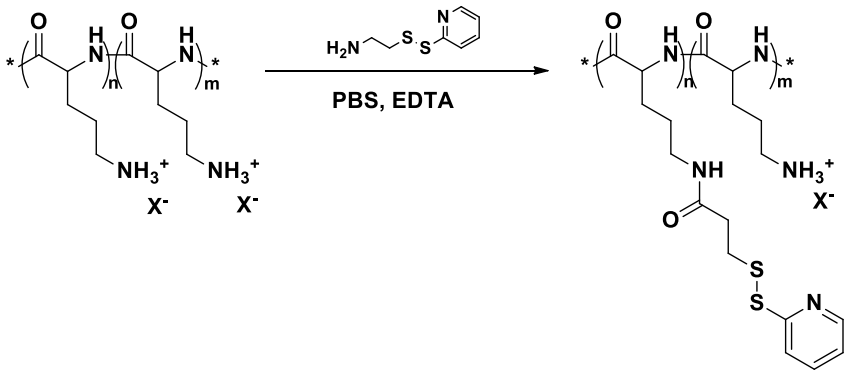

Figure III.30. Schematic representation of POPD synthesis.

The ^{1}H NMR spectrum in D_2O with corresponding assignments for the synthesised POPD compound is depicted in Figure III.31.

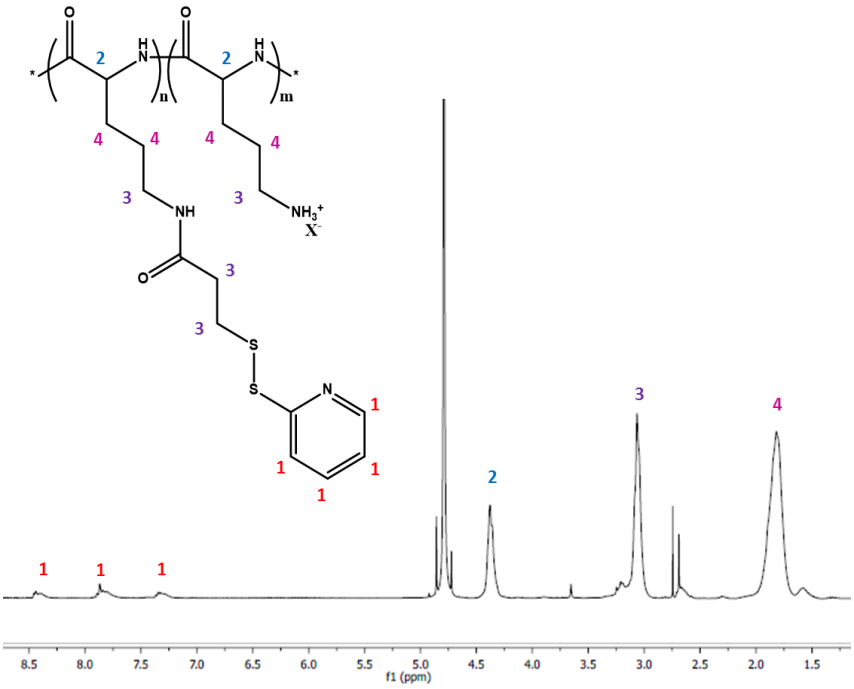

Figure III.31. ^{1}H NMR spectrum with assignments for POPD.

III.2.3.2.2. DNA Binding Assay Electrophoresis

dsDNA (22 bp dsDNA) was covalently linked to P(Orn) backbone via disulphide bond formation, as in the case of System 2, testing afterwards the degree of the reaction and the stability of the final

conjugate (Figure III.32). TCEP (tris(2-carboxyethyl)phosphine) was used as reducing agent.

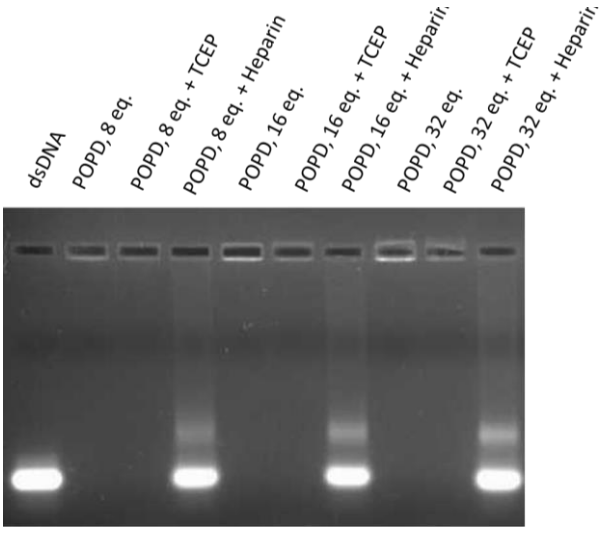

Figure III.32. Gel shift and heparin displacement assays for POPD using different amounts of polymer keeping constant the amount of dsDNA (500 ng).

Figure III.32 demonstrates that if conjugation occurs, free DNA is complexed after cleavage. The addition of TCEP (0.5 M) had no effect while, the addition of heparin 1 IU triggered a clear shift of the dsDNA suggesting that there is no conjugation but there is complexation. Due to the poor stability of Systems 6 and 7, a new system was conceived (**System 8**).

III.2.3.3. System 8 - P(Orn)-Based Conjugates for Oligonucleotide Complexation

III.2.3.3.1. Synthetic Approaches

For System 8, P(Orn) (50 units ornithine) was functionalised in three different manners using PEG (MW 2000, PEG_{2000} and 3000, PEG_{3000}), PEG-*Fmoc* (MW 3000, PEG_{3000}-*Fmoc*) and PD via amide bond formation obtaining four systems: **POP1** and **POP2** (P(Orn) modified with PEG_{2000} and PEG_{3000} respectively), **POPF** (P(Orn) modified with PEG_{3000}-*Fmoc*), and **POPD** (P(Orn) modified with PD). The addition of the non-ionic, hydrophilic PEG polymer aims to provide stealth properties to the final polyplex avoiding recognition by immune system as well as

increasing molecule size, thereby reducing clearance from the bloodstream impeding rapid excretion through the reticulum endothelium system (RES) [61]. Otherwise, the presence of the hydrophobic pendent *Fmoc* moiety will induce conformational changes allowing to compare the behaviour of both POP and POPF conjugates. The obtained products are schematically represented in Figure III.33 and their composition is shown in Table III.13.

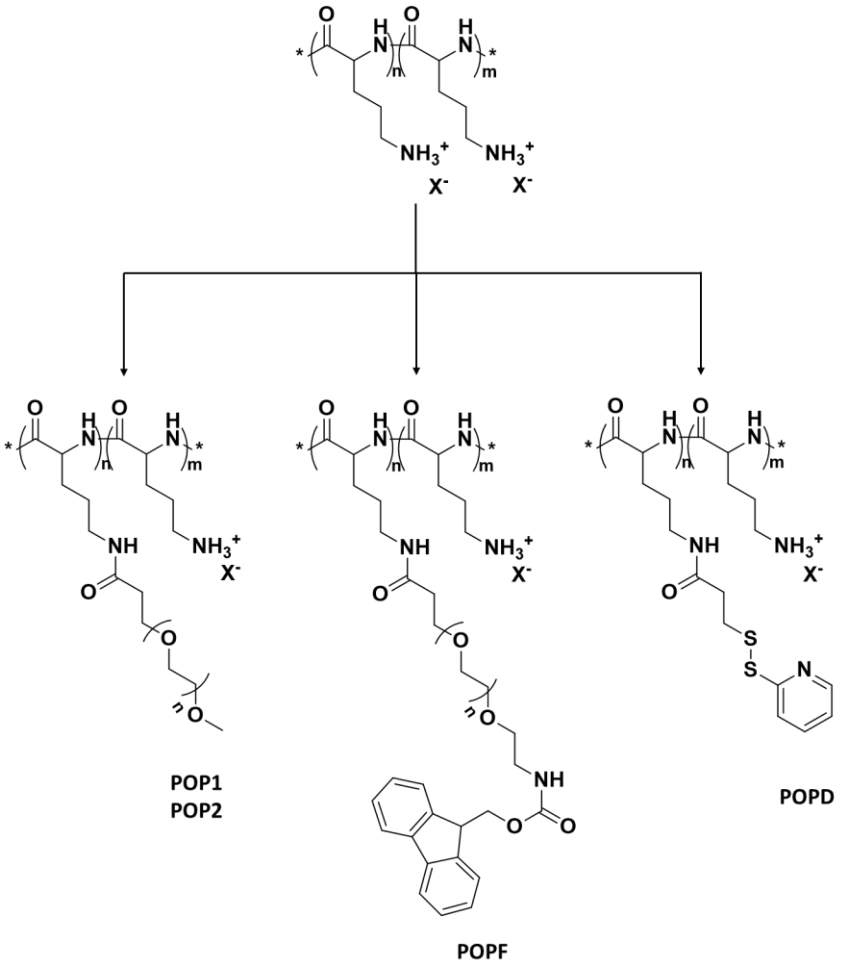

Figure III.33. Schematic representation for the obtained P(Orn) derivatives.

Table III.13. Composition of P(Orn) derivatives estimated by ^{1}H NMR.

Conjugate Polymer	Id	Loading (mol%)
P(Orn)-PEG$_{2000}$	POP1	1.8
P(Orn)-PEG$_{3000}$	POP2	1.4
P(Orn)-PEG$_{3000}$-*Fmoc*	POPF	2.7
P(Orn)-PD	POPD	8

The ^{1}H NMR spectrum in D_2O with corresponding assignments for the synthesised **POP1** and **POP2** compounds are depicted in Figure III.34.

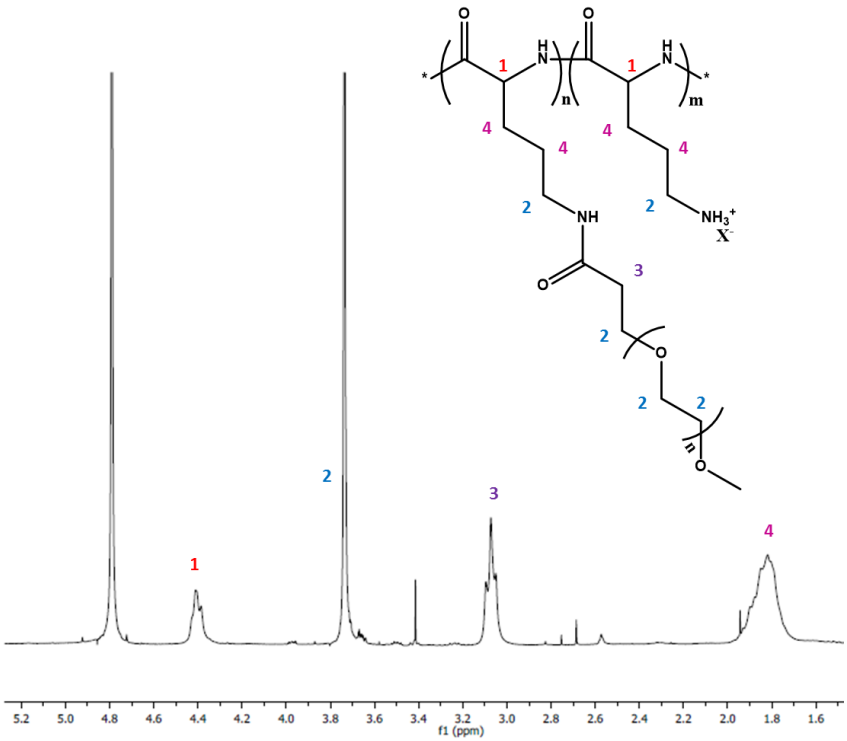

Figure III.34. ^{1}H NMR spectrum with assignments for **POP1** and **POP2**.

III.2.3.3.2. DNA Binding Assay Electrophoresis

Polyplex formation was carried out in HEPES 20 mM pH 7.4, and oligonucleotide complexation was proved by gel shift assay, comparing P(Orn) derivatives with non-modified P(Orn) in order to select the best N/P ratio (Figure III.35). N/P 4 was selected for further assays.

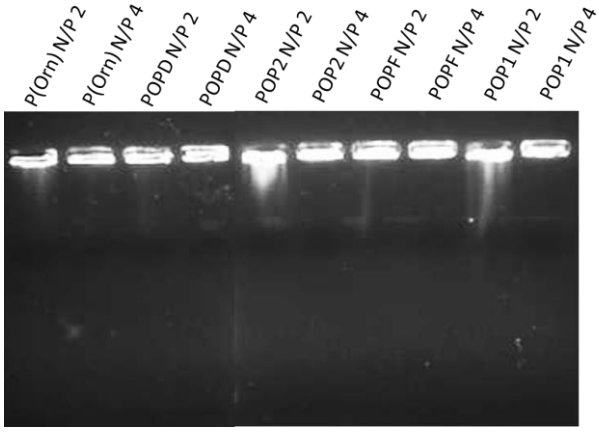

Figure III.35. Gel shift assay for P(Orn)-based polyplexes at different N/P ratios.

III.2.3.3.3. RBC Lysis Assay

Following the same rational and characterisation explained for the previous systems, polyplex ability to induce RBC lysis *in vitro* was determined as a preliminary indicator of haematocompatibility [48]. Haemolytic profiles obtained are represented in Figure III.36. P(Orn) derivatives demonstrated to be non-haemolytic and, therefore, do not promote breakage of the RBC membrane confirming their suitability for IV administration.

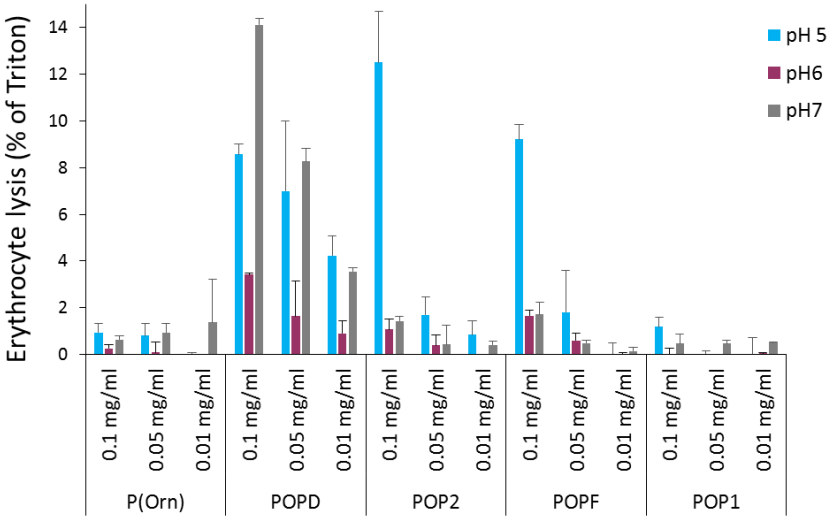

Figure III.36. Erythrocyte leakage assay for P(Orn) derivatives at different pH values: compounds were incubated with erythrocytes at different concentrations at 37°C at indicated pH values. Haemoglobin release was measured after 1 h. Data expressed as mean ± SD, n= 3.

III.2.3.3.4. DLS Measurements- Particle Size and ζ-Potential

Variations in size and ζ-potential of each P(Orn) derivative-polyplex varied slightly comparing data at pH 7.4 and pH 5.5 (Table III.14). These results suggest that the polyplexes will be stable, in terms of pH, along the delivery pathway until reach the desired target.

Table III.14. Particle size and ζ-potential for P(Orn) derivatives at N/P 3 and two different pH, 7.4 and 5.5.

siRNA polyplex	pH 7.4			pH 5.5		
	Size[a] (d, nm)	ζ-potential[a] (mV)	PdI[a]	Size[a] (d, nm)	ζ-potential[a] (mV)	PdI[a]
P(Orn)	55.8 ± 5.2	**29.2 ± 0.4**	0.443 ± 0.011	38.9 ± 9.6	**31.3 ± 1.6**	0.352 ± 0.031
POPD	68.5 ± 3.2	**24.1 ± 1.8**	0.267 ± 0.020	43.5 ± 9.5	**30.5 ± 0.6**	0.217 ± 0.011
POP1	35.7 ± 1.9	**18.2 ± 0.6**	0.366 ± 0.004	36.1 ± 9.1	**17.1 ± 1.3**	0.365 ± 0.015
POP2	27.2 ± 8.9	**10.6 ± 1.4**	0.353 ± 0.085	36.5 ± 2.6	**7.2 ± 0.9**	0.255 ± 0.015
POPF	36.5 ± 2.2	**16.9 ± 1.9**	0.410 ± 0.010	31.5 ± 13.7	**15.7 ± 0.5**	0.377 ± 0.019

[a] As determined by DLS in 20 mM HEPES buffer at 25˚C. Polyplexes were diluted 1:20 before measurement. Size values are expressed in terms of number. Variations refer to the median of three measurements of the sample.

III.2.3.3.5. Biological Evaluation of System 8 Complexes: Gene Silencing, Cell Viability, and Cellular Internalisation *In Vitro*

Gel shift assay with System 8 complexes at N/P 4 was performed to assess their stability in cell culture media in view of later *in vitro* studies. As it can be observed in the figure below (Figure III.37), free siRNA was not detected after 5h incubation at 37˚C proving the stability of the polyplexes under these conditions and their suitability for next experiments.

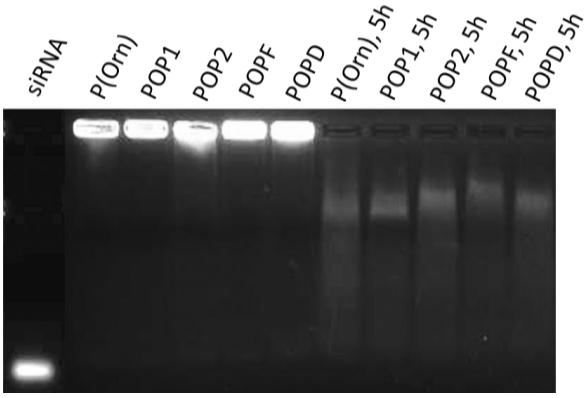

Figure III.37. Gel shift assay for System 8 complexes at N/P 4 with and without cell culture media. Complexes in cell culture media at 37˚C were incubated during 5 h and diluted 1:4.

After these encouraging results, gene knockdown efficiency was investigated following the same silencing study with luciferase (Section III.4.4.19, Figure III.38). B16F10Luc cells were incubated 24 hours with the different P(Orn) derivatives complexed with luc siRNA at N/P 3 and N/P 4 ratios.

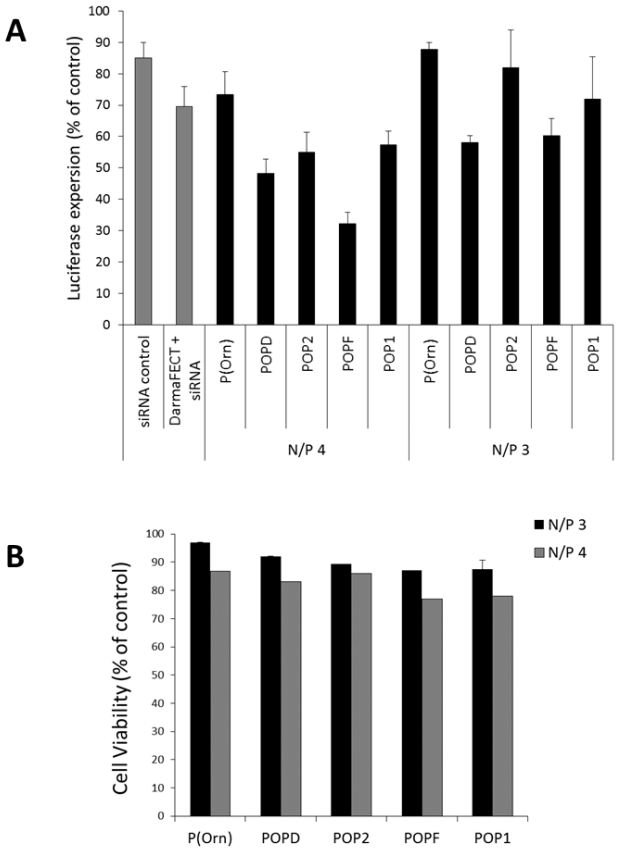

Figure III.38. (A) Gene silencing form System 8 conjugates in B16F10 cell line at N/P 3 and N/P 4, 24 h post-incubation. (B) Determination of cell viability for System 8 complexes in B16F10 cells at N/P 3 and N/P 4 ratios, determined by MTS assay 24 h post-incubation. HEPES was used as control. Data expressed as mean ± SD, n≥4.

In the case of N/P 4 ratio, gene silencing was reliable but cell mortality was higher than 20%. Pursuant to ISO 10993-5, percentages of cell viability above 80% are considered as non-cytotoxicity; within 80%–60% weak; 60%–40% moderate and below 40% strong cytotoxicity respectively [62]. However, at N/P 3, cell viability increased and 40% of gene silencing was obtained.

Aiming to demonstrate gene silencing sustainability, incubation time was increased (48 h) and a clear improvement in terms of silencing was obtained while low toxicity was maintained (Figure III.39).

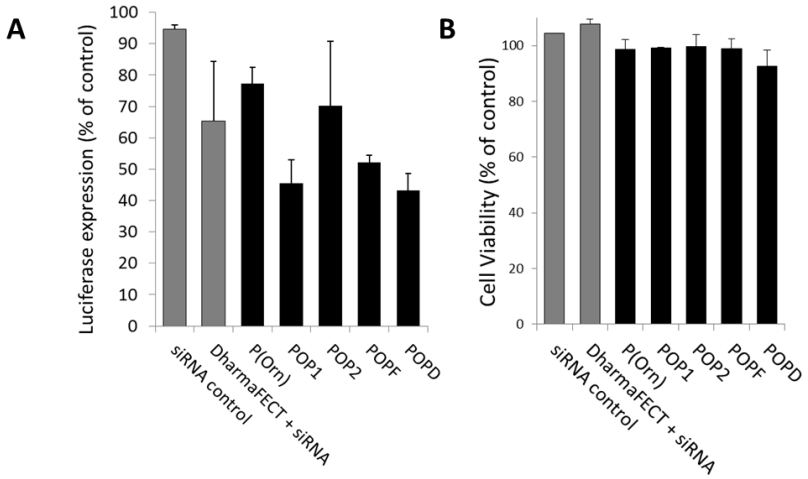

Figure III.39. (A) Gene silencing data form System 8 complexes at N/P 3 in B16F10 cell line, 48 h post-incubation. (B) Cell viability of the polyplexes in B16F10 cell line by MTS assay at N/P 3 ratio and 48 h post-incubation. Data expressed as mean ± SD, n≥4.

Aiming to determine the cell trafficking pathway, a kinetic study using the InCell Analyzer device to observe the cellular internalisation of the P(Orn) derivatives at different times, from 0 min to 5 hours, was carrying out.

Figure III.40A shows one of the images obtained concluding a clear time-dependent internalisation of POP2-6FAM-siRNA. Figure III.40B shows cell internalisation vs. time for all the P(Orn) derivatives.

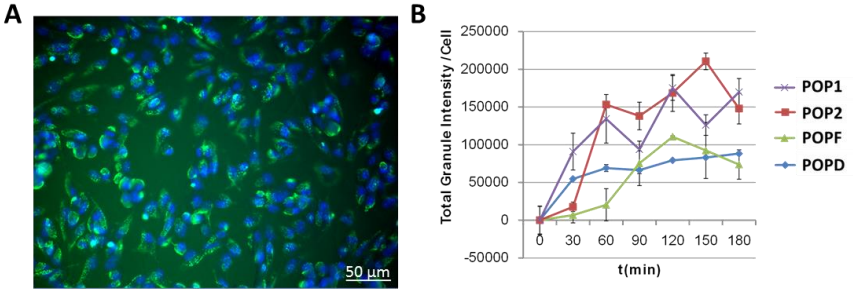

Figure III.40. (A) Cell Internalisation for POP2 at 2 h post-treatment by using InCell Analyzer Device. Green: 6-FAM; Blue: Hoechst. (B) Cell Internalisation vs. time for POP1, POP2, POPF, and POPD.

III.3. CONCLUSIONS

siRNA induced RNA interference is a promising strategy for the treatment of various cancers via the regulation of previously undrugable targets. However, the delivery process remains as the most crucial limitation and this hampers therapeutic/clinical development. Along this thesis chapter, different multifunctional polymeric platforms based on natural or synthetic polyaminoacids (PGA, PArg, and P(Orn)) and their derivatives were synthesised and physicochemically characterised to discover a successful vehicle for an effective gene delivery. It has to be remarked that all systems were display a low index of polydispersity (Đ ~ 1.2) due to the controlled polymerisation techniques employed for their obtaining [26, 27, 31] and, therefore, precise and well-defined structures, allowing reproducibility and the determination of a clear structure activity relationship.

PGA-based systems were successfully designed and synthesised exploring both conjugation and complexation strategies. However, the lack of stability and an inefficient endosomal escape made us focus on the use of polycations under the same rational as previously mentioned PGA systems. The well-known polycationic PArg was explored for oligonucleotide complexation. The guanidine headgroup of arginine would be the critical structural component responsible for the possible biological activity. PArg have been widely used as cell-penetrating agent in the biomedical fields. Polyarginines composed of simple and short sequences are readily applicable as gene delivery carriers and cell permeable enhancers [63-65]. However, in gene delivery systems, such polymers by themselves cannot easily be used as an encapsulating agent due to their unstable linear structures, low molecular weights, and relatively low electron charge density compared to nucleic acids such as DNA and siRNA. To overcome the weak condensation for both short sequences of polyarginine and nucleic acid, different well-defined polymers with more than 50 units of polycation arginine were selected for oligonucleotide complexation. Furthermore, after complexation, the systems were coated with PGA or DB in order to end up with haemo- and bio-compatible systems and to provide “stealth” properties to polyplexes for future *in vivo* application. Nevertheless, probably due to

an inefficient endosomal release, these compounds were not able to transfect efficiently, even using coating agents with endosomolytic moieties. The amount of endosomolytic agent in the coating polymer at non-toxic concentrations could be not enough.

Continuing the exploration of alternatives within the field of polypeptides, another strategy based on positively charged synthetic P(Orn) was investigated. As in the case of PArg, ornithine was expected to enhance the gene delivery ability due to the cationic charge of its pendant amino groups at physiological pH. These can contribute to the binding and condensation of the oligonucleotide and, in parallel with lysine, form parts of cell penetrating peptides [66]. P(Orn) (50 units ornithine) was functionalised in three different manners using PEG (MW 2000, PEG_{2000} and 3000, PEG_{3000}), PEG-*Fmoc* (Mw 3000, PEG_{3000}-*Fmoc*) and PD via amide bond formation obtaining four systems: POP1 and POP2 (P(Orn) modified with PEG_{2000} and PEG_{3000} respectively), POPF (P(Orn) modified with PEG_{3000}-*Fmoc*), and POPD (P(Orn) modified with PD). The addition of the non-ionic, hydrophilic PEG polymer aims to provide stealth properties to the final polyplex avoiding recognition by immune system as well as increasing molecule size, thereby reducing clearance from the bloodstream impeding rapid excretion through the reticulum endothelium system (RES) [63]. Otherwise, the presence of the hydrophobic pendent Fmoc moiety will induce conformational changes allowing to compare the behaviour of both POP and POPF conjugates. Their nanosize and positive surface charge were found to be favourable for *in vitro* application (non-cytotoxic and non-haemolytic). More importantly, the polyplexes successfully transfected a luciferase-transfected melanoma cell model (B16F10-luc-G5), evidencing the potential of this polypeptidic platform. Further analyses are being carried out in order to validate this system.

III.4. MATERIALS AND METHODS

III.4.1. Materials

All chemicals were reagent grade and used without further purification. N-butyl polyglutamic-L-acid sodium salt (PGA), methoxy-poly(ethylene glycol)-poly(L-glutamic acid) sodium salt diblock (DB), n-

butyl poly-L-arginine hydrochloride (PArg), and n-butyl poly-L-ornithine hydrochloride (P(Orn)) were from Polypeptide Therapeutic Solutions SL (PTS, Spain). DMTMM·Cl was synthesised essentially as described in ref [67]. L-Histidine methyl ester dihydrochloride (Hist, 97%) and L-arginine methyl ester dihydrochloride (Arg, 98%) were purchased from ACROS Organics™. 3-Morpholinopropylamine (Morph) and amino-2-propanol (ApOH, 93%) were obtained from Sigma-Aldrich. MeO-PEG(2000)-COOH, MeO-PEG(3000)-NHS, and Fmoc-PEG(3000)- NHS were obtained from Iris Biotech. Single stranded DNA (ssDNA, 16-22 nucleotides) sequences, thiol hexane labelled single stranded DNA sequence (ssDNA-C6-SH), 6-FAM single stranded DNA sequence (ssDNA-FAM) were obtained from Biomers.net GmbH. Luciferase GL3 double stranded siRNA (ds-siRNA), 21 nucleotides per strand, D-001400-01-20, control ds-siRNA and transfecting agent DharmaFECT® 1 were provided by Fisher Scientific. Pyridyl dithiol ethylamine HCl salt was synthesised essentially as described in ref [68]. Deuterated solvent D_2O was purchased from Deutero GmbH. Water is defined in this chapter as deionised water with a conductance below 0.06 µS. Dialysis were performed in dialysis devices featuring proprietary Ultra-pure Biotech Cellulose Ester (CE) Membrane with 1, 3 or 10 kDa MWCO (Float-A-Lyzer®). Preparative SEC was performed using Sephadex G-25 superfine from GE.

III.4.2. Cell Culture

Murine melanoma cells B16F10-luc-G5 which stably expresses firefly luciferase were grown in DMEM medium supplemented with 10% FBS, 2 mM L-glutamine, 100 IU/mL penicillin, 100 µL/mL streptomycin at 37°C in a humidified atmosphere containing 5% CO_2 and 95% air.

III.4.3. Characterisation Techniques

III.4.3.1. Nuclear Magnetic Resonance (NMR) Spectroscopy

^1H and DOSY NMR spectra were recorded on a Bruker AC 300 or on a Bruker AV500 at room temperature (RT) and at a frequency of 300 MHz and 500 MHz respectively. Pulsed field gradient NMR spectroscopy was used to measure translational diffusion by fitting the integrals or

intensities of the NMR signals to the Stejskal-Tanner [69, 70] equation: $I= I_0 \exp[-D\gamma^2g^2\delta^2(\Delta-\delta / 3)]$ where I is the observed intensity, I_0 the reference intensity (unattenuated signal intensity), D the diffusion coefficient, γ the gyromagnetic ratio of the observed nucleus, g the gradient strength, δ the length of the gradient, and Δ the diffusion time. Two-dimensional diffusion-ordered NMR spectroscopy (DOSY) was performed with a stimulated echo sequence using bipolar gradient pulses. The lengths of delays were held constant at Δ= 100 ms, and 32 spectra of 64 scans each were acquired with the strength of the diffusion gradient varying between 5% and 95%. The lengths of the diffusion gradient and the stimulated echo were optimised for each sample. Typical values were δ = 3 ms for the analysis of both oligomers and PGA-based conjugates. All data were processed and analysed using the MestreNova 6.2 software.

III.4.3.2. Dynamic Light Scattering (DLS)

For DLS measurement, the polymer solution was measured in a cell DTS 1070 with laser light scattering using a Zetasizer Nano ZS with backscatter detection (Malvern Instruments, Worcestershire, UK). For size measurements, the equilibration time was 0 min, the temperature was 25˚C, and an automatic attenuator was used. The refractive index of the solvent, in our case water, was 1.330 and hence, the viscosity was 0.8872. For polyplex analysis of the particles the refractive index of polystyrene latex (1.590) was used. Each sample was measured 3 times with 10 subruns. The Zeta (ζ) potential was calculated by the Smoluchowski model. Therefore 10 up to 30 subruns of 10 s at 25°C (n=3) were measured.

III.4.3.3. Cellular Internalisation via InCell Analyzer Device

B16F10 cells were seeded in a black 96-well plate with flat and clear bottom at a density of 7500 cells/cm^2 (100 µL cell suspension per well) and allowed to adhere for 24 h and then medium was replaced with 80µL fresh growth medium. 20 µL of fluorophore-labelled polymer solution were added and the cells incubated for 0 to 5 h at 37˚C. At each sample time, cells were placed on ice, then the medium was removed and the cells were washed twice with 100 µL ice-chilled PBS-BSA 0.1%

and then 200 µL PBS were added. 30 min before washing the cells with PBS-BSA 0.1%, the nuclear marker Hoechst (1 µL from a solution 5 mM) was added in order to identify possible co-localisations. Cell-associated fluorescence was then analysed using an InCell Analyzer 1000 device. Cells incubated without polymer conjugate were used to account for the background fluorescence.

III.4.4. Protocols

III.4.4.1. General Method for PGA-Hist Synthesis

In a one neck round bottom flask fitted with a stir bar and stopper, 1 eq. of PGA sodium salt was suspended in milliQ water. Afterwards 1.3 eq. of DMTMM·Cl was added dissolved also in milliQ water. 10 minutes later, 1 eq. of L-histidine methyl ester dihydrochloride was added and the pH was adjusted to 8 by adding some drops of 1M $NaHCO_3$ solution. Reaction was allowed to proceed 16 hours stirring at room temperature (RT). Dialysis using Float-A-Lyzer at the corresponding MWCO was performed in order to purify the polymer. A white powder was obtained after freeze-drying.

^{1}H NMR δ_H (300 MHz, D_2O): 8.58 (1xH, s), 7.31 (1xH, s), 4.37 (1H, m), 4.14 (1xH, s), 3.81 (3xH, s), 3.36-3.18 (2xH, m), 2.31-1.96 (4H, m). x: percentage of modification.

III.4.4.2. General Method for PGA-Morph Synthesis

In a one neck round bottom flask fitted with a stir bar and stopper, 1 eq. of PGA sodium salt was suspended in milliQ water. Afterwards 1.3 eq. of DMTMM·Cl, also dissolved in milliQ water, was added. 10 minutes later, 1 eq. of 3-morpholinopropylamine was added and the pH was adjusted to 8 by adding drops of 1M $NaHCO_3$ solution. The reaction was allowed to proceed 16 hours stirring at RT. Dialysis using Float-A-Lyzer at the corresponding MWCO was performed in order to purify the polymer. A white powder was obtained after freeze-drying.

^{1}H NMR δ_H (300 MHz, D_2O): 4.33 (1H, m), 3.98 (2xH, s), 3.30-3.15 (4xH, m), 3.36-3.18 (2xH, m), 2.39-1.98 (4H + 2xH, m). x: percentage of modification.

III.4.4.3. General Method for PGA-X-ApOH Synthesis

In a one neck round bottom flask fitted with a stir bar and stopper, 1 eq. of PGA-X (X means Hist or Morph) was suspended in milliQ water. Afterwards 1 eq. of DMTMM·Cl, also dissolved in milliQ water, was added. 10 minutes later, 1 eq. of amino-2-propanol was added and the pH was adjusted to 8 by adding drops of 1M $NaHCO_3$ solution. The reaction was allowed to proceed 16 hours stirring at RT. Dialysis using Float-A-Lyzer at the corresponding MWCO was performed in order to purify the polymer. A white powder was obtained after freeze-drying.

^{1}H NMR δ_H (300 MHz, D_2O): 4.33 (1H, m), 3.21-2.94 (3xH, m), 3.30-3.15 (4xH, m), 2.34-1.98 (4H, m), 1.16 (3xH, s). x: percentage of modification.

III.4.4.4. General Method for PGA-R-Arg Synthesis

In a one neck round bottom flask fitted with a stir bar and stopper, 1 eq. of PGA-R (R means Hist or Morph) was suspended in milliQ water. Afterwards 1 eq. of DMTMM·Cl, also dissolved also in milliQ water, was added. 10 minutes later, 1 eq. of L-arginine methyl ester dihydrochloride was added and the pH was adjusted to 8 by adding drops of 1M $NaHCO_3$ solution. The reaction was allowed to proceed 16 hours stirring at RT. Dialysis using Float-A-Lyzer at the corresponding MWCO was performed in order to purify the polymer. A white powder was obtained after freeze-drying.

^{1}H NMR δ_H (300 MHz, D_2O): 4.45 (1xH, s), 4.33 (1H, m), 3.79 (2xH, s), 2.39-1.87 (4H + 4xH, m). x: percentage of modification.

III.4.4.5. Oligonucleotide Complexation to PGA-R-X

Polyplex formulations for gel shift experiments were prepared as follows: 200 ng of dsDNA and the calculated amount of PGA-R-X (where R is Hist or Morph and X is ApOH or Arg) at indicated +/- ratios were diluted in separate tubes in 10 µL of 20 mM HEPES buffered pH 7.4 each. Only protonatable nitrogens, not amide nitrogens, were considered in the +/- calculations. The nucleic acid and the polymer solution were mixed by rapidly pipetting up and down (at least 5 times) and incubated

for 30-40 min at RT in order to form the polyplexes necessary for gel shift experiments.

III.4.4.6. General Method for PGA-R-X-PD Synthesis

In a one neck round bottom flask fitted with a stir bar and stopper, 1 eq. of PGA-R-X (R means Hist or Morph, and X means ApOH or Arg) was suspended in milliQ water. Afterwards 0.2 eq. of DMTMM·Cl was added dissolved also in milliQ water. 10 minutes later, 0.1 eq. of pyridyl dithiol ethylamine HCl salt was added and the pH was adjusted to 8 by adding some drops of 1M $NaHCO_3$ solution. Reaction was allowed to proceed 16 hours stirring at RT. Dialysis using Float-A-Lyzer at the corresponding MWCO was performed in order to purify the polymer. A white powder was obtained after freeze-drying.

^{1}H NMR δ_H (300 MHz, D_2O): 8.43 (1xH, m), 7.88 (2xH, m), 7.33 (1xH, m), 4.33 (1H, m), 3.48 (2xH, m), 2.95 (2xH, m), 2.39-1.90 (4H, m). x: percentage of modification.

III.4.4.7. General Oligonucleotide Conjugation to PGA-R-X-PD

To conjugate the thiol labelled dsDNA to PGA-R-X-PD, 1-32 eq. of PGA-R-X-PD (depending on the case) were dissolved in PBS and mixed with the same volume of thiolated dsDNA containing x eq. of oligonucleotide (x is the percentage of PD modification) and the reaction mixture was incubated overnight at 37˚C with continuous shaking (500 rpm).

III.4.4.8. General Oligonucleotide Complexation to PArg or P(Orn) and Coating

System 4, 5 and 7 compounds were prepared by mixing the amount of dsDNA (200 ng) or siRNA (500 ng) and PArg or P(Orn) at indicated nitrogen/phosphate (N/P) ratios each in HEPES 20 mM pH 7.4. The nucleic acid was added to the polycation, rapidly mixed and incubated for 15 min at RT. After that, the corresponding amount of coating agent (PGA_{100} or DB_{88}) was added and incubated again during 15 min at RT.

III.4.4.9. POPD Synthesis

30 mg of P(Orn) 50 units (0.153 mmol, 1 eq.) were dissolved in 1 mL of PBS-EDTA under agitation at RT. Then, 0.1 eq. of PD (4.8 mg, 0.015 mmol) were dissolved in 200 µL of DMSO and added drop by drop to the P(Orn) solution. After one hour in agitation, the reaction was lyophilised. Residue was resuspended in 300 µL of milliQ water and purified using a PD10 column containing Sephadex G25 resin.

^{1}H NMR δ_H (300 MHz, D_2O): 8.41-7.31 (4xH, m), 4.34 (1H, m), 3.21-3.06 (4xH + 2H, m), 1.82 (4H, m). x: percentage of modification.

III.4.4.10.System 7 Polyplex Formation

System 7 polyplexes were prepared by dissolving the amount of dsDNA or siRNA and oligomers at indicated nitrogen/phosphate (N/P) ratios each in HEPES 20 mM pH 7.4. The nucleic acid was added to the polycation, rapidly mixed and incubated for 20-30 min at RT.

III.4.4.11. Synthesis of POP1

All reagents were weighed in 5 mL vials and stoppered with rubber septa. Vials were purged under N_2 and P(Orn) was dissolved in 1 mL DMSO anhydrous under magnetic stirring. PEG was dissolved in 1 mL DMSO under the same conditions and after the solution was taken with a syringe and dropped in the P(Orn) vial. A catalytic amount of DMTMM·BF_4 (dissolved in 300 µL DMSO) was added with the same protocol. Then, pH was adjusted to 8 with DIEA and reaction was left under magnetic stirring for 72 h.

The reaction was transferred to a 5 mL round bottom flask and DMSO was evaporated under vacuum. The obtained residue was dissolved in 300 µL of milliQ water and it was purified over a PD10 column. Fractions were lyophilised and the obtained solids were analysed by ^{1}H NMR and DOSY (D_2O).

^{1}H NMR δ_H (300 MHz, D_2O): 4.41 (1H, m), 3.74(44xH + 4H m), 3.07 (2H, m), 1.82 (4H, m). x: percentage of modification.

III.4.4.12. Synthesis of POP2

All reagents were weighed in 5 mL vials and stoppered with rubber septa. Vials were purged under N_2 and P(Orn) was dissolved in 2 mL DMSO anhydrous under magnetic stirring. PEG was dissolved in 1 mL DMSO under the same conditions and placed in the P(Orn) vial. A catalytic amount of DMAP (dissolved in 200 µL DMSO) was added with the same protocol. Then, pH was adjusted to 8 with DIEA and reaction was left under magnetic stirring for 36 h.

The reaction was transferred to a 5 mL round bottom flask and DMSO was evaporated under vacuum. The obtained residue was dissolved in 300 µL of milliQ water and it was purified using a PD10 column (500 µL fraction, t.1-2 of 1 mL each, 30 fractions). Fractions were lyophilised and the obtained solids were analysed by ^{1}H NMR and DOSY (D_2O).

^{1}H NMR δ_H (300 MHz, D_2O): 4.41 (1H, m), 3.74(68xH + 4H m), 3.07 (2H, m), 1.82 (4H, m). x: percentage of modification.

III.4.4.13. Synthesis of POPF

All reagents were weighed in 5 mL vials and stoppered with rubber septa. Vials were purged under N_2 and P(Orn) was dissolved in 2 mL DMSO anhydrous under magnetic stirring. PEG was dissolved in 1 mL DMSO under the same conditions placed in the P(Orn) vial. A catalytic amount of DIEA (dissolved in 200 µL DMSO) was added with the same protocol. Then, pH was adjusted to 8 with DIEA and reaction was left under magnetic stirring for 72 h.

The reaction was transferred to a 5 mL round bottom flask and DMSO was evaporated under vacuum. The obtained residue was dissolved in 300 µL of milliQ water and it was purified using a PD10 column (500 µL fraction, t.1-2 of 1 mL each, 30 fractions). Fractions were lyophilised and the obtained solids were analysed by ^{1}H NMR and DOSY (D_2O).

^{1}H NMR δ_H (300 MHz, D_2O): 4.41 (1H, m), 3.74(68xH + 4H m), 3.07 (2H, m), 1.82 (4H, m). x: percentage of modification.

III.4.4.14. DNA and siRNA Binding Assay by Electrophoresis

For dsDNA, a 1% agarose gel was prepared by dissolving agarose in TAE buffer (Tris base, acetic acid and EDTA) and boiling to 100°C. After cooling down to 50°C and the addition of EtBr, the agarose gel was cast in the electrophoresis unit. Polyplexes or conjugates containing 200 ng of dsDNA in 20 µL HEPES and loading buffer were placed into the sample wells. Electrophoresis was performed at 80 V for 80 min. For siRNA, a 2.5% agarose gel containing EtBr was prepared. Polyplexes or conjugates containing 500 ng of siRNA in 20 µL HEPES and loading buffer were placed into the sample wells. Electrophoresis was performed at 80 V for 40 min.

III.4.4.15. Red Blood Cell (RBC) Lysis Assay

Erythrocytes (RBC, red blood cells) were isolated from fresh whole mouse blood obtained by cardiac puncture after death and placed in a heparinised tube. Blood was diluted with PBS pH 7.4 up to 10 mL and then centrifuged (3000 rpm, 10 min, 4°C) three times, removing the supernatant after each centrifugation and re-suspending the cells in sterile PBS. The final RBC pellet was weighed and re-suspended at 2% (v/v) in PBS. To study the haemolytic activity of the systems, the systems were dissolved in PBS stock solutions adjusted to pH 6.5 or 7.4 and citrate solution adjusted to pH 5.5. Then samples were added to wells (n=3, 100 µL) covering the concentration range 0.1-0.01 mg/mL of systems. Buffer at the corresponding pH was used as a control together with Triton X–100 1% (w/v) to determine a 100% RBC lysis. The plates were then incubated at 37°C for 1 h. To assess haemoglobin (Hb) release the plates were then centrifuged (3000 rpm, 10 min, 20°C) and the supernatant of each well was transferred into a new plate. The Hb released was assessed by measuring the absorbance at 570 nm using Victor^2 Wallac^{eTM} plate reader. The percentage of haemolysis of each sample was calculated relative to 100% haemolysis obtained from incubation with Triton-X 100.

III.4.4.16. Buffer Capacity- Potentiometric Titration

The polymer sample containing 15 µmol protonatable amines was diluted in a total volume of 3.5 mL NaCl solution (50 mM) and the pH was adjusted to 2.1 by addition of 0.1 M HCl. Afterwards, a back titration with 50 mM NaOH solution was performed until a pH of 11 was reached. Furthermore a titration with 50 mM NaCl was performed and the consumption of NaOH in this control titration was subtracted from the consumption in the polymer titrations at the corresponding pH values. Percentage of buffer capacity C in a certain pH range (x - y), where ΔV stands for the volume consumption of NaOH in the considered pH range, was calculated according to Equation III.1

$$C_{pH_{x-y}} = \frac{\Delta V_{pH_{x-y}} \times 0.05M}{0.015\ mmol} \times 100 \qquad \text{Equation III.1}$$

where C is the total buffer capacity between the indicated pH values (%) and ΔV is the volume difference between the indicated pH values (mL).

III.4.4.17. Plasma Stability by Gel Shift Assay

For the investigation of plasma stability, polymer-DNA conjugates prepared as in Section III.4.4.7, were incubated in a solution containing 20% mice serum at 37˚C and different incubation times: 0 h, 0.5 h, 1 h, 2 h, and 5 h. Then, an agarose electrophoresis assay was performed using the same protocol than in Section III.4.4.14.

III.4.4.18. Cell Culture Media Stability by Gel Shift Assay

For the investigation of cell culture media stability, polymer-DNA conjugates prepared as in Section III.4.4.7, were incubated in a solution containing 80% cell culture media at 37˚C and different incubation times. Then, an agarose electrophoresis assay was performed using the same protocol than in Section III.4.4.14.

III.4.4.19. Luciferase Gene Silencing *In Vitro* and Luciferase Assay

B16F10 luc cells were plated on 96-well plates (7500 cells/well) in 100 µL of medium containing 10% FBS 24 h prior to the transfection. Cells were incubated with the developed systems or the positive control (DharmaFECT™) containing luc siRNA or control siRNA. At 48 h after

treatment cells were treated with 20 µL of Bright-Glo™ reagent. Luciferase activity was read spectrophotometrically using Victor^2 Wallac plate reader. Relative light units (RLU) were presented as percentage of the luciferase gene expression obtained with buffer treated control cells.

III.4.4.20. MTS Assay for Cell Viability Evaluation

B16F10 luc cells were seeded into 96-well plates (7500 cells/well) in 100 µL of medium containing 10% FBS. After 24 h, culture medium was replaced with 80 µL fresh growth medium containing 10% FCS and 20 µL of transfection complexes solution at different +/- ratios were added. All studies were performed in quintuplicate. 48 h post-treatment, 20 µL of manufacturer solution containing MTS/PMS (20:1) was added to each well, and the cells were incubated for a further 2 h. Optical density of each well was measured spectrophotometrically at 490 nm using Victor^2 Wallac plate reader. The absorbance values were represented as the percentage of cell viability taken as 100% cell viability of untreated control cells.

REFERENCES

1. Friedmann, T. and R. Roblin, *Gene Therapy for Human Genetic Disease?* Science, 1972. **175**(4025): p. 949-955.
2. Mulligan, R., *The basic science of gene therapy.* Science, 1993. **260**(5110): p. 926-932.
3. Wirth, T., N. Parker, and S. Ylä-Herttuala, *History of gene therapy.* Gene, 2013. **525**(2): p. 162-169.
4. Therapy Clinical Trials Worldwide Database provided by the Journal of Gene Medicine, http://www.wiley.com/legacy/wileychi/genmed/clinical/, April 2016.
5. Fire, A., et al., *Potent and specific genetic interference by double-stranded RNA in Caenorhabditis elegans.* Nature, 1998. **391**(6669): p. 806-811.
6. Elbashir, S.M., et al., *Duplexes of 21-nucleotide RNAs mediate RNA interference in cultured mammalian cells.* Nature, 2001. **411**(6836): p. 494-498.

7. Bernstein, E., et al., *Role for a bidentate ribonuclease in the initiation step of RNA interference.* Nature, 2001. **409**(6818): p. 363-366.
8. Matranga, C., et al., *Passenger-Strand Cleavage Facilitates Assembly of siRNA into Ago2-Containing RNAi Enzyme Complexes.* Cell. **123**(4): p. 607-620.
9. Ameres, S.L., J. Martinez, and R. Schroeder, *Molecular Basis for Target RNA Recognition and Cleavage by Human RISC.* Cell. **130**(1): p. 101-112.
10. Song, J.-J., et al., *Crystal Structure of Argonaute and Its Implications for RISC Slicer Activity.* Science, 2004. **305**(5689): p. 1434-1437.
11. Kanasty, R., et al., *Delivery materials for siRNA therapeutics.* Nat Mater, 2013. **12**(11): p. 967-977.
12. Behlke, M.A., *Progress towards in Vivo Use of siRNAs.* Mol Ther, 2006. **13**(4): p. 644-670.
13. Hannon, G.J. and J.J. Rossi, *Unlocking the potential of the human genome with RNA interference.* Nature, 2004. **431**(7006): p. 371-378.
14. Vannucci, L., et al., *Viral vectors: a look back and ahead on gene transfer technology.* New Microbiol, 2013. **36**(1): p. 1-22.
15. Pack, D.W., et al., *Design and development of polymers for gene delivery.* Nat Rev Drug Discov, 2005. **4**(7): p. 581-593.
16. Yin, H., et al., *Non-viral vectors for gene-based therapy.* Nat Rev Genet, 2014. **15**(8): p. 541-555.
17. Li, S.-D. and L. Huang, *Non-viral is superior to viral gene delivery.* Journal of Controlled Release, 2007. **123**(3): p. 181-183.
18. Wagner, E., *Polymers for siRNA Delivery: Inspired by Viruses to be Targeted, Dynamic, and Precise.* Accounts of Chemical Research, 2012. **45**(7): p. 1005-1013.
19. Yin, L., N. Zheng, and J. Cheng, *Highly Efficient SiRNA Delivery Mediated by Cationic Helical Polypeptides and Polypeptide-Based Nanosystems*, in *SiRNA Delivery Methods: Methods and Protocols*, K. Shum and J. Rossi, Editors. 2016, Springer New York: New York, NY. p. 37-47.
20. Martin, M.E. and K.G. Rice, *Peptide-guided gene delivery.* The AAPS Journal, 2007. **9**(1): p. E18-E29.
21. Thomas, C.E., A. Ehrhardt, and M.A. Kay, *Progress and problems with the use of viral vectors for gene therapy.* Nat Rev Genet, 2003. **4**(5): p. 346-358.

22. Zagorodko, O., et al., *Polypeptide-Based Conjugates as Therapeutics: Opportunities and Challenges.* Macromolecular Bioscience, 2017. **17**(1): p. 1600316-n/a.
23. Maeda, H., H. Nakamura, and J. Fang, *The EPR effect for macromolecular drug delivery to solid tumors: Improvement of tumor uptake, lowering of systemic toxicity, and distinct tumor imaging in vivo.* Advanced Drug Delivery Reviews, 2013. **65**(1): p. 71-79.
24. Duncan, R. and S.C.W. Richardson, *Endocytosis and Intracellular Trafficking as Gateways for Nanomedicine Delivery: Opportunities and Challenges.* Molecular Pharmaceutics, 2012. **9**(9): p. 2380-2402.
25. Thomas, C.M. and J.-F. Lutz, *Precision Synthesis of Biodegradable Polymers.* Angewandte Chemie International Edition, 2011. **50**(40): p. 9244-9246.
26. Conejos-Sanchez, I., et al., *A controlled and versatile NCA polymerization method for the synthesis of polypeptides.* Polymer Chemistry, 2013. **4**(11): p. 3182-3186.
27. VICENT, M.J., et al., *Controlled synthesis of polyglutamates with low polydispersity and versatile architectures*. WO2013/060919A1.
28. Niño-Pariente, A., V. J. Nebot, and M.J. Vicent, *Relevant Physicochemical Descriptors of "Soft Nanomedicines" to Bypass Biological Barriers.* Current Pharmaceutical Design, 2016. **22**(9): p. 1274-1291.
29. Hadjichristidis, N., et al., *Synthesis of Well-Defined Polypeptide-Based Materials via the Ring-Opening Polymerization of α-Amino Acid N-Carboxyanhydrides.* Chemical Reviews, 2009. **109**(11): p. 5528-5578.
30. Deming, T.J., *Synthesis of Side-Chain Modified Polypeptides.* Chemical Reviews, 2016. **116**(3): p. 786-808.
31. Barz, M., A. Duro-Castano, and M.J. Vicent, *A versatile post-polymerization modification method for polyglutamic acid: synthesis of orthogonal reactive polyglutamates and their use in "click chemistry".* Polymer Chemistry, 2013. **4**(10): p. 2989-2994.
32. Kirtane, A.R. and J. Panyam, *Polymer nanoparticles: Weighing up gene delivery.* Nat Nano, 2013. **8**(11): p. 805-806.
33. Lachelt, U. and E. Wagner, *Nucleic Acid Therapeutics Using Polyplexes: A Journey of 50 Years (and Beyond).* Chem Rev, 2015. **115**(19): p. 11043-78.

34. Singer, J.W., et al., *Paclitaxel poliglumex (XYOTAX; CT-2103): an intracellularly targeted taxane.* Anti-Cancer Drugs, 2005. **16**(3): p. 243-254.
35. Duncan, R. and M.J. Vicent, *Polymer therapeutics-prospects for 21st century: The end of the beginning.* Advanced Drug Delivery Reviews, 2013. **65**(1): p. 60-70.
36. Barz, M., et al., *Overcoming the PEG-addiction: well-defined alternatives to PEG, from structure-property relationships to better defined therapeutics.* Polymer Chemistry, 2011. **2**(9): p. 1900-1918.
37. Bertrand, E., et al., *Histidinylated linear PEI: a new efficient non-toxic polymer for gene transfer.* Chemical Communications, 2011. **47**(46): p. 12547-12549.
38. Wen, Y., et al., *Serum tolerance and endosomal escape capacity of histidine-modified pDNA-loaded complexes based on polyamidoamine dendrimer derivatives.* Biomaterials, 2012. **33**(32): p. 8111-8121.
39. Thomas, J.J., M.R. Rekha, and C.P. Sharma, *Unraveling the Intracellular Efficacy of Dextran-Histidine Polycation as an Efficient Nonviral Gene Delivery System.* Molecular Pharmaceutics, 2012. **9**(1): p. 121-134.
40. Gu, J., et al., *Self-assembled carboxymethyl poly (l-histidine) coated poly (β-amino ester)/DNA complexes for gene transfection.* Biomaterials, 2012. **33**(2): p. 644-658.
41. Hashemi, M., et al., *Modified polyethyleneimine with histidine-lysine short peptides as gene carrier.* Cancer Gene Ther, 2011. **18**(1): p. 12-19.
42. Perche, F., et al., *Gene transfer by histidylated lipopolyplexes: A dehydration method allowing preservation of their physicochemical parameters and transfection efficiency.* International Journal of Pharmaceutics, 2012. **423**(1): p. 144-150.
43. Perche, F., et al., *Selective gene delivery in dendritic cells with mannosylated and histidylated lipopolyplexes.* Journal of Drug Targeting, 2011. **19**(5): p. 315-325.
44. Midoux, P., et al., *Chemical vectors for gene delivery: a current review on polymers, peptides and lipids containing histidine or imidazole as nucleic acids carriers.* British Journal of Pharmacology, 2009. **157**(2): p. 166-178.

45. Kim, T.-i., M. Lee, and S.W. Kim, *A guanidinylated bioreducible polymer with high nuclear localization ability for gene delivery systems.* Biomaterials, 2010. **31**(7): p. 1798-1804.
46. Meng, F., W.E. Hennink, and Z. Zhong, *Reduction-sensitive polymers and bioconjugates for biomedical applications.* Biomaterials, 2009. **30**(12): p. 2180-2198.
47. Cleland, W.W., *Dithiothreitol, a New Protective Reagent for SH Groups*.* Biochemistry, 1964. **3**(4): p. 480-482.
48. Murthy, N., et al., *The design and synthesis of polymers for eukaryotic membrane disruption.* Journal of Controlled Release, 1999. **61**(1–2): p. 137-143.
49. Fox, M.E., F.C. Szoka, and J.M.J. Fréchet, *Soluble Polymer Carriers for the Treatment of Cancer: The Importance of Molecular Architecture.* Accounts of Chemical Research, 2009. **42**(8): p. 1141-1151.
50. Boussif, O., et al., *A versatile vector for gene and oligonucleotide transfer into cells in culture and in vivo: polyethylenimine.* Proc Natl Acad Sci U S A, 1995. **92**(16): p. 7297-301.
51. Aigner, A., et al., *Delivery of unmodified bioactive ribozymes by an RNA-stabilizing polyethylenimine (LMW-PEI) efficiently down-regulates gene expression.* Gene Ther, 2002. **9**(24): p. 1700-7.
52. Futaki, S., et al., *Stearylated Arginine-Rich Peptides: A New Class of Transfection Systems.* Bioconjugate Chemistry, 2001. **12**(6): p. 1005-1011.
53. Richard, J.P., et al., *Cell-penetrating Peptides: A REEVALUATION OF THE MECHANISM OF CELLULAR UPTAKE.* Journal of Biological Chemistry, 2003. **278**(1): p. 585-590.
54. Futaki, S., et al., *Arginine-rich Peptides: AN ABUNDANT SOURCE OF MEMBRANE-PERMEABLE PEPTIDES HAVING POTENTIAL AS CARRIERS FOR INTRACELLULAR PROTEIN DELIVERY.* Journal of Biological Chemistry, 2001. **276**(8): p. 5836-5840.
55. Merdan, T., et al., *Pegylated Polyethylenimine−Fab' Antibody Fragment Conjugates for Targeted Gene Delivery to Human Ovarian Carcinoma Cells.* Bioconjugate Chemistry, 2003. **14**(5): p. 989-996.
56. ENGELBERG, H., *Plasma Heparin Levels.* Correlation with Serum Cholesterol and Low-Density Lipoproteins, 1961. **23**(4): p. 573-577.

57. Takechi, Y., et al., *Comparative study on the interaction of cell-penetrating polycationic polymers with lipid membranes.* Chemistry and Physics of Lipids, 2012. **165**(1): p. 51-58.
58. Koloskova, O.O., et al., *Synthesis and evaluation of novel lipopeptide as a vehicle for efficient gene delivery and gene silencing.* European Journal of Pharmaceutics and Biopharmaceutics, 2016. **102**: p. 159-167.
59. Bond, V.C. and B. Wold, *Poly-L-ornithine-mediated transformation of mammalian cells.* Molecular and Cellular Biology, 1987. **7**(6): p. 2286-2293.
60. Pouton, C.W., et al., *Polycation-DNA complexes for gene delivery: a comparison of the biopharmaceutical properties of cationic polypeptides and cationic lipids.* Journal of Controlled Release, 1998. **53**(1–3): p. 289-299.
61. Caliceti, P. and F.M. Veronese, *Pharmacokinetic and biodistribution properties of poly(ethylene glycol)–protein conjugates.* Advanced Drug Delivery Reviews, 2003. **55**(10): p. 1261-1277.
62. *ISO 10993-5:2009: Biological Evaluation of Medical Devices. Part 5: Tests for In Vitro Cytotoxicity. International Organization for Standardization; Geneva, Switzerland.* 2009.
63. Jiang, Q.-Y., et al., *Gene delivery to tumor cells by cationic polymeric nanovectors coupled to folic acid and the cell-penetrating peptide octaarginine.* Biomaterials, 2011. **32**(29): p. 7253-7262.
64. Tai, Z., et al., *Biodegradable Stearylated Peptide with Internal Disulfide Bonds for Efficient Delivery of siRNA In Vitro and In Vivo.* Biomacromolecules, 2015. **16**(4): p. 1119-1130.
65. Verdurmen, Wouter P.R., et al., *Preferential Uptake of L- versus D-Amino Acid Cell-Penetrating Peptides in a Cell Type-Dependent Manner.* Chemistry & Biology, 2011. **18**(8): p. 1000-1010.
66. Yoo, J., et al., *Bioreducible branched poly(modified nona-arginine) cell-penetrating peptide as a novel gene delivery platform.* Journal of Controlled Release, 2017. **246**: p. 142-154.
67. Kunishima, M., et al., *Synthesis and Characterization of 4-(4,6-Dimethoxy-1,3,5-triazin-2-yl)-4-methylmorpholinium Chloride.* Tetrahedron Letters, 1999. **40**(29): p. 5327-5330.
68. van der Vlies, A.J., et al., *Synthesis of Pyridyl Disulfide-Functionalized Nanoparticles for Conjugating Thiol-Containing*

Small Molecules, Peptides, and Proteins. Bioconjugate Chemistry, 2010. **21**(4): p. 653-662.

69. Tsou, C.C. and S.S. Sun, *New fluorescent amide-functionalized phenylethynylthiophene low molecular weight gelator.* Organic Letters, 2006. **8**(3): p. 387-390.
70. Tu, T., et al., *Visual Chiral Recognition through Enantioselective Metallogel Collapsing: Synthesis, Characterization, and Application of Platinum–Steroid Low-Molecular-Mass Gelators.* Angewandte Chemie International Edition, 2011. **50**(29): p. 6601-6605.

Chapter IV

Development of PGA-Based Conjugates for Intraperoxisomal Delivery of Engineered Human Alanine:Glyoxylate Aminotransferase

The work presented within this thesis chapter was carried out thanks to a collaboration between the Polymer Therapeutics lab and the research group of Dr. Barbara Cellini at the Department of Neurological Biomedical and Movement Sciences at the University of Verona (Italy). A publication entitled "Use of Polymer Conjugates for the Intraperoxisomal Delivery of Engineered Human Alanine:Glyoxylate Aminotransferase as a Protein Therapy for Primary Hyperoxaluria Type I" in the journal Nanomedicine: Nanotechnology, Biology and Medicine has been the result of this collaborative work [1].

IV.1. INTRODUCTION AND BACKGROUND

The delivery of active proteins to cells or living organisms constitutes another example of therapy that requires effective cytosolic transport. This therapeutic approach is used for many pathologic conditions and a variety of protein drugs are already in the market [2]. In the case of loss-of-function genetic diseases caused by enzyme deficits, enzyme administration replenishes the target organism with the absent or defective protein, thus partly or completely rescuing the clinical phenotype. Although the initial application of this approach was limited to circulating proteins, in the last few decades enzyme replacement therapy has been successfully applied to other disorders including phenylketonuria, the deficit of adenosine deaminase, and some lysosomal storage diseases [3-5].

Alanine:glyoxylate aminotransferase (AGT) is a pyridoxal 5'-phosphate (PLP)-dependent enzyme that catalyses an overall transamination reaction converting L-alanine and glyoxylate to pyruvate and glycine, respectively [6]. The protein is a homodimer (molecular weight (MW) 86 KDa) belonging to the fold Type I family of PLP-enzymes. Each monomer comprises an N-terminal stretch of 20 residues that wraps the surface of the adjacent subunit, a large domain (residues 21-282) forming most of the active site and of the dimerisation interface, and a small domain (residues 283-392) containing the peroxisomal targeting sequence (PTS) (Figure IV.1A). As with most peroxisomal proteins, AGT folds in the cell cytosol and is then translocated to peroxisomes in its fully-folded dimeric state.

Peroxisomal import occurs through the formation of a complex between AGT and the Pex5p carrier. The interaction is weak and is mediated by a non-canonical –KKL type 1 PTS (PTS1) and by an "extended PTS1" formed by residues 381–388 and 327–330 (Figure IV.1B) [7].

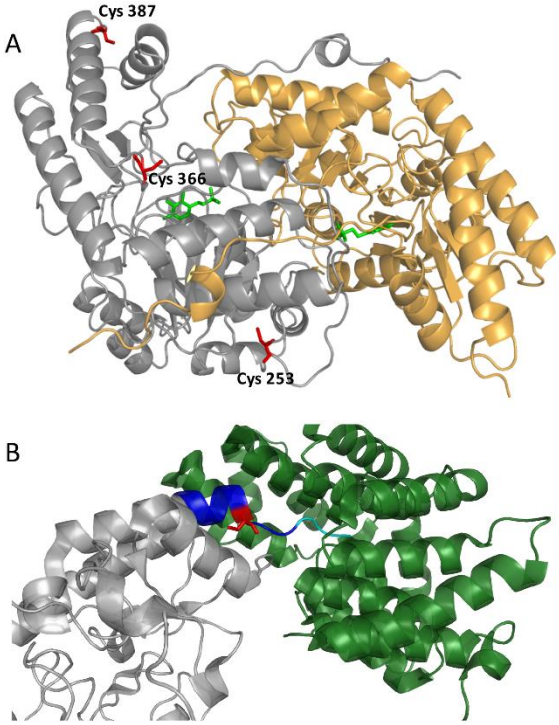

Figure IV.1. AGT dimeric structure. (A) The AGT dimer (PDB file 1H0C) is coloured as follow: one monomer is pale orange and the other is grey with exposed Cys residues represented as red sticks. PLP is represented as green sticks. (B) Representation of the interaction between the C-term domain of Pex5p receptor (green) and AGT (grey). On AGT the PTS1 and the extended PTS1 are coloured cyan and blue, respectively; Cys387 is coloured red.

AGT deficit causes Primary Hyperoxaluria Type I (PH1), a rare genetic disease characterised by an abnormally high concentration of urinary oxalate. This leads to the deposition of calcium oxalate (CaOx) crystals in the kidneys and urinary tract causing urolithiasis and nephrocalcinosis [8-10]. This can progress to end-stage-renal-disease and to a potentially fatal condition called systemic oxalosis with CaOx deposition in various tissues [11, 12]. The only pharmacologic approach

available to treat PH1 is the administration of vitamin B6, although this is only effective in a minority of the patients (25-35%). The best option for unresponsive subjects is liver transplantation, which replaces the entire enzyme pool but entails several undesired side effects [12, 13]. Thus, the design of new treatment strategies represents an urgent need.

PH1 displays a loss-of-function pathogenesis because the absence of functional AGT prevents the detoxification of glyoxylate inside liver peroxisomes, leading to its cytosolic accumulation and oxidation to the metabolic end-product oxalate [8, 10]. Thus, an enzyme administration strategy to replenish the liver with active AGT may relieve disease symptoms. In this regard, a study recently demonstrated that an AGT-cell-penetrating Tat-peptide fusion protein (Tat-AGT) can be successfully transduced in a mammalian model of PH1 and restores the glyoxylate detoxification ability of the cells [14]. Although these data provided the proof-of-principle for the feasibility of AGT administration, the direct intravenous administration of Tat-AGT is not feasible as it would elicit an aggressive immune response [15].

In the present thesis chapter, we evaluated the feasibility of the delivery of AGT by conjugating the enzyme with a polymeric nanocarrier. This masks the proteins from the immune system, improves its stability in the bloodstream, and increases cargo transport across the plasma membrane [16]. Multifunctional telechelic biodegradable polymers represent an exciting technology in the field of protein delivery by means of polymer conjugation approaches. Many polymer conjugates are already in the market with demonstrated clinical benefit including the well-known PEGylated proteins [17-20]. Polypeptide-based carriers, in particular poly-L-glutamic acid homopolymers (PGA) as polymer-drug conjugates and polyethylenglycol (PEG)-PGA block-*co*-polymers as polymeric micelles have been widely exploited as delivery systems as they have demonstrated safety and excellent pharmacologic properties in the clinic [17, 21]. However, PGA-derived carriers have not been widely studied for protein conjugation [22]. Recently, in our laboratory, the formation of disulphide bonds between reactive thiol groups after PGA

derivatisation and free cysteines (Cys) exposed on the protein surface has been described [23, 24]. Once internalised, the reducing environment of the cell cytosol can cleave the covalent linkage, thus allowing the release of the free protein cargo [24, 25]. Based on this, a strategy has been constructed to efficiently conjugate recombinant purified AGT with a PEG-PGA block-*co*-polymer functionalised with pyridyl dithiol (PD) groups able to react with free thiol groups forming a reversible disulphide bond. We show that conjugation with PEG-PGA does not significantly alter the functional properties of AGT and endows the protein with the ability to cross the plasma membrane and localise in the cytosol of a cellular model of PH1. Engineering AGT by the insertion of a stronger PTS and the mutation of one of the polymer anchoring points located on the "extended PTS1" partly decreases the conjugation efficiency. However, this allows peroxisomal targeting of the conjugates, resulting in the enhanced ability to detoxify intraperoxisomal glyoxylate with respect to the wild-type protein.

IV.2. RESULTS AND DISCUSSION

IV.2.1. Synthetic Methodologies

IV.2.1.1. Synthesis of Pyridyl Disulphide Modified PEG-PGA

We modified PEG-PGA diblock with pyridyl dithiol ethylamine using 4-(4,6-Dimethoxy-1,3,5-triazin-2-yl)-4-methylmorpholinium chloride (DMTMM·Cl) as a carboxylic acid activator according to methodology previously described in Chapter II. After purification via ultrafiltration, we analysed the freeze-dried product by NMR to determine the degree of modification. This achieved a total loading of 14 mol% corresponding to 11 glutamic acid units (GAU) out of the total 80. From the percentage of modification, the MW of the pyridyl dithiol PEG-PGA was calculated to be 15,715 Da.

IV.2.1.2. Conjugation of PEG-PGA with AGT

To conjugate purified recombinant AGT with PEG-PGA the formation of reduction-sensitive disulphide bonds after PGA derivatisation with free Cys exposed on the protein surface was used [24, 25]. The crystal structure of AGT shows that Cys253, Cys366 and

Cys387 are located near the surface of the protein and could be employed as conjugation sites (Figure IV.1A) [26]. As a preliminary experiment, we used the thiol-reactive probe 5,5-dithiobis(2-nitrobenzoate) (DTNB) to verify the presence of solvent-exposed cysteine residues potentially available for the conjugation process. It was discovered that three out of the six Cys residues present on each monomer were reactive toward DTNB, although with different kinetics. Titration of the first thiol group of each monomer occurred with a $t_{1/2}$ of 4.4 min, while the titration of the other two groups occurred with a $t_{1/2}$ of 65 min, thus suggesting that one of the Cys was more exposed to the solvent. Moreover, by measuring the transaminase activity of the DTNB-treated enzyme, it was found that the titration did not significantly compromise the enzyme catalytic activity. These data support the use of a strategy based on the formation of disulphide bonds to allow PEG-PGA conjugation.

The conjugation was carried out by mixing equal volumes of AGT and PEG-PGA. Preliminary experiments were performed at different polymer:protein molar ratios (from 5:1 to 15:1) and also at different incubation times (from 1 to 48 h) to achieve optimal conjugation conditions. The achieved yield was greater than 90% by using a 5:1 ratio and by incubating the mixture over night at 25°C. The unbound polymer was then removed by forced dialysis. Conjugation of AGT with PEG-PGA, altered the electrophoretic pattern of AGT, which appeared as a smeared band at MWs higher than that of the unconjugated monomer (Figure IV.2). As PEG-PGA alone does not give any signal upon staining [24, 27], the smeared band is probably indicative of different levels of conjugation. The incubation of PEG-PGA-AGT conjugates with 10 mM reduced glutathione for 1 h at 37°C, a condition mimicking the reducing environment of the cell cytosol, led to the disappearance of the smear and the complete recovery of the band corresponding to the unconjugated monomer.

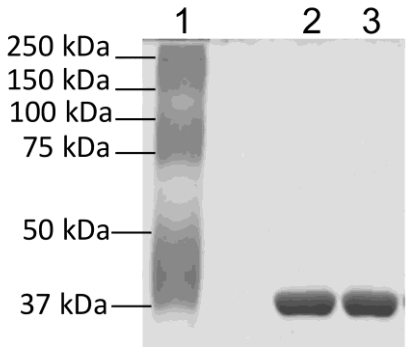

Figure IV.2. Evaluation of the PEG-PGA-AGT conjugation efficiency. 6 µg of protein were loaded in each lane and stained with Coomassie Blue. Lanes were loaded as follow: 1. PEG-PGA-AGT conjugation mixture; 2 PEG-PGA-AGT conjugates treated with GSH. 3. Unconjugated AGT.

These results confirm that pyridyl dithiol functionalised PEG-PGA can be used to efficiently conjugate AGT at room temperature. The process can be reversed by application of mild reducing conditions, confirming specificity of the conjugation and supporting the possibility of intracellular payload release.

IV.2.2. Biochemical Characterisation of the PEG-PGA-AGT Conjugates

One main challenge in the development of protein-polymer conjugates is the possible irreversible modification of the protein that may compromise its functionality [25]. To assess if PEG-PGA conjugation of AGT altered the biochemical properties of the enzyme, we compared spectroscopic and kinetic properties of the PEG-PGA-AGT conjugates with those of the unmodified protein. The molar extinction coefficient at 280 nm cannot be used to determine protein concentration in the conjugates due to interference from the polymer moiety. Thus, we determined AGT concentration by Bradford assay or an indirect assay based on the measurement of the PLP content of the sample (taking into account that AGT binds two moles of PLP per dimer). In each experiment, the results obtained using the two methods did not differ by more than 10%.

As already described [6], purified recombinant AGT displays an absorbance band in the visible region centred at 423 nm associated with

a positive dichroic band at 429 nm, and a shoulder at about 340 nm, associated with a negative dichroic band at 335 nm. These bands have been previously attributed to the ketoenamine and enolimine tautomers of the internal aldimine. Additionally, the circular dichroism (CD) spectrum displayed positive dichroic bands in the aromatic region at 285 and 290 nm and a negative dichroic band in the 256–266 nm region, probably related to the position of aromatic amino acids located in the microenvironment of the active site [6]. As shown in Figure IV.3A, conjugated and unconjugated AGT displayed similar dichroic features in the UV-visible region, thus indicating that the conjugation process did not significantly alter the coenzyme binding mode and the AGT tertiary structure. This is in agreement with the finding that intrinsic fluorescence emission spectra of the two species are characterised by an identical emission maximum at 337 nm and by a similar emission intensity (Figure IV.3B).

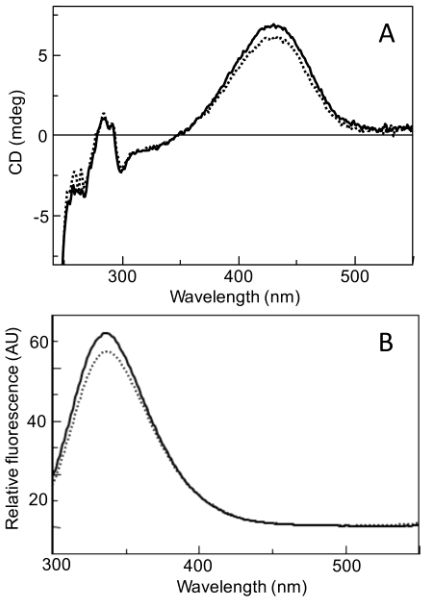

Figure IV.3. Spectral properties of PEG-PGA-AGT (dotted line) and unconjugated AGT (continuous line). (A) CD spectra were taken at 8 μM enzyme concentration. (B) Intrinsic fluorescence spectra were taken at 1 μM enzyme concentration (λ_{exc} 280 nm). All measurement were performed in 100 mM KP buffer pH 7.4.

Next, the steady-state kinetic parameters of conjugated and unconjugated AGT for the overall transamination of the L-alanine/glyoxylate pair was measured (Table IV.1). PEG-PGA-AGT conjugates displayed K_m for the substrates comparable to those of native AGT and a maximum specific activity value equal to ~80% with respect to unconjugated AGT. Upon GSH treatment, the specific activity of the released enzyme was not significantly different from that of the unconjugated enzyme. Thus, the conjugation process has only a limited impact on the catalytic properties of AGT and the small modification caused by the polymer does not irreversibly compromise the protein properties. This is in line with the finding that the DTNB titration does not alter the AGT activity.

Table IV.1. Kinetic parameters for the L-alanine/glyoxylate transamination of unconjugated and conjugated AGT.

Species	Substrate	Co-substrate	K_{cat} (s^{-1})	K_m (mM)
AGT	L-alanine	Glyoxylate	45 ± 2[a]	31 ± 4[a]
	Glyoxylate	L-alanine	45 ± 3[a]	0.23 ± 0.05[a]
PEG-PGA-AGT	L-alanine	Glyoxylate	33 ± 1	39 ± 3
	Glyoxylate	L-alanine	35 ± 2	0.18 ± 0.04
PEG-PGA-AGT after GSH treatment	L-alanine	Glyoxylate	48 ± 5	35 ± 4
	Glyoxylate	L-alanine	42 ± 4	0.21 ± 0.05

[a] From ref. [5]

Dynamic Light Scattering (DLS) and Size-Exclusion Chromatography (SEC) analyses were also used to gain insight into the molecular dimensions of the PEG-PGA-AGT conjugates. As shown in Figure IV.4A, the unconjugated polymer was mainly present as two species characterised by a hydrodynamic diameter of 5.1 ± 0.3 nm and 199 ± 10 nm. Since the DLS intensity signal is proportional to the sixth power of a particle diameter, the specie at the lower diameter was the most abundant in solution. Unconjugated AGT displayed a hydrodynamic diameter of 7.9 ± 0.3 nm, in agreement with previous reports [28-30]. Upon conjugation, a main peak with a size of 15 ± 4 nm was present, consistent with the formation of the protein-polymer complex. Accordingly, while the elution volume of unconjugated AGT on SEC was

30.6 mL, PEG-PGA-AGT conjugates eluted as a mixture of two peaks at 23.2 and 25.6 mL, along with a shoulder at 30 mL, the elution volume of unconjugated AGT (Figure IV.5B). By collecting fractions corresponding to each peak and analysing by sodium dodecyl sulphate-polyacrylamide gel electrophoresis (SDS-PAGE), we found that fraction 1 mainly contained conjugates at high molecular weight (HMW) (>200 KDa) and fraction 2 mainly contained conjugates at low molecular weight (LMW) (<200 KDa). Meanwhile, fraction 3 was predominantly made up of the small amount of unconjugated AGT remaining in the mixture. The formation of conjugates at different MWs is not unexpected based on the previous SDS-PAGE results and can be rationalised in terms of a different conjugation degree, which in turn depends on the different reactivity of the three -SH groups exposed on the surface of each AGT subunit. In agreement with this hypothesis, no free -SH was titrated in the HMW fraction of conjugates, thus implying that they are characterised by the highest conjugation degree. Since a higher conjugation degree should improve the transduction efficiency [31-34], we investigated if an increased PEG-PGA/AGT ratio drove the formation of HMW conjugates. However, neither a 10:1 nor a 15:1 ratio led to any significant change in the relative population of the different PEG-PGA-AGT conjugates, probably due to steric hindrance and accessibility of the protein reactive sites.

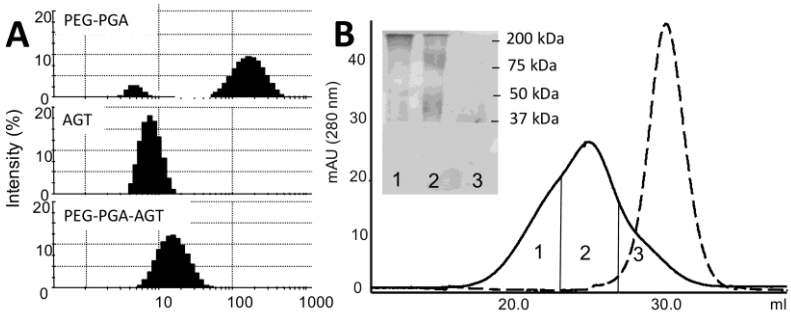

Figure IV.4. Molecular dimension analyses of AGT and PEG-PGA-AGT. (A) DLS evaluation of the average diameter of the species. (B) Elution profile (absorbance at 280 nm) of AGT 7.5 µM (- -) and PEG-PGA-AGT conjugation mixture 7.5 µM (-). The solutions were loaded on a Superdex S200 H10/30 SEC column and fractions were collected by peak. In the inset the SDS-PAGE analyses of SEC fractions of PEG-PGA-AGT. Al measurements were performed in phosphate buffered saline (PBS).

Overall, these data indicate that AGT can be efficiently bound to PEG-PGA leading to the formation of conjugates at different MWs without significantly compromising the enzyme structural and functional properties. This finding is an important prerequisite for the use of the PEG-PGA-AGT conjugates as therapeutics, as it guarantees that the protein will function once internalised in the cell.

IV.2.3. Cellular Uptake of PEG-PGA-AGT Conjugates in Eukaryotic Cells

While the ability of PGA-based nanocarriers to be internalised into eukaryotic cells has already been well documented, the internalisation mechanisms are still debated [33, 34]. We investigated the cellular uptake of PEG-PGA-AGT conjugates using a well-recognized cellular model of PH1 based on Chinese Hamster Ovary (CHO) cells stably expressing glycolate oxidase (GO) [35]. The system has proven to be useful not only to understand the molecular bases of the disease, but also to test the effectiveness of compounds used to rescue the effect of disease-causing mutations [36-42].

In preliminary experiments, PEG-PGA-AGT conjugates were added at 1 μM concentration to the culture medium of CHO-GO cells for different times, ranging from 1 to 24 hours. Thereafter, we harvested, extensively washed (to remove conjugates present in the medium) and lysed cells, before subjecting the lysates to Western-blotting and enzyme activity assays. The expression levels and specific activities of CHO-GO cells stably expressing wild-type AGT (CHO-GO-AGT) or treated with unconjugated AGT as positive and negative controls, respectively, were analysed. Although the presence of intracellular AGT and the transaminase activity were detectable starting from 1 hour after treatment, maximal internalisation occurred around 7 hours and remained stable until 24 hours (Figure IV.5).

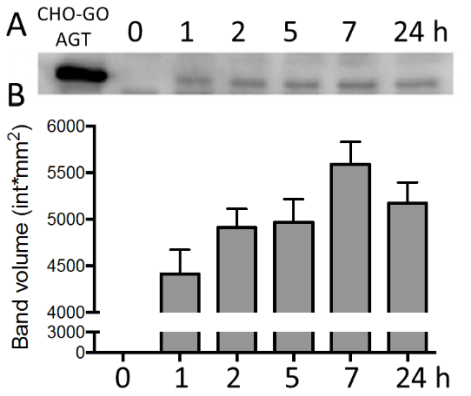

Figure IV.5. Time course analysis of the delivery of PEG-PGA-AGT to CHO-GO cells. CHO-GO cells were treated with 1 µM PEG-PGA-AGT. At different times (0, 1, 2, 5, 7, and 24 hours) cells were harvested and analysed by Western-blot and enzymatic activity assays. (A) 6 µg of lysate of cells treated with PEG-PGA-AGT or of CHO-GO-AGT cells were subjected to SDS-PAGE, immunoblotted with anti-AGT from rabbit (1:6000) and then detected with a chemiluminescent substrate. (B) Histogram representative of the immunoblot band. Bars represent the mean ± standard error mean (SEM) of three different experiments.

To test if the transduction efficiency varied with the conjugation degree, cells were treated with either HMW or LMW conjugates purified by SEC. As shown in Figure IV.6, a faint band of immunoreactive AGT was observed upon treatment with LMW conjugates (LMWC), but a stronger signal upon treatment with HMW conjugates (HMWC). These data suggest that HMWC are more efficiently transduced in cells, in line with the finding that larger particles are usually endowed with an enhanced ability to be internalised [32].

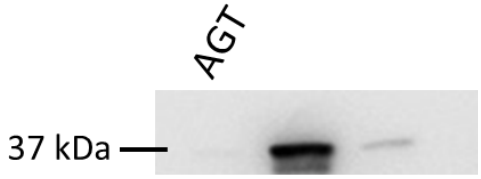

Figure IV.6. Internalisation of HMWC and LMWC in CHO-GO cells. Cells were treated with 5 µM HMWC, LMWC or unconjugated AGT for 24 hours. For western-blot analyses 6 µg of cell lysate were subjected to SDS-PAGE, immunoblotted with anti-AGT from rabbit (1:6000) and detected using a chemiluminescent substrate.

Upon treatment of CHO-GO cells with increasing amounts of HMW PEG-PGA-AGT, as exhibited in Figure IV.7A and Figure IV.7B, the presence of intracellular AGT starting from 0.6 µM concentration and this increased up to 5 µM concentration was detected. It should be noted that, the treatment concentration of the conjugates being equal, the amount of immunoreactive AGT and the specific activity level achieved by CHO-GO cells transduced with unpurified conjugates was about 3-fold lower than that observed in cells treated with purified HMWC, in line with the increased transduction ability of the latter.

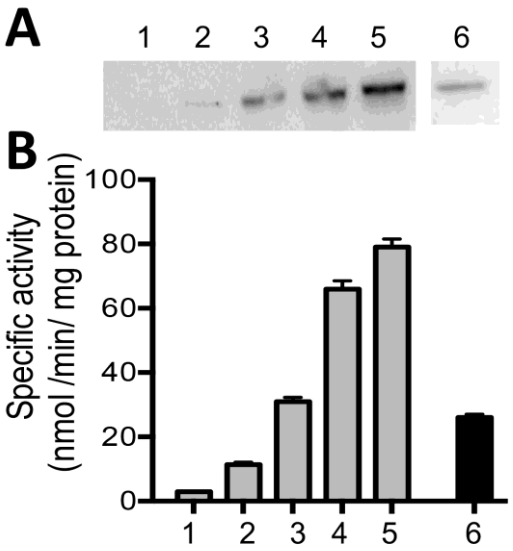

Figure IV.7. Dose-response analysis of CHO-GO cells treated with HMW PEG-PGA-AGT and unpurified PEG-PGA-AGT. Cells were treated with increasing concentrations of HMW PEG-PGA-AGT or with 5 µM unpurified PEG-PGA-AGT for 24 hours. (A) Western-blot. 6 µg of cell lysate were subjected to SDS-PAGE, immunoblotted with anti-AGT from rabbit (1:6000) and detected using a chemiluminescent substrate. (B) Histogram representative of specific activity values of CHO-GO cells treated with increasing concentration of HMW PEG-PGA-AGT (grey) or with 5 µM unpurified PEG-PGA-AGT (black). The AGT transaminase activity was measured by incubating 100 µg of lysate with 0.5 M L-alanine, 10 mM glyoxylate and 200 µM PLP at 25°C in 100 mM KP, pH 7.4. Bars represent the mean of three different experiment + SEM. Immunoblot lanes and histogram bars are coded as follow lane 1 to 5: CHO-GO cells treated with HMW PEG-PGA-AGT at 0.3, 0.6, 1.15, 2.5 and 5.0 µM concentration, respectively; lane 6: CHO-GO cells treated with 5 µM unpurified PEG-PGA-AGT.

The internalisation of PEG-PGA-AGT conjugates was further investigated by confocal microscopy to confirm that transaminase activity and presence of immunoreactive AGT in CHO-GO cells treated with PEG-PGA-AGT was due to the presence of intracellular AGT and not to conjugates non-specifically bound to the plasma membrane. Furthermore, this analysis can provide insight into the subcellular localisation of the protein. As a first approach, we performed imaging experiments in which AGT was labelled with a fluorescein isothiocyanate (FITC) fluorescent probe before conjugation and visualised in live cells. Due to the high absorbance of the dye in the visible region, we could not analyse the effect of the labelling on the absorbance, dichroic, and fluorescence features of the enzyme. However, by comparing the enzyme activity of the labelled and unlabelled enzyme, we found that AGT-FITC displays transaminase activity at saturating substrate concentrations equal to 36 s^{-1}, a value very similar to the k_{cat} of the unlabelled enzyme [6]. This strongly suggests that the labelling does not significantly alter the AGT functional and structural properties.

AGT-FITC was conjugated to PEG-PGA and the resultant conjugates were purified as previously described. CHO-GO cells were treated for 24 h with either PEG-PGA-AGT-FITC conjugates or unconjugated AGT-FITC at 5 µM AGT-equiv. concentration, then extensively washed and immediately analysed cells by live cell microscopy after plasma membrane staining with the Cell Mask™ Deep Red dye. While no FITC signal was present in cells treated with unconjugated AGT-FITC, a clear signal was detected within the plasma membrane of cells treated with PEG-PGA-AGT-FITC conjugates, as shown in Figure IV.8A. The protein appeared partly spread-out in the cytosol and partly located in discrete compartments. In agreement with these data, immunofluorescence microscopy (IFM) experiments also indicated that AGT was both diffused in the cytosol and present as bright spots (Figure IV.8B). However, the bright spots staining for AGT did not co-localise with the peroxisomal marker (Figure IV.8C), thus suggesting that the conjugated protein was not imported into peroxisomes or the levels present were below detection limits.

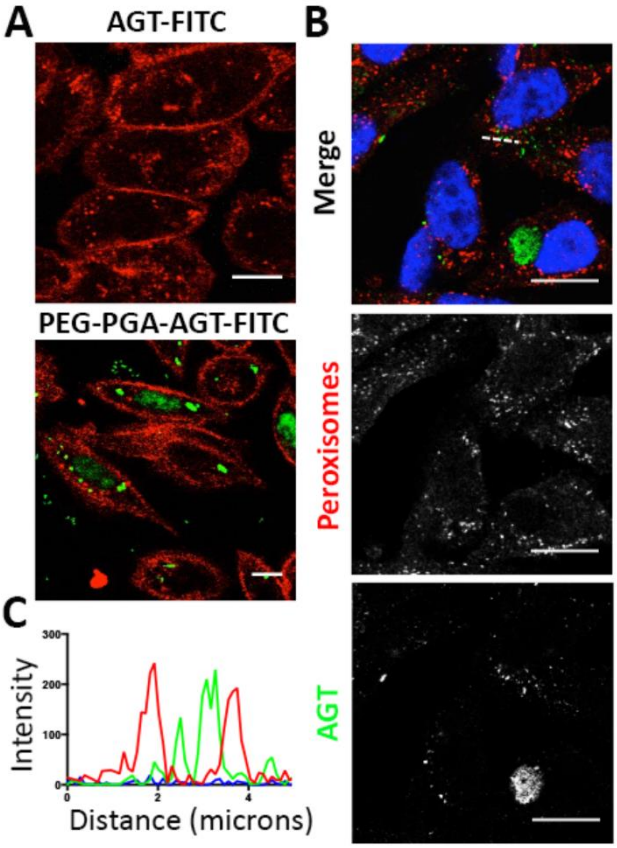

Figure IV.8. Analysis of PEG-PGA-AGT internalisation in CHO-GO cells. Cells were treated for 24 hours with 5 µM unconjugated or conjugated AGT-FITC (A) or 5 µM PEG-PGA-AGT (B). (A) In live cell imaging AGT-FITC is shown in green and the plasma membrane is labelled with Cell Mask™ Deep Red (red). (B) For IFM experiments cells were fixed, AGT and peroxisomes were detected by using the anti-AGT-antibody (green) and the anti-peroxisomal protein antibody (red), respectively. Nuclei were stained with DAPI (blue). Merge and individual channel images came from a single z-stack. (C) RGB profile plotted along the line drawn in the merged image. Scale bar: 10 µm.

Overall, these data demonstrate that the conjugation to PEG-PGA provides catalytically active AGT with the capacity to cross the plasma membrane and localise in the intracellular milieu, even if the protein seems to be mainly localised in the cell cytosol rather than imported into peroxisomes.

The details surrounding uptake and intracellular trafficking of polymeric nanosystems are still debated and different studies point to governance by multiple mechanisms, including macropinocytosis, caveolae-mediated endocytosis, and clathrin-mediated endocytosis. Notably, macropynosomes can acidify but do not interact with lysosomes thus contents escape degradation [34, 43], while contents carried via the caveolae-mediated pathway can also possibly avoid lysosomal degradation [44]. Therefore, while PEG-PGA-AGT conjugates are internalised through various mechanisms and a portion of them becomes entrapped inside endosomes, another portion may be released in the cell cytosol. Matrix peroxisomal proteins fold in the cell cytosol and are then translocated into peroxisomes in the fully folded form thanks to the interaction with a specific carrier [45]. AGT should be released from the cytosolic portion of PEG-PGA-AGT conjugates and should interact with the peroxisomal import machinery. However, the failure to detect co-localisation between the AGT signal and the peroxisomal marker in IFM experiments led us to conclude that the import of transduced AGT was either prevented or strongly affected following polymer conjugation of the protein. As previously mentioned, the import of AGT depends on the interaction with Pex5p, which is mediated by a weak PTS1 made up of a -KKL C-terminal tripeptide [7]. A study has recently reported that the substitution of the -KKL sequence with the canonical -SKL sequence enhances by ≈50-fold the binding affinity of AGT for Pex5p [46]. Moreover, the binding between AGT and Pex5p involves ancillary stretches of amino acids in the C-terminal region called “extended PTS1” (Figure IV.1B) [7, 47] and the mutation of residues located at or near the ancillary targeting region may alter the relative position of the receptor with respect to AGT, thus compromising the import of the protein [46]. As one of the reactive Cys residues exposed on the AGT surface (Cys387) is part of the “extended PTS1”, we cannot exclude that PEG-PGA-AGT conjugates underwent a partial reduction and that part of the polymer remained bound to Cys387, thus explaining the compromised import into peroxisomes.

IV.2.4. Engineering of AGT to Promote Peroxisomal Localisation

On the basis of the above results and considerations, it was reasoned that engineering AGT by the insertion of an -SKL targeting sequence at the C-terminus and/or by the mutation of Cys387 may promote the correct peroxisomal localisation of the transduced protein. Thus, we inserted the K390S mutation in AGT either alone or in combination with the C387S mutation, the latter choice dictated by the need to induce the smallest perturbation of the chemical-physical features of the C-terminus. As a preliminary experiment, we confirmed that, when expressed in CHO-GO cells, both variants showed clear peroxisomal localisation (data not shown). This implies that the mutations do not affect the interaction with the peroxisomal import machinery. Thus, purification was made to homogenise and characterise the K390S single variant (AGT-SKL) and the C387S/K390S double variant (AGT-SSKL). The Lys390 and the Cys387 mutations did not induce any significant change to AGT enzymatic activity (Table IV.2) and they did not affect the spectroscopic features of the enzyme (data not shown).

Table IV.2. Kinetic parameters for the AGT-SKL and AGT-SSKL variants.

AGT variant	Substrate	Co-substrate	K_{cat} (s^{-1})	K_m (mM)
AGT-SKL	L-alanine	Glyoxylate	43 ± 2	52 ± 8
	Glyoxylate	L-alanine	42 ± 2	0.11 ± 0.02
AGT-SSKL	L-alanine	Glyoxylate	46 ± 2	53 ± 8
	Glyoxylate	L-alanine	47 ± 2	0.16 ± 0.02

Recombinant purified AGT-SKL displayed a conjugation efficiency to PEG-PGA analogous to that of wild-type AGT and gave similar amounts of HMW and LMW conjugates purified by SEC. However, the C387S/K390S double mutation displayed a 50% reduction in conjugation efficiency and no changes were observed upon increasing the protein:polymer ratio from 1:5 to 1:15. Moreover, AGT-SSKL only formed LMW conjugates. As expected, the unconjugated variant exhibited two Cys residues per monomer titrated by DTNB with kinetics characterised by a $t_{1/2}$ of 40 min. These data suggest that the Cys387

mutation eliminated the most solvent exposed thiol group and this may explain why the conjugation equilibrium of AGT-SSKL shifted toward the unconjugated protein with respect to wild-type AGT. Nevertheless, PEG-PGA-AGT-SSKL conjugates displayed no exposed cysteine residues, thus indicating that the variant achieved the highest possible conjugation degree.

CHO-GO cells were treated for 24 h with either purified PEG-PGA-AGT-SKL or PEG-PGA-AGT-SSKL conjugates as well as with the corresponding unconjugated variants at 5µM concentration as negative controls. Then transduced cells were analysed by confocal microscopy and, as expected, we did not observe intracellular AGT after treatment with the unconjugated variants (data not shown). Treatment of CHO-GO cells with PEG-PGA-AGT-SKL conjugates led to the accumulation of AGT both in the cytosol and in discrete compartments whose signal did not co-localise with that of the peroxisomal marker (Figure IV.9), a pattern similar to that observed with PEG-PGA-AGT conjugates. Interestingly, upon treatment of CHO-GO cells with PEG-PGA-AGT-SSKL conjugates, the majority of AGT localised inside peroxisomes, even given the presence of AGT staining that did not co-localise with peroxisomes (Figure IV.9). These data indicate that the removal of the polymer-attachment point at the C-terminus of AGT and the insertion of a stronger peroxisomal targeting sequence promoted correct peroxisomal localisation. Since the peroxisomal import was not effective for the PEG-PGA-AGT-SKL conjugates, it can be concluded that the C387S mutation made the conjugates incompatible with the import machinery. Based on these results, it can be speculated that when PEG-PGA-AGT conjugates are transduced into CHO-GO cells, they do not undergo complete reduction in the cytosolic environment and that the polymer linked to Cys387 may change the conformation of the C-terminus thus compromising the interaction with Pex5p and consequently preventing the peroxisomal import. In the AGT-SSKL variant, the C387S mutation does not affect the subcellular localisation of AGT *per se*, but rather avoids the binding of a polymer moiety at the C-terminus. This effect, along with the K390S mutation that promoted the peroxisomal import [46], explains why the transduction with PEG-

PGA-AGT-SSKL conjugates results in the presence of intraperoxisomal AGT in CHO-GO cells.

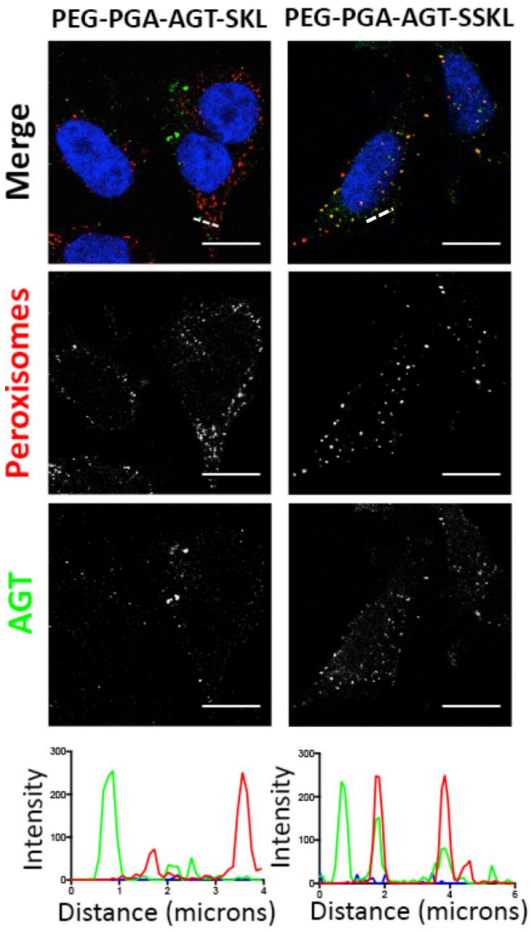

Figure IV.9. Analysis of the subcellular localisation of PEG-PGA-AGT-SKL and PEG-PGA-AGT-SSKL in CHO-GO cells. Cells were treated for 24 hours with 5 µM PEG-PGA-AGT-SKL (A) or 5 µM PEG-PGA-AGT-SSKL (B). Cells were then fixed, AGT and peroxisomes were detected by using the anti-AGT-antibody (green) and the anti-peroxisomal protein antibody (red), respectively. Nuclei were stained with DAPI (blue). Below are reported the RGB profiles plotted along the line drawn in the merged image. Merge and individual channel images came from a single z-stack. Scale bar: 10 µm.

To quantify the internalisation yield of AGT-SSKL, the transaminase activity of the transduced cells was measured. As expected, any activity was detected in cells treated with the unconjugated variant, while cells

treated with PEG-PGA-AGT-SSKL conjugates exhibited a specific activity of 11.5 nmol/min/mg, a value 7.2-fold lower compared with the value obtained in cells transduced with PEG-PGA-AGT conjugates. Taking into account the similar k_{cat} values of the double variant in the purified form and the wild-type AGT (Table IV.2), the specific activity observed upon treatment with the conjugates indicates the amount of transduced protein present inside the cell. On this basis, we concluded that PEG-PGA-AGT-SSKL conjugates are characterised by a lower transduction efficiency with respect to PEG-PGA-AGT. This result can be understood considering that the conjugation of AGT-SSKL with PEG-PGA only generates LMWC, which are expected to have a lower internalisation yield with respect to the HMWC formed by wild-type AGT.

IV.2.5. Glyoxylate-Detoxification Activity of the PEG-PGA-AGT Conjugates

To test whether the internalisation of conjugated AGT was effective in restoring the glyoxylate detoxification ability, 1 mM glycolate was added to CHO-GO cells transduced for 24 h with either PEG-PGA-AGT or PEG-PGA-AGT-SSKL conjugates at 5 µM concentration and measured cell viability after 24 h. Cells treated with unconjugated AGT and cells stably expressing AGT as negative and positive control, respectively, were used. Treatment with glycolate leads to the formation of glyoxylate inside CHO-GO cell peroxisomes, due to the catalytic activity of GO. Glyoxylate is toxic for the cell, but if catalytically active AGT is present, it detoxifies glyoxylate to glycine and prevents cell death. Thus, the viability of CHO-GO cells in the presence of glycolate is an indirect measure of the amount of functional AGT present in the cell [35].

Figure IV.10 demonstrates a viability of cells stably expressing AGT of around 80%, while a 20% viability of untreated cells and of cells treated with unconjugated AGT. Treatment with PEG-PGA-AGT or PEG-PGA-AGT-SSKL conjugates increased cell viability up to 70% and 45%, respectively. These data indicate that the conjugation of AGT to PEG-PGA mediates the delivery of a functional enzyme with the ability to restore the glyoxylate detoxification of CHO-GO cells. It was noted that

cells treated with PEG-PGA-AGT-SSKL displayed an AGT specific activity about 7-fold lower than that of cells treated with PEG-PGA-AGT. Nevertheless, we found that cell viability upon transduction with PEG-PGA-AGT-SSKL was only 1.5-fold lower as compared to cells transduced with PEG-PGA-AGT. Although cell viability does not linearly depend on the AGT specific activity of the cells, these results suggest that, given an equal transduction efficiency, PEG-PGA-AGT-SSKL conjugates are significantly more effective in restoring the glyoxylate detoxifying ability of the cells. This may be explained by the finding that conjugated wild-type AGT has a cytosolic localisation, while the conjugated AGT-SSKL variant is able to reach the peroxisomal matrix, where glyoxylate is formed. In this regard, the finding that conjugated AGT present in the cytosol still protects cells from glycolate toxicity is probably due to the fact that glyoxylate formed inside peroxisomes is exported to the cytosol, where it can be detoxified by the enzyme.

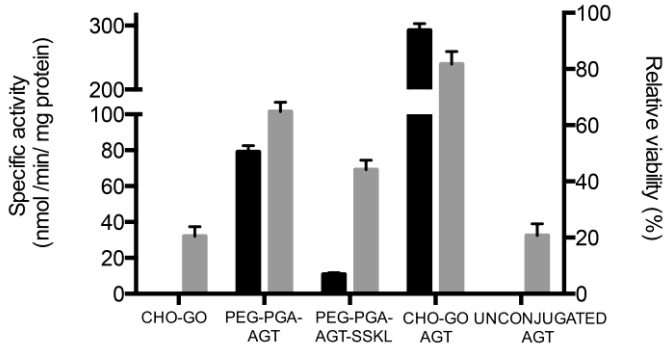

Figure IV.10. Specific activity and viability in the presence of glycolate of CHO-GO cells treated with different conjugated and unconjugated AGT variants. Grey bars: cell viability after 24 hours of treatment with 0.9 mM glycolate measured by the crystal violet colorimetric assay and expressed as percentage with respect to the untreated control. Six replicates have been measured for each sample. Black bars: AGT transaminase activity in the cell lysate detected by incubating 100 µg of lysate with 0.5 M L-alanine, 10 mM glyoxylate and 200 µM PLP at 25°C in 100 mM KP, pH 7.4. Histogram Bars are coded as follow: CHO-GO; untreated cells, PEG-PGA-AGT; CHO-GO cells treated with 5 µM PEG-PGA AGT for 24 h, PEG-PGA-AGT-SSKL; CHO-GO cells treated with 5 µM PEG-PGA AGT-SSKL for 24 h, CHO-GO-AGT; CHO-GO cells stably expressing AGT and AGT; CHO-GO cells treated with 5 µM unconjugated AGT for 24 h. Vertical bar indicate the SEM.

IV.2.6. Stability and Haemocompatibility Studies

To assess stability in the circulation, PEG-PGA-AGT conjugates and unconjugated AGT were incubated in human plasma at 37°C and time-dependent changes of the total amount of soluble protein in each sample were determined. The results reported in Figure IV.11A indicate the progressive disappearance of the signal corresponding to immunoreactive AGT for the unconjugated protein starting from 24 h and reaching a value of 30% at 48 h incubation. However, a loss of immunoreactive AGT was observed upon incubation of PEG-PGA-AGT conjugates in plasma, thus suggesting that conjugation protects the enzyme from degradation. A similar behaviour was observed with PEG-PGA-AGT-SSKL conjugates.

We then performed an *ex vivo* red blood cells (RBC) haemolysis assay to assess the biocompatibility of the conjugates. Human RBCs were incubated at 37°C with PEG-PGA-AGT or PEG-PGA-AGT-SSKL conjugates at 5 μM concentration and the percentage of haemolysis after a 1 h incubation was determined. Phosphate buffered saline (PBS) and 0.9% NaCl as negative controls and 1% Triton X-100 as the positive control were used. The results (Figure IV11B) indicate that the presence of the conjugates did not significantly increase haemolysis with respect to the negative controls.

Overall, the data obtained suggest that the conjugates are stable in biological fluids and will not induce toxic effects in circulating cells. Considering that circulation stability and biocompatibility are two of the most important parameters influencing the performance of polymeric conjugates under *in vivo* conditions [2, 48], these results represent important findings in view of the possible future development of PEG-PGA-AGT and PEG-PGA-AGT-SSKL for therapeutic applications.

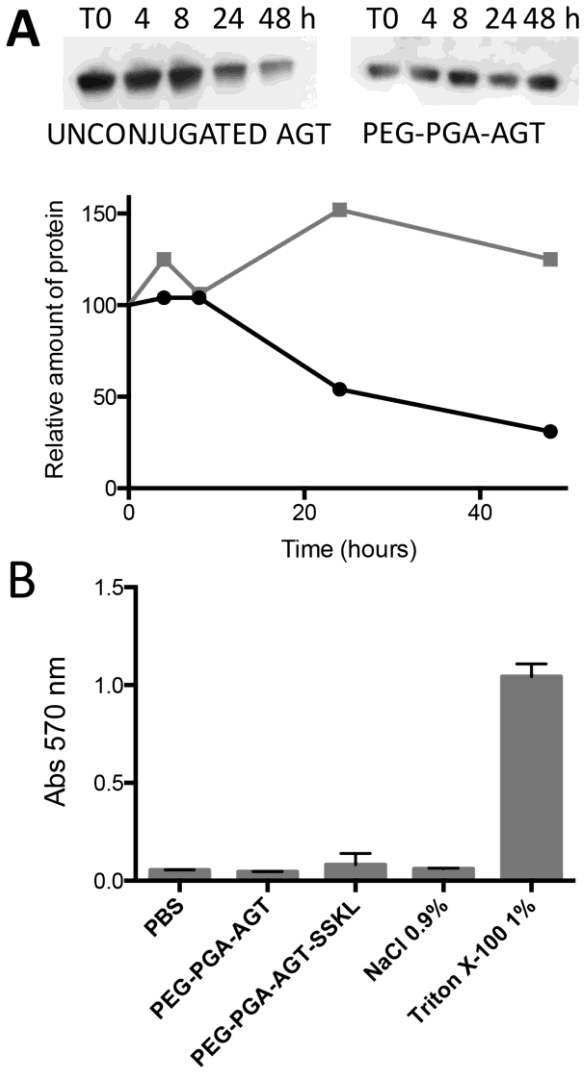

Figure IV.11. Stability and haemocompatibility of AGT conjugates. (A) 5 µM conjugated and unconjugated AGT were incubated in human serum at 37°C. At different times 2 µl of the mixtures were withdrawn, subjected to SDS-PAGE, immunoblotted with anti-AGT from rabbit (1:6000) and detected by using a chemiluminescent substrate. The WB bands of conjugated (grey) and unconjugated (black) AGT were quantified and plotted as function of time. (B) Absorbance at 570 nm representative of the haemolytic activity under the indicated conditions.

IV.3. CONCLUSIONS

We report a strategy to conjugate AGT to PEG-PGA diblock-co-polymers through the formation of disulphide bonds, as well as the successful use of the obtained conjugates to restore glyoxylate detoxification in eukaryotic cells mimicking a PH1 phenotype. Our protocol allowed us to achieve a high conjugation yield without significant effects to the functional properties of the enzyme. The obtained conjugates are internalised by CHO-GO cells, a well-accepted cellular model of PH1, and are mainly found in discrete compartments in the cytosol. Furthermore, they efficiently detoxify endogenously produced glyoxylate. By applying a protein engineering approach, we generated a mutated form of AGT bearing the substitution of Cys387-to-Ser and of Lys390-to-Ser (AGT-SSKL), to favour the interaction with the peroxisomal targeting machinery. PEG-PGA-AGT-SSKL conjugates internalised into CHO-GO cells are imported into peroxisomes and are more effective in glyoxylate detoxification with respect to PEG-PGA-AGT conjugates. *In vitro* data confirm a high stability in plasma and an excellent hemocompatibility of conjugated AGT, thus suggesting that the conjugates are suitable for intravenous injection. Overall, these data support the exploitation of this system to replenish PH1 patients with a catalytically active and correctly localised enzyme able to counteract the deficit responsible for oxalate accumulation. As polymer-based nanoconjugates have been widely employed for the delivery of therapeutic proteins, mainly due to their versatility and biocompatibility [19, 20, 49], these results using a biodegradable carrier constitute a fundamental step in the future development of a safer enzyme administration therapy effective for all PH1 patients independent of the type of mutation.

The correct targeting of a protein drug is an important issue, particularly in the case of disorders involving peroxisomal enzymes whose functionality is strongly influenced by the subcellular localisation [50]. Previous reports on the administration of catalase inside peroxisomes to rescue reactive oxygen species (ROS)-induced damage were based on the use of an enzyme derivative endowed with a non-covalently bound cell-penetrating peptide [51-53]. To the best of our

knowledge, the strategy outlined in this chapter is the first report of a PGA-based conjugate designed for the efficient delivery of a catalytically active therapeutic protein to the peroxisome. Thus, it represents an exciting strategy to implement for other diseases caused by deficiencies of peroxisomal enzymes.

IV.4. MATERIALS AND METHODS

IV.4.1. Materials

PLP, L-alanine, sodium glyoxylate, L-lactic dehydrogenase from rabbit muscle, isopropyl-β-D-thiogalactoside (IPTG), EDTA and imidazole were all purchased from Sigma Aldrich. Ham's F12 Glutamax medium, PBS, FITC, zeocin and Hoechst were purchased from Life Technologies. The rabbit polyclonal anti-AGT human antibody was kindly provided by Prof. C.J. Danpure of University College London (UK); the anti-rabbit HRP antibody and the AlexaFluor 488 and 555 were purchased from Life Technologies. Methoxy-poly(ethylene glycol)-poly(L-glutamic acid) sodium salt diblock (mPEG(2000)-PGA(80)[Na]; Mn = 14200, Mw/Mn = 1.16) was provided from Polypeptide Therapeutic Solutions SL (PTS, Spain). DMTMM chloride was synthesised according to literature [22]. Pyridyl dithiol ethylamine HCl salt was synthesised as described in [54]. ^{1}H NMR spectra were obtained at 300 MHz using a FT-spectrometer (Bruker) and analysed using the MestReNova 6.2 software. Vivaspin centrifugal concentrator tubes were from GE Healthcare.

IV.4.2. Synthesis of Pyridyl Disulphide (PD) Modified Diblock (PEG-PGA-PD)

PD-modified diblock was synthesised by post-polymerisation modification with DMTMM chloride using a modified published method [55]. In detail, 100 mg of diblock PEG-PGA in its sodium salt form (0.570 mmol, 1 equivalent (eq.)) was suspended in 6 mL of milliQ water. Next, 47.2 mg of DMTMM chloride (0.170 mmol, 0.3 eq.) dissolved in 2 mL of water were added, and the mixture was stirred for 15 min to activate the carboxyl acid groups of PGA. Then, 19 mg of pyridyl dithiol ethylamine (0.085 mmol, 0.15 eq.) dissolved in 2 mL of water were

added, the pH was adjusted to 8 by the addition of 1M $NaHCO_3$ solution, and the reaction mixture was stirred overnight. Finally, the reaction mixture was purified by ultrafiltration using vivaspin tubes with a molecular weight cut-off (MWCO) of 3 kDa. The purified product was recovered by freeze-drying. Yield: 85%. Labelling efficiency: 99%.

^{1}H NMR (300 ppm, D_2O, δ): 8.43 (1xH, m), 7.84 (2xH, m), 7.28 (1xH, m), 4.36 ppm (1H, m), 3.74 ppm (s, PEG chain), 2xH, m), 2.95 (2xH, m), 2.39-1.90 (4H, m). x: percentage of modification.

IV.4.3. Protein Expression and Purification

The vectors coding the K390S variant (AGT-SKL) and the C387S/K390S double variant (AGT-SSKL) were obtained from the AGT-Ma-NoHis construct [56] using the QuikChange II site-directed mutagenesis kit (Stratagene). The mutations were introduced by using the primers: 5'-GAT GGT CTC ACA GCT TGC TCT TGG GGC AGT GCT G and its complement, and the primer 5'-GGT CTC ACA GCT TGC TCT TGG GGC TGT GCT GCA GGG C-3' and its complement for the K390S and the C387S mutation, respectively. All mutations were confirmed by DNA sequencing. Protein expression and purification were performed as previously reported [57]. Protein concentration was determined using the apparent molar absorption coefficient of 95400 M^{-1} cm^{-1} at 280 nm. The PLP content was determined either by releasing the cofactor in 0.1 M NaOH using the apparent molar absorption coefficient of 6600 M^{-1} cm^{-1} at 388 nm, or by high performance liquid chromatography (HPLC) analysis as previously described [57].

IV.4.4. AGT-FITC Conjugation

10 mg of FITC (Molecular Probes) was dissolved in 1 mL of dimethyl sulfoxide (DMSO), following the manufacturer protocol. 100 µL of the FITC solution was added to 1 mL of AGT (1 mg/mL) in 0.1 M $NaHCO_3$, pH 9.0, to reach a final FITC: AGT ratio of 100:1 (w/w). The mixture was then incubated in the dark at room temperature for 1 hour. In order to remove excess FITC, the mixture was loaded on a PD-10 column previously equilibrated in phosphate saline buffer and the eluate was collected in 0.5 mL fractions. 5 µL of each fraction was diluted in 100 µL

of PBS on a 96 well/plate and the absorbance at 495 nm was measured. Fractions with the highest absorbance were pooled and the protein content was quantified by Bradford assay.

IV.4.5. Polymer-AGT Conjugation

Purified recombinant AGT, AGT-FITC, AGT-SKL, and AGT-SSKL were diluted in PBS to a final concentration of 15 µM. PEG-PGA was dissolved in 150 mM ammonium acetate, pH 6 to a final concentration of 75 µM. The two solutions were mixed in equal volumes to obtain a 5:1 molar ratio between polymer and protein. The mixture was incubated overnight at 25°C to allow conjugation and then concentrated by using Amicon Ultra centrifugal devices (MWCO 30 kDa) and washed twice with PBS to remove the excess of PEG-PGA. The conjugation efficiency was verified by SDS-PAGE under non-reductive conditions or after 1h incubation at 37°C with 10 mM reduced glutathione.

IV.4.6. Conjugate Purification

AGT-Ma, AGT-SKL, and AGT-SSKL conjugates were loaded onto a Sephacryl S300 SEC column (GE Healthcare), equilibrated in PBS, using an AKTA FPLC system (Amersham Biosciences). Elution was monitored by following absorbance at 280 nm and fractions corresponding to each peak were collected. The protein content of each fraction was determined using Bradford assay and the conjugation degree was verified by SDS-PAGE.

IV.4.7. Enzymatic Activity Assays

The transaminase activity of the analysed AGT variants in the purified recombinant form and conjugated form were determined by incubating each enzyme sample (0.1 µM) with saturating concentrations of the two substrates (0.5 M L-alanine, 10 mM glyoxylate) in 100 mM potassium phosphate buffer (KP) pH 7.4 in the presence of 200 µM PLP. Mixtures were incubated at 25°C for 10 minutes, and the reaction was stopped by adding 10% trichloroacetic acid (w/v). The amount of pyruvate produced was measured by a spectrophotometric assay coupled with lactate dehydrogenase [6]. For the measurement of the AGT specific activity in CHO-GO cells, 90 µg of

cell lysate were incubated with 0.5 M L-alanine and 10 mM glyoxylate at 25°C in 100 mM KP, pH 7.4 in the presence of 200 µM PLP. The reaction time was set to 10 min for cells stably expressing AGT and to 60 min for cells transduced with PEG-PGA-AGT and PEG-PGA-AGT-SSKL conjugates. The reactions were stopped by adding 10% TCA (w/v) and pyruvate production was measured by the spectrophotometric assay described above [6].

IV.4.8. Titration of Cysteinyl Groups

For the titration of exposed -SH groups, a solution of PEG-PGA conjugates or unconjugated protein at 5 µM concentration in 100 mM KP, pH 7.4 was treated with DTNB at 100-fold excess over the protein cysteinyl content as determined by amino acid composition. The increase in the absorbance at 412 nm was registered with time and a molar extinction coefficient of 13600 M^{-1} cm^{-1} was used to calculate the concentration of titrated -SH groups from the total absorbance change. The rate constants for the reaction of the exposed -SH groups with DTNB were calculated by fitting the time-dependent change in the absorbance at 412 nm to a double or a single exponential curve for PEG-PGA-AGT or PEG-PGA-AGT-SSKL, respectively.

IV.4.9. Spectroscopic Measurements

Absorption measurements were made with a Jasco V-550 spectrophotometer with 1 cm path length quartz cuvettes at a protein concentration of 1-10 µM in 100 mM KP, pH 7.4. Intrinsic fluorescence emission spectra were recorded on a Jasco FP-750 spectrofluorimeter equipped with a thermostatically controlled cell holder by using a 1 cm path length quartz cuvette. Protein emission spectra were taken from 300 to 500 nm (excitation at 280 nm) with both the excitation and the emission slits set to 5 nm. The protein concentration was 0.1-1 µM. Spectra of blanks were taken immediately before the measurements of samples containing protein. CD measurements were taken with a Jasco J-710 spectropolarimeter at a protein concentration of 5–10 µM, by using 1 cm path length cells. Routinely, three spectra were recorded at a scan speed of 50 nm/min with a bandwidth of 2 nm and averaged

automatically. All the spectral measurements were carried out in 100 mM KP, pH 7.4, at 25°C.

IV.4.10. Dynamic Light Scattering (DLS) Measurements

DLS measurements were performed on a Zetasizer Nano S device from Malvern Instruments in PBS at a protein concentration of 7.5 µM for unconjugated and conjugated proteins and 0.5 mg/mL for the free polymer. The temperature of sample cell was set to 25°C by a Peltier temperature control system and 12.5 Å ~45-mm disposable cells with stopper were used.

IV.4.11. Cell Culture and Conjugates Transduction

CHO cells stably expressing GO and CHO-GO cells stably expressing AGT were cultured as previously reported [42]. For protein transduction experiments, CHO-GO cells were seeded in a 6 cm dish at 6.0 x 10^5 cells/dish. After 24 hours the medium was replaced with fresh Ham's F12 medium containing purified PEG-PGA-AGT-Ma, PEG-PGA-AGT-SKL, or PEG-PGA-AGT-SSKL conjugates at a concentration range of 0.3–5 µM. After 24 hours, cells were extensively rinsed with PBS, trypsinised, and lysed according to a previously published protocol [56]. The protein concentration in the cell lysate was determined by Bradford assay.

IV.4.12. Western Blot Analyses

Ten micrograms of cell lysate were loaded per lane on a MiniProtean TGX™ pre-cast gel (Biorad) along with the Precision plus protein Kaleidoscope™ (Bio-Rad) molecular mass markers. Proteins were transferred to a nitrocellulose membrane by the iBlot device (Invitrogen) and the membrane was blocked in 5% milk solution in TBST (50 mM Tris-HCl pH 7.5, 150 mM NaCl, 0.1% Tween 20) for 1 hour at room temperature. For AGT detection, the membrane was incubated with polyclonal rabbit anti-AGT serum (dilution 1:6000), washed three times in TBST, and then incubated with peroxidase-conjugated anti-rabbit IgG (dilution 1:10000).

IV.4.13. Live Cell Imaging and Immunofluorescence Microscopy (IFM)

For live cell imaging experiments, 3 x 10^5 cells were seeded into each well of a 4-well chamber slide (µ-Slides, Ibidi) with a 13-mm glass bottom, treated with 5 µM AGT-FITC or PEG-PGA-AGT-FITC and grown for 24 hours. For plasma membrane and nuclei staining, the Cell Mask™ Deep Red fluorescent dye and Hoechst, respectively, were added at 1:1000 dilution in the culture media 5 minutes before the measurement. Before the acquisition, the medium was replaced with a special medium without phenol red (DMEM/F12 NoPhenolRED, Invitrogen). In IFM experiments, 3 x 10^5 cells were seeded into each well of a 24-well plate containing a 13-mm glass coverslip, and treated with unconjugated or conjugated AGT, AGT-SKL, and AGT-SSKL (5 µM) for 24 hours. Cells were then fixed in 4% (w/v) paraformaldehyde, permeabilised with 0.3% Triton X-100 in PBS and blocked in 3% bovine serum albumin in PBS. For the immunolabeling, rabbit polyclonal anti-human AGT and guinea-pig anti-PMP70 were used as primary antibody, and Alexa Fluor conjugated antibodies (AF488 and AF555, Life technologies) were used as secondary antibodies. Nuclei were stained with DAPI (Molecular Probes) and the coverslips were mounted over slides in AF1 medium (Dako). In both live cell imaging and IFM experiments, images were captured using a confocal laser-scanning fluorescence microscope Leica SP5 (Molecular Probes, Leica Microsystem, Manheim, Germany) at 63× magnification. For qualitative analyses, the ImageJ software was used (Rasband, W.S., ImageJ, U. S. National Institute of Health, Bethesda, Maryland, USA (http://rsb.info.nih.gov/ij/,1997–2008). Images were processed using Adobe Photoshop.

IV.4.14. Glycolate Toxicity Assay

CHO-GO-AGT or CHO-GO cells treated with PEG-PGA-AGT or PEG-PGA-AGT-SSKL were cultured as described above. After 24 hours, glyoxylate production was induced by adding HEPES buffered glycolate, pH 7.0 at a final concentration of 0.9 mM. Cell viability was evaluated after a 24 hour incubation using the crystal violet staining (Sigma

Aldrich) as previously reported [27]. The absorbance at 595 nm, which is proportional to the number of viable cells, was measured with a TECAN plate reader. Six replicates were performed for each assay condition.

IV.4.15. Stability and Biocompatibility Studies

Human plasma and RBC isolated from the buffy coat fractions of healthy volunteers were centrifuged on Ficoll-Paque PLUS gradient (1078 g/ml density, GE Healthcare, Little Chalfont, United Kingdom) at 400 *g* for 30 min, at room temperature, at a 1:1 ratio. For stability studies 7.5 µM AGT and AGT-SSKL either in the unconjugated or in the purified conjugated forms were incubated in fresh human plasma at 37°C. At scheduled times (0, 4, 8, 24 and 48 hours) 2 µL of the mixtures were withdrawn and subjected to SDS-PAGE. The gel was then blotted on a nitrocellulose membrane and incubated with anti-AGT antibody as previously described. For haemolysis studies RBC were resuspended 1:1 in PBS and treated with purified PEG-PGA-AGT (5 µM), purified PEG-PGA-AGT-SSKL (5 µM), NaCl (0.9% w/v) or Triton X-100 (1% v/v) at 37°C in a 96 well plate. After 1 h incubation, the plate was centrifuged at 3000 *g* and the absorbance at 570 nm of the supernatants was measured. Each sample was performed in triplicate.

IV.4.16. Statistical Analysis

Experiments were performed at least in triplicate. Statistical analysis was performed with the Origin® 7.03 (Origin Lab) or GraphPad Prism Version 5.0 (GraphPad software, San Diego, CA, USA) software packages.

REFERENCES

1. Roncador, A., et al., *Use of polymer conjugates for the intraperoxisomal delivery of engineered human alanine:glyoxylate aminotransferase as a protein therapy for primary hyperoxaluria type I.* Nanomedicine, 2016. **18**(16): p. 30228-3.
2. Leader, B., Q.J. Baca, and D.E. Golan, *Protein therapeutics: a summary and pharmacological classification.* Nat Rev Drug Discov, 2008. **7**(1): p. 21-39.

3. Al Hafid, N. and J. Christodoulou, *Phenylketonuria: a review of current and future treatments.* Transl Pediatr, 2015. **4**(4): p. 304-17.
4. Lachmann, R.H., *Enzyme replacement therapy for lysosomal storage diseases.* Curr Opin Pediatr, 2011. **23**(6): p. 588-93.
5. Vellard, M., *The enzyme as drug: application of enzymes as pharmaceuticals.* Curr Opin Biotechnol, 2003. **14**(4): p. 444-50.
6. Cellini, B., et al., *Human wild-type alanine:glyoxylate aminotransferase and its naturally occurring G82E variant: functional properties and physiological implications.* Biochem J, 2007. **408**(1): p. 39-50.
7. Fodor, K., et al., *Molecular requirements for peroxisomal targeting of alanine-glyoxylate aminotransferase as an essential determinant in primary hyperoxaluria type 1.* PLoS Biol, 2012. **10**(4): p. e1001309.
8. Salido, E., et al., *Primary hyperoxalurias: disorders of glyoxylate detoxification.* Biochim Biophys Acta, 2012. **1822**(9): p. 1453-64.
9. Harambat, J., et al., *Primary hyperoxaluria.* Int J Nephrol, 2011. **2011**: p. 864580.
10. Danpure, C.J. and P.R. Jennings, *Peroxisomal alanine:glyoxylate aminotransferase deficiency in primary hyperoxaluria type I.* FEBS Lett, 1986. **201**(1): p. 20-4.
11. Lorenzo, V., A. Torres, and E. Salido, *Primary hyperoxaluria.* Nefrologia, 2014. **34**(3): p. 398-412.
12. Cochat, P., et al., *Primary hyperoxaluria Type 1: indications for screening and guidance for diagnosis and treatment.* Nephrol Dial Transplant, 2012. **27**(5): p. 1729-36.
13. Cellini, B., et al., *The chaperone role of the pyridoxal 5'-phosphate and its implications for rare diseases involving B6-dependent enzymes.* Clin Biochem, 2014. **47**(3): p. 158-65.
14. Roncador, A., et al., *TAT-Mediated Delivery of Human Alanine:Glyoxylate Aminotransferase in a Cellular Model of Primary Hyperoxaluria Type I.* International Journal of Peptide Research and Therapeutics, 2013. **19**(2): p. 175-184.
15. Dinca, A., W.M. Chien, and M.T. Chin, *Intracellular Delivery of Proteins with Cell-Penetrating Peptides for Therapeutic Uses in Human Disease.* Int J Mol Sci, 2016. **17**(2).
16. Moritz, M. and M. Geszke-Moritz, *Recent Developments in the Application of Polymeric Nanoparticles as Drug Carriers.* Adv Clin Exp Med, 2015. **24**(5): p. 749-58.

17. Canal, F., J. Sanchis, and M.J. Vicent, *Polymer--drug conjugates as nano-sized medicines.* Curr Opin Biotechnol, 2011. **22**(6): p. 894-900.
18. Duncan, R., *Polymer therapeutics: Top 10 selling pharmaceuticals - what next?* J Control Release, 2014. **190**: p. 371-80.
19. Ginn, C., et al., *PEGylation and its impact on the design of new protein-based medicines.* Future Med Chem, 2014. **6**(16): p. 1829-46.
20. Pasut, G. and F.M. Veronese, *State of the art in PEGylation: the great versatility achieved after forty years of research.* J Control Release, 2012. **161**(2): p. 461-72.
21. Duncan, R. and M.J. Vicent, *Polymer therapeutics-prospects for 21st century: the end of the beginning.* Adv Drug Deliv Rev, 2013. **65**(1): p. 60-70.
22. Duro-Castano, A.C.-S., I.; Vicent, M.J., *Peptide-Based Polymer Therapeutics.* Polymers, 2014. **6**(2): p. 36.
23. Barz, M.D.-C., A.; Vicent, M.J., *A versatile post-polymerization modification method for polyglutamic acid: synthesis of orthogonal reactive polyglutamates and their use in "click chemistry".* Polymer Chemistry, 2013. **4**: p. 5.
24. Talelli, M. and M.J. Vicent, *Reduction sensitive Poly(l-glutamic acid) (PGA)-protein conjugates designed for polymer masked-unmasked protein therapy.* Biomacromolecules, 2014. **15**(11): p. 4168-77.
25. Gong, Y., J.C. Leroux, and M.A. Gauthier, *Releasable Conjugation of Polymers to Proteins.* Bioconjug Chem, 2015. **26**(7): p. 1172-81.
26. Zhang, X., et al., *Crystal structure of alanine:glyoxylate aminotransferase and the relationship between genotype and enzymatic phenotype in primary hyperoxaluria type 1.* J Mol Biol, 2003. **331**(3): p. 643-52.
27. Montioli, R., et al., *S81L and G170R mutations causing Primary Hyperoxaluria type I in homozygosis and heterozygosis: an example of positive interallelic complementation.* Hum Mol Genet, 2014. **23**(22): p. 5998-6007.
28. Cellini, B., R. Montioli, and C.B. Voltattorni, *Human liver peroxisomal alanine:glyoxylate aminotransferase: characterization of the two allelic forms and their pathogenic variants.* Biochim Biophys Acta, 2011. **1814**(11): p. 1577-84.

29. Cellini, B., et al., *Human liver peroxisomal alanine:glyoxylate aminotransferase: Different stability under chemical stress of the major allele, the minor allele, and its pathogenic G170R variant.* Biochimie, 2010. **92**(12): p. 1801-11.
30. Cellini, B., et al., *Molecular defects of the glycine 41 variants of alanine glyoxylate aminotransferase associated with primary hyperoxaluria type I.* Proc Natl Acad Sci U S A, 2010. **107**(7): p. 2896-901.
31. Zhu, C., et al., *Co-delivery of siRNA and paclitaxel into cancer cells by biodegradable cationic micelles based on PDMAEMA-PCL-PDMAEMA triblock copolymers.* Biomaterials, 2010. **31**(8): p. 2408-16.
32. Merkel, O.M., et al., *Integrin alphaVbeta3 targeted gene delivery using RGD peptidomimetic conjugates with copolymers of PEGylated poly(ethylene imine).* Bioconjug Chem, 2009. **20**(6): p. 1270-80.
33. Li, M., et al., *Nanoscaled poly(L-glutamic acid)/doxorubicin-amphiphile complex as pH-responsive drug delivery system for effective treatment of nonsmall cell lung cancer.* ACS Appl Mater Interfaces, 2013. **5**(5): p. 1781-92.
34. Peng, S.F., et al., *Mechanisms of cellular uptake and intracellular trafficking with chitosan/DNA/poly(gamma-glutamic acid) complexes as a gene delivery vector.* Biomaterials, 2011. **32**(1): p. 239-48.
35. Lumb, M.J., G.M. Birdsey, and C.J. Danpure, *Correction of an enzyme trafficking defect in hereditary kidney stone disease in vitro.* Biochem J, 2003. **374**(Pt 1): p. 79-87.
36. Fargue, S., et al., *Effects of alanine:glyoxylate aminotransferase variants and pyridoxine sensitivity on oxalate metabolism in a cell-based cytotoxicity assay.* Biochim Biophys Acta, 2016. **1862**(6): p. 1055-62.
37. Fargue, S., et al., *Four of the most common mutations in primary hyperoxaluria type 1 unmask the cryptic mitochondrial targeting sequence of alanine:glyoxylate aminotransferase encoded by the polymorphic minor allele.* J Biol Chem, 2013. **288**(4): p. 2475-84.
38. Fargue, S., G. Rumsby, and C.J. Danpure, *Multiple mechanisms of action of pyridoxine in primary hyperoxaluria type 1.* Biochim Biophys Acta, 2013. **1832**(10): p. 1776-83.
39. Oppici, E., et al., *Pyridoxamine and pyridoxal are more effective than pyridoxine in rescuing folding-defective variants of human*

alanine:glyoxylate aminotransferase causing primary hyperoxaluria type I. Hum Mol Genet, 2015. **24**(19): p. 5500-11.
40. Oppici, E., R. Montioli, and B. Cellini, *Liver peroxisomal alanine:glyoxylate aminotransferase and the effects of mutations associated with Primary Hyperoxaluria Type I: An overview.* Biochim Biophys Acta, 2015. **1854**(9): p. 1212-9.
41. Oppici, E., et al., *S250F variant associated with aromatic amino acid decarboxylase deficiency: molecular defects and intracellular rescue by pyridoxine.* Febs Journal, 2013. **280**: p. 174-174.
42. Oppici, E., et al., *The Chaperoning Activity of Amino-oxyacetic Acid on Folding-Defective Variants of Human Alanine:Glyoxylate Aminotransferase Causing Primary Hyperoxaluria Type I.* ACS Chem Biol, 2015. **10**(10): p. 2227-36.
43. Almeida, C.S., et al., *Tailoring Cellular Uptake of Conjugated Polymer Nanoparticles Using Modular Amphiphilic Peptide Capping Ligands.* Chemistry of Materials, 2015. **27**(19): p. 6879-6889.
44. Rejman, J., M. Conese, and D. Hoekstra, *Gene transfer by means of lipo- and polyplexes: role of clathrin and caveolae-mediated endocytosis.* J Liposome Res, 2006. **16**(3): p. 237-47.
45. Rucktaschel, R., W. Girzalsky, and R. Erdmann, *Protein import machineries of peroxisomes.* Biochim Biophys Acta, 2011. **1808**(3): p. 892-900.
46. Mesa-Torres, N., et al., *Molecular recognition of PTS-1 cargo proteins by Pex5p: implications for protein mistargeting in primary hyperoxaluria.* Biomolecules, 2015. **5**(1): p. 121-41.
47. Fodor, K., et al., *Ligand-induced compaction of the PEX5 receptor-binding cavity impacts protein import efficiency into peroxisomes.* Traffic, 2015. **16**(1): p. 85-98.
48. Sanchis, J., et al., *Polymer-drug conjugates for novel molecular targets.* Nanomedicine (Lond), 2010. **5**(6): p. 915-35.
49. Du, A.W. and M.H. Stenzel, *Drug carriers for the delivery of therapeutic peptides.* Biomacromolecules, 2014. **15**(4): p. 1097-114.
50. Terlecky, S.R. and J.I. Koepke, *Drug delivery to peroxisomes: employing unique trafficking mechanisms to target protein therapeutics.* Adv Drug Deliv Rev, 2007. **59**(8): p. 739-47.
51. Giordano, C.R., et al., *Catalase therapy corrects oxidative stress-induced pathophysiology in incipient diabetic retinopathy.* Invest Ophthalmol Vis Sci, 2015. **56**(5): p. 3095-102.

52. Nell, H.J., et al., *The targeted antioxidant, catalase-SKL, reduces beta-amyloid toxicity in the rat brain.* Brain Pathol, 2016.
53. Undyala, V., S.R. Terlecky, and R.S. Vander Heide, *Targeted intracellular catalase delivery protects neonatal rat myocytes from hypoxia-reoxygenation and ischemia-reperfusion injury.* Cardiovasc Pathol, 2011. **20**(5): p. 272-80.
54. Kunishima, M., et al., *Synthesis and Characterization of 4-(4,6-Dimethoxy-1,3,5-triazin-2-yl)-4-methylmorpholinium Chloride.* Tetrahedron Letters, 1999. **40**(29): p. 5327-5330.
55. Barz, M., A. Duro-Castano, and M.J. Vicent, *A versatile post-polymerization modification method for polyglutamic acid: synthesis of orthogonal reactive polyglutamates and their use in "click chemistry".* Polymer Chemistry, 2013. **4**(10): p. 2989-2994.
56. Oppici, E., et al., *Gly161 mutations associated with Primary Hyperoxaluria Type I induce the cytosolic aggregation and the intracellular degradation of the apo-form of alanine:glyoxylate aminotransferase.* Biochim Biophys Acta, 2013. **1832**(12): p. 2277-88.
57. Cellini, B., et al., *Construction, purification and characterization of untagged human liver alanine-glyoxylate aminotransferase expressed in Escherichia coli.* Protein Pept Lett, 2008. **15**(2): p. 153-9.

Chapter V

Use of SANS and SAXS to Study the Inner Structure of Drug Delivery Systems in Solution

The work presented in this thesis chapter was made possible by a collaboration between the Polymer Therapeutics lab at the Centro de Investigación Príncipe Felipe, in Valencia and the School of Chemistry from Cardiff University in Dr. Alison Paul's group.

V.1. INTRODUCTION AND BACKGROUND

V.1.1. Small Angle Scattering Techniques

The application of new, robust, and sophisticated methodologies has complemented existing techniques to meet the challenge of studying the conformation of nanomedicines under physiological or near-physiological conditions [1]. Remarkable progress in the design of nanoscale drug delivery systems (nanoDDS) has precipitated the formation of developmental guidelines to be followed to achieve a specific therapeutic effect [2]. Therefore, the exhaustive physicochemical characterisation of new nanosized entities, which allows the control of pharmacokinetics and biodistribution, will permit the generation of more efficient nanomedicinal therapeutic strategies.

Small angle scattering (SAS) techniques are included within the methodologies recently used to study nanoDDS solution conformation. In SAS, radiation is elastically scattered by the sample and analysis of resultant patterns are used to infer sample structure. SAS techniques such as small angle neutron scattering (SANS), small angle X-ray scattering (SAXS), and small angle light scattering (SLS) provide information on the size, shape, and orientation of structures [3]. The main difference between these methods is the nature of the radiation employed to obtain complementary information. Otherwise, they share several similarities and the same mathematical formalism can be used to analyse data. By using a suitable and physically rational model for the data, any change in solution is quantifiable. However, this analysis can be laborious, requires considerable prior knowledge, and the information obtained must often be combined with complementary physicochemical characterisation techniques to fully describe the systems under investigation. In some cases, the radius of gyration, R_g, and the inner structure of the nanosystems can be obtained without making any assumptions in a preliminary analysis of the data [4-6].

SANS is a neutron-based non-destructive technique that can probe structural information at length scales ranging from 1 to 100 nm. SANS is used in a wide range of scientific fields, including the study of soft matter, biophysics, and biology. Importantly, SANS experiments are relevant for the elucidation of links between biological activity and solution conformation, as characterisation can be carried out under physiologically relevant conditions. Thanks to this technique, researchers analysed the physicochemical properties and conformational behaviour under physiological conditions of PK1, a clinically evaluated polymer-anticancer drug conjugate (N-(2-hydroxypropyl)methacrylamide-doxorubicin (HPMA-DOX) conjugate) [7]. Subsequent complementary studies [8] demonstrated the influence of drug type, drug loading, and pH on sample conformation and, therefore, changes in properties such as conjugate biodistribution, potential toxicity, and pharmacological activity.

This process also permitted the investigation of conformational changes in endosomolytic polymers for the intracellular delivery of proteins and genes as a function of pH and salt type [4, 9]. This revealed the potential for SANS to analyse samples under complex environmental conditions. Another interesting example allowed the correlation of the different *in vitro* biological outputs of *tert*- or *block*-diethylstilbestrol (DES)-polyacetal conjugates in two different human prostate cancer cell lines (PC3 hormone independent and LNCaP hormone dependent) with the different solution conformations [10].

SANS has the crucial feature of differentiating the scattering length densities between isotopes and, more precisely, between hydrogen and deuterium (though they are essentially identical in X-rays and light analyses). In biological systems, hydrogen can be exchanged with deuterium producing a minimal effect on the sample. However, this has dramatic effects on the scattering, so allowing intriguing contrast variation studies [11-13] and provides the ability to independently characterise the different deuterium labelled domains within a drug delivery system structure in solution (Figure V.1).

Figure V.1. Example of SANS contrast variation study.

In the case of SAXS experiments, the elastic scattering of X-rays is recorded using wavelengths comparable to neutrons and, therefore, measures similar length scales. The difference lies in the radiation employed and the sample behaviour in response. In SANS, the neutrons are scattered by the nuclei and the interaction depends on the isotope used, while in SAXS, the X-rays are scattered by the electrons. Therefore, the bigger the element, the bigger the intensity of the scattering, and this has a direct impact on the selection of samples and their observed properties.

Examples of SAXS application in soft matter include the investigation of non-viral gene delivery systems [14], block copolymer micelles [12], and peptide amphiphile self-assembled nanovectors [15]. Additionally, studies also used synchrotron based X-ray radiation to investigate the nanostructure of PEGylated lipid nanosystems in order to study the protein corona effect [16]. As for SANS, SAXS is generally a non-destructive method, although biomaterials such as DNA or proteins may be susceptible to radiation damage at high intensities. Moreover, unlike the SANS technique, heavier elements mask the scattering from lighter elements in SAXS.

In this chapter, we will report, for the first time, a rigorous and detailed structural investigation of polymeric nanosystems already classified as successful drug delivery nanocarriers: (i) the three-dimensional (3D) structure of 3- and 4-arm star shaped polyglutamates including information on the size, shape, and internal structure with varying different parameters such as glutamic acid-units (GAU) content (from 100 to 250 GAU) or core composition, and (ii) the conformational

analysis of the first example of polymer combination therapy combining an endocrine disruptor (DES) and a chemotherapeutic drug (paclitaxel, PTX) attached to the same polyacetal backbone.

V.1.2. Small Angle Scattering Essentials

When incident radiation is scattered by a particle, it does so in an elastic fashion, experiencing a change in momentum but not energy. Therefore the wave vector, *k*, of the incident radiation will have the same magnitude as the wave vector of the scattered radiation, *k'*. Using vector triangles then allows a scattering vector, *Q*, to be derived where *Q = k →k'* (Figure V.2) [17].

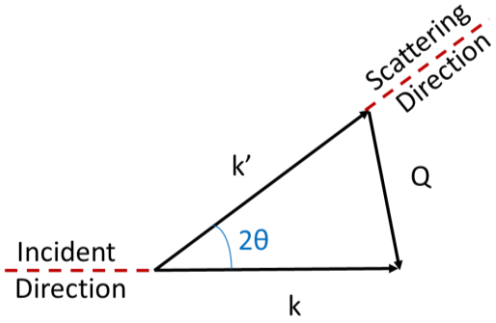

Figure V.2. Vector triangle showing how the scattering vector, *Q*, is derived.

As the wave vector has the value of

$$k = k' = 2\pi/\lambda \qquad \text{(Equation V.1)}$$

from simple trigonometry on the vector triangle

$$Q = \frac{4\pi}{\lambda} \sin\left(\frac{\theta}{2}\right) \qquad \text{(Equation V.2)}$$

The magnitude *Q* has dimensions of reciprocal length, meaning that larger objects scatter at low *Q* values and smaller objects scatter at high *Q* values.

In SAS experiments, the scattering intensity, *I(Q)*, is measured as a function of *Q* and is described in terms of the relative contributions of the form factor, *P(Q)* (which describes the size and shape of the scattering body), the structure factor, *S(Q)* (which describes interactions between different scattering bodies), and B_{inc} which is a flat background

arising from incoherent scattering, principally from hydrogenated material within the sample (Equation V.3).

$$\mathrm{I(Q)} = \phi V_p (\Delta\rho)^2 P(Q) S(Q) + B_{inc} \qquad \text{(Equation V.3)}$$

$\phi V_p(\Delta\rho)^2$ is a sample-dependent scale factor modulated by the polymer volume fraction ϕ, the volume of a single particle V_p, and the contrast term $(\Delta\rho)^2$, which describes the difference in scattering length density between the solvent and the polymer, $\Delta\rho=\rho_{solvent}-\rho_{polymer}$.

In the specific case of SANS, as hydrogen and deuterium are at opposite ends of the scattering length density scale, we achieved contrast by dissolving the different studied polymers in D_2O. In the case of SAXS, we prepared the solutions by dissolving the different substances in H_2O, phosphate buffer saline (PBS), or D_2O, to compare the results obtained using both techniques, thereby complementing the obtained information.

V.2. USE OF SAS TO STUDY STAR SHAPED POLYGLUTAMATES

V.2.1. SAS from Branched Polymers

A huge number of SAS investigations have focused on characterising branched polymer systems such as star polymers, dendrimers, and graft polymers, so demonstrating the effectiveness of these techniques in the characterisation of such polymeric nanocarriers. For example, conformational and size information, such as R_g, were obtained using Guinier and Kratky standard plots in dilute solutions of poly(ethylene oxide) star polymers ranging from 30 arms (G3 dendrimer) to 150 arms (G10 dendrimer) with a polyamidoamine (PAMAM) dendrimer core [18].

Another example is the thermodynamic measurements made after mixing star branched and linear polymers [19]. The Flory-Huggins interaction parameters, χ, (which take account of the energy of interdispersing polymer and solvent molecules) were determined for a number of branching architectures and polymer chemistry. This study demonstrated that χ increases with the number of branch points and

with the number of chain ends. This may be understood based on chain topology.

The group of Jones *et al.* [20] published a study focused on measuring the contribution of χ on chain architecture for a blend of star branched and linear polymers finding that χ increased upon star presence (number of arms). The thermodynamics of miscibility of star-star polymers, including isotopic mixtures with different number of arms, has also been investigated [21].

Other SANS investigations involved stars with dendrimer cores and deuterated arms in solution [22]. The solvent scattering length density was matched to that of the arms (zero contrast condition) in order to obtain characteristic sizes (R_g) and Porod (fractal) exponents. This study found that such properties depend strongly on core branching architecture in the dilute region and inter-particle structure factors were obtained for semi-dilute solutions. Rathgeber *et al.* [23] studied the application of the Beaucage model on branched dendrimers in solution, which allowed the characterisation of the degree of branching and its regularity. Star polymers with a dendrimer core have also been investigated in the bulk state (without any solvent) with ordered structures resolved employing transmission electron microscopy (TEM), SAXS and SANS [24].

V.2.2. Star Shaped Polyglutamates

Star polymers are branched polymers made up of several linear chains attached to a central core. Their unique mechanical, rheological, and biomedical properties make them optimal platforms for drug delivery and offer improved yield compared to conventional linear polymers [25]. When compared to linear polymers with similar molecular weight (MW), star-shaped systems present a more compact structure, a large surface area, and an increased concentration of functionalised end groups. Furthermore, multi-arm stars, as well as hyperbranched polymers, show enhanced solubility, lower melt viscosity, and different thermal and physical properties. Such properties depend more on arm MW than on the total MW of the star polymer.

When compared to dendrimers, star polymers offer the advantages of feature accelerated and tuneable methods of synthesis. However, the most appealing feature is their self-assembly behaviour. Recent studies suggest that macromolecular architecture is a key parameter for the tuning of micellar behaviour and properties. Therefore both potential biological applications as well as architecture must be taken into consideration when designing new materials such as nanoDDS.

A recent study described the synthesis, physicochemical characterisation, preliminary *in vitro* evaluation, and exhaustive *in vivo* biodistribution and pharmacokinetics of a new star shaped polyglutamate family (St-PGA) [25]. This study highlighted the advantages of such branched systems when compared with their linear counterparts in terms of cell uptake enhancement and prolonged plasma half-life. In order to understand even better the prospective in aqueous solution of these nanoDDS systems in particular, and any other in general, revealing their inner structure and the detailed delivery mechanisms, more sophisticated methods are needed. Surprisingly, there is a lack of such studies for clinically relevant systems except for recent works by Paul *et al*. [7, 13].

In this section, we will present the 3D structure of 3- and 4-arm star shaped polyglutamates including information on the size, shape, and internal structure.

V.2.3. Results and Discussion

The strategy and tactics generally followed during the SAS data analysis to obtain the desired structural information are schematically shown in Figure V.3.

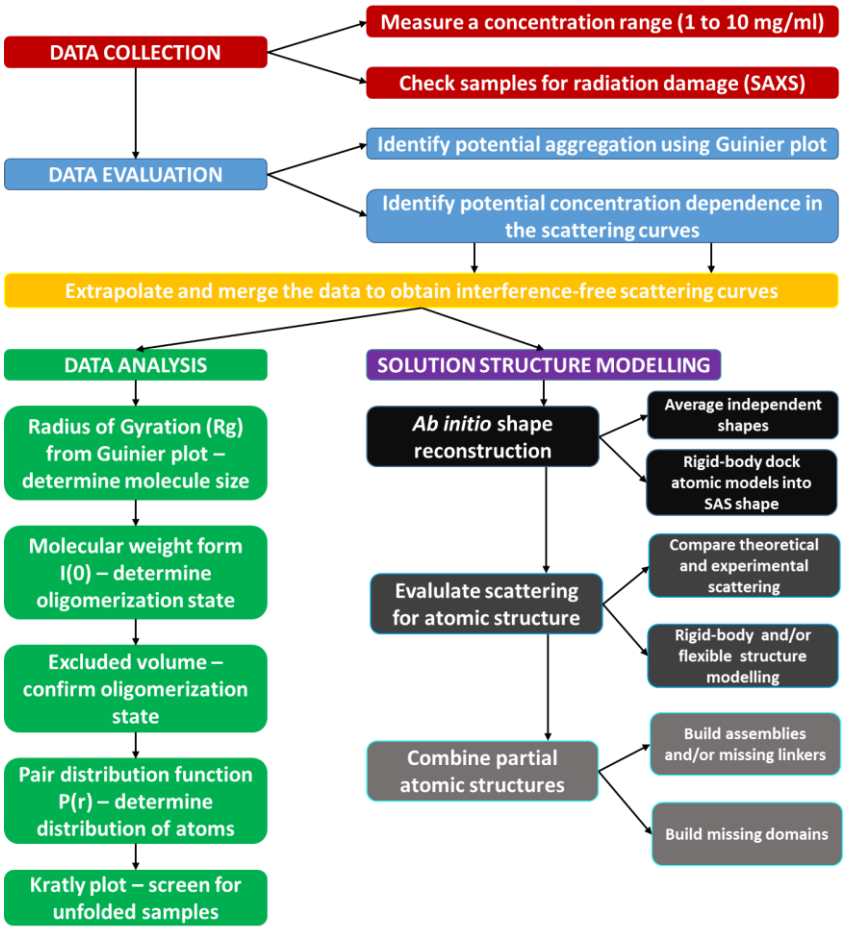

Figure V.3. Schematic for SAS data collection, evaluation, analysis, modelling, and interpretation. Adapted from [26].

Conceptually the SAS experiment can be divided into four major steps: data collection, data evaluation, data analyses, and solution structure modelling, each of which will be detailed below.

V.2.3.1. 3- and 4-Arm Star Shaped Polyglutamates

3- and 4-arm star shaped polyglutamates were previously synthesised by Duro-Castaño and colleagues using a recently published versatile methodology yielding well-defined carriers with tunable MW and low polydispersities [25]. The schematic structure of the 3-arm shaped polyglutamates is presented in Figure V.4.

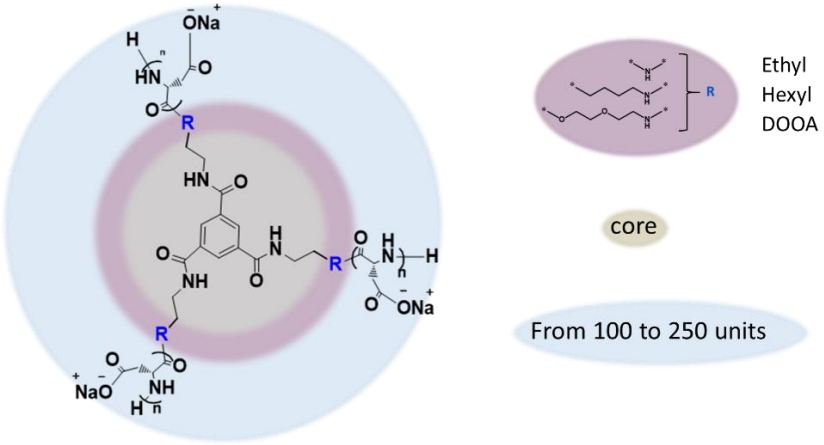

Figure V.4. Schematic structure of 3-arm star shaped polyglutamates. R: -NH- in ethyl based polymers; -$CH_2CH_2CH_2CH_2NH$- in hexyl based polymers; and -$OCH_2CH_2OCH_2CH_2NH$- in 3,6-dioxa-octanediamine (DOOA) based polymers.

Five different sets of polymers were synthesised for study by SANS and SAXS. The first polymer set (**Set 1**) comprised 3-arm star polymers with the same multifunctional core coupled with three different amines (*R*: -NH- in ethyl based polymers; -$CH_2CH_2CH_2CH_2NH$- in hexyl based polymers; and -$OCH_2CH_2OCH_2CH_2NH$- in 3,6-dioxa-octanediamine, DOOA, based polymers) and different number of GAU. We studied these compounds by SANS on the D11 instrument at the Institute Laue-Langevin (ILL), Grenoble and the physicochemical characteristics studied are listed in Table V.1.

Table V.1. Physicochemical characteristics of the 3-arm star shaped polyglutamates, Set 1, studied by SANS. Adapted from [25].

Star Polymer	Amine (R)	DP^{theo}	Mn^{a} (kDa)	Mn^{b} (kDa)	DP^{a}	DP^{b}	$Đ^{a}$
SE1	Ethyl	100	21.3	21.0	97	96	1.26
SE3	Ethyl	250	50.3	51.5	229	235	1.09
SD2	DOOA	100	22.2	24.1	101	110	1.23
SD4	DOOA	200	40.5	41.6	185	190	1.12
SH3	Hexyl	250	51.5	52.6	235	240	1.17

[a] Determined by SEC in DMF; [b] Estimated by ^{1}H NMR. DP= degree of polymerisation. DP^{theo}= monomer concentration/initiator concentration. Mn= number average MW. Đ= polydispersity= MW/Mn. S= 3-arm star polymer. E= ethyl; D= DOOA; H= hexyl.

A second set of polymers (**Set 2**) consisted of 3-arm star shaped polyglutamates with ethyl as a coupled amine certain GAU functionalised with propargylamine or ethylene glycol azide amine. The presence of these functionalities allows site-specific conjugation of relevant molecules such as antibodies, proteins, or imaging probes enabling the design of advanced theranostics or polymer-based combination nanopharmaceutics [27]. Set 2 polymers also include the physical mixture of both compounds as well as their covalent attachments. We studied these compounds by SANS on the SANS2d diffractometer at the ISIS Spallation Neutron Source, Rutherford Appleton Laboratory, Didcot, UK. Their physicochemical characteristics are listed in Table V.2.

Table V.2. Physicochemical characteristics of the functionalised ethyl derivatives 3-arm star shaped polyglutamates, Set 2, studied by SANS.

Star Polymer	Amine (R)	DP^{theo}	Mn^{a} (kDa)	Đ
SP	Ethyl	150	22.9	1.23
SN	Ethyl	150	24.0	1.23
SP+SN	Ethyl	150+150	-	-
SP-SN	Ethyl	150+150	-	-

[a] Estimated after ^{1}H NMR. SP= 3-arm star polymer functionalised with 10 mol% propargylamine. SN= 3-arm star polymer functionalised with 5 mol% ethylene glycol azide amine. SP+SN= physical mixture. SP-SN= covalent capture.

In order to probe the regions occupied by the core *vs.* the corresponding amine, *R*, we performed contrast variation experiments with a third set of 3-arm star shaped polyglutamates (**Set 3**). Set 3 polymers contained star polymers with ethyl as a substituent and certain GAU functionalised with propargylamine or ethylene glycol azide amine as in the previous case. However, Set 3 polymers contained a deuterated core. We studied these compounds by SANS on the time-of-flight LOQ diffractometer at the ISIS Spallation Neutron Source, Rutherford Appleton Laboratory, Didcot, UK. Their physicochemical characteristics are listed in Table V.3.

Table V.3. Physicochemical characteristics of deuterated 3-arm star shaped polyglutamates, Set 3, studied by SANS.

Star Polymer	Amine (R)	DP^{theo}	Mn^{a} (kDa)	Đ
SDP	Ethyl	120	18.3	1.19
SDN	Ethyl	120	19.4	1.19

[a] Estimated after ^{1}H NMR. SDP= 3-arm star polymer with deuterated core and functionalised with 12 mol% propargylamine. SDN= 3-arm star polymer with deuterated core and functionalised with 5mol% ethylene glycol azide amine.

The fourth set of polymers (**Set 4**) is composed of all previously studied 3-arm star shaped polyglutamates with ethyl as substituent. However, we studied these polymers by SAXS at the beamline NCD11 at ALBA Synchrotron Light Facility, Barcelona, Spain. Set 4 and their physicochemical characteristics are listed Table V.4.

Table V.4. Physicochemical characteristics of the ethyl derivatives 3-arm star shaped polyglutamates studied by SAXS.

Star Polymer	Amine (R)	DP^{theo}	Mn^{a} (kDa)	Mn^{b} (kDa)	Đ
S	Ethyl	150	23.1	-	1.23
SD	Ethyl	120	18.1	-	1.19
SDP	Ethyl	120	-	18.3	1.19
SDN	Ethyl	120	-	19.4	1.19

[a] Data obtained by SEC in DMF. [b] Estimated after ^{1}H NMR. S= 3-arm star polymer. SD= 3-arm star polymer with deuterated core. SDP= 3-arm star polymer with deuterated core and functionalised with 12 mol% propargylamine. SDN= 3-arm star polymer with deuterated core and functionalized with 5 mol% ethylene glycol azide amine.

The final set (**Set 5**) comprised star polyglutamates with 4 arms (*4S*) with certain GAU functionalised with bisdemethoxycurcumin (BDMC) to assess how polymer shape and size change as function of this pendant moiety. BDMC was chosen instead of curcumin due to its greater stability in physiological conditions and its ability to inhibit inflammation while reducing plaque deposition in Alzheimer's disease models [28]. We studied Set 5 by SANS on the SANS2d diffractometer at the ISIS Spallation Neutron Source, Rutherford Appleton Laboratory, Didcot, UK. Their physicochemical characteristics are listed in Table V.5.

Table V.5. Physicochemical characteristics of 4-arm star polymers studied by SANS.

Star Polymer	DP^{theo}	Mn^{a} (kDa)	Mn^{b} (kDa)	DP^{a}	DP^{b}	Đ
4S	200	16.8	16.0	111	106	1.34
4S(PEG-PGA)	200	-	28.8	-	--	1.34
4SCα	200	-	18.2	-	-	1.34
4SCβ	200	-	19.7	-	-	1.34

[a] Data obtained by SEC in DMF; [b] Estimated after ^{1}H NMR. 4S= 4-arm star polymer. 4SC = 4-arm star polymer functionalised with BDMC. α= 4 mol% modification. β= 8 mol% modification.

V.2.3.2. SANS Data Analysis: Set 1

We employed SANS to determine the solution conformation of the polymers presented in Table V.1. Scattering data for the studied polymers obtained before and after subtracting the solvent (D_2O) are depicted in Figure V.5.

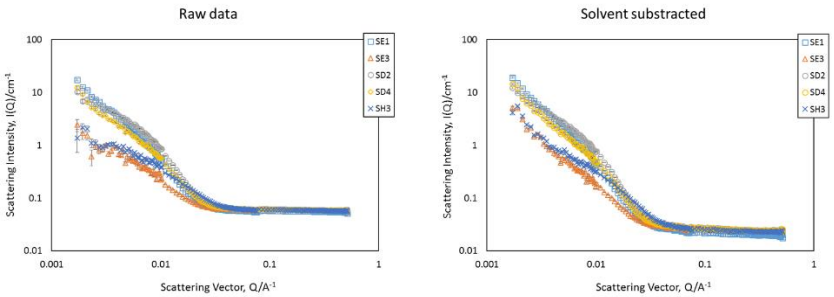

Figure V.5. Scattered intensity obtained by SANS, *I(Q)*, as a function of the scattering vector, *Q*, for the Set 1 before and after subtracting the solvent (D_2O) at concentration of 1 wt% (weight percent). Error bars are shown.

Determination of experimental parameters such as R_g, *I(0)*, D_{max} (maximum dimension), excluded volume, and MW usually represents the first step in reconstruction of the solution structure (Figure V.3). In some cases, R_g and *I(0)* can be determined from the SAS curve using the Guinier plot or through calculation of the pair-distribution function, *P(r)* [29, 30]. Disagreement between the values may be a sign of improper

assignment of D_{max} for the indirect Fourier transformation or other problems such as heterogeneity or unfolding.

V.2.3.2.1. Guinier Approximation

R_g may be extracted from *I(Q)* by treating the compounds as particles of unspecified size and shape and conducting a Guinier analysis. Guinier demonstrated that, in dilute systems where *S(Q) = 1*, at low *Q* values (where large length scales are observed), the scattering from a single particle can be simplified to

$$\ln\big(I(Q)\big) \approx \ln(I(0)) - {Q^2 R_g^2}/{3} \qquad \text{(Equation V.4)}$$

where R_g (the root-mean-square distance of all scattering elements from the centre of gravity) gives an idea of the overall size of the particle. A plot can be produced of *I(Q) vs.* Q^2 where, from Equation V.4, the slope of the data at low *Q* (provided $QR_g < 1$ or $QR_g<1.3$ for globular substances) is $-R_g^2/3$ [30]. Strictly speaking, Equation V.4 is an approximation valid only where $Q<<Rg^{-1}$. However, for quasi-spherical particles, the upper limit of the useful *Q* range is extended because the scattering form factor of a sphere is approximated well by Equation V.4 even for $Q \approx R_g$.

Non-linear behaviour in the Guinier plot in the range $Q<1.3/R_g$ indicates the presence of aggregation or inappropriate *Q* range (Figure V.6). Scattering from aggregation influences the entire dataset and any further data processing should proceed with caution.

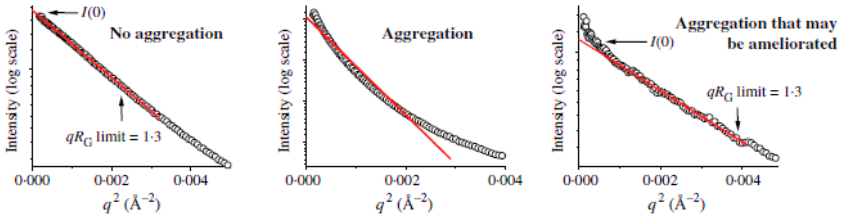

Figure V.6. Different behaviours in the Guinier plot. Adapted from [26].

For the studied set of star polymers, there is no Guinier region in the range $Q<1.3/R_g$, indicating the presence of larger substances than unimers in D_2O, the solvent used. This is most likely due to self-assembly

behaviour. When the sample is dissolved in PBS instead of D_2O or H_2O, the presence of smaller substances were observed, indicating lower interaction between particles due to the effect of salt concentration (Section V.2.3.5). These findings demonstrate the powerful influence of salt in the conformation of star shaped polyglutamates due to ionic strength as well as counterion (Duro-Castano *et al.,* submitted).

V.2.3.2.2. Kratky Approach

Kratky plots emphasise deviation from the high-*Q* behaviour of the scattering intensity *I(Q)*. The Kratky plot, $Q^2I(Q)$ *vs. Q*, which also can be calculated directly from the scattering curve, provides an excellent tool for evaluating the folding of samples. For folded domains, the Kratky plot yields a parabolic-like curve. Additionally, the position of the curve peak provides some information about overall size. However, this position is shape-dependent, like R_g, and thus cannot directly provide information regarding MW. In contrast, extended semi-flexible polymers, such as random coil peptides, follow the Porod-Kratky worm-like chain model [31, 32]. Random coil or unstructured peptides lack the characteristic folded peak and are linear with respect to *Q* in the large *Q*-region. Therefore, SAS is sensitive to the overall shape of the macromolecule, and samples that are unfolded are clearly visible in the Kratky plot (Figure V.7).

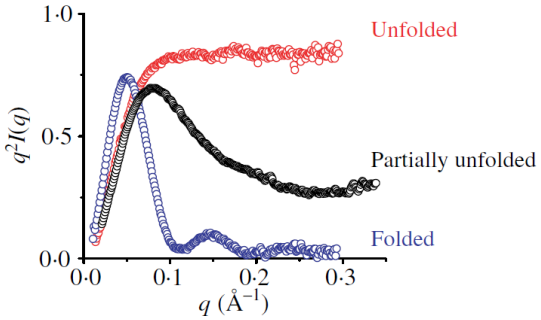

Figure V.7. Kratky plot identifies unfolded samples. Adapted from [26].

For the polymers under study in this section, the Kratky plots (Figure V.8) depicts smooth growth of $I(Q)Q^2$, suggesting that the compounds are folded or partially unfolded. However, more accurate

conclusions require further modelling of the obtained data (Section V.2.3.2.3).

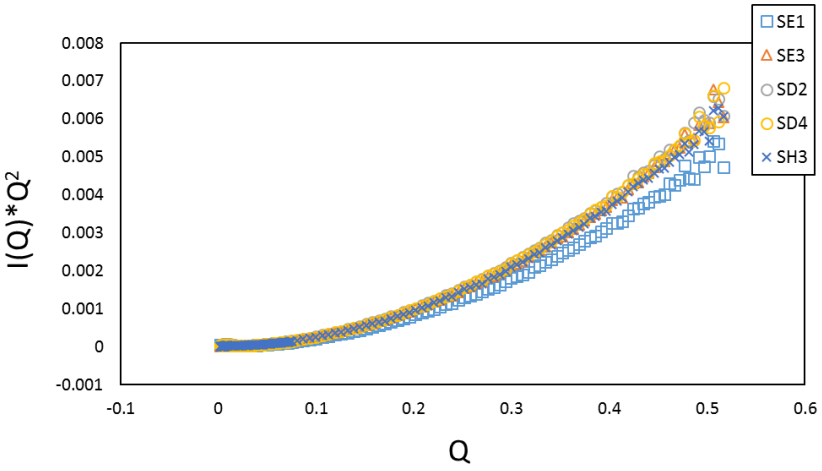

Figure V.8. Kratky representation of the SANS scattering from Set 1.

V.2.3.2.3. FISH Data Fitting

If a solution of macromolecules is monodisperse (or quasi-monodisperse as in the case of the polymers under study), the measured scattering profiles can be used for solution structure determination. Comparison of multiple reconstructions is extremely important to verify the stability of the solution and multiple repetitions of the modelling process significantly decreases the risk of inferring erroneous shapes. Unfortunately, given incorrect symmetries, *ab-initio* programs will often find shapes that also fit the scattering profiles [26].

If the atomic structure of the sample is known or an atomic model can be proposed, comparisons of theoretical SANS profiles with the experimental data is the first step in the structure evaluation. For this reason, we carried out modelling of the data to already defined precise form factors to gain more detailed information on the polymer conformation. To achieve this, we calculated the theoretical SANS profile with the FISH program [33], using the sum of square errors (SSE) to evaluate the best models.

We tested a multitude of form factors and fits which are presented in the following sections: rods, solid ellipsoids, and Gaussian coil for a Dozier star polymer. However, overinterpretation of the data must be avoided, and hence, beginning with the simplest models, such as those for solid geometric shapes, is most appropriate. A comprehensive description of all the models, including all written equations, can be found in the FISH manual [33].

V.2.3.2.3.1. Rod Form Factor

Equations V.5 and V.6 give the form factor for *N* randomly orientated rods from which a rod length, *L*, and cross-sectional radius, *R*, can be obtained. $J_1(x)$ is the first order Bessel function, and the volume, $V = \pi R^2 L$.

$$P(Q) = N \int_0^{\pi/2} F^2(Q) \sin(\gamma)\, d\gamma \qquad \text{(Equation V.5)}$$

where: $F(Q) = (\Delta\rho)V \frac{\sin(1/2\, QL\cos\gamma)}{1/2 QL\cos\gamma} \frac{2J_1(QR\sin\gamma)}{QR\sin\gamma}$ (Equation V.6)

Table V.6 shows the best fit parameters obtained for the rod form factor and Figure V.9 shows scattering data for the star polymers with best fits to the mentioned rod model.

Table V.6. Best fit parameters and SSE for the rod model.

Star Polymer	Rod Model		
	L (nm)	R (nm)	SSE
SE1	17.6	188.4	3.94e+03
SE3	3.4	168.7	1.90e+03
SD2	18.3	43.3	5.39e+03
SD4	12.2	109.9	4.52e+03
SH3	4.8	26.0	4.50e+03

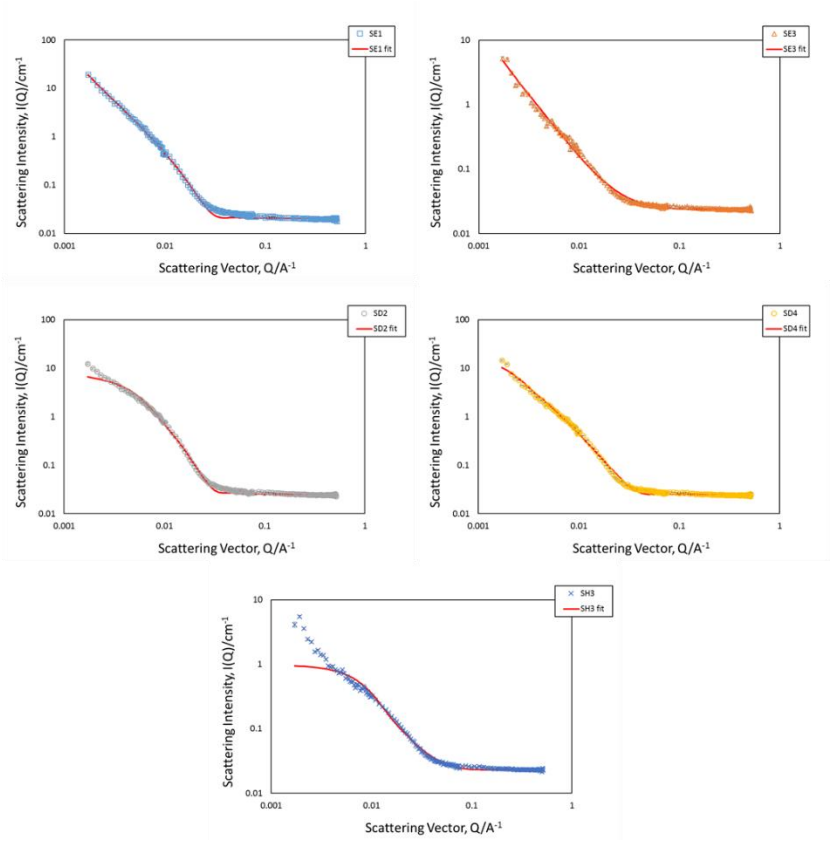

Figure V.9. Scattering data for the Set 1 star polymers with best fits to the rod form factor.

Both the fitted curves (Figure V.9) and the obtained parameters (Table V.6) suggest a preferred disc shape. However, values lie out of range of SANS technique and SSE values are high, leading to a mismatch between the fit and the curve. For these reasons, we suggest that the rod model is not the most suitable approach for the studied compounds and continued analyses of other forms.

V.2.3.2.3.2. Ellipsoid Form Factor

Equations V.7, V.8, and V.9 are applied for solid ellipsoids from which radius, *A*, and axial ratio, *X*, can be obtained.

$$I(Q) = I(Q) + SCALE \int_0^{\pi/2} \Phi^2(u) \sin(\propto) d \propto \qquad \text{(Equation V.7)}$$

where $\phi(u) = 3(\sin(u) - u \cdot \cos(u))/u3$ (Equation V.8)

and $u = QA(sin^2(\propto) + X^2 cos^2(\propto))^{1/2}$ (Equation V.9)

Table V.7 shows the best fit parameters obtained for the ellipsoid model and Figure V.10 shows scattering data for the Set 1 star polymers with best fits to the ellipsoid form factor.

Table V.7. Best fit parameters and SSE for the ellipsoid model.

Star Polymer	Ellipsoid Model		
	A (nm)	X (nm)	SSE
SE1	86.7	0.010	4.26e+03
SE3	198.2	0.001	2.04e+03
SD2	45.6	0.020	7.80e+03
SD4	528.7	0.001	5.79e+03
SH3	26.0	0.010	5.27e+03

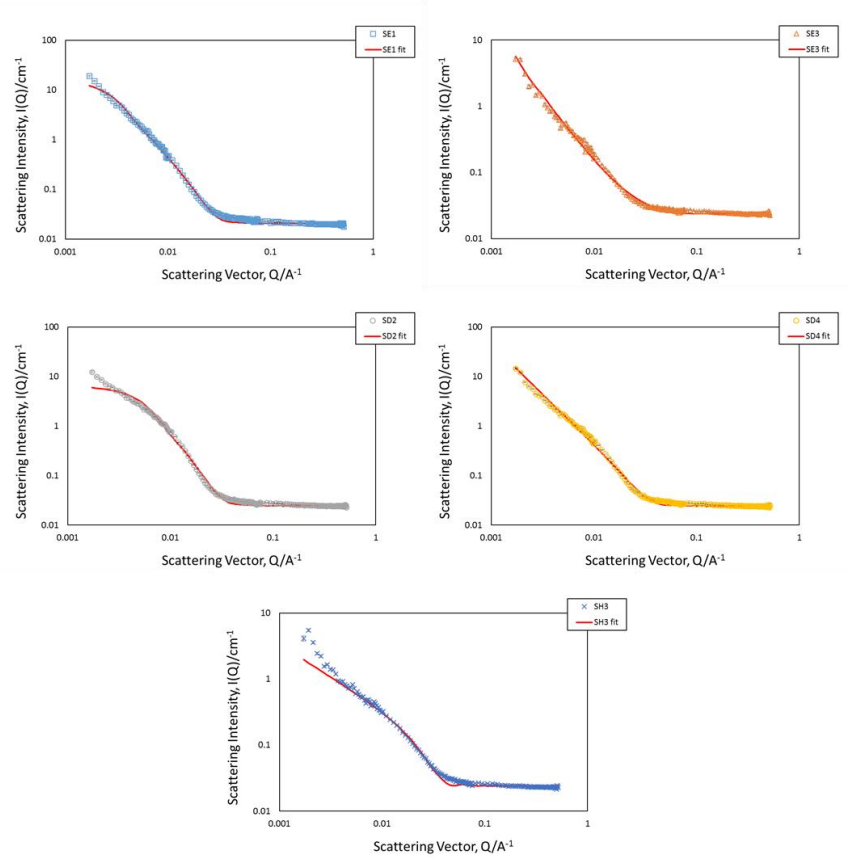

Figure V.10. Scattering data for the star polymers with fits to the ellipsoid form factor.

Both the fitted curves (Figure V.10) and the obtained parameters (Table V.7) suggest a preferred thin disc shape. However, values lie out of range of SANS technique and SSE values are high, leading to a mismatch between the fit and the curve. For these reasons, we suggest that the solid ellipsoid model is not the most suitable approach for the studied compounds and continued analyses of other forms.

V.2.3.2.3.3. Gaussian Coil for a Dozier Star Polymer Form Factor

In this case, R_g is obtained from the form factor, by fitting the data to the following equation:

$$P(Q) = Nf\left(exp\{-Q^2R_g^2/3\} + \frac{4\pi\alpha}{Q\xi(\mathrm{Nf})}\frac{\sin(\mu\tan^{-1}(Q\xi))}{(1+Q^2\xi^2)^{\mu/2}}\right) \quad \text{(Equation V.10)}$$

where *Nf* is the scale, *α/Nf* is the relative scale of the fractal term, *ξ* is the exponential damping length and $\nu = 1/(\mu + 1)$ is the Flory exponent (*3/5* in good solvent, *1/2* in theta solvent (*i.e.* $\mu = 2/3$ to *1*)).

In Figure V.11 the scattering data with fits are shown and Table V.8 shows the best fit parameters obtained by using this model.

Table V.8. Best fit parameters and SSE values obtained with the Gaussian coil for a Dozier star polymer mathematical model.

Dozier Model	SE1	SE3	SD2	SD4	SH3
I(0)	11.3	8.0	2.0	16.9	12.9
Rg (nm)	95.6	95.7	80.2	94.8	97.1
α/Nf	0.011	0.007	0.019	0.007	0.005
ξ (nm)	19.5	18.9	13.2	15.3	12.8
ν	0.34	0.38	0.31	0.33	0.36
HS S(Q) VOL	0.052	0.046	0.050	0.076	0.096
SPH R	21.7	21.1	19.4	17.3	12.8
BKG A	0.007	0.018	0.004	0.014	0.017
BKG B*Q	-0.007	-0.009	-0.004	-0.012	-0.009
BKG C*Q^2	0.009	0.012	0.006	0.015	0.010
SSE	5.13e+02	4.76e+02	4.81e+02	5.58e+02	5.09e+02

Errors on the refined parameter are Rg (±15); ξ (±5); υ (±0.05).

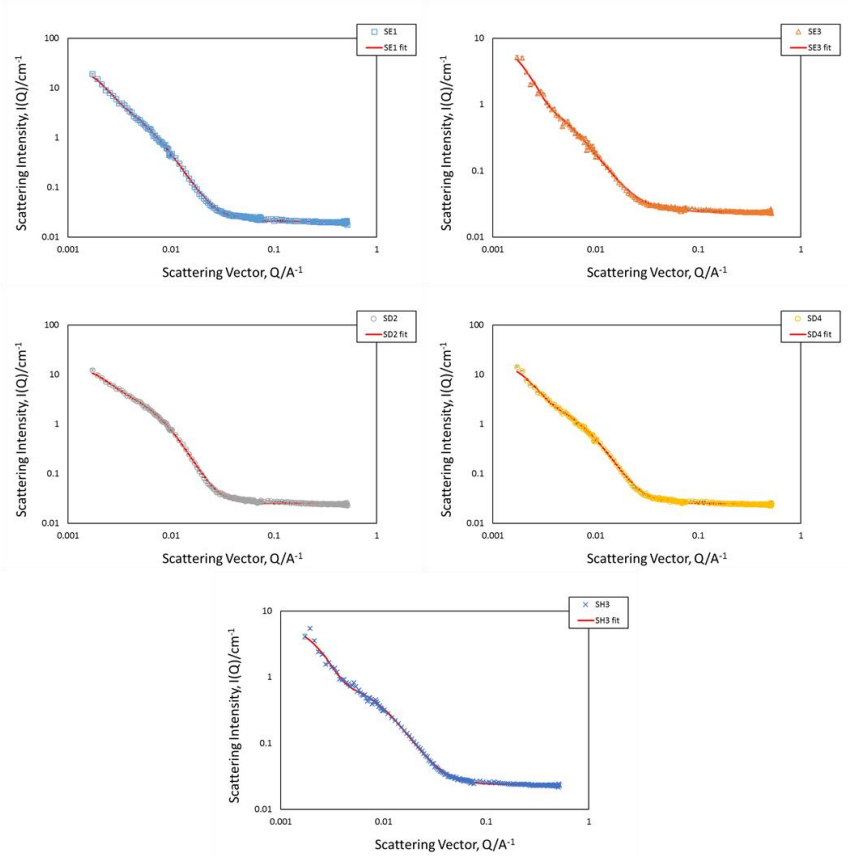

Figure V.11. Scattering data for Set 1 with fits to the Gaussian coil for a Dozier star polymer form factor obtained by using all the possible parameters.

Looking at both fit curves (Figure V.11) and the obtained parameters (Table V.8), we note that the values obtained for all the parameters are acceptable and within the detection limits for SANS. Furthermore, SSE values have diminished considerably compared to those obtained in previous models indicating the selection of an appropriate model. Additionally, as shown in Figure V.11, the theoretical curves match the experimental findings. Critically, the star model is the only model that reproduces the inflexion point feature observed in the scattering curves at approximately Q= 0.006 A^{-1}.

Based on these results, we performed a second data adjustment in order to minimise the number of fit parameters by using a flat background (*Q* independent background) which will be dominated by

any incoherent scattering, if present, but will also contain any instrument background not perfectly subtracted during data analysis. The obtained results are shown in Figure V.12 and Table V.9.

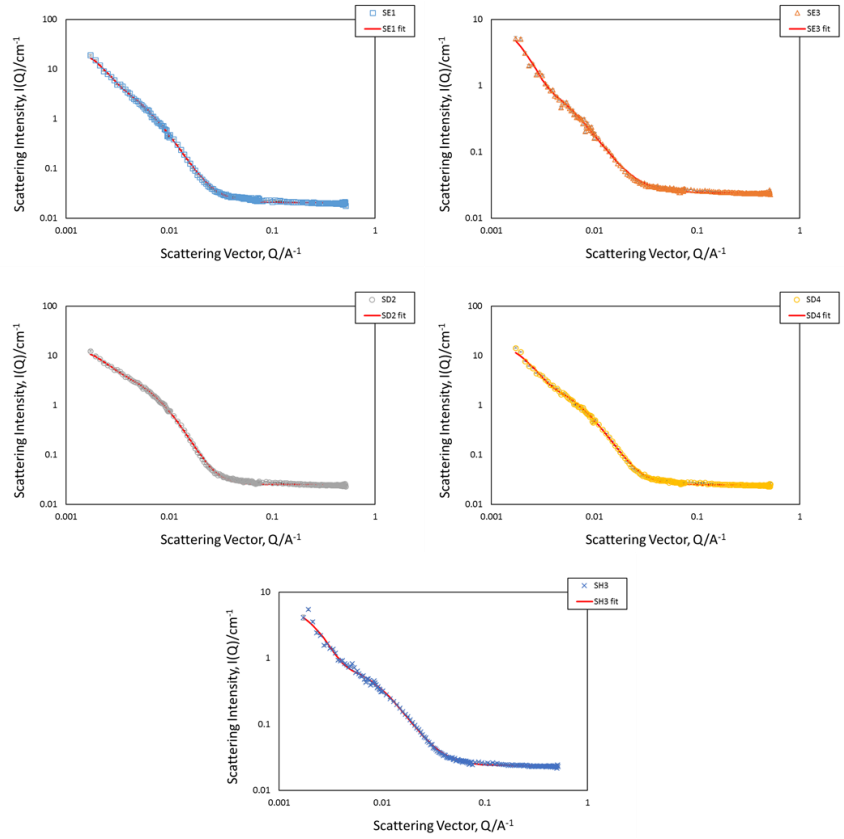

Figure V.12. Scattering data for the star polymers with fits to the Gaussian coil for a Dozier star polymer form factor without backgrounds *B* and *C* contribution.

The obtained results using a flat background demonstrate that the theoretical and experimental curves still match and SEE values remain low.

Table V.9. Best fit parameters and SSE for the Gaussian coil for a Dozier star polymer without backgrounds *B* and *C* contribution.

Dozier Model	SE1	SE3	SD2	SD4	SH3
I(0)	5.77	7.61	55.2	104.4	11.9
Rg (nm)	116.2	94.4	130.0	130.9	92.1
α/Nf	0.012	0.009	0.014	0.007	0.006
ξ (nm)	25.8	18.2	20.4	24.8	12.6
ν	0.36	0.40	0.34	0.36	0.39
HS S(Q) VOL	0.055	0.217	0.098	0.104	0.046
SPH R	23.8	175.1	22.0	20.9	13.4
BKG A	0.020	0.024	0.025	0.024	0.023
BKG B*Q	-	-	-	-	-
BKG C*Q^2	-	-	-	-	-
SSE	1.58e+03	1.02e+03	1.87e+03	1.44e+03	9.32e+02

Errors on the refined parameter are Rg (±15); ξ (±5); υ (±0.05).

In a final attempt, we minimised the number of fitting parameters using a flat background and negating the *S(Q)* term in the model, *i.e.* assuming absence of interparticle interactions. Figure IV.13 shows the perfectly matched fit and Table IV.10 shows the fit parameters.

We obtained confirmation of the global (rather than local) minimum in the fit by varying the initial parameters and refitting the data set. We established the error in each component by determining when a difference in the fit could be visually determined after manual alteration of the chosen setting and relaxation of the coupled parameters. Associated errors are indicated in Table V.10.

Table V.10. Best fit parameters and SSE for the Gaussian coil for a Dozier star polymer without both *S(Q)* and backgrounds *B* and *C* contribution.

Dozier Model	SE1	SE3	SD2	SD4	SH3
I(0)	30.18	9.99	12.90	19.52	6.32
Rg (nm)	101.2	102.0	91.0	92.5	82.1
α/Nf	0.010	0.007	0.016	0.007	0.007
ξ (nm)	18.8	18.9	12.8	13.4	9.6
ν	0.35	0.40	0.32	0.34	0.38
HS S(Q) Vol	-	-	-	-	-
SPH R (nm)	15.0	15.0	15.0	15.0	15.0
BKG A	0.020	0.024	0.025	0.025	0.023
B*Q	-	-	-	-	-
C*Q^2	-	-	-	-	-
SSE	1.94e+03	1.06e+03	2.65e+03	1.92e+03	1.12e+03

Errors on the refined parameter are Rg (±15); ξ (±5); υ (±0.05).

Fit parameters demonstrate that, in the absence of interparticle interactions (*S(Q)*= 1), the R_g of the analysed compounds ranged from 80 to 100 nm. R_g values decrease in the order *Ethyl*>*DOOA*>*Hexyl* but, surprisingly, there was no dependence on MW. This is a key concept towards the elucidation of the 3D shape of the molecules. The Flory component values variation was found to be small, closed to ⅓, indicating a relatively poor solvent and suggesting that the polymers studied are in a collapsed conformation (dense stars). Packing close to the core is influenced by the packing efficiency of the substituents (*i.e.* the polymer packs around a larger overall excluded volume for Ethyl than Hexyl). Moving towards the outer layers, it appears that the arms tend to reorganise themselves around a fixed core, hence the core is simply more "wrapped" as MW increases allowing R_g to remain relatively unchanged.

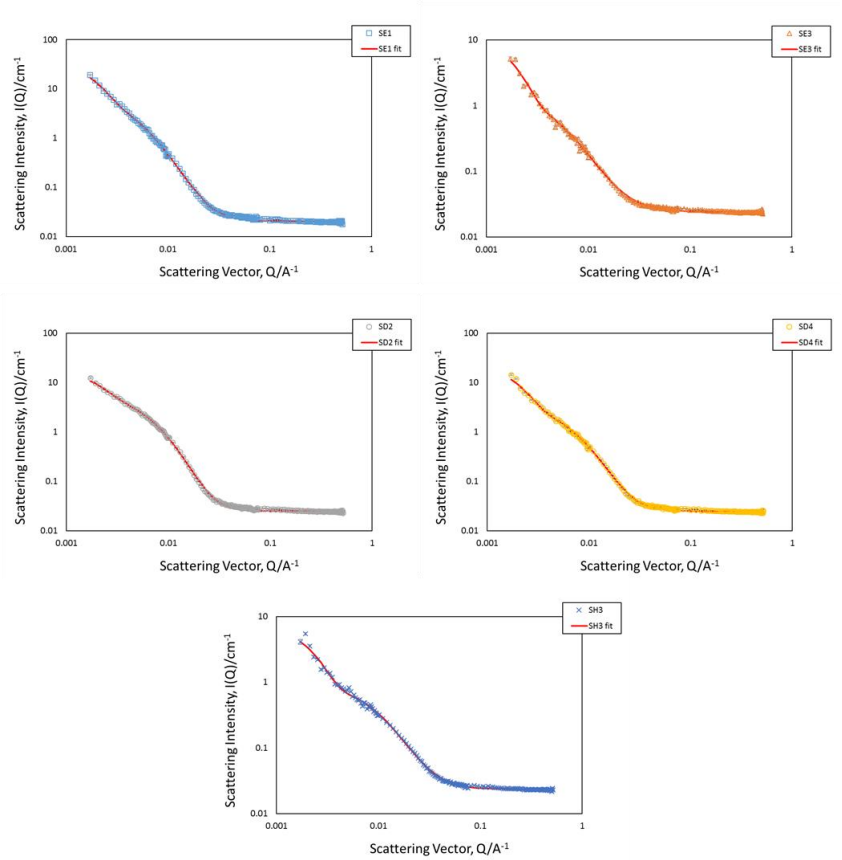

Figure V.13. Scattering data for the star polymers with fits to the Gaussian coil for a Dozier star polymer form factor without both *S(Q)* and backgrounds *B* and *C* contribution.

The ξ parameter provides an indication of how the polymer swelling changes upon the distance from the core. As with the R_g values, the ξ parameters are clearly dependent on the substituent used, and vary in the same order as R_g (Ethyl>DOOA>Hexyl). When combined with the Flory parameter, this provides a consistent picture of how the conformation varies with MW: for larger R_g values the larger core area to cover results in more swollen outer layers and higher ξ values.

V.2.3.3. SANS Data Analysis: Set 2

We also used SANS to determine the solution conformation of the Set 2 polymers presented in Table V.2. A summary of every compound tested with the different measured conditions is shown in Table V.11.

Table V.11. Summary of the different conditions tested with the different star-shape polymers from set 2.

Star Polymer	Arms	GAU	Solvent	Concentration (mg/mL)
SPc	3	150	D_2O	2
SPd	3	150	D_2O	1
SNd	3	150	D_2O	1
(SP+SN)c	3+3	150+150	D_2O	2
(SP+SN)e	3+3	150+150	D_2O	0.1
(SP-SN)c	3-3	150-150	D_2O	2
(SP-SN)e	3-3	150-150	D_2O	0.1

c= 2 mg/mL; d= 1 mg/mL; e= 0.1 mg/mL. SP= 3-arm star polymer functionalised with 10 mol% propargylamine. SN= 3-arm star polymer functionalised with 5 mol% ethylene glycol azide amine. SP+SN= physical mixture. SP-SN= covalent capture.

We studied the ***SP polymer*** (ethyl as substituent, 150 GAU, functionalised with propargylamine) in D_2O at two different concentrations, 2 and 1 mg/mL (*SPc* and *SPd* respectively), values above its critical aggregation concentration (CAC), 0.5 mg/mL (Duro-Castano *et al.,* submitted). This CAC value not only represents the concentration above which aggregation processes are taking place, but also represents the maximum concentration of free non-aggregated polymer species present in the sample under specific conditions (temperature, ionic strength, pH). Scattering data after subtracting the solvent and scaling the curves for the two different concentrations are shown in Figure V.14.

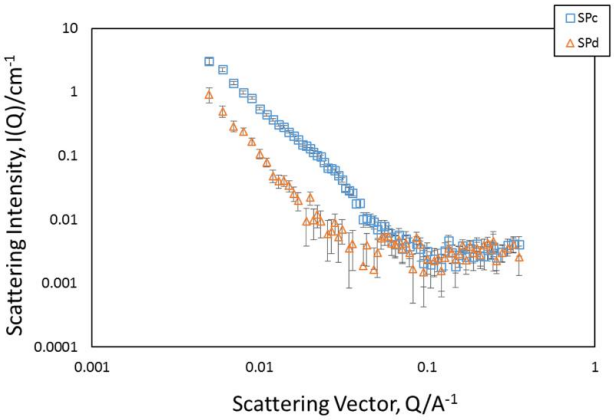

Figure V.14. Scattered intensity obtained by SANS, *I(Q)*, as a function of the scattering vector, *Q*, for the studied star polymer after subtracting the solvent (D_2O) and scaling at two different concentrations: 2 and 1 mg/mL (*SPc* and *SPd* respectively). Error bars are shown.

We studied the ***SN polymer*** (ethyl as substituent, 150 GAU, functionalised with ethylene glycol azide amine) in D_2O at 1 mg/mL (*SNd*), value above its CAC (0.5 mg/mL) (Duro-Castano *et al.,* submitted). Scattering data after subtracting the solvent are shown in Figure V.15.

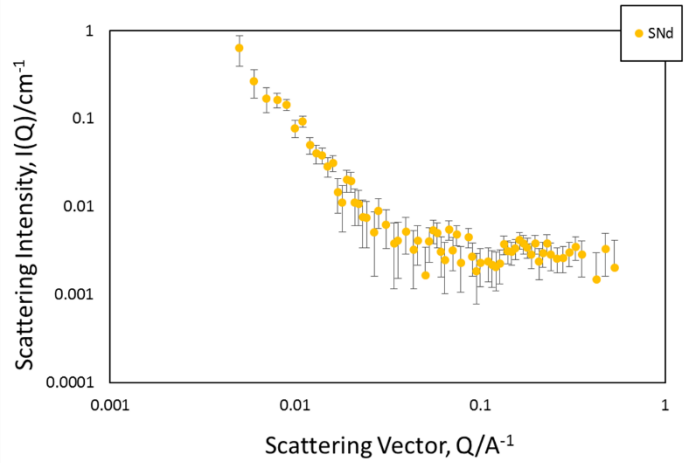

Figure V.15. Scattered intensity obtained by SANS, *I(Q)*, as a function of the scattering vector, *Q*, for the studied star polymer after subtracting the solvent (D_2O) at 1 mg/mL. Error bars are shown.

When *SP* and *SN* polymers are compared at the same concentration (1 mg/mL, Figure V.16) we observed similar curve shapes, suggesting that the propargylamine and ethylene glycol azide amine

used has no significant effect in the conformation of the parent star polymers or that the effect produced is exactly the same.

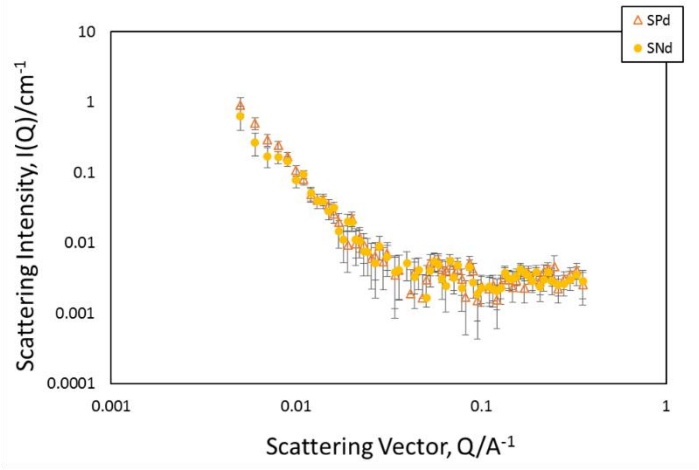

Figure V.16. Comparison between *SPd* and *SNd*. Error bars are shown.

We next measured a physical mixture of SP and SN polymers (*SP+SN*) in D_2O at two different concentrations: 2 and 0.1 mg/mL (*(SP+SN)c* and *(SP+SN)e* respectively), values above and below CAC respectively. Scattering data after subtracting the solvent are shown in Figure V.17.

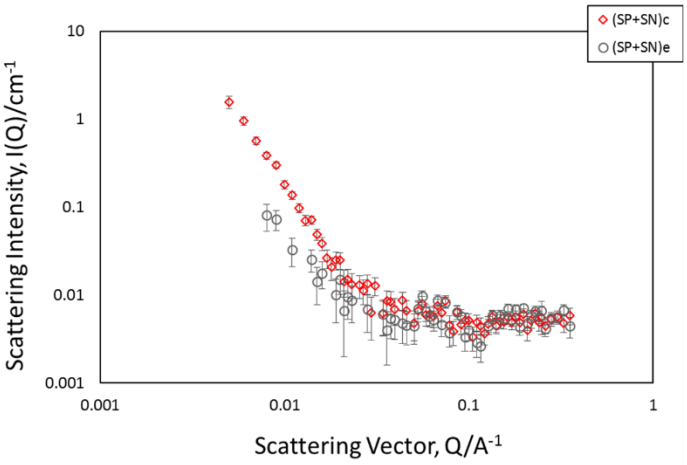

Figure V.17. Scattered curve for the mixture *SP+SN* after subtracting the solvent (D_2O) at two different concentrations: 2 mg/mL ((*SP+SN)c*) and 0.1 mg/mL ((*SP+SN)e*). Error bars are shown.

As shown in Figure V.17, the curve at 0.1 mg/mL presents with a poor signal/noise ratio, although, at high *Q* values, the shape of the curve is similar for both concentrations.

When covalent attachment is carried out at the same concentrations as in the previous case (2 and 0.1 mg/mL), the scattered curve of the resulting compound (*SP-SN*) presents itself as shown in Figure V.18.

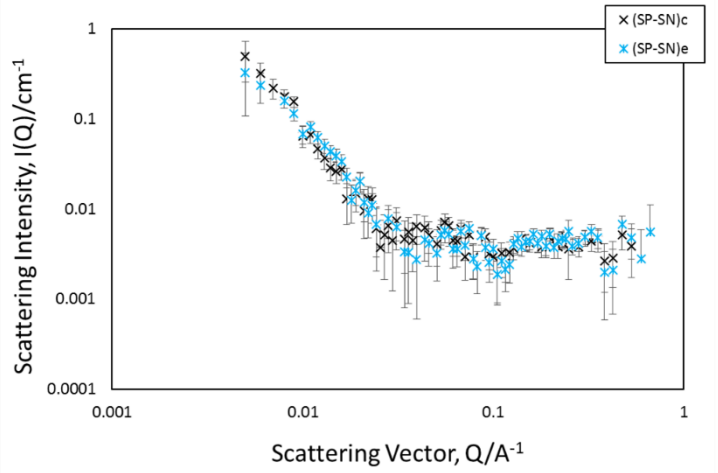

Figure V.18. Scattered curve for the compound *SP-SN* after subtracting the solvent (D_2O) and scaling the curves at two different concentrations: 2 mg/mL ((*SP-SN)c*) and 0.1 mg/mL ((*SP-SN)e*). Error bars are shown.

In this case, we observed that the effect of the concentration does not affect the shape of the obtained compound after covalent capture.

Comparing both the physical mixture and the covalent attachment in the same graph at the same concentration (Figure V.19), we noted a small difference in the shape of the curve at low *Q* values, suggesting that both solutions could contain different substances.

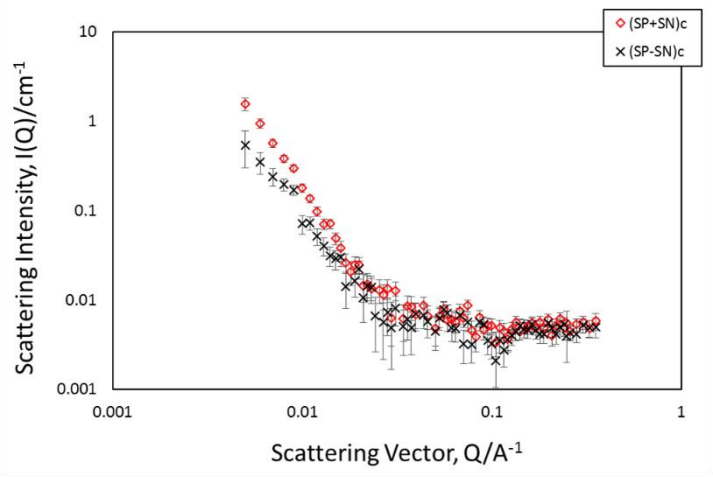

Figure V.19. Comparison between (*SP+SN)c* and ((*SP-SN)c*. Error bars are shown.

V.2.3.3.1. FISH Data Fitting

Taking the results obtained for the Set 1 polymers as a starting point, we selected the Gaussian Coil for a Dozier Star Polymer model in order to elucidate the parameters related to size and shape for this second set of star polymers.

During the fitting, we minimised the number of parameters using a flat background and negating the *S(Q)* term in the model.

Regarding ***SP* polymer**, Figure V.20 shows the scattering data with fits and Table IV.12 shows the best fit parameters obtained for the two different concentrations: 2 mg/mL (*SPc*) and 1 mg/mL (*SPd*).

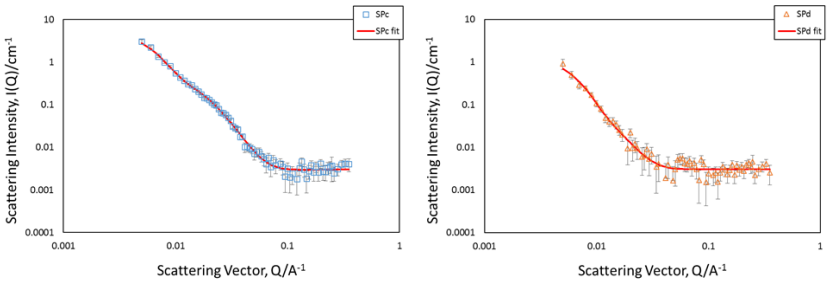

Figure V.20. Scattering data for with fits to the Gaussian coil for a Dozier star polymer form factor without both *S(Q)* and backgrounds *B* and *C* contribution.

Comparing these parameters with those obtained for Set 1 (obviating the functionalisation and GAU), we observed a strong concentration-dependence on the self-assembly process. Table V.12 shows similar parameters for the *SP* compound at 2 mg/mL and at 1 mg/mL. Therefore, when the concentration increases, the self-assembling process increases exponentially.

Table V.12. Best fit parameters and SSE for the Gaussian coil for a Dozier star polymer without both *S(Q)* and backgrounds *B* and *C* contribution.

Dozier Model	SPc	SPd
I(0)	5.14	1.30
Rg (nm)	31.9	32.1
α/Nf	0.004	0.005
ξ (nm)	5.1	8.1
ν	0.31	0.31
HS S(Q) Vol	-	-
SPH R (nm)	15.0	15.0
BKG A	0.003	0.024
B*Q	-	-
C*Q²	-	-
SSE	5.60e+01	6.30e+01

Errors on the refined parameter are Rg (±15); ξ (±5); υ (±0.05).

In the case of the ***SN* polymer**, Figure V.21 shows the scattering data with fit and Table V.13 shows the best fit parameters obtained for 1 mg/mL (*SNd*).

Despite the associated error bars in the measurement, Figure V.21 and Table V.13 demonstrate that the modification of the GAU does not affect the conformation of the star polymer (with these percentages of functionalisation).

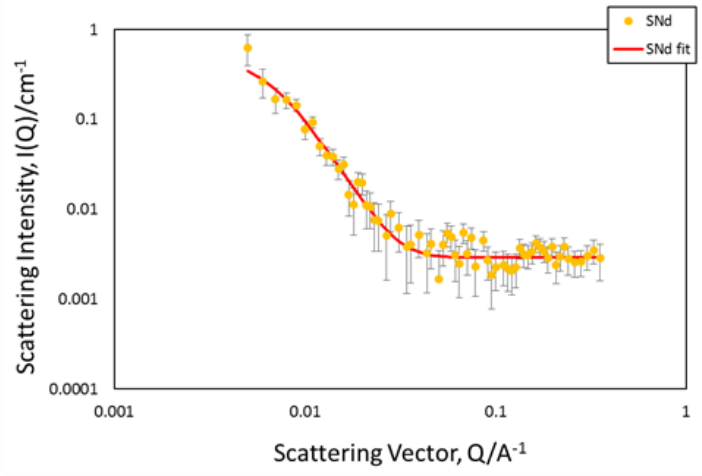

Figure V.21. Scattering data for with fit to the Gaussian coil for a Dozier star polymer form factor without both *S(Q)* and backgrounds *B* and *C* contribution.

Table V.13. Best fit parameters and SSE for the Gaussian coil for a Dozier star polymer without both *S(Q)* and backgrounds *B* and *C* contribution.

Dozier Model	SNd
I(0)	0.31
Rg (nm)	29.4
α/Nf	0.034
ξ (nm)	8.9
ν	0.31
HS S(Q) Vol	-
SPH R (nm)	15.0
BKG A	0.003
B*Q	-
C*Q^2	-
SSE	6.03e+01

Errors on the refined parameter are Rg (±15); ξ (±5); υ (±0.05).

Concerning to the physical mixture ***(SP+SN)*** and the covalent attachment ***(SP-SN)*** of the functionalised compounds, Figure V.22 shows the scattering data with fits and Table V.14 shows the best fit parameters obtained at 2 mg/mL (*(SP+SN)c* and *(SP-SN)c*). Due to the

signal/noise ratio, we did not study 0.1 mg/mL samples (*(SP+SN)e* and *(SP-SN)e*) at length.

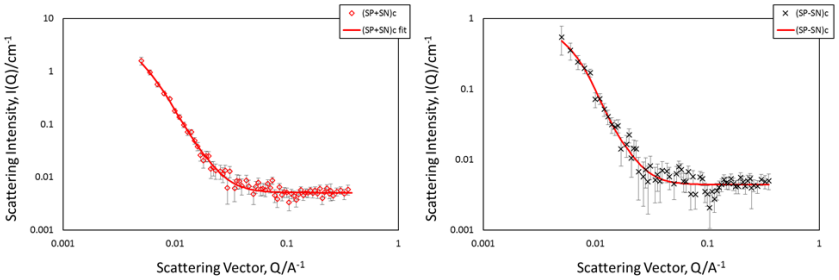

Figure V.22. Scattering data for with fit to the Gaussian coil for a Dozier star polymer form factor without both *S(Q)* and backgrounds *B* and *C* contribution.

Table V.14. Best fit parameters and SSE for the Gaussian coil for a Dozier star polymer without both *S(Q)* and backgrounds *B* and *C* contribution.

Dozier Model	(SP+SN)c	(SP-SN)c
I(0)	0.92	0.56
Rg (nm)	33.8	29.7
α/Nf	0.276	0.021
ξ (nm)	24.4	11.8
ν	0.34	0.34
HS S(Q) Vol	-	-
SPH R (nm)	15.0	15.0
BKG A	0.005	0.004
B*Q	-	-
C*Q²	-	-
SSE	5.64e+01	5.70e+01

Errors on the refined parameter are Rg (±15); ξ (±5); υ (±0.05).

The fit parameters obtained demonstrate that, in the absence of interparticle interactions (*S(Q)*=1), the R_g of the analysed Set 2 polymers are around 30 nm, independent of the conjugate substituent. Comparing these findings with the previous result (Table V.13) suggests that the self-assembly process has decreased. As in Set 1, the Flory component values vary little, and are close to ⅓, indicating a relatively

poor solvent. Therefore, the polymer is collapsed (dense stars) and the arms tend to reorganise themselves around the fixed core.

When *(SP+SN)* and *(SP-SN)* systems are compared, the only difference found is the ξ value. In the case of physical mixture, this value is higher than for covalent attachment suggesting that this linkage gives rise to a more compact structure with no major influence on the final conformation of the star polymer.

V.2.3.4. SANS Data Analysis: Set 3

A crucial feature of SANS is the difference in scattering length densities between isotopes and, more precisely, between hydrogen and deuterium, -0.3741 x 10^{-12} cm and 0.6671 x 10^{-12} cm, respectively (though they are essentially identical in X-ray and light analyses). This difference allows us to change the scattering power of part of a molecule by substituting hydrogen for deuterium with a minimal effect on the sample.

Table V.15. Summary of the different conditions tested for the different deuterated star polymers within Set 3.

Star Polymer	Arms	GAU	Solvent	Concentration (mg/mL)
SDN2a	3	120	H_2O	10
SDN3a	3	120	D_2O	10
SDN3c	3	120	D_2O	2
SDN4b	3	120	dPBS	5
SDP3a	3	120	D_2O	10

2= H2O. 3= D2O. 4= deuterated PBS (dPBS). a= 10 mg/mL. b= 5 mg/mL. c= 2 mg/mL. SDN= 3-arm star polymer with deuterated core and functionalised with 6 mol%$_I$ ethylene glycol azide amine. SDP= 3-arm star polymer with deuterated core and functionalised with 12 mol% propargylamine.

However, this change has dramatic effects on the scattering allowing intriguing contrast variation studies [11-13] and provides the ability to independently characterise the different deuterium labelled domains within a drug delivery system structure in solution. To this end,

we attempted to demonstrate the regions occupied by the core *vs.* the substituent using contrast variation experiments by analysing the scattering data obtained for the compounds listed in Table V.3 (Set 3). A summary of every compound tested with the different measured conditions is shown in Table V.15.

Due to elevated experimental difficulty, the number of accumulations per run had to be significantly increased in order to minimise error bars. Unfortunately, due to beam-time allowance, the measured *Q*-range was insufficient for the elucidation of the compound structure (Figure V.23). To complete the data, future studies will require an extension of the measured *Q*-range, and will hopefully provide interesting results, as we observed a remarkable difference in the behaviour of the systems when comparing *SDN2a* and *SDN3a* graphs (Figure V.24).

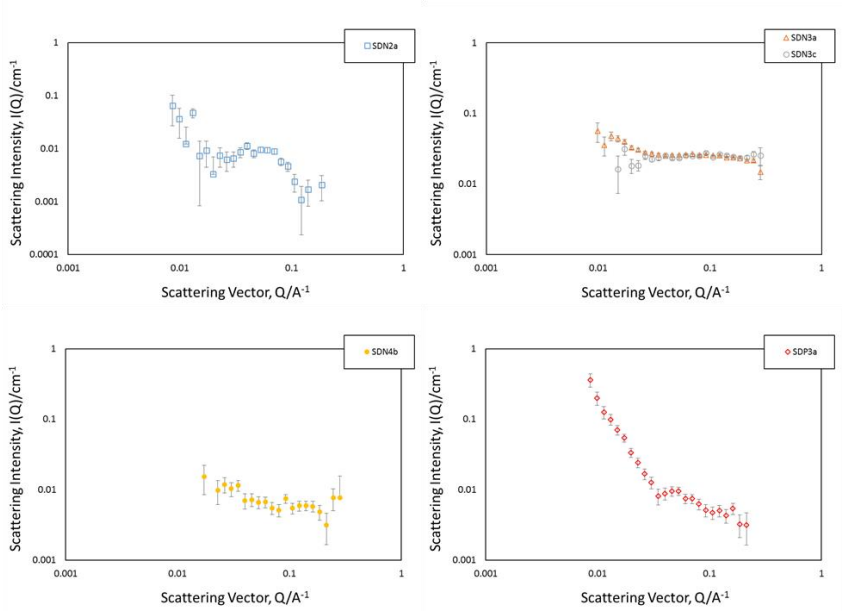

Figure V.23. Scattered curve for the deuterated core star polymers presented in Table V.15 after subtracting the solvent different. Error bars are shown.

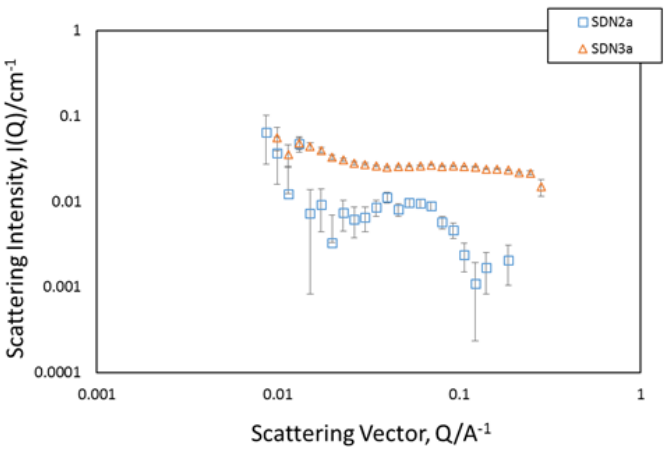

Figure V.24. Comparison between *SDN* in H_2O (*SDN2a*) and D_2O (*SDN3a*) at the same concentration (10 mg/mL). Error bars are shown.

V.2.3.5. SAXS Data Analysis: Set 4

As a complement to SANS, we used SAXS to determine the solution conformation of the polymers presented in Table V.4. In this section, we will present the analysis of all studied compounds, divided by different issues (ionic strength and concentration).

Table V.16 contains a summary of every compound tested with the different measured conditions.

Table V.16. Summary of the different conditions tested for Set 4 of 3-arm star polymers.

Star Polymer	Arms	GAU	Solvent	Concentration (mg/mL)
S1a	3	150	PBS	10
S2a	3	150	H_2O	10
S2b	3	150	H_2O	5
S2c	3	150	H_2O	2
S2d	3	150	H_2O	1
SD1a	3	150	PBS	10
SD2b	3	150	H_2O	5
SD2c	3	150	H_2O	2
SD2d	3	150	H_2O	1
SDP2a	3	150	H_2O	10
SDN2a	3	150	H_2O	10
SDN3a	3	150	D_2O	10
(SDP+SDN)1a	3+3	150+150	PBS	10
(SDP+SDN)1b	3+3	150+150	PBS	5
(SDP+SDN)1c	3+3	150+150	PBS	2
(SDP+SDN)1d	3+3	150+150	PBS	1
(SDP+SDN)2a	3+3	150+150	H_2O	10
(SDP+SDN)2b	3+3	150+150	H_2O	5
(SDP+SDN)2c	3+3	150+150	H_2O	2
(SDP+SDN)2d	3+3	150+150	H_2O	1
(SDP-SDN)2a	3+3	150-150	H_2O	10

1= PBS. 2= H_2O. 3= D_2O. a=10 mg/mL. b= 5 mg/mL. c= 2 mg/mL. d= 1 mg/mL. S= 3-arm star polymer. SD= 3-arm star polymer with deuterated core. SDP= 3-arm star polymer with deuterated core and functionalised with 10 mol% propargylamine. SDN= 3-arm star polymer with deuterated core and functionalised with 5 mol% ethylene glycol azide amine. SDP+SDN= physical mixture. SDP-SDN= covalent capture.

We studied the ***S polymer*** (ethyl as substituent, 150 GAU) in both PBS (*S1a*, at 10 mg/mL) and H_2O (*S2a*, *S2b*, *S2c*, *S2d,* at concentrations between 10 and 1 mg/mL).

Figure V.25 shows the scattering data, before and after subtracting the solvent, for these polymers and a comparison between the same concentration of star polymer in PBS and H_2O.

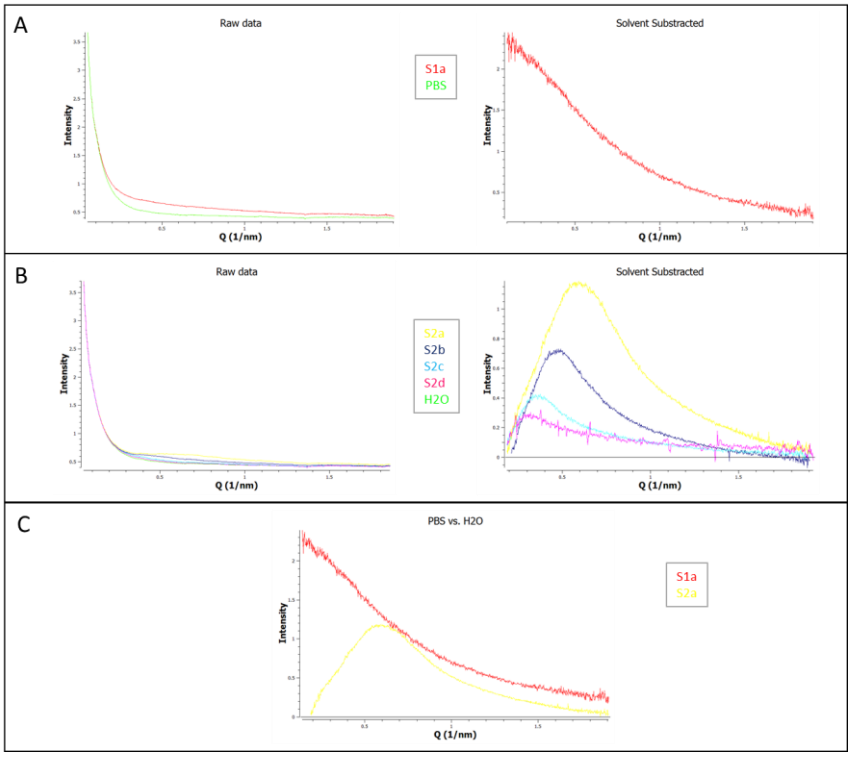

Figure V.25. (A) Scattered curve for *S1a* polymer before and after subtracting the solvent (PBS). (B) Scattered curve for *S2* polymers before and after subtracting the solvent (H_2O) at different concentrations: 10 mg/mL (*S2a*), 5 mg/mL (*S2b*), 2 mg/mL (*S2c*), 1 mg/mL (*S2d*). (C) Comparison between *S1a* and *S2a*.

As shown in Figure V.25, ionic strength has a clear influence on the self-assembling behaviour. When the star polymers are dissolved in H_2O (as in the case of polymers studied by SANS above reported), the observed particle size increased compared to PBS-polymer solutions (Figure V.25C). These findings demonstrate that salt concentration has a significant effect on the polymer size by decreasing the incidence of polymer aggregation. The superposition of scattering curves from different concentrations in H_2O (Figure V.25B) reveals a clear concentration-dependent trend similar to the findings from Section V.2.3.1: when the polymer concentration diminishes, the structures become smaller.

To verify the effect of core deuteration and to compare with the information obtained in previous sections, we performed the same analysis for ***SD*** polymers (ethyl as substituent, deuterated core, 150 GAU). We studied *SD* polymer in both PBS (*SD1a,* at 10 mg/mL) and H_2O (*SD2*), measuring concentrations between 5 and 1 mg/mL (*SD2b*, *SD2c*, *SD2d*) in H_2O. Figure V.26 shows the scattering data before and after subtracting the solvent for these polymers in PBS and H_2O. As shown in Figure V.26, again, we found a clear influence of the ionic strength on nanostructure size. Additionally, when concentration increases, the size also increases.

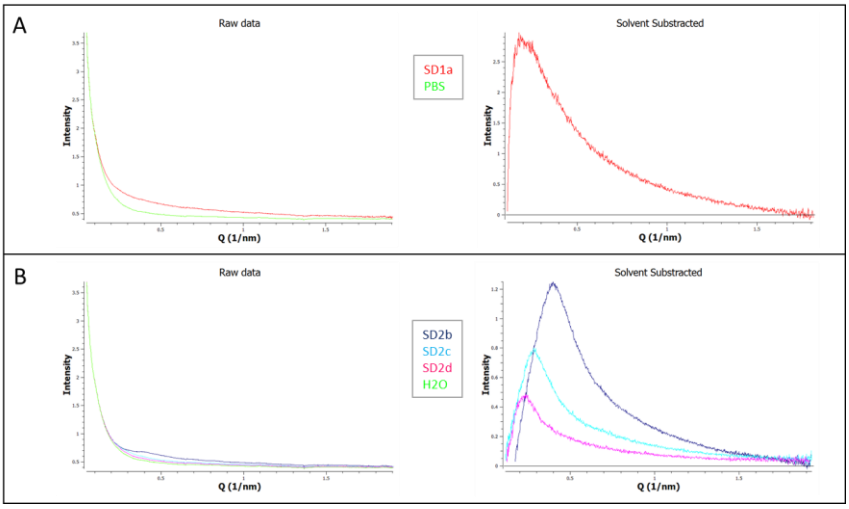

Figure V.26. (A) Scattered curve for *SD1a* polymer before and after subtracting the solvent (PBS). (B) Scattered curve for *S2* polymers before and after subtracting the solvent (H_2O) at different concentrations: 5 mg/mL (*SD2b*), 2 mg/mL (*SD2c*) and 1 mg/mL (*SD2d*).

We analysed the ***SDP*** polymer (ethyl as substituent, deuterated core, 10 mol% functionalised with propargylamine, 150 GAU) in H_2O at a concentration of 10 mg/mL (*SDP2a*) (Figure V.27).

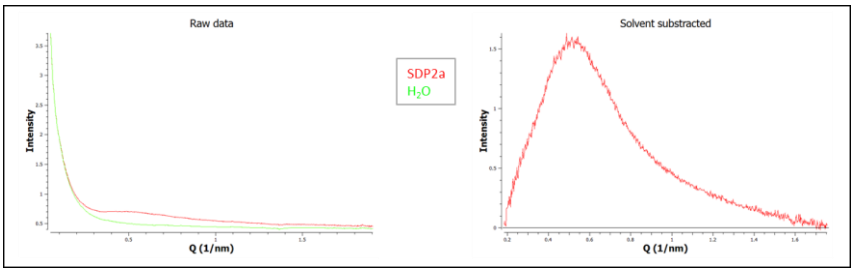

Figure V.27. Scattered curve for *SDP2a* polymer before and after subtracting the solvent (H_2O).

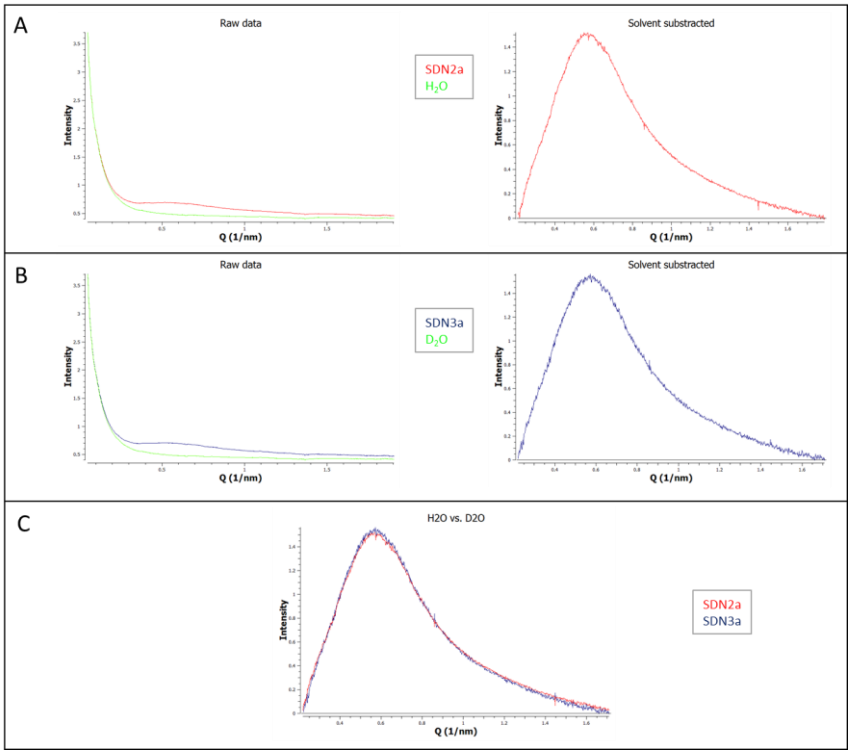

Figure V.28. (A) Scattered curve for *SDN2a* polymer before and after subtracting the solvent (H_2O) at 10 mg/mL. (B) Scattered curve for *SDN3a* polymer before and after subtracting the solvent (D_2O) at 10 mg/mL. (C) Comparison between *SDN2a* and *SDN3a*.

We also measured the ***SDN* polymer** (ethyl as substituent, deuterated core, 5 mol% functionalised with ethylene glycol azide amine, 150 GAU) in both H_2O and D_2O at 10 mg/mL (*SDN2a* and *SDN3a* respectively). As expected (Figure V.28C), the size and shape of polymer

dissolved in H_2O and D_2O were exactly the same. These findings therefore suggest that the data obtained by SANS in deuterated solvents is perfectly valid and can be extrapolated to non-deuterated solvents in the same conditions.

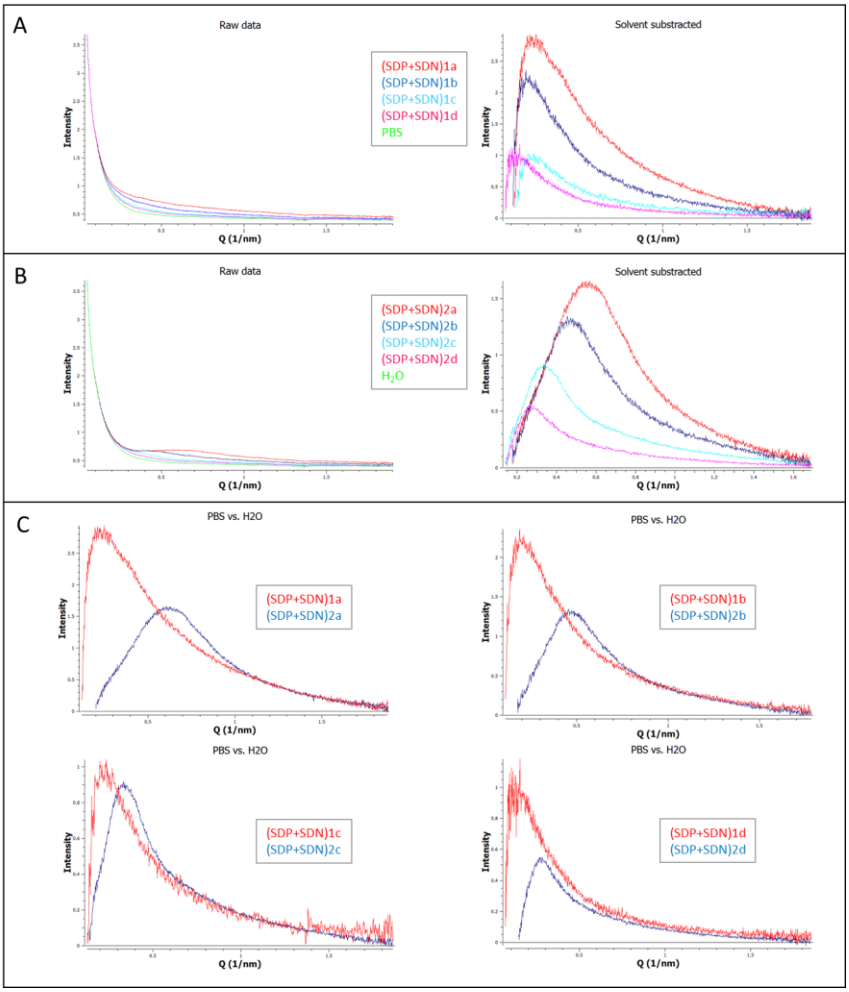

Figure V.29. (A) Scattered curve for the mixture *SDP+SDN* before and after subtracting the solvent (PBS) at different concentrations: 10 mg/mL [(*SDP+SDN)1a*], 5 mg/mL [(*SDP+SDN)1b*], 2 mg/mL [(*SDP+SDN)1c*], 1 mg/mL [(*SDP+SDN)1d*]. (B) Scattered curve for the mixture *SDP+SDN* before and after subtracting the solvent (H_2O) at different concentrations: 10 mg/mL [(*SDP+SDN)2a*], 5 mg/mL [(*SDP+SDN)2b*], 2 mg/mL [(*SDP+SDN)2c*], 1 mg/mL [(*SDP+SDN)2d*]. (C) Comparison between polymers inside PBS and H_2O at the same concentration.

In order to ratify the behaviour of the studied polymers in terms of mobility and deformability, we studied the physical mixture and covalent attachment of *SDP* and *SDN* polymers in both PBS and H_2O. Firstly, we measured the physical mixture *SDP+SDN* at four selected concentrations, from 1 to 10 mg/mL (Figure V.29). Figure V.29A and Figure V.29B demonstrate how size increases when concentration also increases. However, this growth is less pronounced when PBS is used, demonstrating once again the influence of ionic strength on nanostructure size.

When both *SDP* and *SDN* compounds are covalently attached and dissolved in PBS, the scattered curve changes, suggesting the presence of higher nanostructures compared to the physical mixture (Figure V.30).

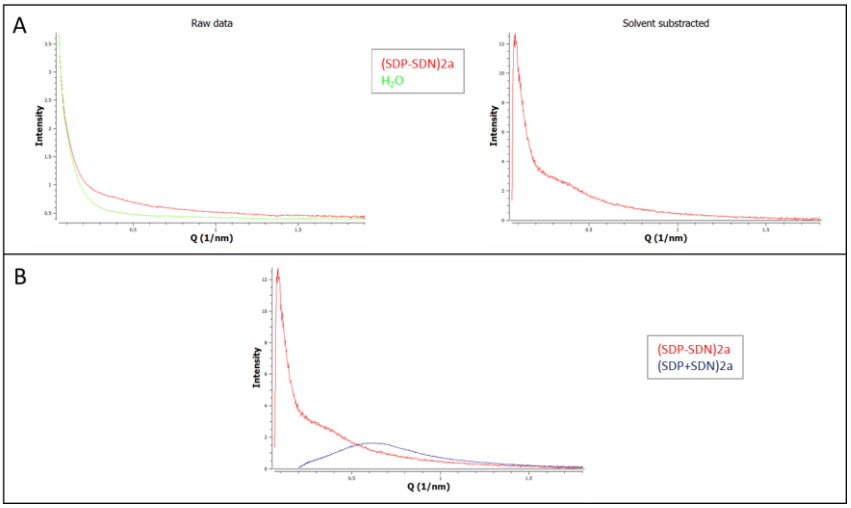

Figure V.30. (A) Scattered curve for the compound *SDP-SDN* before and after subtracting the solvent (H_2O) at 10 mg/mL [(*SDP-SDN)2a*]. (B) Comparison between the physical mixture and the covalently attached compound at the same concentration (10 mg/mL).

V.2.3.5.1. Guinier Approximation

As stated previously, at low resolution, scattering can be described by the Guinier approximation (Equation V.4). The Guinier plot will give a straight line from which R_g and *I(0)* can be extracted.

Concerning ***S*** polymers, Table V.17 shows the results obtained when the Guinier approximation is applied, confirming the previous assumptions about the size of the polymers in different solvents and different concentrations.

Table V.17. Guinier approximation applied to *S* polymers.

Star Polymer	Rg	I(0)	QRg limit	QRg limit	Fidelity
S1a	2.26 ± 0.09	2.32 ± 0.0044	0.31	1.30	0.96
S2a	No data*	-	-	-	-
S2b	No data*	-	-	-	-
S2c	2.41 ± 0.54	0.53 ± 0.01	0.79	1.11	0.60
S2d	3.31 ± 0.26	0.31 ± 0.0055	0.54	1.30	0.78

1= PBS. 2= H2O. 3= D2O. a=10 mg/mL. b= 5 mg/mL. c= 2 mg/mL. d= 1 mg/mL. S= 3-arm star polymer.* This indicates no linear Guinier region (*e.g.* because the sample is severely polydisperse) or the Guinier region is too short (because the sample is too big in size for the given minimum Q).

Concerning ***SD* polymers**, Table V.18 shows the results obtained when the Guinier approximation is applied, again confirming the previous assumptions about the size of the polymers under different ionic strengths and different concentrations.

Table V.18. Guinier approximation applied to *SD* polymers.

Star Polymer	Rg	I(0)	QRg limit	QRg limit	Fidelity
SD1a	3.47 ± 0.06	3.78 ± 0.015	0.60	1.29	0.80
SD2b	No data*	-	-	-	-
SD2c	No data*	-	-	-	-
SD2d	3.43 ± 0.56	0.58 ± 0.027	0.74	0.72	0.51

1= PBS. 2= H2O. 3= D2O. a=10 mg/mL. b= 5 mg/mL. c= 2 mg/mL. d= 1 mg/mL. SD= 3-arm star polymer with deuterated core.* This indicates no linear Guinier region (*e.g.* because the sample is severely polydisperse) or the Guinier region is too short (because the sample is too big in size for the given minimum Q).

As previously mentioned, the ***SDP2a***, ***SDN2a,*** and ***SDN3a*** polymers are functionalised with propargylamine (*SDP2a*) and ethylene glycol azide amine (*SDN2a* and *SDN3a*). In all these cases, the samples proved to be too large in size for the given minimum *Q* and the Guinier plots did not provided any coherent results.

When *SDP* and *SDN* polymers are physically mixed under different conditions (PBS and H_2O) and at different concentrations (from 1 to 10 mg/mL), Guinier approximation provides the results shown in Table V.19.

Table V.19. Guinier approximation applied to the physical mixture of *SDP* and *SDN* polymers at different concentrations.

Star Polymer	Rg	I(0)	QRg limit	QRg limit	Fidelity
(SDP+SDN)1a	2.63 ± 0.05	3.25 ± 0.012	0.58	1.30	0.82
(SDP+SDN)1b	3.45 ± 0.07	2.62 ± 0.017	0.64	1.30	0.81
(SDP+SDN)1c	3.29 ± 0.06	1.17 ± 0.012	0.64	1.30	0.80
(SDP+SDN)1d	4.30 ± 0.48	1.08 ± 0.015	0.46	1.29	0.89
(SDP+SDN)2a	No data*	-	-	-	-
(SDP+SDN)2b	No data*	-	-	-	-
(SDP+SDN)2c	No data*	-	-	-	-
(SDP+SDN)2d	3.28 ± 0.32	0.70 ± 0.017	0.86	1.09	0.54

1= PBS. 2= H2O. 3= D2O. a=10 mg/mL. b= 5 mg/mL. c= 2 mg/mL. d= 1 mg/mL. SDP= 3-arm star polymer with deuterated core and functionalised with 10 mol% propargylamine. SDN= 3-arm star polymer with deuterated core and functionalised with 5 mol% ethylene glycol azide amine. SDP+SDN= physical mixture. SDP-SDN= covalent capture.* This indicates no linear Guinier region (*e.g.* because the sample is severely polydisperse) or the Guinier region is too short (because the sample is too big in size for the given minimum Q).

When *SDP* and *SDN* polymers are covalently conjugated and dissolved in H_2O, the Guinier approximation provides the results shown in Table V.20.

Table V.20. Guinier approximation applied when SDP and SDN are covalently attached at 10 mg/mL.

Star Polymer	Rg	I(0)	QRg limit	QRg limit	Fidelity
(SDP-SDN)2a	11.32 ± 1.20	16.19 ± 0.84	0.84	1.26	0.78

2= H2O. a=10 mg/mL. SDP= 3-arm star polymer with deuterated core and functionalised with 10%$_{mol}$ propargylamine. SDN= 3-arm star polymer with deuterated core and functionalised with 5%$_{mol}$ ethylene glycol azide amine. SDP-SDN= covalent capture.

To confirm that the data obtained via Guinier plots are reliable, the fidelity value shown in all tables should to be close to 1. Therefore, the

obtained data needs to be further modelled for a more accurate conclusion. We will performe this thorough analysis in the near future.

V.2.3.6. SANS Data Analysis: Set 5

We applied SANS to determine the solution conformation of the Set 5 polymers presented in Table V.5. Table V.21 shows a summary of every compound tested with the different measured conditions.

Table IV.21. Summary of the different conditions tested for Set 5 of 4-arm star polymers.

Star Polymer	Arms	GAU	Solvent	Concentration (mg/mL)
4S3d	4	200	D_2O	1
4S(PEG-PGA)3d	4	200	D_2O	1
4SCα3c	4	200	D_2O	2
4SCβ3c	4	200	D_2O	2

4S= 4-arm star polymer. 4SC = 4-arm star polymer functionalised with BDMC. α= 4 mol% modification. β= 6 mol% modification

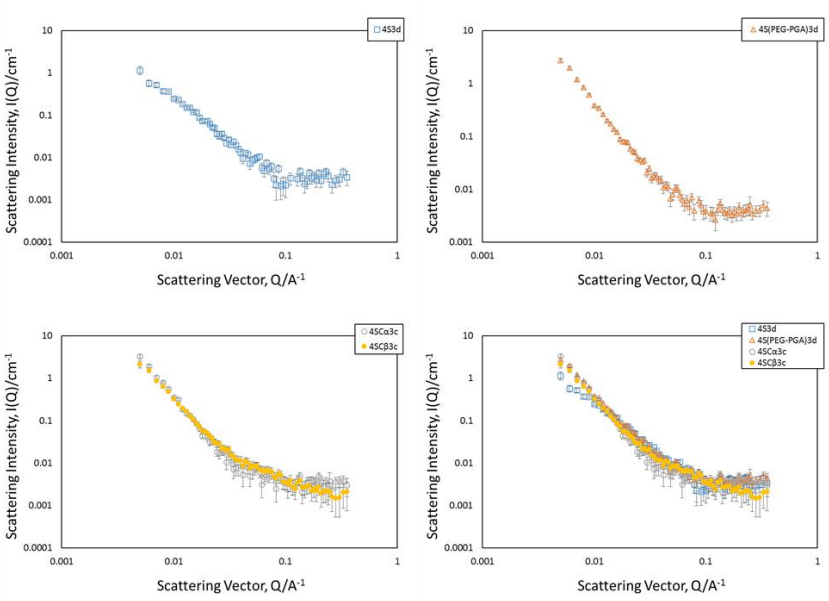

Figure V.31. Scattered intensity obtained by SANS, *I(Q)*, as a function of the scattering vector, *Q*, for the studied 4-ar star polymers after subtracting the solvent (D_2O) and scaling the curves. Error bars are shown.

Figure V.31 shows the scattering data for the studied 4-arm star polymers obtained after subtracting the solvent (D_2O) and scaling the curves.

We noted that all curves exhibit the similar patterns, so we expect similar results after mathematically analysing each polymer.

V.2.3.6.1. FISH Data Fitting

Following the results obtained for the Set 1 and Set 2 polymers, we selected the Gaussian Coil for a Dozier Star Polymer model to elucidate the parameters related to size and shape for this 5th set of star polymers. As in previous cases, during the fitting, we minimised the number of parameters using a flat background and negating the *S(Q)* term in the model.

Figure V.32 shows the scattering data with fits and Table V.22 shows the best fit parameters obtained.

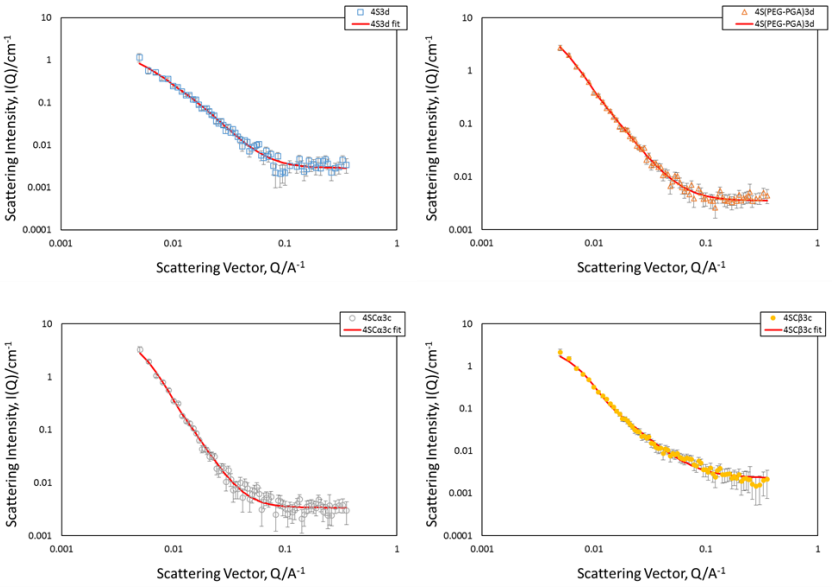

Figure V.32. Scattering data for the star polymers with fits to the Gaussian coil for a Dozier star polymer form factor without both *S(Q)* and backgrounds *B* and *C* contribution.

Table V.22. Best fit parameters and SSE for the Gaussian coil for a Dozier star polymer without both *S(Q)* and backgrounds *B* and *C* contribution.

Dozier Model	4S3d	4S(PEG-PGA)3d	4SCα3c	4SCβ3c
I(0)	0.75	3.08	4.28	4.25
Rg (nm)	34.0	37.0	37.0	28.7
α/Nf	0.037	0.128	0.041	0.040
ξ (nm)	9.6	25.4	17.5	18.7
ν	0.39	0.39	0.35	0.43
HS S(Q) Vol	-	-	-	-
SPH R (nm)	15.0	15.0	15.0	15.0
BKG A	0.002	0.003	0.003	0.005
B*Q	-	-	-	-
C*Q^2	-	-	-	-
SSE	6.20e+01	6.38e+01	6.86e+01	1.92e+03

Errors on the refined parameter are Rg (±15); ξ (±5); υ (±0.05).

As expected, the results obtained for all structures are similar. The exception is the observed variations in the *ξ* value, indicating that the presence of PEG or BDMC increased the effective volume occupied by the arms of the star polymer.

V.2.4. Conclusions

SAS techniques have proven to be suitable for the elucidation of the solution conformation of all studied star polymers.

Concerning SANS experiments, we made several attempts to fit the data with different models commonly used for polymers. After extensive analysis, we found the Gaussian coil for a Dozier star polymer to be the most appropriate model to fit the data for both 3- and 4 arm star polymers. This generated information about the radius of gyration, as well as other conformational parameters.

During the fitting, we made attempts to minimise the number of parameters using a flat background and negating the *S(Q)* term in the model (*S(Q)*=1). Fit parameters (Table V.10 for Set 1; Tables V.12, V.13

and V.14 for the Set 3; and Table V.22 for the Set 5), together with the results obtained by SAXS, show that, in the absence of interparticle interactions (*S(Q)*=1), the R_g deeply depends on the polymer used and salt concentration. Furthermore, the R_g is directly related to both conditions, although there is no dependence on the MW. This important information allowed us to elucidate the 3D shape of the nanostructures. When H_2O or D_2O were used as a solvent (given that the Flory component values vary little, and are close to ⅓, indicating a relatively poor solvent) the polymer is relatively collapsed (dense stars) and the arms tend to reorganise themselves around the fixed core. Therefore, the core is more "wrapped" as molecular weight increases, allowing R_g to remain relatively unchanged. When PBS was used, the self-assembling behaviour diminished, resulting in much smaller structures due to a greater ionic strength.

Moreover, the functionalization of GAU with minimal amounts of relevant biomolecules did not lead to significant changes in structure, allowing the opportunity of site-specific conjugation of different bioactive agents. This will enable the design of advance theranostics or polymer-based combination nanopharmaceutics.

V.3. USE OF SANS TO STUDY POLYACETAL-BASED CONJUGATES

V.3.1. Polyacetal-Based Conjugates

During recent decades, great advances have been made in combination therapy for cancer treatment, among other diseases and disorders. The term "combination therapy" is used when more than one drug or type of therapy (*i.e.* chemotherapy, radiotherapy, etc.) are simultaneously administrated to treat a disease. One of the advantages of using combination therapy is the possibility of modulating more than one signalling pathway in diseased cells, maximising the therapeutic effect, and possibly overcoming mechanisms of resistance [34].

The Combination Index (CI) is used to determine whether or not the combination of the drugs is effective [35,36]. CI allows the calculation of *n* chemical interactions (synergism, additive effect, antagonism) simultaneously, while not requiring knowledge of

mechanisms of action. The toxicity of a mixture depends on the toxicity of the components and how the components interact with each other in a dose-dependent way. Chemicals in a mixture may show zero interaction or may provide more than an additive effect (synergism) or less than an additive effect (antagonism).

Polymer drug conjugates are nanoDDS in which a drug is covalently bound to a polymer carrier. The main benefits compared to the parent free drug are: (a) the passive tumor targeting by the enhanced permeability and retention (EPR) effect [37], (b) decreased toxicity [38], (c) increased solubility in biological fluids [39], (d) the ability to overpass some mechanisms of drug resistance [40], and (e) the ability to elicit immunostimulatory effects [41, 42]. After the success of first generation of polymer-drug conjugates on the market and in clinical trials, a second generation has been developed based on combination therapy [27]. Polymer-drug conjugates for combination therapy involve at least four types of systems, including polymer-drug conjugate plus free drugs (Type I), polymer-drug conjugate plus polymer-drug conjugate (Type II), a single polymeric carrier carrying a combination of drugs (Type III), and polymer-directed enzyme prodrug therapy (PDEPT) and polymer enzyme liposome therapy (PELT) (Type IV). In this work we chose to focus on Type III conjugates to permit the delivery of two different drugs on the same carrier to the tumor site and ensure a simultaneous action.

The present section aims to structurally investigate a family of polyacetals synthesised to improve the therapeutic effect of already reported polyacetal-DES conjugates [10, 43, 44]. For this purpose, we added PTX as a second drug covalently bound to the carrier in order to obtain a polymer-based combination conjugate with endocrine plus chemotherapy looking for anticancer synergism in advanced prostate and breast cancer models.

PTX is a microtubule-interfering agent and a clinically well-established anti-neoplastic agent used for the treatment of breast and prostate cancers among others. However, PTX has serious drawbacks limiting its efficacy. Due to its lack of aqueous solubility, PTX must be solubilised in a formulation vehicle, Cremophor EL (CrEL) or ethanol

when used clinically causing additional undesirable sides effects (hypersensitivity) to those caused by the drug itself. Additionally, due to its short half-life and low selectivity, only a small amount of drug normally reaches the tumour sites.

Different approaches have been developed to enhance solubility of PTX and improve its pharmacokinetics to overcome these problems and numerous anticancer conjugates are currently in advanced phase of clinical trials [45]. An albumin-based PTX nanoparticle, Abraxane (ABI-007, Celgene Corporation), was approved by the Food and Drug Administration (FDA) in 2004 for the treatment of breast cancer [46,47]. The most advanced PTX-conjugated system is a PGA-PTX conjugate (Opaxio®) which displays a better safety profile compared to free PTX in cancer treatment alone or in combination with radiotherapy or other small drugs such as cisplatin [48-53]. Micellar-based drugs containing PTX [54] or PTX-inclusive anticancer agent combinations (such as estramustine plus PTX [55] or docetaxel (DCX) plus PTX [56]) have been studied for the treatment of prostate cancer. Anti-prostate cancer effects can be improved by combining PTX with other drugs, such as DES. Indeed, combination of DES with another taxane family member, DCX, improves therapeutic effect of DCX in the treatment of metastatic androgen-independent prostate cancer [57].

Herein, we report the conformational analysis of the first example of polymer combination therapy combining endocrine (DES) and chemotherapeutic (PTX) drugs attached to the same polymer backbone. The design of a successful prodrug requires a stability in the bloodstream but reasonably quickly conversion into active agents at the site of action. Chemical derivatisation of PTX at the C 2' or the C 7' position offered the best options in the creation of the prodrug. Therefore, we synthesised 2' ester derivatives of PTX to increase aqueous solubility and permit PTX release under physiological conditions.

V.3.2. Results and Discussion

The strategy and tactics followed to obtain the desired structural information from SANS data analysis are schematically shown in Figure V.3.

V.3.2.1. *Tert*- and *Block*-Polyacetals

A series of polyacetal-based combination conjugates were prepared by J. Movellan and V. Gimenez following a polyacetal synthetic strategy previously described (Figure V.33) [10, 43]. Both drugs, Serinol (Ser) and DES were incorporated in a random distribution to form *tert*-polymers, or in a sequential approach to form *block*-*co*-polymers. DES and Ser moieties were used as *co*-monomers during the polymerisation reaction and form part of the polymer main-chain.

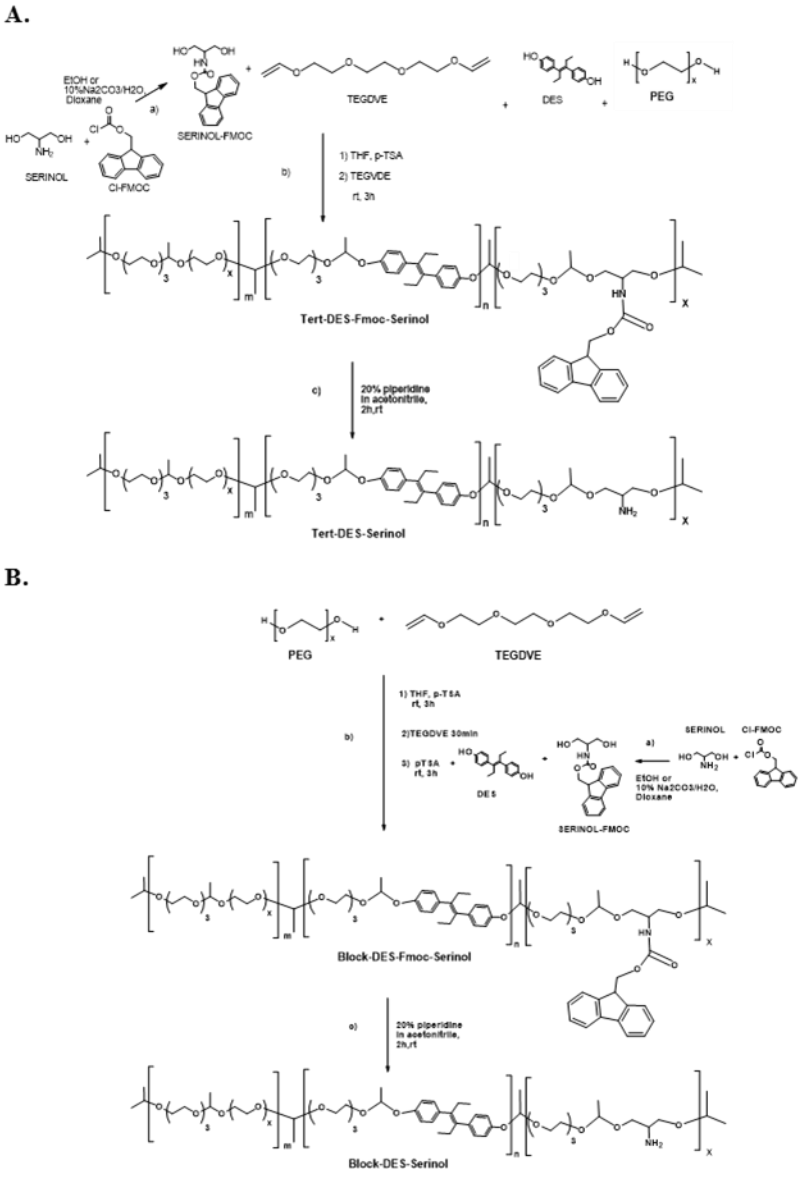

Figure V.33. Synthetic approach followed to obtain (A) *tert*-DES-Ser, (B) *block*-DES-Ser. Adapted from [10].

Ser moieties offer new anchoring positions to incorporate PTX in a second conjugation step (Figure V.34).

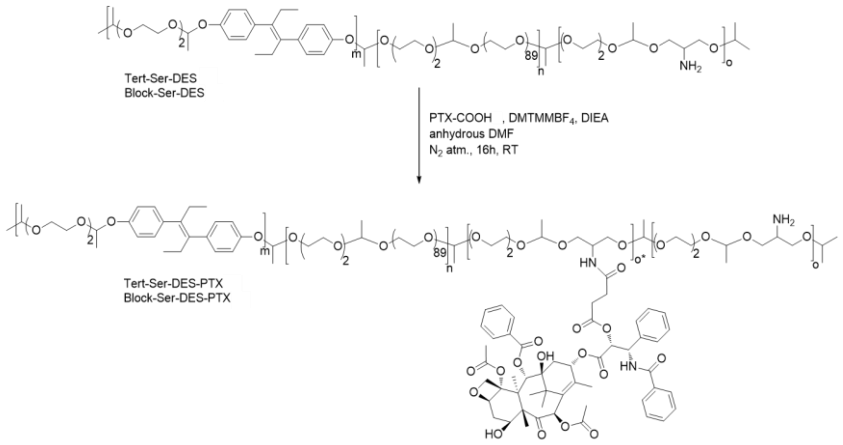

Figure V.34. Synthetic approach followed to obtain *tert*-DES-SerPTX and *block*-DES-SerPTX.

The structures of these novel systems consisted of a diol drug, DES, incorporated into the polymer main-chain and a functionalised drug, PTX, conjugated to polymer side-chains by post-polymerisation modifications yielding *tert*-DES-SerPTX and *block*-DES-SerPTX combination conjugates. The schematic structure and characteristics of the studied polyacetals are presented in Figure V.35 and Table V.23, respectively.

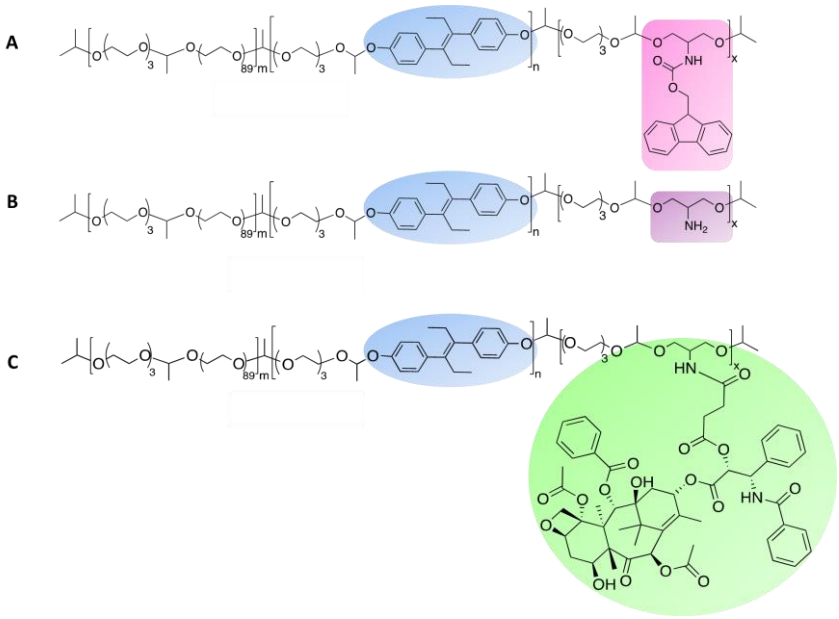

Figure V.35. Schematic representation of some studied polyacetals. (A) *tert/bock*-DES-SerFmoc (9-fluorenylmethoxycarbonyl protected Ser); (B) *tert/block*-DES-Ser; (C) *tert/block*-DES-SerPTX.

Table V.23. Characteristics of studied polyacetals.

Conjugate Polymer	Loading[a] (wt%)			Free content[b] (wt% of TDL)	
	DES	SerFmoc/Ser	PTX	DES	PTX
***Tert*-DES**	3.5	-	-	0.2 ± 0.1	-
***Tert*-DES-SerFmoc**	3.5	3.0	-	0.1 ± 0.1	-
***Tert*-DES-Ser**	3.5	3.0	-	0.1 ± 0.1	-
***Tert*-DES-SerPTX**	3.5	2.3	0.7	0.1 ± 0.1	0.2 ± 0.1
***Block*-DES**	3.0	-	-	0.2 ± 0.1	-
***Block*-DES-SerFmoc**	3.0	3.0	-	0.1 ± 0.1	-
***Block*-DES-Ser**	3.0	3.0	-	0.1 ± 0.1	-
***Block*-DES-SerPTX**	3.0	2.3	0.7	0.1 ± 0.1	0.2 ± 0.1

[a] Estimated by ^{1}H NMR. [b] Determined by HPLC analysis. TDL: total drug loading.

We studied these compounds by SANS on the D11 instrument at the Institute Laue-Langevin (ILL), Grenoble.

V.3.2.2. SANS Data Analysis

V.3.2.2.1. Influence of SerFmoc in Polyacetal Conformation

Previously published DES-polyacetal SANS studies [10] focused on the elucidation of the solution conformation of *tert*- and *block*-copolymer conjugates containing a fixed DES content of 4 wt% using deuterated solvents (dPBS and methanol, MeOD). A single short rod represented the most appropriate model for both conjugates in methanol (1.5 nm diameter, 18.5 nm in length). This demonstrated that a loss of solvophobicity of the *block*-DES occurred in methanol compared to dPBS. Such an effect inhibited the aggregation, observed in the case of dPBS, of the DES-rich region of the molecule, and with it, the large difference in solution structures observed between the *block*-DES and *tert*-DES conjugates. Hence, the solution behaviour in aqueous media was driven by the hydrophobicity of DES (Figure V.36).

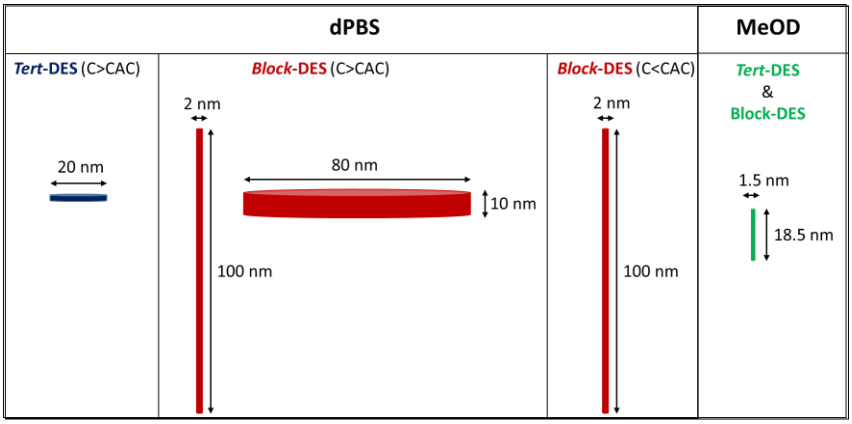

Figure V.36. Graphic representation of previously obtained results [10].

In the light of these results, we first used SANS to study possible changes in polyacetal conformation derived from the addition of another pendent hydrophobic moiety, SerFmoc (9-fluorenylmethoxycarbonyl protected Ser). We then compared the findings of this study with previously published results. As mentioned previously, all compounds were prepared in dPBS and MeOD using deuterated solvents to provide contrast.

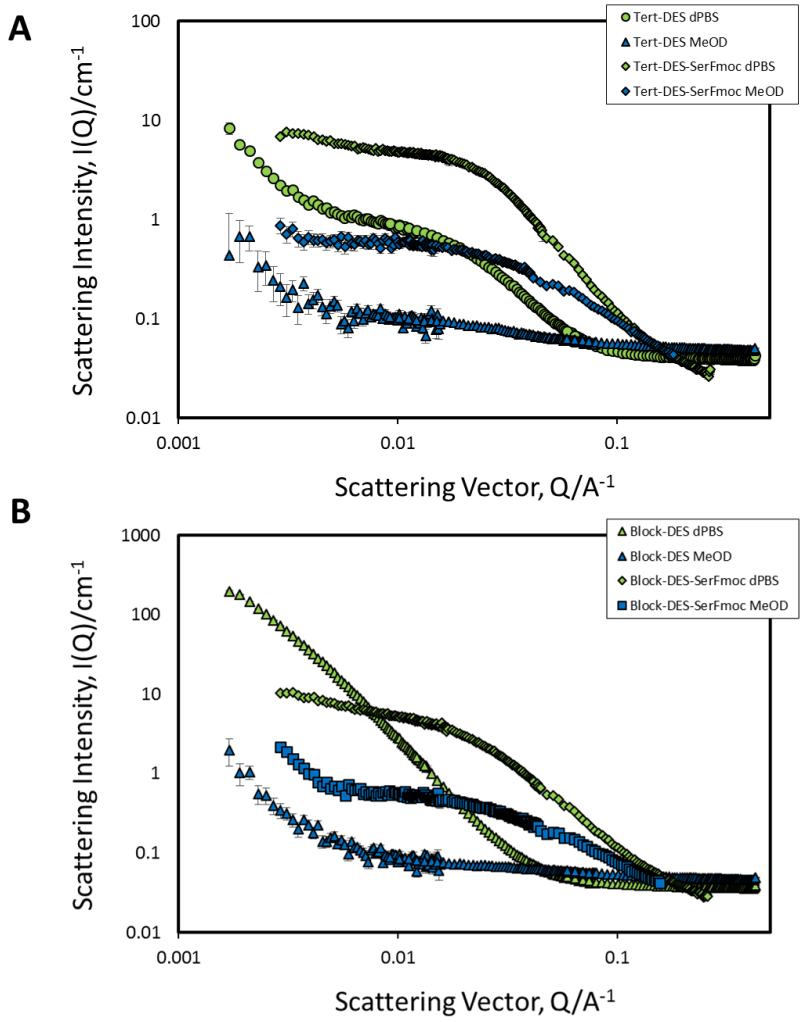

Figure V.37. SANS data from 1 wt% conjugate solutions. (A) *tert*-DES and *tert*-DES-SerFmoc in dPBS and MeOD. (B) *block*-DES and *block*-DES-SerFmoc in dPBS and MeOD. Representative error bars are shown.

Figure V.37 shows critical comparisons of the scattering obtained from *tert*- (Figure V.37A) and *block*- (Figure V.37B) conjugates in dPBS and MeOD. This includes previously presented data for *tert*-DES and *block*-DES conjugates for clarity and comparison purposes. The addition of SerFmoc moiety produces a clear change in solution conformation for *tert*- and *block*- polymers both in dPBS and in MeOD. In MeOD,

scattering plots are identical for *tert*- and *block*- systems indicating that in dPBS there is a small influence of the *tert*- or *block*- nature of the polymer on the solution conformation. Figure V.36 shows the comparison scattering from the *tert*- and *block*- polymers containing SerFmoc in MeOD and dPBS. This figure demonstrates that the scattering curves for *tert*- and *block*- conjugates become similar in shape following the introduction of SerFmoc. There still remains a difference in the curvature of the two profiles, although this is less pronounced when compared with polyacetals in dPBS.

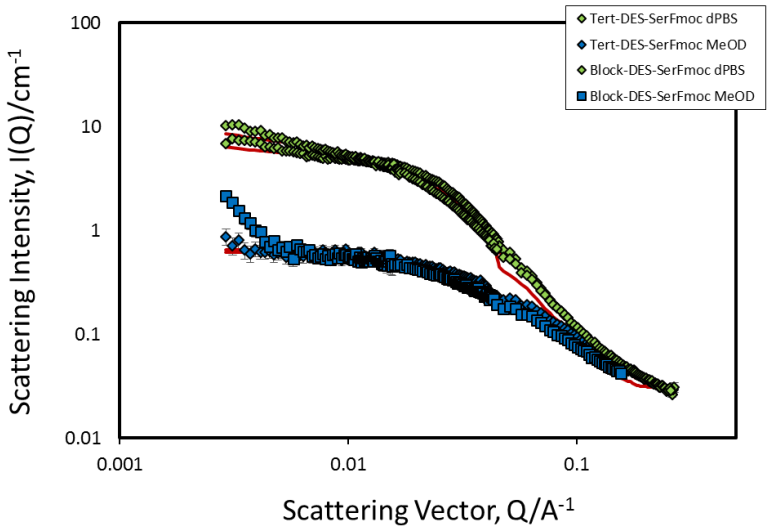

Figure V.38. SANS data from 1 wt% conjugate solutions. In dPBS: *tert*-DES-SerFmoc, *block*-DES-SerFmoc. In MeOD: *tert*-DES-SerFmoc, *block*-DES-SerFmoc. Red lines are best fits to the data. Representative error bars are shown.

However, the difference between *tert*- and *block*- polymers is much smaller with the SerFmoc than without, indicating that SerFmoc induced a more dominant effect on solution conformation with the *block*- distribution. Thus, the addition of SerFmoc dramatically changed the scattering shape and the differences seen between *tert*-DES and *block*-DES polymers were significantly reduced.

For the *tert*-DES-SerFmoc polymer in dPBS, the modelling analysis indicates the presence of two different co-existing disks in solution. The biggest disk is approximately 30 nm in diameter and 6 nm in length, and

the other disk is 10 nm in diameter and 3 nm in length. In the case of *block*-DES-SerFmoc polymer, the modelling also indicates the presence of two sets of disks, one approximately 15 nm in diameter and 6 nm in length, the other larger than can be accurately quantified by SANS over this Q range.

V.3.2.2.2. Influence of PTX in Polyacetal Conformation

Continuing this study, we compared combination polymers containing DES and PTX moieties to their single parent drug. In Figure V.39, *tert*-DES-SerPTX and both parent single conjugates, one conjugate without PTX (*tert*-DES-Ser), one conjugate without DES (*tert*-SerPTX), and *tert*-DES for comparison, have been represented in order to resolve any effect on solution conformation following incorporation of each component.

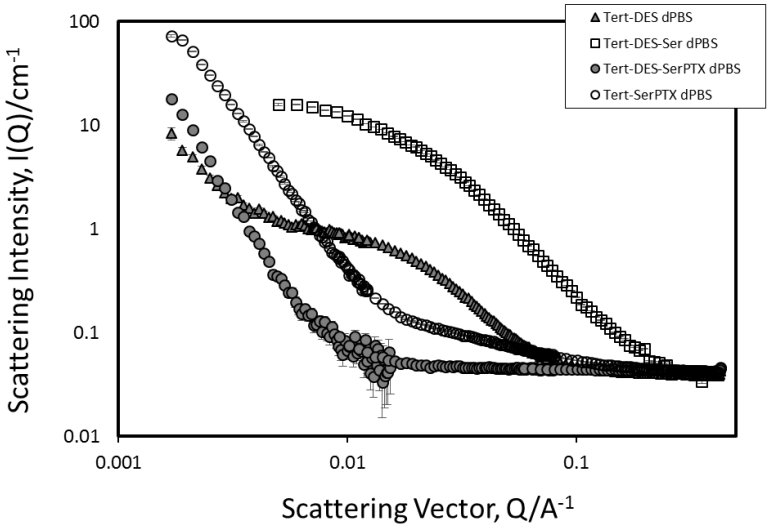

Figure V.39. SANS data from 1 wt% *tert*-polymer solutions in dPBS: *tert*-DES, *tert*-DES-Ser, *tert*-DES-SerPTX, and *tert*-SerPTX. Error bars are shown.

We made the same comparisons for the *block*- family of polymers in Figure V.40.

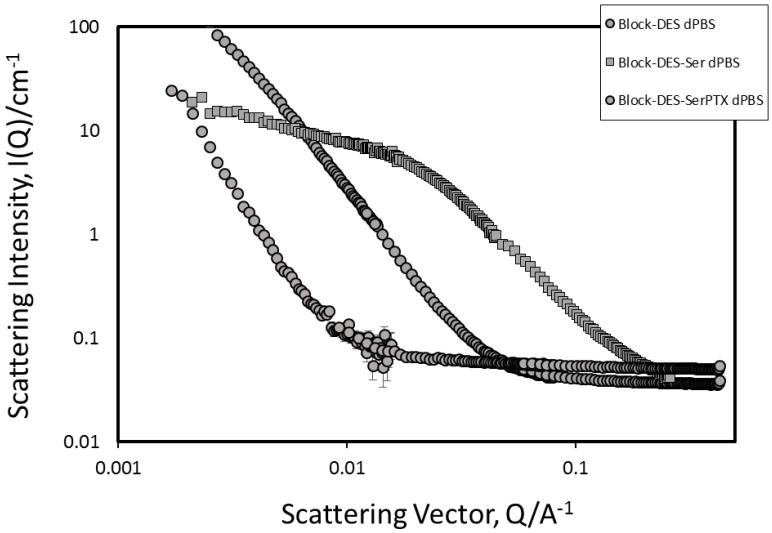

Figure V.40. SANS data from 1 wt% *block*-polymer solutions in dPBS: *block*-DES, *block*-DES-Ser, *block*-DES-SerPTX. Error bars are shown.

We observed significant scattering profile differences after comparing *tert*-DES with the synthesised polyacetals containing PTX, *tert*-DES-SerPTX and *tert*-SerPTX, both with profiles similar in shape but different with regards to intensity. This fact clearly demonstrated that the incorporation of PTX is the major driving force behind solution conformation. This is confirmed by studying the *block*-polymer series, as the shape of the scattering profiles changes substantially following the addition of PTX. *Block*-polymers take on the same characteristics at that shown by the *tert*-DES-SerPTX and *tert*-SerPTX polymers.

Scattering from the *tert*-SerPTX sample was best fit to a thin rod of radius 1 nm, length 30 nm with a Q^{-n} term with n= 3.5. For *tert*-DES-SerPTX the scattering was dominated by a Q^{-4} term, possibly indicating the presence of an extremely large structure out with the resolution of SANS experiments. We also observed similar findings for the *block*-DES-SerPTX. This experiment clearly confirmed that PTX drives solution conformation of the polyacetals due to high hydrophobicity inducing significant differences in aggregation parameters. Overall, this drives polymers to form larger structures in solution.

V.3.3. Conclusions

We developed polyacetal-based combination conjugates through the modification of DES-polyacetals with Ser-*co*-monomers, thus allowing the conjugation of PTX. SANS studies confirmed that following *fmoc*-protected Ser and PTX incorporation the hydrophobic pendant chain exerted a dominant effect on the polymer conformation.

V.4. MATERIALS AND METHODS

V.4.1. Materials

All 3- and 4-arm star shaped polyglutamates studied in this chapter were synthesised by Duro-Castaño and colleges using a recently published methodology [25]. Polyacetal-based combination conjugates were prepared by J. Movellan and V. Gimenez following a polyacetal synthetic strategy previously reported [10, 43]. D_2O, deuterated methanol, and deuterated PBS were purchased form Deuter GmbH. Any water used was of Millipore grade. Polymer solutions were prepared by simply dissolving the desired material in its respective solvent.

V.4.2. SANS Data Acquisition

SANS experiments were performed using the D11 diffractometer at the Institute Laue-Langevin (ILL, Grenoble), and diffractometers SANS2d and LOQ at ISIS Spallation Neutron Source (Didcot, UC). All solutions were prepared in D_2O at a concentration of 1 wt% and were placed in 2-mm path length, UV-spectrophotometer grade, quartz cuvettes (Hellma UK) and mounted in aluminium holders on top of an enclosed, computer-controlled, sample chamber. Sample volumes were approximately 0.6 cm^3. Temperature control was achieved using a thermostatted circulating bath pumping fluid through the base of the sample chamber, achieving a temperature stability of ±2 ºC. Data were collected and corrected for the scattering and transmission of the solvent and cell and were placed on an absolute intensity scale with reference to a flat scatterer. Scattering data are expressed in terms of the scattering vector Q which is given by $Q = 4n\pi/\lambda \sin(\theta/2)$ in which n is the refractive index for neutrons ($n \approx 1$), λ is the wavelength, and θ is the scattering angle.

V.4.3. SAXS Data Acquisition

SAXS spectra of 1 mg/mL to 10 mg/mL filtered star polymer solutions were collected at the beamline NCD11 at ALBA Synchrotron Light Facility (Barcelona, Spain). The energy of the incident beam was 12.6 KeV (λ= 0.995 Å). Samples were placed in a thermostated liquid cell using 150 µL of sample per measurement. The scattered X-ray was recorded in a two-dimensional CCD detector Quantum 210r (4096 x 4096 pixels highest achievable resolution - pixel size 51 microns), converted to one-dimensional scattering by radial averaging, and represented as a function of the momentum transfer vector $Q=4\pi\sin\theta/\lambda$, in which θ is half the scattering angle and λ is the wavelength of the incident X-ray beam. The sample-to-detector distance was maintained at 1.4 m. Measurements of each sample were collected over 0.1 to 1 s each. Solutions were prepared using deionised water, deionised water buffered with PBS at pH = 7.4, or deuterated water at 20˚C. The comparison of the successive exposures of an acquisition experiment indicated no changes in the scattering patterns (*i.e.* no measurable radiation damage to the samples). Data were normalised to the intensity of the transmitted beam, and the scattering data from the background solvent, tested before and after each corresponding sample measure, were averaged and used to subtract the background.

V.4.4. FISH Modelling

The FISH data fitting program [33] was used to predict size and shape of the different species in solution through the obtained SANS data. This program uses an iterative, linear least-squares process to fit data to models which contain the equations describing the scattering expected for different form factors, structure factors, contrast steps, polydispersities, and background scattering. Known model parameters, such as volume fraction and polydispersities, can be fixed manually and the program is then allowed to optimise the fit by refining the remaining parameters.

V.4.5. ATSAS Programs

The SAXS data were processed using standard procedures for ATSAS programs [58]. The forward scattering *I(0)* and the radius of gyration, *Rg*, were computed using the Guinier approximation for $QR_g < 1.3$.

REFERENCES

1. Lane, L.A., et al., *Physical Chemistry of Nanomedicine: Understanding the Complex Behaviors of Nanoparticles in Vivo.* Annual Review of Physical Chemistry, 2015. **66**(1): p. 521-547.
2. Blanco, E., H. Shen, and M. Ferrari, *Principles of nanoparticle design for overcoming biological barriers to drug delivery.* Nat Biotech, 2015. **33**(9): p. 941-951.
3. Hyland, L.L., M.B. Taraban, and Y.B. Yu, *Using small-angle scattering techniques to understand mechanical properties of biopolymer-based biomaterials.* Soft Matter, 2013. **9**(43): p. 10218-10228.
4. Griffiths, P.C., et al., *Understanding the Mechanism of Action of Poly(amidoamine)s as Endosomolytic Polymers: Correlation of Physicochemical and Biological Properties.* Biomacromolecules, 2004. **5**(4): p. 1422-1427.
5. Wan, K.-W., et al., *Poly(amidoamine) Salt Form: Effect on pH-Dependent Membrane Activity and Polymer Conformation in Solution.* Biomacromolecules, 2004. **5**(3): p. 1102-1109.
6. Glatter, O. and O. Kratky, *Small angle xray scattering.* London: Academic Press 1982, 1982.
7. Paul, A., M.J. Vicent, and R. Duncan, *Using Small-Angle Neutron Scattering to Study the Solution Conformation of N-(2-Hydroxypropyl)methacrylamide Copolymer–Doxorubicin Conjugates.* Biomacromolecules, 2007. **8**(5): p. 1573-1579.
8. Griffiths, P.C., et al., *Conformational consequences of cooperative binding of a coiled-coil peptide motif to poly(N-(2-hydroxypropyl) methacrylamide) HPMA copolymers.* Journal of Controlled Release, 2011. **153**(2): p. 173-179.
9. Filippov, S., et al., *Novel pH-Responsive Nanoparticles.* Langmuir, 2008. **24**(17): p. 9295-9301.
10. Giménez, V., et al., *Demonstrating the importance of polymer-conjugate conformation in solution on its therapeutic output: Diethylstilbestrol (DES)-polyacetals as prostate cancer*

treatment. Journal of Controlled Release, 2012. **159**(2): p. 290-301.
11. Filippov, S.K., et al., *Hydrolytically Degradable Polymer Micelles for Drug Delivery: A SAXS/SANS Kinetic Study.* Biomacromolecules, 2013. **14**(11): p. 4061-4070.
12. Pedersen, J.S., et al., *A Small-Angle Neutron and X-ray Contrast Variation Scattering Study of the Structure of Block Copolymer Micelles: Corona Shape and Excluded Volume Interactions.* Macromolecules, 2003. **36**(2): p. 416-433.
13. Paul, A., et al., *Drug Mimic Induced Conformational Changes in Model Polymer−Drug Conjugates Characterized by Small-Angle Neutron Scattering.* Biomacromolecules, 2010. **11**(8): p. 1978-1982.
14. Angelov, B., et al., *Topology and internal structure of PEGylated lipid nanocarriers for neuronal transfection: synchrotron radiation SAXS and cryo-TEM studies.* Soft Matter, 2011. **7**(20): p. 9714-9720.
15. Moyer, T.J., et al., *pH and Amphiphilic Structure Direct Supramolecular Behavior in Biofunctional Assemblies.* Journal of the American Chemical Society, 2014. **136**(42): p. 14746-14752.
16. Pozzi, D., et al., *Effect of polyethyleneglycol (PEG) chain length on the bio-nano-interactions between PEGylated lipid nanoparticles and biological fluids: from nanostructure to uptake in cancer cells.* Nanoscale, 2014. **6**(5): p. 2782-2792.
17. Pynn, R., *Neutron Scattering- A primer.* Los Alamos National Laboratory: Los Alamos., 1990.
18. Hedden, R.C. and B.J. Bauer, *Structure and Dimensions of PAMAM/PEG Dendrimer−Star Polymers.* Macromolecules, 2003. **36**(6): p. 1829-1835.
19. Lee, J.S., R.P. Quirk, and M.D. Foster, *Effect of Butadiene End-Capping of Arms in a Star Polystyrene on Solution Properties, Bulk Dynamics, and Bulk Thermodynamic Interactions in Binary Blends.* Macromolecules, 2004. **37**(26): p. 10199-10204.
20. Greenberg, C.C., et al., *Effective interaction parameter between branched and linear polystyrene.* Journal of Polymer Science Part B: Polymer Physics, 2001. **39**(21): p. 2549-2561.
21. Martter, T.D., et al., *Thermodynamic interaction parameter of star–star polybutadiene blends.* Journal of Polymer Science Part B: Polymer Physics, 2003. **41**(3): p. 247-257.

22. Stancik, C.M., et al., *Impact of Core Architecture on Solution Properties of Dendrimer-like Star Copolymers.* Macromolecules, 2003. **36**(15): p. 5765-5775.
23. Rathgeber, S., et al., *Starlike dendrimers in solutions: Structural properties and internal dynamics.* The Journal of Chemical Physics, 2006. **125**(20): p. 204908.
24. Mackay, M.E., et al., *Microphase Separation of Hybrid Dendron−Linear Diblock Copolymers into Ordered Structures.* Macromolecules, 2002. **35**(22): p. 8391-8399.
25. Duro-Castano, A., et al., *Well-Defined Star-Shaped Polyglutamates with Improved Pharmacokinetic Profiles As Excellent Candidates for Biomedical Applications.* Molecular Pharmaceutics, 2015. **12**(10): p. 3639-3649.
26. Putnam, C.D., et al., *X-ray solution scattering (SAXS) combined with crystallography and computation: defining accurate macromolecular structures, conformations and assemblies in solution.* Quarterly Reviews of Biophysics, 2007. **40**(03): p. 191-285.
27. Greco, F. and M.J. Vicent, *Combination therapy: Opportunities and challenges for polymer–drug conjugates as anticancer nanomedicines.* Advanced Drug Delivery Reviews, 2009. **61**(13): p. 1203-1213.
28. Koronyo, Y., et al., *Alzheimer's Disease in the Retina: Imaging Retinal Aβ Plaques for Early Diagnosis and Therapy Assessment.* Neurodegenerative Diseases, 2012. **10**(1-4): p. 285-293.
29. Farrow, C.L. and S.J.L. Billinge, *Relationship between the atomic pair distribution function and small-angle scattering: implications for modeling of nanoparticles.* Acta Crystallographica Section A, 2009. **65**(3): p. 232-239.
30. Guinier, A. and G. Fournet, *Small-angle scattering of X-rays. New York: Wiley Interscience.* 1955.
31. Kratky, O. and G. Porod, *Röntgenuntersuchung gelöster Fadenmoleküle.* Recueil des Travaux Chimiques des Pays-Bas, 1949. **68**(12): p. 1106-1122.
32. Kratky, O. and G. Porod, *Diffuse small-angle scattering of X-rays in colloid systems.* J Colloid Sci, 1949. **4**(1): p. 35-70.
33. Heenan, R.K., *FISH: Rutherford Appleton Laboratory, Didcot, U.K.*
34. Broxterman, H.J. and N.H. Georgopapadakou, *Anticancer therapeutics: “Addictive” targets, multi-*

targeted drugs, new drug combinations. Drug Resistance Updates. **8**(4): p. 183-197.
35. Peer, D., et al., *Nanocarriers as an emerging platform for cancer therapy.* Nat Nano, 2007. **2**(12): p. 751-760.
36. Rodea-Palomares, I., et al., *Application of the combination index (CI)-isobologram equation to study the toxicological interactions of lipid regulators in two aquatic bioluminescent organisms.* Water Research, 2010. **44**(2): p. 427-438.
37. Matsumura, Y. and H. Maeda, *A New Concept for Macromolecular Therapeutics in Cancer Chemotherapy: Mechanism of Tumoritropic Accumulation of Proteins and the Antitumor Agent Smancs.* Cancer Research, 1986. **46**(12 Part 1): p. 6387-6392.
38. Vasey, P.A., et al., *Phase I Clinical and Pharmacokinetic Study of PK1 [N-(2-Hydroxypropyl)methacrylamide Copolymer Doxorubicin]: First Member of a New Class of Chemotherapeutic Agents—Drug-Polymer Conjugates.* Clinical Cancer Research, 1999. **5**(1): p. 83-94.
39. Meerum Terwogt, J.M., et al., *Phase I clinical and pharmacokinetic study of PNU166945, a novel water-soluble polymer-conjugated prodrug of paclitaxel.* Anti-Cancer Drugs, 2001. **12**(4): p. 315-323.
40. Minko, T., et al., *HPMA copolymer bound adriamycin overcomes MDR1 gene encoded resistance in a human ovarian carcinoma cell line.* Journal of Controlled Release, 1998. **54**(2): p. 223-233.
41. Říhová, B., et al., *Cytostatic and immunomobilizing activities of polymer-bound drugs: experimental and first clinical data.* Journal of Controlled Release, 2003. **91**(1–2): p. 1-16.
42. Sirova, M., et al., *Treatment with HPMA copolymer-based doxorubicin conjugate containing human immunoglobulin induces long-lasting systemic anti-tumour immunity in mice.* Cancer Immunology, Immunotherapy, 2007. **56**(1): p. 35-47.
43. England, R.M., et al., *Polyacetal-stilbene conjugates — The first examples of polymer therapeutics for the inhibition of HIF-1 in the treatment of solid tumours.* Journal of Controlled Release, 2012. **164**(3): p. 314-322.
44. Vicent, M.J., et al., *Polyacetal-diethylstilboestrol: a polymeric drug designed for pH-triggered activation.* J Drug Target, 2004. **12**(8): p. 491-501.

45. Luo, C., et al., *Advances of Paclitaxel Formulations Based on Nanosystem Delivery Technology.* Mini-Reviews in Medicinal Chemistry, 2012. **12**(5): p. 434-444.
46. Miele, E., et al., *Albumin-bound formulation of paclitaxel (Abraxane ABI-007) in the treatment of breast cancer.* Int J Nanomedicine, 2009. **4**: p. 99-105.
47. Gradishar, W.J., *Albumin-bound paclitaxel: a next-generation taxane.* Expert Opinion on Pharmacotherapy, 2006. **7**(8): p. 1041-1053.
48. Pearson, O.H., et al., *Endocrine versus endocrine plus five-drug chemotherapy in postmenopausal women with stage II estrogen receptor-positive breast cancer.* Cancer, 1989. **64**(9): p. 1819-23.
49. Chipman, S.D., et al., *Biological and clinical characterization of paclitaxel poliglumex (PPX, CT-2103), a macromolecular polymer–drug conjugate.* International Journal of Nanomedicine, 2006. **1**(4): p. 375-383.
50. Li, C. and S. Wallace, *Polymer-drug conjugates: Recent development in clinical oncology.* Advanced Drug Delivery Reviews, 2008. **60**(8): p. 886-898.
51. Langer, C.J., et al., *Phase III Trial Comparing Paclitaxel Poliglumex (CT-2103, PPX) in Combination with Carboplatin Versus Standard Paclitaxel and Carboplatin in the Treatment of PS 2 Patients with Chemotherapy-Naïve Advanced Non-small Cell Lung Cancer.* Journal of Thoracic Oncology. **3**(6): p. 623-630.
52. Paz-Ares, L., et al., *Phase III trial comparing paclitaxel poliglumex vs docetaxel in the second-line treatment of non-small-cell lung cancer.* Br J Cancer, 2008. **98**(10): p. 1608-1613.
53. O'Brien, M.E.R., et al., *Randomized Phase III Trial Comparing Single-Agent Paclitaxel Poliglumex (CT-2103, PPX) with Single-Agent Gemcitabine or Vinorelbine for the Treatment of PS 2 Patients with Chemotherapy-Naïve Advanced Non-small Cell Lung Cancer.* Journal of Thoracic Oncology. **3**(7): p. 728-734.
54. Soga, O., et al., *Physicochemical Characterization of Degradable Thermosensitive Polymeric Micelles.* Langmuir, 2004. **20**(21): p. 9388-9395.
55. Speicher, L.A., L. Barone, and K.D. Tew, *Combined Antimicrotubule Activity of Estramustine and Taxol in Human Prostatic Carcinoma Cell Lines.* Cancer Research, 1992. **52**(16): p. 4433-4440.

56. Izbicka, E., et al., *Biomarkers for Sensitivity to Docetaxel and Paclitaxel in Human Tumor Cell Lines In Vitro.* Cancer Genomics - Proteomics, 2005. **2**(4): p. 219-226.
57. Montgomery, R.B., et al., *Diethylstilbestrol and docetaxel.* Cancer, 2007. **110**(5): p. 996-1002.
58. Petoukhov, M.V., et al., *New developments in the ATSAS program package for small-angle scattering data analysis.* Journal of Applied Crystallography, 2012. **45**(2): p. 342-350.

General Discussion

Many nanosized drug delivery systems aim to deliver bioactive agents to a specific intracellular compartment, such as the cytosol, and may represent a powerful tool for the treatment and/or prevention of several currently relevant human diseases. However, while we have made great advances in biomacromolecules, such as oligonucleotides or proteins, this strategy still requires improvements to the approaches employed to transport therapeutic molecules into specific cell types. While the last 20 years has seen the emergence of a range of promising methods, shortcomings such as low/variable delivery efficiency, high cytotoxicity, and perhaps most importantly, ineffective endosomal/lysosomal escape still exist. A potential solution to these problems lies in the field of Polymer Therapeutics (PT) [1]: well-defined polypeptide-based therapeutics with suitable biodegradability, predictable structure and conformation, high homogeneity, and high drug loading capacity [2-4].

Within the field of PT, the use of advanced physicochemical techniques has generated efficient therapeutic strategies by controlling pharmacokinetics and biodistribution. Small angle neutron scattering (SANS) or small angle X-ray scattering (SAXS) offer means to gather information on the size, shape, and orientation of structures of samples at length scales ranging from 1 to 100 nm, even under physiological conditions [5]. By using suitable and physically rational models for data analysis, we can quantify changes in solution; however, this analysis can be laborious and requires considerable prior knowledge.

With this in mind, the objective of this thesis dissertation focused on two key topics:

i) The design, development, and validation of nanosized polypeptide-based carriers to facilitate the cytosolic delivery of bioactive agents that display an impaired capability to cross biological membranes by themselves or exhibit low lysosomal stability. This includes plasmid DNA (pDNA), small interfering RNA (siRNA), and proteins.

ii) The exhaustive physicochemical characterisation of polymeric drug delivery systems to determine their solution conformation.

Initial efforts addressed the fundamental question of whether negatively charged well-defined polyglutamic acid (PGA) polymers functionalised with positively charged oligomer domains could be used as oligonucleotide delivery systems. To this end, we designed different conjugates of PGA with succinyl tetraethylene pentamine (Stp) oligoaminoamides (Table II.3). Optionally, we included histidines for modulation of endosomal buffer capacity and cysteines for pDNA or siRNA complex stabilisation, followed by the characterisation of biophysical properties and gene transfer efficiency in N2a neuroblastoma or 4T1 breast cancer cells.

The first three developed systems were based on PGA polymers (homopolymers or block-*co*-polymers) modified with a monodisperse Stp-based oligoaminoamide. In System 1, we orthogonally modified PGA side-chains with oligomer **S** by means of amide bond formation using the **S** terminal amine (Figure II.3) and DMTMM·Cl (4-(4,6-Dimethoxy-1,3,5-triazin-2-yl)-4-methylmorpholinium chloride) coupling chemistry [6]. In System 2, we modified PGA side-chains analogously with **SH** (additionally containing histidines to improve the endosomolytic effect) [7], **SC** (containing cysteine to stabilise the pDNA complex via disulphide formation) [8, 9], or **SHC** (containing both histidines and cysteine). To generate System 3, we performed the conjugation via bioreducible disulphide bonds using the terminal cysteine of **SHC** to avoid possible side-chain crosslinking reactions. For this purpose, we employed a pyridyl disulphide modified PGA (PGA-PD) as the starting material (Figure II.25) [6]. Due to the similar behaviour of SHC and PCSH polyplexes, we designed an alternative system (System 4) hoping to improve the activity of SHC by promoting complex stability. First, we generated a polyplex between pDNA and oligoaminoamide **SHC** and subsequently coated the positively charged pDNA complex with a negatively charged PGA-polymer in an attempt to improve the biocompatibility of **SHC**. We employed two different lengths of PGA and diblock PEG-PGA as coating agents [10].

Unfortunately, our studies suggested that the systems assessed were not suitable for siRNA delivery. We propose the poor stability of complexes as the major factor contributing to a lack of transfection ability. Nanoparticle formulations with siRNA present important differences to plasmid formulation. Although both self-assemble through electrostatic forces, plasmids are several hundred-fold larger than siRNA, suggesting that different kinds of polycations may be optimal. This again demonstrates that pDNA and siRNA differ considerably in their properties and suitable delivery vectors must be tailored individually [11].

Concerning pDNA, the conjugation of Stp derivatives to the PGA chain through amide bond formation (System 1 and System 2) resulted in stable non-toxic nanosystems with the ability to efficiently transfer pDNA. This improved the efficiency of both PGA and Stp-based compounds as transfection agents, with a more pronounced effect for Stp derivatives bearing histidine moieties. Moreover, the complexation capacity depended on the content of the oligoaminoamide. Complexation of pDNA with System 1 or 2 polymers exceeded the effectiveness of PEI in gene delivery. Thus, the presence of PGA promoted the enhanced transfection capacity of the Stp_5 family.

In the case of System 3, **SHC** conjugated to PGA by disulphide bonds improved cell viability, even given the relatively high amount of PGA-based polymer required. Upon coating (System 4), we did not observe significant improvements in gene transfer efficiency, mainly as **SHC** itself already demonstrated a high gene transfer capability. However, coating did permit a slight enhancement in cell viability. We also expected that a coating strategy would provide advantages when compared with **SHC** *in vivo* due to the enhanced permeability and retention (EPR) effect and possible alterations to pharmacokinetics. Further experiments are ongoing to explore this hypothesis.

The obtained results permitted the generation of guidelines for the synthesis and physicochemical characterisation of new multifunctional polymeric platforms for effective gene delivery. These new systems were composed of natural or synthetic polyaminoacids (and their

derivatives) with low polydispersity (Đ~ 1.2) and, therefore, precise and well-defined structures, allowing reproducibility and the determination of structure-activity relationships.

As a first step, we designed, synthesised, and evaluated PGA-based systems modified with different endosomolytic moieties containing secondary and tertiary amines as possible gene delivery carriers. However, the proposed systems did not form complexes with the desired oligonucleotide. With these results in mind, we designed a second set of PGA-based polymers containing pyridyl disulphide (PD) to form a conjugate via a disulphide bond between the polymer and the oligonucleotide. However, these conjugates were not stable in plasma or cell culture media even at short incubation times.

Using the same rational as for PGA, we explored the potential of polyarginine (PArg) in oligonucleotide complexation. We designed different systems aiming to avoid negative charges in the PGA chain and to employ non-modified polymers. However, these compounds did not display cell transfection capabilities.

Continuing the exploration of alternatives within the field of polypeptides, we next developed a strategy based on positively charged synthetic polyornithine (P(Orn)). As in the case of PArg, we expected ornithine to enhance gene delivery due to the cationic charge of its pendant amino groups at physiological pH. These can contribute to the binding and condensation of the oligonucleotide and, in parallel with lysine, form parts of cell penetrating peptides. We chemically modified P(Orn) derivatives and complexed the resulting structures (POP1, POP2, POPF, and POPD) to siRNA at an optimised N/P ratio. We demonstrated their nanosized appearance and positive surface charge to be favourable for *in vitro* applications (non-cytotoxic and non-haemolytic). More importantly, the polyplexes successfully transfected a luciferase-transfected melanoma cell model (B16F10-luc-G5), evidencing the potential of this polypeptidic platform. We are currently carrying out further analyses to validate this system.

Continuing the design of systems for cytosolic drug delivery, we reported a strategy to conjugate alanine:glyoxylate aminotransferase

(AGT) to PEG-PGA diblock-co-polymers through the formation of disulphide bonds [12]. Furthermore, we successful applied the obtained conjugates to restore glyoxylate detoxification in eukaryotic cells mimicking a primary hyperoxaluria type I (PH1) phenotype. Our protocol permitted high conjugation yields without significantly affecting the functional properties of the enzyme. CHO-GO cells, a well-accepted cellular model of PH1, internalised the obtained conjugates, which located to discrete compartments in the cytosol. Furthermore, conjugate-treated cells efficiently detoxified endogenously produced glyoxylate. By applying a protein engineering approach, we then generated a mutated form of AGT bearing the substitution of Cys387-to-Ser and of Lys390-to-Ser (AGT-SSKL) to favour the interaction with the peroxisomal targeting machinery. These modified conjugates displayed peroxisomal import in CHO-GO cells and more effectively detoxified glyoxylate when compared to PEG-PGA-AGT conjugates. *In vitro* data confirmed high plasma stability and hemocompatibility of conjugated AGT, thus suggesting that the developed conjugates are suitable for intravenous administration. Overall, our data supports the exploitation of this system to replenish PH1 patients with a catalytically active and correctly localised enzyme with the ability to counteract the deficit responsible for oxalate accumulation. As polymer-based nanoconjugates have been widely employed for the delivery of therapeutic proteins, mainly due to their versatility and biocompatibility [13-15], these results, using a biodegradable carrier, constitute a fundamental step towards the future development of a safer enzyme administration therapy effective for all PH1 patients independent of the type of mutation.

The correct targeting of a protein represents an important issue, particularly in the case of disorders involving peroxisomal enzymes whose functionality is strongly influenced by subcellular localisation [16]. Previous reports on the administration of catalase to peroxisomes to rescue reactive oxygen species (ROS)-induced damage employed an enzyme derivative endowed with a non-covalently bound cell-penetrating peptide [17-19]. To the best of our knowledge, our strategy represents the first report of a PGA-based conjugate designed to

efficiently deliver a catalytically active therapeutic protein to the peroxisome. Thus, our work also represents an example to implement in other diseases caused by peroxisomal enzyme deficiency.

Finally, we have demonstrated the successful application of powerful physicochemical techniques (SANS and SAXS) to better understand the behaviour of polymer-based therapeutics. These techniques permitted the elucidation of the solution conformation of polymers with the possibility of changing several experimental parameters to allow measurements close to physiological conditions.

In the first project, we analysed 3- and 4 arm star-shaped polyglutamates by SANS. All 3-arm systems comprised the same multifunctional core coupled with three different amines and a different number of polyglutamate units (GAU). We made several attempts to fit the data with different models commonly used for polymers. After extensive analysis, we found the Gaussian coil for a Dozier star polymer to be the most appropriate model for both 3- and 4 arm star polymers. This generated information regarding the radius of gyration and other conformational parameters.

During data fitting, we attempted to minimise the number of parameters using a flat background and negating the *S(Q)* term in the model (*S(Q)*=1). Fit parameters, together with the results obtained by SAXS, show that, in the absence of interparticle interactions (*S(Q)*=1), R_g deeply depended on the polymer used and the salt concentration. Furthermore, R_g is directly related to both conditions, although there is no dependence on MW. This important information allowed us to elucidate the 3D shape of the nanostructure. When H_2O or D_2O were used as a solvent (given that the Flory component values vary little, and are close to ⅓, indicating a relatively poor solvent), the analysed polymer was relatively collapsed (dense star) and the arms tended to reorganise themselves around the fixed core. Therefore, the core is more “wrapped” as molecular weight increases, allowing R_g to remain relatively unchanged. When we employed PBS as a solvent, self-assembly behaviour diminished, resulting in much smaller structures due to a greater ionic strength.

Moreover, the functionalization of GAU with minimal amounts of relevant biomolecules did not significantly alter the structure, allowing the opportunity of site-specific conjugation of different bioactive agents. This will enable the design of advance theranostics or polymer-based combination nanopharmaceuticals.

In the last project, we developed polyacetal-based combination conjugates through the modification of DES-polyacetals with Ser-*co*-monomers, thus allowing the conjugation of paclitaxel (PTX). SANS studies confirmed that following *fmoc*-protected serinol (Ser) and PTX incorporation the hydrophobic pendant chain exerted a dominant effect on the polymer conformation.

These results demonstrate the potency of these techniques in the field of PT by using relevant physiological conditions.

REFERENCES

1. Duncan, R., *The dawning era of polymer therapeutics.* Nat Rev Drug Discov, 2003. **2**(5): p. 347-360.
2. Duncan, R. and M.J. Vicent, *Polymer therapeutics-prospects for 21st century: The end of the beginning.* Advanced Drug Delivery Reviews, 2013. **65**(1): p. 60-70.
3. Conejos-Sánchez, I., et al., *Polymer-doxycycline conjugates as fibril disrupters: An approach towards the treatment of a rare amyloidotic disease.* Journal of Controlled Release, 2015. **198**: p. 80-90.
4. Barz, M., et al., *Overcoming the PEG-addiction: well-defined alternatives to PEG, from structure-property relationships to better defined therapeutics.* Polymer Chemistry, 2011. **2**(9): p. 1900-1918.
5. Niño-Pariente, A., V.J. Nebot, and M.J. Vicent, *Relevant Physicochemical Descriptors of "Soft Nanomedicines" to Bypass Biological Barriers.* Current Pharmaceutical Design, 2016. **22**: p. 1-1.
6. Barz, M., A. Duro-Castano, and M.J. Vicent, *A versatile post-polymerization modification method for polyglutamic acid: synthesis of orthogonal reactive polyglutamates and their use in "click chemistry".* Polymer Chemistry, 2013. **4**(10): p. 2989-2994.

7. Pichon, C., C. Gonçalves, and P. Midoux, *Histidine-rich peptides and polymers for nucleic acids delivery.* Advanced Drug Delivery Reviews, 2001. **53**(1): p. 75-94.
8. Schaffert, D., et al., *Solid-Phase Synthesis of Sequence-Defined T-, i-, and U-Shape Polymers for pDNA and siRNA Delivery.* Angewandte Chemie International Edition, 2011. **50**(38): p. 8986-8989.
9. Fröhlich, T., et al., *Structure–activity relationships of siRNA carriers based on sequence-defined oligo (ethane amino) amides.* Journal of Controlled Release, 2012. **160**(3): p. 532-541.
10. Niño-Pariente, A., et al., *Design of Poly-l-Glutamate-Based Complexes for pDNA Delivery.* Macromolecular Bioscience, 2017: p. 1700029-n/a.
11. Scholz, C. and E. Wagner, *Therapeutic plasmid DNA versus siRNA delivery: Common and different tasks for synthetic carriers.* Journal of Controlled Release, 2012. **161**(2): p. 554-565.
12. Roncador, A., et al., *Use of polymer conjugates for the intraperoxisomal delivery of engineered human alanine:glyoxylate aminotransferase as a protein therapy for primary hyperoxaluria type I.* Nanomedicine, 2016. **18**(16): p. 30228-3.
13. Du, A.W. and M.H. Stenzel, *Drug carriers for the delivery of therapeutic peptides.* Biomacromolecules, 2014. **15**(4): p. 1097-114.
14. Ginn, C., et al., *PEGylation and its impact on the design of new protein-based medicines.* Future Med Chem, 2014. **6**(16): p. 1829-46.
15. Pasut, G. and F.M. Veronese, *State of the art in PEGylation: the great versatility achieved after forty years of research.* J Control Release, 2012. **161**(2): p. 461-72.
16. Terlecky, S.R. and J.I. Koepke, *Drug delivery to peroxisomes: employing unique trafficking mechanisms to target protein therapeutics.* Adv Drug Deliv Rev, 2007. **59**(8): p. 739-47.
17. Giordano, C.R., et al., *Catalase therapy corrects oxidative stress-induced pathophysiology in incipient diabetic retinopathy.* Invest Ophthalmol Vis Sci, 2015. **56**(5): p. 3095-102.
18. Nell, H.J., et al., *The targeted antioxidant, catalase-SKL, reduces beta-amyloid toxicity in the rat brain.* Brain Pathol, 2016.
19. Undyala, V., S.R. Terlecky, and R.S. Vander Heide, *Targeted intracellular catalase delivery protects neonatal rat myocytes*

from hypoxia-reoxygenation and ischemia-reperfusion injury. Cardiovasc Pathol, 2011. **20**(5): p. 272-80.

Final Conclusions

• Non-viral vectors based on poly-L-glutamic acid (PGA)-derivatives modified with pentameric succinyl tetraethylene pentamine (Stp_5) were designed, developed, and *in vitro* validated. Histidines for modulation of endosomal buffer capacity and cysteines for pDNA or siRNA complex stabilisation were included. Vectors were characterised for biophysical properties and gene transfer efficiency in N2a neuroblastoma or 4T1 breast cancer cells.

• The conjugation of Stp derivatives to the PGA chain through amide bond formation resulted in stable non-toxic nanosystems with the ability to efficiently transfer pDNA. This improved the efficiency of both PGA and Stp-based compounds as transfection agents, with a more pronounced effect for Stp derivatives bearing histidine moieties. Thus, the presence of PGA enhanced transfection capacity of the Stp_5 family.

• PGA conjugation of Stp derivatives through post-polymerisation modification via disulphide bonds significantly improved Stp cell viability.

• Multifunctional polymeric platforms based on PGA, poly-L-arginine (PArg), poly-L-ornithine (P(Orn)), and their derivatives, were also obtained through post-polymerisation modifications. Polymeric carriers were fully characterised and biologically evaluated as non-viral vectors for siRNA delivery in cell models.

•P(Orn)-based nanosystems with a net positive surface charge demonstrated the most promising cell silencing results. Furthermore, these nanosystems displayed acceptable cytotoxic and haemolytic profiles using the concentrations tested previously in B16F10-luc-G5 melanoma cells.

• The conjugation of poly(ethylene glycol)-*co*-poly(L-glutamic acid) (PEG-PGA) block-*co*-polymer to alanine:glyoxylate aminotransferase (AGT) via the formation of disulfide bonds between the polymer and cysteine residues of the enzyme was performed as a novel treatment for Primary Hyperoxaluria type I (PH1). PEG-PGA conjugation did not affect AGT structural/functional properties and allowed internalisation

of the enzyme in a cellular model of PH1 and the restoration of glyoxylate-detoxification. The insertion of the C387S/K390S amino acid substitutions reduced conjugation efficiency but endowed conjugates with the ability to reach the peroxisomal compartment. These results, along with the finding that conjugates are hemocompatible, stable in plasma, and non-immunogenic, hold promise for the development of polypeptide-based AGT conjugates as a therapeutic option for PH1 patients. Furthermore, these findings lay the groundwork for applications in other diseases related to deficits in peroxisomal proteins.

- SAS techniques elucidated of the solution conformation of all studied polymers. A Gaussian coil for a Dozier star polymer was the most appropriate model to fit the data for both 3- and 4 arm star-shaped PGA polymers. These assessments also generated information about the radius of gyration as well as other conformational parameters.

- SANS studies in polyacetal-based combination conjugates confirmed that, following *fmoc*-protected serinol (SerFmoc) and paclitaxel (PTX) incorporation, the hydrophobic pendant chain exerted a dominant effect on the polymer conformation.

Appendix

Thesis Project, Objectives, Main Methodology, Results and Conclusions in Spanish

1. INTRODUCCIÓN Y MARCO TEMÁTICO DE LA TESIS

Un transporte citosólico adecuado puede ser utilizado como una poderosa herramienta para el tratamiento y/o prevención tanto de cáncer como de otras muchas enfermedades que nos afectan hoy en día. Junto con los avances recientes dentro de las tecnologías terapéuticas basadas en biomacromoléculas, tales como genes, oligonucleótidos y proteínas, se requiere un desarrollo tecnológico enfocado a la mejora en la eficiencia del trasporte celular de esas moléculas terapéuticas [1]. Una gran variedad de métodos prometedores han salido a la luz en los últimos 20 años. Por ejemplo el uso de péptidos de penetración celular (*cell-penetrating peptides*, CPPs), liposomas o polímeros. Sin embargo, a pesar de este progreso tan significativo, estos métodos presentan serios inconvenientes como baja/variable eficiencia en el transporte, alta citotoxicidad y, quizá más importante, escape endosomal/lisosomal inefectivo. En este contexto, los llamados Polímeros Terapéuticos (PT) [2] emergen como una potente y prometedora alternativa para superar dichas limitaciones. Específicamente, los PT basados en polipéptidos bien definidos son unos excelentes candidatos para el transporte de fármacos debido a su adecuada biodegradabilidad, conformación y estructuras predecibles, alta homogeneidad así como alta capacidad de carga de fármaco [3-5].

La aparición de técnicas de caracterización novedosas, potentes y sofisticadas ha complementado la tarea realizada por las técnicas ya existentes a la hora de afrontar el reto de trabajar en condiciones fisiológicas. El notable desarrollo en el diseño de sistemas de administración de fármacos ha obligado a establecer unas pautas que seguir en dicho diseño con el fin de lograr el efecto terapéutico deseado. Por lo tanto, la importancia de una exhaustiva caracterización fisicoquímica de estructuras complejas ha quedado patente, dando lugar a estrategias terapéuticas más eficientes controlando tanto la biodistribución como la farmacocinética de dichas nanomedicinas [6].

Partiendo de estas bases, el objetivo de la tesis doctoral se ha centrado en dos temas principales.

i) Diseño y desarrollo de portadores polipeptídicos de tamaño nanométrico, capaces de facilitar el transporte citosólico de agentes bioactivos que no son capaces de traspasar las membranas biológicas por sí solos o que exhiben baja estabilidad lisosomal, tales como DNA plasmídico (*plasmid DNA*, pDNA), pequeño RNA de interferencia (*small interfering* RNA, siRNA) o proteínas.

ii) Caracterización fisicoquímica exhaustiva de diferentes moléculas con una base polimérica similar a los compuestos anteriores. Para cumplir este último propósito se utilizaron técnicas altamente avanzadas intentando simular las condiciones fisiológicas.

2. OBJETIVOS DE LA INVESTIGACIÓN

El objetivo global de la presente tesis se centra tanto en el transporte citosólico de biomacromoléculas a través de portadores polipeptídicos de tamaño nanométrico como en la exhaustiva caracterización fisicoquímica en disolución de sistemas poliméricos similares. Estos objetivos principales pueden desglosarse en cuatro objetivos específicos:

(i) Diseño de complejos basados en ácido poli-L-glutámico (PGA) para terapia génica. Esto engloba el diseño, la síntesis, la caracterización fisicoquímica y evaluación biológica *in vitro* de sistemas basados en cadenas de PGA funcionalizadas con diferentes poliamidoaminas sintéticas lineales que serán utilizados como sistemas para el transporte de oligonucleótidos.

(ii) Desarrollo de portadores polipeptídicos no virales para el transporte de siRNA. Dentro de este punto se encuentra tanto el desarrollo como la evaluación biológica de una metodología versátil en la que diferentes poliaminoácidos, tanto sintéticos como naturales, serán modificados con el fin de obtener vehículos adecuados para el transporte de siRNA.

(iii) Desarrollo de conjugados basados en PGA para el transporte intraperoxisomal de alanina:glioxilato aminotransferasa (AGT). En este

punto se estudiará la factibilidad del transporte de AGT mediante la conjugación de la encima a un portador polimérico compuesto por polietilenglicol y PGA (PEG-PGA).

(iv) Uso se Dispersión de Neutrones de Ángulo Pequeño (*Small Angle Neutron Scattering*, SANS) y Dispersión de Rayos X de Ángulo Pequeño (*Small Angle X-ray Scattering*, SAXS) para estudiar la estructura en disolución de sistemas de transporte de fármacos. Este último objetivo se centra en la exhaustiva caracterización fisicoquímica de diferentes nanosistemas en disolución a través de complejas y avanzadas técnicas como SANS o SAXS, intentando mimetizar las condiciones fisiológicas.

3. METODOLOGÍA

3.1. Materiales e Instrumentación

3.1.1. Materiales

Todos los reactivos y disolventes utilizados durante el desarrollo de la tesis fueron de grado analítico o superior y se usaron sin purificación adicional, a no ser que se indique lo contrario. De manera general, las reacciones llevadas a cabo en disolventes orgánicos se realizaron bajo atmósfera inerte de nitrógeno. El agua utilizada fue desionizada con una conductancia por debajo de 0.06 µS (agua milliQ).

Los métodos más utilizados de purificación de los conjugados poliméricos se basaron en el uso de diálisis o cromatografías por exclusión de tamaño. Para las diálisis se utilizaron Vivaspin®, Float-A-Lyzer® o membranas moleculares. En el caso de purificación por cromatografía, se utilizaron resinas Sephadex o columnas comerciales pre-empaquetadas PD10.

3.1.2. Instrumentación

Espectroscopía de Resonancia Magnética Nuclear (NMR). Los espectros ^{1}H NMR y DOSY NMR se llevaron a cabo en un sistema Bruker Advance AC 300 (300 MHz) o AV500 (500 MHz) utilizando para ello al menos 5 mg de compuesto, temperatura ambiente y disolventes

deuterados. Los datos obtenidos se analizaron mediante la utilización del software MestreNova 6.2.

Dispersión de Luz Dinámica (DLS). Las medidas tanto de tamaño de partícula como de potencial ζ se realizaron a 25˚C en un dispositivo Malvern Zetasizer Nano ZS equipado con un láser (532 nm) a un ángulo de dispersión fijo de 90˚. La celda utilizada fue DTS 1070. Para las medidas de tamaño, el tiempo de equilibrado fue de 0 min con atenuación automática. El índice de refracción del disolvente, en este caso agua, fue 1,330 y, por lo tanto, la viscosidad fue 0,8872. Para el análisis de los diferentes polímeros se utilizó el índice de refracción del látex de poliestireno (1,590). Cada muestra se midió tres veces con 10 submedidas. El potencial ζ se calculó a través del modelo Smoluchowski. Se utilizaron entre 10 y 30 medidas de 10 s cada una a 25˚C (n=3).

Espectroscopía Ultravioleta-Visible (UV-Vis). Los espectros se tomaron en un espectrofotómetro Jasco V-630 UV/Vis a 25˚C con celdas de plástico o cuarzo (en su caso) de 1 cm y ancho de banda de 0.5 nm.

Microscopía Electrónica de Transmisión (TEM). Las imágenes se adquirieron en un microscopio de transmisión electrónica FEI Tecnai G2 Spirit (FEI Europe, Eindhoven, Netherlands) usando una cámara digital Morada (Olympus Soft Image Solutions GmbH, Münster, Germany). Para su preparación, las muestras se adsorbieron en rejillas de cobre recubiertas por una película de carbón de 200 mallas. Tras ello, se realizó una tinción de contraste negativo con una disolución de acetato de uranilo al 2%.

Microscopía de Fluorescencia Confocal. Las imágenes fueron adquiridas con un microscopio (invertido) láser confocal Leica, modelo TCS SP8 AOBS (Leica Microsystems Heidelberg and MBH, Germany). Todas las imágenes se adquirieron bajo las mismas condiciones y se analizaron mediante el software de Leica LAS AF Lite (Leica Microsystems Heidelberg and MBH, Germany).

Dispersión de Neutrones de Ángulo Pequeño (SANS). Los experimentos de SANS se llevaron a cabo utilizando el difractómetro D11 del Instituto Laue-Langevin (ILL, Grenoble) y los difractómetros

SANS2d y LOQ en ISIS Spallation Neutron Source (Didcot, UK). Todas las disoluciones fueron preparadas en disolventes deuterados a la concentración máxima de 1 wt% y se colocaron en celdas de cuarzo de 2 mm de camino óptico. Los volúmenes de muestra fueron aproximadamente de 0,6 cm^3. Los datos fueron recogidos y corregidos de la transmisión y dispersión de la celda y del disolvente y se pusieron en una escala de intensidad absoluta. Los datos de dispersión fueron expresados en función del vector de dispersión Q, el cual viene dado por $Q = 4n\pi/\lambda \sin(\theta/2)$ en el que *n* es el índice de refracción para los neutrones ($n \approx 1$), λ es la longitud de onda, y θ es el ángulo de dispersión.

Dispersión de Rayos X de Ángulo Pequeño (SAXS). Los espectros de SAXS de disoluciones filtradas de concentraciones entre 1 mg/mL y 10 mg/mL, fueron obtenidos en la línea de luz NCD11 del Sincrotrón ALBA (Barcelona, España). La energía del haz incidente fue 12,6 KeV (λ= 0.995 Å). Las muestras se colocaron en una celda termostatada utilizando aproximadamente 150 µL por medida. Los rayos X dispersados fueron recogidos en un detector bidimensional CCD Quantum 210r, convertidos a monodimensionales y representados como función del vector $Q=4\pi\sin\theta/\lambda$, en el que θ es la mitad del ángulo de dispersión y λ es la longitud de onda del haz de rayos X incidente. La distancia entre la muestra y el detector se mantuvo constante a 1,4 m. Las medidas de cada muestra se hicieron durante tiempos entre 0,1 y 1 s cada una. Las disoluciones fueron preparadas utilizando agua desionizada, agua tamponada con PBS a pH = 7,4 o agua deuterada a 20˚C. La comparación de las exposiciones sucesivas de un experimento de adquisición no indicó cambios en los patrones de dispersión (es decir, ningún daño de radiación medible a las muestras). Los datos fueron normalizados con respecto a la intensidad del haz transmitido, y los datos de dispersión por el fondo del disolvente, medido antes y después de la correspondiente muestra, haciendo la media y utilizándolo para eliminar el fondo.

Modelado con FISH. El programa FISH [7] fue la herramienta utilizada para predecir tanto el tamaño como la conformación de las distintas especies en disolución a través los datos obtenidos en los diferentes experimentos de SANS. Dicho programa emplea un proceso

lineal de mínimos cuadrados iterativo para ajustar los datos a modelos que contienen las ecuaciones que describen la dispersión esperada para diferentes factores de forma, factores de estructura, pasos de contraste, polidispersidades y dispersión de fondo. Parámetros de modelo conocidos, tales como fracción de volumen y polidispersidades, se pueden fijar manualmente y se permite al programa optimizar el ajuste refinando los parámetros restantes.

Programas ATSAS. Los datos obtenidos de los experimentos de SAXS fueron procesados utilizando procedimientos estándar de los programas ATSAS [8].

Ensayos Celulares. Todos los procesos relacionados con el cultivo celular se llevaron a cabo en una cabina de flujo laminar recirculante vertical con seguridad biológica clase II (Telsar). En todo momento se utilizó material estéril.

Medidas de absorbancia o luminiscencia de ensayos *in vitro*. Estas medidas se realizaron en un equipo Victor^2 Wallac 1420 Multilabel HTS counter Perkin Elmer (Northwolk, CT, EEUU) utilizando placas de 96 pocillos y las correspondientes longitudes de onda propias de cada compuesto.

3.2. Métodos más Relevantes

3.2.1. Protocolos de Síntesis

Síntesis de Fmoc-Stp(boc)$_3$-OH. La síntesis de Fmoc-Stp(boc)$_3$-OH se reprodujo básicamente de la referencia [9] realizando algunas modificaciones.

Carga de la Resina 2-Chlorotrityl Chloride con Fmoc-L-Trp(boc)-OH. Todas las síntesis en fase sólida fueron realizadas utilizando una resina 2-chlorotrityl chloride (CTC-resin, 200-400 mesh). La resina (1,56 mmol chloride/g) fue pre-hinchada en diclorometano (DCM) anhidro (1 mL/100 mg resina) durante 20 min. 0,45 equivalentes (eq.)/g (150% de la carga deseada) del aminoácido protegido con 9-fluorenilmetiloxicarbonil (Fmoc-L-Trp(boc)-OH) por gramo de resina y N,N-diisopropiletilamina (DIPEA, 0,9 eq./g) fueron disueltos en DCM

anhidro, añadidos a la resina y mezclados durante 1 h. Después del acoplamiento, una mezcla de DCM/metanol (MeOH)/DIPEA (80/15/5; v/v/v) fue añadida durante 30 min para capturar los cloruros residuales.

Para determinar la carga de resina, una pequeña cantidad de ésta (∼10 mg) fue lavada dos veces con DCM y dos veces más con n-hexano y secada a vacío. 1 mg de la resina seca (por triplicado) se mezcló con 1 mL de piperidina 20% (v/v) en N,N-dimetilformamida (DMF) y se incubó durante 1 h. La cantidad de grupo protector Fmoc fue cuantificada midiendo la absorción a 301 nm. La carga fue calculada usando la siguiente ecuación:

$$carga\ [mmol/g] = \frac{1000 \times A_{301}}{m\ [mg] \times 7800 \times D}$$

Donde D es el factor de dilución. Después de la determinación de la carga, la resina fue incubada cuatro veces durante 10 min con piperidina 20% (v/v) en DMF, lavada tres veces con DMF, tres veces con DCM, tres veces con n-hexano y secada a vacío.

Procedimiento General de Síntesis de Péptidos en Fase Sólida. Las poliamidoaminas fueron sintetizadas en una resina 2-chlorotrityl chloride cargada previamente con Fmoc-L-Trp(boc)-OH utilizando un tamaño de lote de 25 µmol. La resina fue pre-hinchada durante 20 min con DCM antes del primer paso de desprotección. El grupo fmoc fue eliminado durante tres tratamientos secuenciales con piperidina (20% piperidina en DMF, 5 min, 10 min, 10 min) seguidos de un exhaustivo lavado con DCM (3 veces) y DMF (3 veces). Los acoplamientos de succinil tetraetilen pentamina (Stp) fueron hechos disolviendo el Fmoc-*building block* amino ácido (4 eq.) y DIPEA (8 eq.) en la mínima cantidad de DCM, PyBOP® (4 eq.) y 1-hidroxibenzotriazol (HOBt, 4 eq.) en la mínima cantidad de DMF, y seguidamente transferidas al reactor. Después de 120 minutos, la resina fue lavada con DMF seguida de DCM. Para comprobar que el acoplamiento había terminado se utilizó en test de Kaiser [10]. Si el test de Kaiser muestra que el acoplamiento no ha acabado se repite el ciclo. Después del paso final de desprotección del grupo Fmoc, la resina fue lavada con DMF (3 veces) seguida de DCM (3 veces) y secada a vacío en un desecador.

Escisión del Enlace Péptido-Resina. La escisión de la resina se realizó mediante el tratamiento con una disolución que contenía ácido trifluoroacético (TFA)/triisopropilsilano (TIS)/H_2O (95/2,5/2,5) durante 1,5 h. Después de lavar la resina dos veces con TFA y dos veces con DCM, todas las disoluciones se juntaron, concentraron y precipitaron. Para ello la disolución concentrada se añadió gota a gota sobre una mezcla de n-hexano y *tert*-butilmetileter (MTBE; 1:1) previamente enfriada a -20˚C. El producto obtenido después de centrifugar fue secado bajo nitrógeno y disuelto en un tampón de exclusión por tamaño conteniendo 10 mM HCl y 30% acetonitrilo (ACN). Tras la purificación por exclusión por tamaño en una columna G-10, se juntaron las fracciones adecuadas, se congeló en nitrógeno líquido y se liofilizó.

Método General de Modificación de PGA utilizando DMTMM·Cl. 1 eq. de PGA sal de sodio (MW 151 por unidad, 50 unidades) fue disuelto en la mínima cantidad de agua milliQ. Seguidamente, la correspondiente cantidad de 4-(4,6-dimetoxi-1,3,5-triazin-2-il)-4-metilmorfolina (DMTMM·Cl) para el % de modificación deseado (para el 50%, 1 eq.) fue disuelta también en agua milliQ. 10 min después, la mitad de cantidad de la correspondiente amina a introducir fue disuelta en agua milliQ y añadida a la mezcla de reacción. El pH se ajustó a 8 añadiendo algunas gotas de disolución 1M $NaHCO_3$. Se dejó reaccionar agitando a temperatura ambiente durante 16 h. Transcurrido ese tiempo, se paró la reacción y se purificó a través de Vivaspin® o Float-A-Lyzer® del correspondiente MWCO.

Método General de modificación de PGA-PD a través de la Formación de un Enlace Disulfuro. 1 eq. de PGA-PD (sintetizado utilizando una modificación del método recientemente publicado [11]) y la correspondiente cantidad del compuesto portador del grupo tiol fueron disueltos por separado en PBS a pH 7.4. Seguidamente, ambas disoluciones se mezclaron y se dejó reaccionar a con agitación continua y a temperatura ambiente durante 5 h. Transcurrido ese tiempo, una diálisis mediante Vivaspin® o Float-A-Lyzer® del correspondiente MWCO.

Método General de Formación de Poliplejos. Las formulaciones de poliplejos que fueron utilizadas tanto para transfecciones como para electroforesis fueron preparadas del siguiente modo: 200 ng de pDNA o 500 ng de siRNA y la cantidad adecuada de polímero al ratio +/- o N/P indicado, fueron diluidos individualmente en tubos separados en 10 μL de tampón 20 mM HEPES a pH 7.4. Solamente los nitrógenos protonables, fueron considerados en los cálculos de +/- o N/P. El ácido nucleico correspondiente y la disolución de polímero fueron mezclados a través de un pipeteo rápido (arriba-abajo, al menos 5 veces) e incubados durante 30-40 min a temperatura ambiente.

3.2.2. Caracterización

Ensayos de Unión de pDNA y siRNA mediante Electroforesis. Para pDNA, el gel 1% agarosa fue preparado disolviendo la agarosa en tampón TAE y calentando hasta ebullición por encima de los 100°C. Una vez enfriado más o menos a 50°C y añadido el EtBr, el gel de agarosa se introdujo dentro de la unidad de electroforesis. Los poliplejos conteniendo 200 ng de pDNA en 20 μL de 20 mM HEPES y tampón de carga, fueron introducidos dentro de los pocillos. La electroforesis se llevó a cabo a 80 V durante 80 min. Para siRNA, el gel 2,5% agarosa fue preparado de la misma manera que antes. Los poliplejos conteniendo 500 ng de siRNA en 20 μL de HEPES y tampón de carga fueron introducidos en los pocillos. La electroforesis se llevó a cabo a 80 V durante 40 min.

3.2.3. Evaluación Biológica

Ensayo de Transfección con pCMVluc. Células N2a o 4T1 fueron sembradas en placas de 96 pocillos con 100 μL de medio (10000 o 5000 células por pocillo respectivamente). Pasadas 24 h, el medio fue reemplazado por 80 μL de medio fresco. Los poliplejos formados conteniendo 200 ng de pCMVluc en cada pocillo fueron añadidos en un volumen de 20 μL e incubados a 37˚C. LPEI a un N/P óptimo no tóxico fue utilizado como patrón positivo. Todos los experimentos se realizaron por quintuplicado. 24 h después de la transfección, las células fueron tratadas con 20 μL del reactivo Bright-Glo™. La actividad de la

luciferasa fue medida espectroscópicamente con el equipo Victor^2 Wallac^{TM}.

Ensayo de Silenciamiento con siRNA. Los experimentos de silenciamiento se realizaron utilizando células N2a/EGFPluc o B16F10 luc en placas de 96 pocillos libres de RNasa (5000 o 7500 células por pocillo respectivamente, por triplicado). Las células fueron sembradas 24 h antes del tratamiento, después el medio fue reemplazado por 80 μL de medio fresco. 20 μL de disolución de poliplejo a su correspondiente +/-, conteniendo 500 ng de siRNA se añadieron a cada pocillo y se incubaron a 37°C. 48 h después de la transfección, las células fueron tratadas con 20 μL del reactivo Bright-Glo™. La actividad de la luciferasa fue medida espectroscópicamente con el equipo Victor^2 Wallac^{TM}.

Ensayo de Viabilidad Celular (MTS). Células N2a, 4T1 o B16F10 luc fueron sembradas en placas de 96 pocillos a una densidad de 10000, 5000 o 7500 células por pocillo respectivamente. Pasadas 24 h, el medio fue reemplazado por 80 μL de medio fresco y 20 μL de disolución de poliplejo a su correspondiente +/- fueron añadidos. Todos los estudios se realizaron por quintuplicado. 24 h después de la transfección, 20 μL de una disolución MTS/PMS (20:1) se añadió a cada pocillo, y la placa se incubó durante 2 h más. La densidad óptica de cada pocillo fue medida espectrofotométricamente a 490 nm utilizando el equipo Victor^2 Wallac^{TM}. Los valores de absorbancia fueron representados como porcentaje de viabilidad celular tomando como 100% de viabilidad celular células control sin tratar.

4. RESULTADOS

4.1. Diseño de Poliplejos como Vectores No Virales para Terapia Génica Basados en PGA (Capítulo II)

Debido a la naturaleza polianiónica tanto del DNA como del RNA, normalmente formulaciones catiónicas o neutras han sido utilizadas para el transporte de dichos oligonucleótidos. Dando un nuevo enfoque a esta cuestión, nuestro estudio se centró en el diseño, desarrollo y validación de vectores zwiteriónicos no virales con base polipeptídica.

Con este fin, se diseñaron derivados de PGA modificados con diferentes pentamino succinil tetraetilen pentaminas (Stp_5) [12]. Opcionalmente, se incluyeron histidinas para la modulación de la capacidad tampón endosomal y cisteínas para la estabilización del complejo de pDNA o siRNA, seguido por la caracterización de las propiedades biofísicas y la eficiencia de transferencia de oligonucleótidos en células de neuroblastoma N2a o células de cáncer de mama 4T1.

Los tres primeros sistemas desarrollados se basaron en polímeros de PGA (homopolímeros o copolímeros en bloque) modificados con una oligoaminoamida monodispersa basada en Stp. En el Sistema 1, las cadenas laterales del PGA fueron ortogonalmente modificadas con el oligómero S mediante la formación de enlace amida con la amina terminal de S (Figura II.3). En el Sistema 2, las cadenas laterales del PGA fueron modificadas análogamente con SH (portando histidinas para mejorar el efecto endosomolítico) [13], SC (que contiene cisteína para estabilizar el complejo pDNA a través de la formación de enlaces disulfuro) [9, 14], o SHC (conteniendo histidinas y cisteínas). Para generar el Sistema 3, realizamos la conjugación mediante enlaces disulfuro biorreducibles utilizando la cisteína terminal de SHC. El Sistema 4 difiere de los sistemas anteriores en varias maneras. En primer lugar, se generó un poliplejo entre pDNA y oligoaminoamide SHC, y posteriormente se recubrió el complejo cargado positivamente con PGA (cargado negativamente) en un intento de mejorar la biocompatibilidad de SHC. Se emplearon dos longitudes diferentes de PGA y dibloque PEG-PGA como agentes de recubrimiento.

Lamentablemente, nuestros estudios sugirieron que los sistemas evaluados no son adecuados para el transporte de siRNA. Este hecho puede ser debido a la baja estabilidad de los complejos que contribuye a la falta de capacidad de transfección. La formulación de nanopartículas con siRNA presenta algunas diferencias importantes con respecto a la de pDNA. Aunque ambos se auto-ensamblan por fuerzas electrostáticas, los plásmidos son varios cientos de veces más grandes que el siRNA, sugiriendo que diferentes tipos de policationes pueden ser válidos. Esto demuestra nuevamente que pDNA y siRNA difieren

considerablemente en sus propiedades y el diseño de vectores debe de ser llevado a cabo de manera individual para cada uno de ellos [15].

En cuanto al pDNA, la conjugación de los derivados de Stp a la cadena lateral de PGA mediante reacciones de postpolimerización (enlace amida, Sistema 1 y Sistema 2) dio como resultado nanosistemas no tóxicos, estables, con la capacidad de transferir eficientemente pDNA. Los conjugados PGA-Stp presentaron una mayor eficacia como vectores no virales de transfección comparados con los compuestos de partida (PGA y Stp) observando un efecto más pronunciado para los derivados de Stp que portaban restos de histidina, superando incluso a los resultados obtenidos con PEI (control positivo). Además, se encontró que la capacidad de complejación depende del contenido de la oligoaminoamida.

En el caso de los Sistemas 3-4, la conjugación de SHC a la cadena de PGA mediante enlaces disulfuro mejoró significativamente la viabilidad celular de sistemas anteriores aunque no fue capaz de mejorar la capacidad de transfección de la oligoamina de partida (SHC), incluso tras el revestimiento (Sistema 4). Cabe resaltar que una estrategia de revestimiento además de conjugación polimérica, podría proporcionar ventajas cuando se compara con SHC libre *in vivo* debido al efecto EPR, que proporciona una mayor acumulación de tales macromoléculas en el tumor. Otros experimentos están en curso para demostrar este punto.

4.2. Desarrollo de Vectores Polipeptídicos No Virales para el Transporte de siRNA (Capítulo III)

El RNA interferente (iRNA) inducido por siRNA es una estrategia prometedora para el tratamiento de diversas enfermedades mediante la regulación de dianas previamente “undruggable”. Sin embargo, el proceso de transporte sigue siendo la limitación más crucial, lo que dificulta el desarrollo terapéutico/clínico. En este proyecto, diferentes plataformas poliméricas multifuncionales fueron sintetizadas y físico-químicamente caracterizadas utilizando poliaminoácidos naturales o sintéticos y sus derivados con el fin de encontrar un vector no viral para un transporte génico eficaz. Todos los sistemas se sintetizaron a partir

compuestos poliméricos con baja polidispersidad (Đ ~ 1.2) y, por lo tanto, estructuras precisas y bien definidas, lo que permite la reproducibilidad y la determinación de una clara relación estructura-actividad.

En primer lugar, se diseñaron y sintetizaron sistemas basados en PGA modificados con éxito con diferentes residuos endosomolíticos que contenían aminas secundarias y terciarias, evaluándose como posibles poliplejos de administración génica. Sin embargo, los sistemas propuestos no dieron lugar a la formación complejos con el oligonucleótido deseado. Con estos resultados en mente, se diseñó un segundo set de polímeros basados en PGA conteniendo además piridil disulfuro (PD) para formar un conjugado a través de un enlace disulfuro entre el polímero y el oligonucleótido. Sin embargo, estos conjugados no fueron estables ni en plasma ni en medio de cultivo celular incluso a tiempos de incubación cortos.

Utilizando los mismos conceptos pero con polipéptidos intrínsecamente catiónicos a pH fisiológico, se seleccionó poli-L-arginina (PArg) y su precursor poli-L-ornitina (P(Orn)) para explorar su potencial como vectores no virales después de la complejación de siRNA. Ningún resultado positivo fue encontrado con la PArg, sin embargo la derivatización química de P(Orn) ofreció estrategias muy prometedoras. Los derivados de P (Orn) fueron químicamente modificados, complejando las estructuras resultantes (POP1, POP2, POPF y POPD) al siRNA a una relación N/P optimizada. Su tamaño nanométrico y su carga superficial positiva resultaron favorables para la aplicación *in vitro* (no citotóxica y no hemolítica). Más importante aún, los polipéptidos transfectaron con éxito un modelo de células de melanoma transfectadas con luciferasa (B16F10-luc-G5), evidenciando el potencial de esta plataforma polipéptidica. Se están realizando más análisis para validar este sistema tanto *in vitro* como *in vivo*.

4.3. Desarrollo de Conjugados Basados en PGA para el Transporte Intraperoxisomal de Alanina Glioxilato Aminotransferasa (Capítulo IV)

En este trabajo, se presentó una estrategia para conjugar la enzima Alanina Glioxilato Aminotransferasa (AGT) a copolímeros dibloque de

PEG-PGA a través de la formación de enlaces disulfuro, así como el uso exitoso de los conjugados obtenidos para restablecer la destoxificación de glioxilato en células eucarióticas imitando un fenotipo hiperoxaluria primaria tipo I (PH1), considerada una enfermedad rara letal. Un transporte eficiente de AGT a peroxisomas es requerido para obtener una actividad terapéutica adecuada [16].

El protocolo utilizado permitió conseguir un alto rendimiento de conjugación sin efectos significativos sobre las propiedades funcionales de la enzima. Los conjugados polímero-proteína obtenidos demostraron una internalización adecuada en células CHO-GO, un modelo celular bien aceptado de PH1, encontrándose principalmente en compartimentos discretos del citosol. Además, desintoxican eficientemente el glioxilato producido endógenamente. Mediante la aplicación de un enfoque de ingeniería de proteínas, se generó una forma mutada de AGT con la sustitución de Cys387-a-Ser y de Lys390-a-Ser (AGT-SSKL), para favorecer la interacción con la maquinaria de focalización peroxisomal. Los conjugados de PEG-PGA-AGT-SSKL internalizados en células CHO-GO se importan a peroxisomas y son más eficaces en la destoxificación de glioxilato con respecto a los conjugados de PEG-PGA-AGT. Los datos *in vitro* confirmaron una alta estabilidad en plasma y una excelente hemocompatibilidad del conjugado proteico, lo que sugiere que los conjugados son adecuados para inyección intravenosa. En general, estos datos respaldan la utilización de este sistema para reponer a los pacientes de PH1 con una enzima catalíticamente activa y correctamente localizada capaz de contrarrestar el déficit responsable de la acumulación de oxalato. Debido a que los nanoconjugados con base polimérica han sido ampliamente utilizados para el transporte de proteínas terapéuticas, principalmente por su versatilidad y biocompatibilidad [17-19], estos resultados constituyen un paso fundamental en el futuro desarrollo de una terapia efectiva de administración de enzimas más seguras para todos los pacientes PH1, independientemente del tipo de mutación.

La correcta focalización de un fármaco proteico es un tema importante, particularmente en el caso de trastornos que involucran enzimas peroxisomales cuya funcionalidad está fuertemente

influenciada por la localización subcelular [20]. Los informes anteriores sobre la administración de catalasa en el interior de peroxisomas para solventar el daño inducido por la especie reactiva de oxígeno (ROS) se basaron en el uso de un derivado enzimático dotado de un péptido de penetración celular unido de manera no covalente [21-23]. Hasta donde sabemos, la estrategia esbozada en este capítulo es el primer reporte de un conjugado basado en PGA, diseñado para el suministro eficiente de una proteína terapéutica catalíticamente activa al peroxisoma. Por lo tanto, representa un ejemplo a implementar para otras enfermedades causadas por deficiencias de enzimas peroxisomales.

4.4. Uso de SANS y SAXS para el Estudio Conformacional en Disolución de Sistemas de Transporte de Fármacos (Capítulo V)

Las técnicas SAS han demostrado ser adecuadas para la elucidación conformacional en solución de todos los polímeros estudiados en esta tesis.

En un primer lugar y tras varios intentos de ajustar los datos de SANS a los modelos comúnmente utilizados, se encontró que el modelo de Dozier para polímeros en forma de estrella era el modelo más apropiado para los poliglutamatos en forma de estrella de 3 y 4 brazos. Esto permitió obtener información sobre el radio de giro, así como otros parámetros conformacionales. Durante el ajuste, se intentó minimizar el número de parámetros utilizando un fondo plano y negando el término S (Q) en el modelo (S (Q) = 1). Los parámetros de ajuste (Tabla V.10 para el Set 1; Tablas V.12, V.13 y V.14 para el Set 3; y Tabla V.22 para el Set5), junto con los resultados obtenidos por SAXS, muestran que, en ausencia de interacciones entre partículas (S (Q) = 1), el radio de giro (R_g) depende en gran medida del polímero utilizado y de la concentración de sal. Además, el R_g está directamente relacionado con ambas condiciones, aunque no hay dependencia del peso molecular. Esta importante información permitió elucidar la estructura 3D de los sistemas estudiados. Cuando se utilizó H_2O o D_2O como disolvente (dado que los valores de los componentes de Flory varían poco, y están próximos a ⅓, lo que indica un disolvente relativamente pobre) el polímero se colapsa relativamente (estrellas densas) y los brazos

tienden a reorganizarse alrededor del núcleo. Por lo tanto, el núcleo está más "envuelto" a medida que aumenta el peso molecular, permitiendo que R_g permanezca relativamente sin cambios. Cuando se utilizó el mismo sistema en un medio iónico como PBS, el comportamiento de autoensamblaje disminuyó, dando lugar a estructuras mucho más pequeñas debido a una mayor fuerza iónica.

Además, la funcionalización de las cadenas de ácido glutámico con cantidades mínimas de biomoléculas relevantes no condujo a cambios significativos en la estructura, permitiendo la conjugación específica de diferentes agentes bioactivos, como es el caso de anticuerpos o proteínas, o de agentes de imagen.

Por último, los estudios de SANS en conjugados de combinación basados en poliacetales confirmaron que después de la incorporación de residuos o fármacos hidrofóbicos, tales como serinol protegido con *fmoc* (SerFmoc) y paclitaxel (PTX), la cadena lateral hidrófoba ejercía un efecto dominante sobre la conformación del polímero de partida.

5. CONCLUSIONES

La novedad y relevancia del presente trabajo radica en haber logrado los siguientes objetivos:

- El diseño y validación *in vitro* de derivados de PGA modificados con Stp_5 para su utilización como vehículos no virales para el transporte de oligonucleótidos. Opcionalmente, se incluyeron histidinas para la modulación de la capacidad tampón endosomal y cisteínas para la estabilización del complejo de pDNA o siRNA, seguido por la caracterización de las propiedades biofísicas y la eficiencia de transferencia génica en células de neuroblastoma N2a o de cáncer de mama 4T1.

- La conjugación de los derivados de Stp a la cadena de PGA a través de la formación del enlace amida dio lugar a nanosistemas no tóxicos, estables y con la capacidad de transfectar eficazmente pDNA en modelos celulares. Dicho efecto fue más pronunciado para los derivados de Stp que portaban restos de histidina. La conjugación de

derivados de Stp a la cadena de PGA a través de enlaces disulfuro mejoró la viabilidad celular.

- Se obtuvieron plataformas poliméricas multifuncionales basadas en PGA, PArg, P (Orn) y sus derivados mediante modificaciones post-polimerización y se caracterizaron fisicoquímicamente para encontrar un vehículo para el transporte de siRNA. Se obtuvieron varios conjugados y complejos de oligonucleótidos y se realizaron estudios preliminares *in vitro*. Comparando los resultados obtenidos del silenciamiento de los sistemas P(Orn), fueron los que ofrecieron los resultados más prometedores.

- Los derivados de P(Orn) modificados químicamente, se complejaron al siRNA a una relación N/P optimizada. Su tamaño nanométrico y su carga superficial positiva resultaron favorables para la aplicación *in vitro* (no citotóxica y no hemolítica). Más importante aún, los polipéptidos transfectaron con éxito un modelo de células de melanoma transfectadas con luciferasa (B16F10-luc-G5), evidenciando el potencial de esta plataforma polipéptida. Se están realizando más análisis para validar este sistema.

- Se evaluó la viabilidad del transporte de la enzima AGT mediante su conjugación al copolímero PEG-PGA. AGT es la enzima responsable de la desintoxicación de glioxilato intraperoxisomal, su fallo desencadena la enfermedad de Hiperoxaluria Tipo I (PH1). Tal conjugación no produjo cambios significativos en las propiedades funcionales de AGT, dando a la proteína la capacidad de atravesar la membrana plasmática. Cabe destacar que la conjugación permitió una localización intracellular adecuada, ya que AGT fue localizada en los peroxisomas de un modelo cellular validado de PH1. La modificación de AGT mediante la inserción de una secuencia de focalización peroxisomal más fuerte (PTS) y la mutación de uno de los puntos de anclaje del polímero situados en el "PTS1 extendido", permitió un mayor direccionamiento peroxisomal, clave en la eficiencia del sistema.

- Las técnicas SAS han demostrado ser adecuadas para la elucidación de la conformación en disolución de todos los polímeros estudiados. El modelo de Dozier para poliglutamatos estrella de 3 y 4

brazos fue el más apropiado para ajustar los datos obtenidos. Esto generó información sobre el radio de giro, así como otros parámetros conformacionales.

- Los estudios de SANS en conjugados de combinación basados en poliacetales confirmaron que después de la incorporación de fármacos hidrofóbicos en polímeros hidrofílicos mediante conjugación química, ejercen un efecto dominante sobre la conformación del polímero.

REFERENCIAS

1. Au, J.L.S., et al., *Delivery of cancer therapeutics to extracellular and intracellular targets: Determinants, barriers, challenges and opportunities.* Advanced Drug Delivery Reviews, 2016. **97**: p. 280-301.
2. Duncan, R., *The dawning era of polymer therapeutics.* Nat Rev Drug Discov, 2003. **2**(5): p. 347-360.
3. Duncan, R. and M.J. Vicent, *Polymer therapeutics-prospects for 21st century: The end of the beginning.* Advanced Drug Delivery Reviews, 2013. **65**(1): p. 60-70.
4. Conejos-Sánchez, I., et al., *Polymer-doxycycline conjugates as fibril disrupters: An approach towards the treatment of a rare amyloidotic disease.* Journal of Controlled Release, 2015. **198**: p. 80-90.
5. Barz, M., et al., *Overcoming the PEG-addiction: well-defined alternatives to PEG, from structure-property relationships to better defined therapeutics.* Polymer Chemistry, 2011. **2**(9): p. 1900-1918.
6. Niño-Pariente, A., V. J. Nebot, and M.J. Vicent, *Relevant Physicochemical Descriptors of "Soft Nanomedicines" to Bypass Biological Barriers.* Current Pharmaceutical Design, 2016. **22**(9): p. 1274-1291.
7. Heenan, R.K., *FISH: Rutherford Appleton Laboratory, Didcot, U.K.*
8. Petoukhov, M.V., et al., *New developments in the ATSAS program package for small-angle scattering data analysis.* Journal of Applied Crystallography, 2012. **45**(2): p. 342-350.
9. Schaffert, D., et al., *Solid-Phase Synthesis of Sequence-Defined T-, i-, and U-Shape Polymers for pDNA and siRNA Delivery.* Angewandte Chemie International Edition, 2011. **50**(38): p. 8986-8989.

10. Kaiser, E., et al., *Color test for detection of free terminal amino groups in the solid-phase synthesis of peptides.* Analytical Biochemistry, 1970. **34**(2): p. 595-598.
11. Talelli, M. and M.J. Vicent, *Reduction sensitive Poly(l-glutamic acid) (PGA)-protein conjugates designed for polymer masked-unmasked protein therapy.* Biomacromolecules, 2014. **15**(11): p. 4168-77.
12. Niño-Pariente, A., et al., *Design of Poly-l-Glutamate-Based Complexes for pDNA Delivery.* Macromolecular Bioscience, 2017: p. 1700029-n/a.
13. Pichon, C., C. Gonçalves, and P. Midoux, *Histidine-rich peptides and polymers for nucleic acids delivery.* Advanced Drug Delivery Reviews, 2001. **53**(1): p. 75-94.
14. Fröhlich, T., et al., *Structure–activity relationships of siRNA carriers based on sequence-defined oligo (ethane amino) amides.* Journal of Controlled Release, 2012. **160**(3): p. 532-541.
15. Scholz, C. and E. Wagner, *Therapeutic plasmid DNA versus siRNA delivery: Common and different tasks for synthetic carriers.* Journal of Controlled Release, 2012. **161**(2): p. 554-565.
16. Roncador, A., et al., *Use of polymer conjugates for the intraperoxisomal delivery of engineered human alanine:glyoxylate aminotransferase as a protein therapy for primary hyperoxaluria type I.* Nanomedicine, 2016. **18**(16): p. 30228-3.
17. Du, A.W. and M.H. Stenzel, *Drug carriers for the delivery of therapeutic peptides.* Biomacromolecules, 2014. **15**(4): p. 1097-114.
18. Ginn, C., et al., *PEGylation and its impact on the design of new protein-based medicines.* Future Med Chem, 2014. **6**(16): p. 1829-46.
19. Pasut, G. and F.M. Veronese, *State of the art in PEGylation: the great versatility achieved after forty years of research.* J Control Release, 2012. **161**(2): p. 461-72.
20. Terlecky, S.R. and J.I. Koepke, *Drug delivery to peroxisomes: employing unique trafficking mechanisms to target protein therapeutics.* Adv Drug Deliv Rev, 2007. **59**(8): p. 739-47.
21. Giordano, C.R., et al., *Catalase therapy corrects oxidative stress-induced pathophysiology in incipient diabetic retinopathy.* Invest Ophthalmol Vis Sci, 2015. **56**(5): p. 3095-102.

22. Nell, H.J., et al., *The targeted antioxidant, catalase-SKL, reduces beta-amyloid toxicity in the rat brain.* Brain Pathol, 2016.
23. Undyala, V., S.R. Terlecky, and R.S. Vander Heide, *Targeted intracellular catalase delivery protects neonatal rat myocytes from hypoxia-reoxygenation and ischemia-reperfusion injury.* Cardiovasc Pathol, 2011. **20**(5): p. 272-80.